THE UNIVERSITY
of EDINBURGH

Heteroleptic Thorium Terphenolate Complexes for Small Molecule Activation

Jamie McKinven

University of Edinburgh

Submitted for the degree of Doctor of Philosophy

October 2015

Declaration

The work described in this thesis is entirely my own, except where I have either acknowledged help from a named person or given reference to a published source. Text taken from another source will be enclosed in quotation marks and a reference given. This thesis has not been submitted, in whole or in part, for any other degree.

Signature:

Date:

Abstract

The chemistry and physical properties of actinide complexes has become increasingly significant and relevant since the dawn of the nuclear age. In addition to increasing the potency of nuclear power and the safety and disposal of its subsequent waste products, exploration of the chemistry of actinide complexes provides a fascinating insight into the increased complexity and divergence of reactivity of these complexes when compared to transition metal complexes. Chapter One provides a brief introduction to the chemistry of actinides and in particular, the major focus of this work, of thorium. This is followed by a survey of examples of rare examples of thorium complexes with a formal oxidation state other than Th (IV). Following this is a review of selected examples of thorium (IV) complexes exhibiting unusual reactivity surveying thorium hydride and alkyl complexes initially. This progresses into reviewing the chemistry of thorium complexes containing multiple bonds to non-metal atoms, beginning with carbon atoms and then progressing to atoms in the chalcogen and pnictogen groups. The introduction finishes with an investigation into the properties of the terphenolate ligands used in this study, including examples of unusual complexes that they have been shown to stabilise.

In Chapter Two, an exploration into the catalytic activity of fairly simple actinide amide catalysts, N''_2Th (IV) $\{\kappa^2\text{-}N(SiMe_3)SiMe_2CH_2$, N''_2U (IV) $\{\kappa^2\text{-}N(SiMe_3)SiMe_2CH_2\}$ and UN''_3, upon terminal acetylenes is presented. The chapter begins with a brief introduction summarising the previous reactivity observed in the catalysis of terminal acetylenes, with particular focus on actinide-based catalyst mediated reactions. The catalytic results on a variety of terminal acetylenes with different steric and electronic properties is then reported upon. It is found that high conversions and selectivities can be achieved upon optimisation of the catalytic process. It was also found that the different catalysts and substrates favoured different products, with selective oligomerisation and cyclotrimerisation reactions observed. The differing reactivities lend support to the role of f-electrons upon the catalytic route of the reaction. Conclusions are discussed at the end of the chapter.

In Chapter Three, the synthesis and characterisation of heteroleptic terphenolate thorium chloride complexes and their subsequent reactivity was investigated. The synthesis and characterisation of $ThCl_2(OTer^{Mes})_2DME$ and $ThCl_2(OTer^{Mes})_2(H_2O)_3$ are initially described. The reactivity of these complexes favoured transmetallation of the

terphenolate ligands, with the complexes; $[Li(OTer^{Mes})THF]_2$, $[Li(OTer^{Mes})]_2THF$, μ^{3}-$(Ter^{Mes}O)\mu^{3}$-$(CH_2SiMe_3)_3Li_4$, $LiAlH_2(OTer^{Mes})_2$, $[(THF)K(OTer^{Mes})]_2$, $MgCl(OTer^{Mes})(THF)_2$, $MgBr(OTer^{Mes})(THF)_2$ and $Fe(OTer^{Mes})_2(py)_2$ synthesised and characterised from reactions attempting to transform the ancillary chlorido-ligands. The reactivity of $ThCl_2(OTer^{Mes})_2DME$ was found to not be solely transmetallation of the terphenolate ligands as elucidated by the synthesis and characterisation of $[Th(OTer^{Mes})_2(Cl)_2(4,4'\text{-bipyridyl})_{1.5}]_\infty$ and $[MgTh_2\mu^{2}\text{-}Cl_2\mu^{3}\text{-}Cl(OTer^{Mes})_2(C_4H_7)_2\mu\text{-}\eta^3\text{:}\eta^3(C_4H_7)H]$. The synthesis of $[MgTh_2\mu^{2}\text{-}Cl_2\mu^{3}\text{-}Cl(OTer^{Mes})_2(C_4H_7)_2\mu\text{-}\eta^3\text{:}\eta^3(C_4H_7)H]$ was found to proceed *via* a reductive elimination route with concomitant formation of a terphenolate transmetallation product $Mg(OTer^{Mes})_2(THF)_2$. The formation of$[Th(OTer^{Mes})_2(Cl)_2(4,4'\text{-bipyridyl})_{1.5}]_\infty$ was achieved *via* reaction with the Lewis base 4-4' bipyridine. Reactions attempting to form heteroleptic uranium terphenolate complexes were also detailed. Conclusions are discussed at the end of the chapter.

In Chapter Four, the synthesis and characterisation of heteroleptic terphenolate thorium borohydride complexes and their subsequent reactivity was investigated. It was found that the conversion of $ThCl_2(OTer^{Mes})_2DME$ to $Th(BH_4)_2(OTer^{Mes})_2DME$ proceeded smoothly using a precedented reaction route. In contrast to $ThCl_2(OTer^{Mes})_2DME$, reaction with a Lewis acid was found to result in abstraction of the solvating DME molecule, resulting in the synthesis and characterisation of $Th(BH_4)_2(OTer^{Mes})_2$. In similarity to $ThCl_2(OTer^{Mes})_2DME$, $Th(BH_4)_2(OTer^{Mes})_2DME$ was found to react with a Lewis base (4-4' bipyridine) to form $Th(BH_4)_2(OTer^{Mes})_2(4,4'\text{ bipyridine})_\infty$. However, despite the increased robustness and versatility of the borohydride complexes, transmetallation of the terphenolate complexes remained an issue as shown by the synthesis and characterisation of $Mg(OTer^{Mes})((\mu\text{-}H)_3BH)THF)_2$. $Th(BH_4)_2(OTer^{Mes})_2$ was found to be able to facilitate small molecule activation in a variety of substrates, encompassing CO, CO_2 and CS_2 amongst others. In most cases this small molecule activation favoured the formation of BMe_3, with the concomitant formation of $HB(OTer^{Mes})_2$ in the case of CO_2 and CS_2. Attempts at catalysis of isonitriles and terminal acetylenes by $Th(BH_4)_2(OTer^{Mes})_2$ are presented with mixed results. Conclusions are discussed at the end of the chapter.

In Chapter Five, investigations into the effects of changing the donor atom of the terphenyl moiety were probed. The chapter began by examining the differing properties of a phosphorous atom acting as a ligating atom, as opposed to the oxygen atom seen in Chapters Three and Four. The chapter continued by detailing the result of

reactions attempting to synthesise and characterise terphenyl phosphino-actinide complexes. It was found that in the case of actinides with easily accessible lower oxidation states, i.e. U (IV), that reductive elimination was favoured, culminating in the isolation of $(Ter^{Mes}PH)_2$. Following this result attempts were made to modify the ligand system in an attempt to divert the reaction away from this product, in the hope of isolating a phosphino-actinide complex. Reactions attempting to ligate the terphenyl moiety *via* the aryl α-carbon to thorium were also detailed, resulting in radicular degeneration and the isolation of $^{n}BuTer^{Trip}$ and $ClTer^{Trip}$. Conclusions are discussed at the end of the chapter.

Experimental and characterising data are provided in Chapter Six.

Lay Summary

This piece of work details research carried out towards the aim of transforming ubiquitous, simple feedstocks to more complex and useful derivatives. This work concentrates almost solely upon the chemistry of a particular type of thorium complex in facilitating these transformations.

The work begins with an introductory chapter detailing selected literature examples of relevant thorium chemistry. This chapter continues by looking at the types of complex that have previously been shown to cause transformations of feedstocks similar to those targeted within this piece of work. As a result of this examination, a strategy for forming complexes hoped to facilitate these transformations was proposed.

Chapter Two presents results of the transformation of simple molecules into more complex ones by simple thorium (and uranium) catalysts. These catalysts are found to be highly active and under certain conditions highly selective, however there are areas of this catalysis that could be improved.

Chapter Three reports upon the synthesis and attempted synthesis of thorium complexes that may be able to enable either improvements in the catalytic process outlined in Chapter Two or divergent transformations of the targeted feedstocks.

Chapter Four reports upon an alternative alteration to the thorium complexes described in Chapter Three that resulted in a different transformation of the targeted ubiquitous feedstocks. The preliminary results of a catalytic process are discussed.

Chapter Five reports upon further alternative alterations to the thorium complexes described in Chapter Three. Chapter Six provides experimental details of the reactions carried out within the course of this work.

Acknowledgements

I would like to thank my supervisor Polly for her constant enthusiasm and guidance during my PhD, as well as her patience in allowing me to carry out some of my hare-brained schemes! I also cannot have been the easiest PhD student to deal with at times. I am also grateful to the ESPRC for funding my project.

I am very grateful for all the vital help I have received from Dr Lorna Murray and Mr Juraj Bella with NMR spectroscopy, and the monumental contribution that Dr Gary Nichol has made with my understanding of X-ray crystallography and the workings of diffractometers.

Thank you to all the excellent postdocs in the Love/Arnold group who were so patient, wise and generous with their time. Thank you to Stephen for his constant enthusiasm and unique way of laughing when dispensing, usually apt, criticisms. Thank you to Joy, for being such an inspiring person and excellent chemist, your effect on my life both inside and outside of chemistry was immense. Thank you to Thomas, for being such a fantastic chemist and person, I hope that Ecuador suits you and your family well. Thank you to Rowan for your never-ending attempts to assume a mentor position, I hope that the wonders of Singapore treat you well. I would also like to give a large thank you to Johann, who is probably the person I spoke the most to about chemistry during my PhD (just nudging out Joy with a dip at the line perhaps), however it was far from a one-way street and I believe that you will do great things.

I would also like to thank my fellow Love/Arnold PhD students for making working in the lab so enjoyable. Thank you to Guy, Colin, Isobel and Rebecca for their helpfulness in showing me the ropes and making me feel welcome in what must have been a stressful time for them. Thank you to Aaron for being such a wonderful person, full of fun and enthusiasm for life. Thank you to Charlotte for not letting, admittedly horrendous first impressions of me, cloud her judgement of what became a wonderfully rich and mutually beneficial friendship. Thank you to Andrew for his solid and calming presence, particular in the face of pyrotechnics. Thank you to Markus, for always being an entertaining individual, many good discussions were had at your fume hood. To Emma, the thanks I give here are unlikely to reach the tip of help that you have given me, but you are an astonishingly good friend, who should have more belief in your qualities. Thank you to Danny for putting up with me for so long and apologies for any stress that I caused you. Thanks also to Marketa, James and Jordann, who have

the great burden on their shoulders of continuing the Sussex mafia! All three of you will do exceedingly well, there may be bumps in the road to come but you will get there (mostly, if not completely) unscathed. Thank you to Kai for displaying his continued passion for chemistry despite some setbacks. I am proud to know you all.

There are also people outside of the immediate vicinity of the lab, without whom this work would not have progressed as well, or quickly. A massive thank you to Georg, the Thomas group, JR, Ruth and Mike for their contributions to my sanity during these three years. A particularly large thank you to Georg for all the good times and bad, I hope that there ended up being more of the good!

Finally, thank you to my friends and family for their contribution in allowing me to complete this work. I couldn't have done it without you.

Abbreviations

General

Alk	Alkyl	py	Pyridine
Ar	Aryl	pyr	pyrrole/pyrrolide
Cp	C_5H_5	RT	room temperature
Cp*	C_5Me_5	s.u.s	standard uncertainties
Ct	Centroid	SQUID	Superconducting Quantum Interference Device
Cy	Cyclohexane	^{t}Bu	*tert*-butyl
DFT	Density Functional Theory	THF	tetrahydrofuran
Dipp	2,6-diisopropylphenyl	Ter^{Dipp}	2,6 di-isopropyl diphenyl terphenyl
DME	Dimethoxyethane	Ter^{Mes}	dimesityl terphenyl
DMF	Dimethylformamide	Ter^{Trip}	2,4,6 tri-isopropyl diphenyl terphenyl
EPR	Electron Paramagnetic Resonance	Tp	Trispyrazolylborate
gem	geminal	ν_{eff}	Effective steric factor
HOMO	Highest Occupied Molecular Orbital		
Ind	Indenyl	δ	chemical shift
^{i}Pr	Isopropyl	s	singlet
IR	Infra-red	d	Doublet
Me	Methyl	t	Triplet
Mes	mesityl, 2,4,6-$C_6H_2(Me)_3$	q	quartet
ODtbp	2,6 ditertbutyl phenolate	p	pentet
N″	$N(SiMe_3)_2$	*J*	coupling constant
^{n}Bu	'normal' Butyl		
NMR	Nuclear Magnetic Spectroscopy		
PBV	Percentage Buried Volume		
Ph	Phenyl		

Table of Contents

Chapter 1: Introduction

1.1 Brief introduction into general thorium chemistry – common oxidation state, radioactivity, abundance

Investigation into the chemistry of the actinides has been of increasing importance since the beginning of the nuclear age as a means of producing electricity over 65 years ago. The majority of nuclear power stations use uranium as fuel, with ^{238}U the key isotope in allowing the process to occur. A problem with using ^{238}U to produce nuclear power is the production of radio-active nuclear waste containing components with long half-life, particularly transuranic elements such as plutonium and neptunium. The current disposal procedure for waste from uranium-powered nuclear power stations is to either subject the 'spent' fuel to nuclear reprocessing or disposal in an area deemed inaccessible to the general public whilst still being retrievable, i.e., deep underground. Further understanding of the chemistry of the actinides may aid in the disposal of nuclear waste becoming more sustainable. An alternative to the uranium-fuel cycle is using thorium as nuclear fuel in the thorium fuel cycle. In the thorium fuel cycle the 100% naturally abundant ^{232}Th isotope is transmuted into ^{233}U, a fissile isotope of uranium, which initiates a nuclear chain reaction. Benefits of the thorium fuel cycle over the uranium fuel cycle include: thorium's greater abundance;[1] increased resistance to nuclear weapons proliferation;[2] superior physical and nuclear properties; and reduced production of the highly radioactive higher actinides.[3] A drawback of the thorium fuel cycle is the need for a secondary neutron source to activate the thorium.[4]

Beyond the nuclear fuel industry the chemistry of the actinides is underdeveloped, compared to that of the transition metals. Investigations into the reactivity and bonding of actinide complexes, when compared to transition metal complexes, provide a fascinating case study into the differences that exist due to the influence of *f*-orbitals. Investigation into thorium chemistry compared to uranium chemistry is even further underdeveloped.[5] Below will be described key differences that exist between thorium and transition metals in terms of electronics.

The chemistry of thorium differs from that of most transition metals as it tends not to undergo redox type reactions and the bonding within thorium compounds is decidedly

less covalent and more ionic in character. This is primarily due to the radial contraction of the valence orbitals, which reduces the orbital overlap with ligands. This is a result of relativistic effects acting on the electrons of thorium meaning that the mass of these electrons has increased relative to that of an electron of hydrogen. The Bohr radius is inversely proportional to the mass of the electron and therefore this mass increase has a substantial affect upon the atomic orbitals of thorium as the *s* and *p* functions experience a direct relativistic orbital contraction. This increase in contraction leads to a stronger shielding by outer shell *s* and *p* electrons of similar radial distribution, which results in the indirect relativistic orbital expansion of the *f* and *d* orbitals as their wavefunctions are expanded and destabilised with respect to their hypothetical non-relativistic analogues.[1]

The properties of the lanthanide series of elements also differ from those of thorium, as although thorium does experience the lanthanide contraction, its valence 5f orbitals are far more diffuse than the lanthanides' valence 4f orbitals. This is due to the relativistic expansion of the f-orbitals being more pronounced with increasing principal quantum number, as a consequence of increased shielding by the 'core' electrons. This means that they are more available for bonding covalently as it is possible for them to overlap more efficiently with other orbitals.

Thorium has a crustal abundance of 8.1 ppm, *cf*. the crustal abundance of uranium of 2.4 ppm.[1] However, thorium differs quite significantly from uranium in terms of chemistry, particularly due to the favourability of only one oxidation state, as discussed below. This reduces thorium's tendency to undergo redox chemistry. In contrast uranium complexes are stable under anaerobic conditions in the U (III) to U (VI) oxidation states with recent reports of isolation of compounds in the U (II) oxidation state.[6, 7] As predominantly an α-emitter thorium is a radioactive element, but at 8.14 Bq per mg this radioactive emission is small.

Due to its favourable ionisation potentials with regards to forming the +4 state, thorium is rarely found in any other oxidation state. This results in part from the energetically favourable 'closed shell' electronic configuration that results from thorium adopting a +4 oxidation state, which makes it isoelectronic to radon. The high thermodynamic stability of the +4 state results in a high reduction potential for the Th^{4+}/Th^{3+} pair (E_{red} = -3.0 V),[8] which is comparable to the reduction potential of K^{+}/K (E_{red} = -2.93 V)[9]. In addition the reduction potential for the Th^{4+}/Th^{0} pair is

comparatively low at -1.82 V,[8] meaning that under highly reducing conditions, a ligand system which stabilises the metal centre must be used to prevent formation of elemental thorium metal. For this reason the formation of thorium(III) complexes has so far required the use of alkali metal reduction of thorium(IV) complexes as seen in Equation 1.1. As a result, reports of thorium (III) complexes in the literature are limited to merely five well characterised examples.

1.2 Thorium (III) complexes

A thorium (III) complex is one in which the formal oxidation state upon the thorium metal centre is defined to be 3+. However, in practice, the actual charge upon this centre differs from the official '+3' oxidation state in accordance with Pauling's electroneutrality principle, which states that the distribution of charge in a molecule or ion is such that the charge on a single atom is within the range +0.5 to –0.5 (ideally close to zero).[10]

The first report of a thorium(III) compound came in 1974 from the Baumgärtner group based in Karlsruhe.[11] This compound was $ThCp_3$, **A**, and was synthesised via sodium reduction of the $ThCp_3Cl$ (Equation 1.1). However, characterisation was limited to magnetic susceptibility measurements.

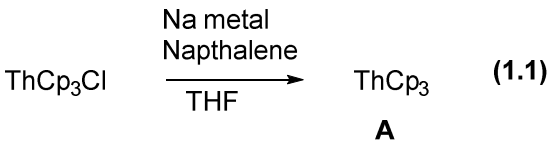

(1.1)

The synthesis of the first thorium(III) compound, $ThCp_3$ as reported by Baumgärtner *et al*.[11]

The magnetic moment for **A** was found to be 0.403 μ_B at 293 K and to decrease to 0.10 μ_B when the temperature was lowered to almost absolute zero, thus displaying paramagnetic behaviour distinguishing Th(III) from Th(IV). Using the spin only formula, (which is not strictly applicable to thorium, due to the large spin orbit coupling component of angular momentum) the calculated magnetic moment for one unpaired electron is 1.73 μ_B and this does not compare favourably with the moment obtained for $ThCp_3$. However, due to the large spin-orbit coupling component of the angular momentum of thorium atoms, much of this angular momentum and hence magnetism is quenched, resulting in a lower magnetic moment being observed.

Importantly, the observation of a non-zero magnetic moment suggests that this complex was paramagnetic, indicating the formation of a thorium(III) compound.

The temperature dependency of the paramagnetism means that the maximum number of unpaired spin states in this compound is not populated at room temperature. The magnetic moment at room temperature is therefore unlikely to be the maximum magnetic moment that could be observed, explaining the disagreement with the calculated value of magnetic moment for a one electron system.

In the early 1980s, Marks also reported the synthesis and characterisation of thorium(III) complexes by photo-induced β-hydride elimination of tris Cp alkyl (methyl, n butyl, isopropyl) complexes of thorium to give the thorium(III) compounds as displayed in **Scheme 1.1.**[12]

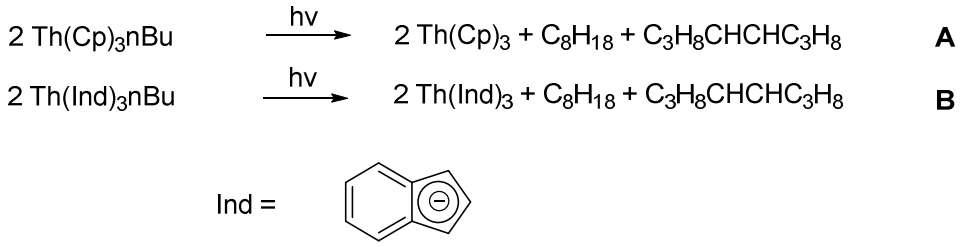

Scheme 1.1: Synthesis of $Th(Ind)_3$, **B**, and $Th(Cp)_3$, **A**.as reported by Marks *et al*.[12]

A and **B** were synthesised from thorium(IV) precursors, which contained alkyl groups with β hydrogens that were eliminated via photolytic activation, producing an alkene and the desired thorium(III) compounds. Unfortunately, neither compound was structurally defined using X-ray diffractometry. It was noted, however, that both compounds were green in colour, unless formed within a frozen toluene glass, in which case a purple colour was observed, which, for **A**, is in agreement with the earlier sodium reduction synthesis.[11] **A** was characterised by IR spectroscopy and mass spectrometry, which showed no evidence of a metal hydride, providing good evidence to support the formation of a thorium(III) compound. This was further underpinned by a magnetic moment of 0.404 μ_B at room temperature, although this property was temperature dependent and could drop as low as 0.1 μ_B at 4 K, again displaying good agreement with the earlier synthesis.[11] Despite the lack of crystallographic confirmation, it is likely that the reports by Baumgärtner and Marks describe the first examples of isolated Th(III) complexes.

The first reported Th(III) crystal structure was obtained for the Th(III) compound, $Th(Cp^{TMS})_3$, by Lappert in 1986[13] (**Figure 1.1, C**).

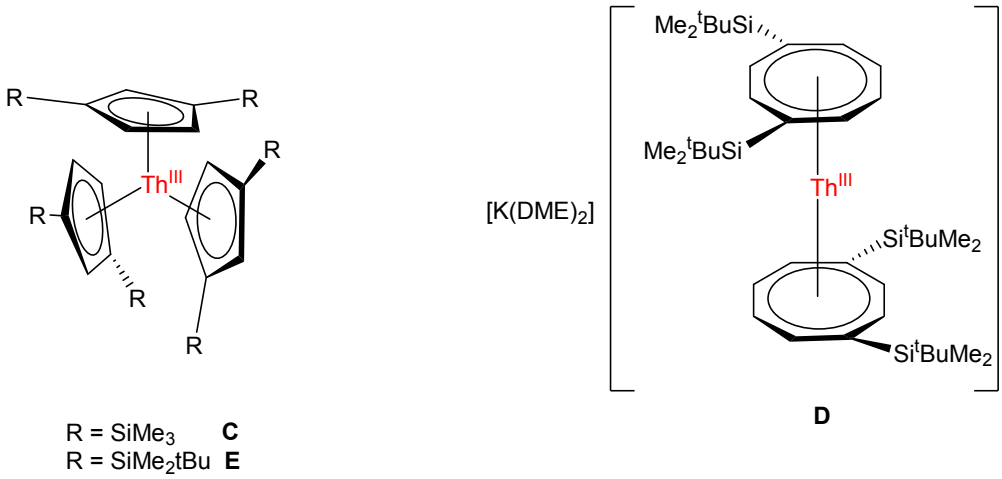

Figure 1.1: The structures of C**,** $Th(Cp^{SiMe3})_3$, **D**, $[K(DME)_2][(COT^{SitBuMe2})_2Th]$, **E,** $Th(Cp^{SitBuMe2})_3$ as reported by Lappert and Cloke *et al*.[13-15]

As can be seen from **Figure 1.1, C**, the stabilisation of the thorium(III) centre, which is inherently thermodynamically unstable with respect to the +4 oxidation state, can be attributed to two main properties of the modified Cp ligands. The first is the steric protection afforded by the bulky $SiMe_3$ groups, which prevent access to the thorium centre. The second, and perhaps the more important consideration in the stabilisation of the metal centre, is that the Cp^{SiMe3} ligands can more readily accept electron density (*cf*. Cp) by acting as π electron acceptors from the thorium centre, which, due to its additional electron is more electron dense in its +3 oxidation state than the thorium +4 state. **C** was reported to be blue, and was analysed by UV-Vis spectroscopy. Optical spectral data for **C** in methylcyclohexane was recorded at 298, 77 and 4 K, resulting in very similar spectra. The bands were broad, spanning 1000–1500 cm^{-1} and were therefore unlike the usual sharp f-f transitions and very intense (*cf*. the much lower oscillation strengths, by two to three orders of magnitude, of typical lanthanide f-f transitions[16]).[15] These bands likely originate from *d*- transitions of the additional electron, even though at the time they were was assigned to be within the $5f^1$ orbital. However, thermodynamic calculations predict the electron to be more likely found within the $6d^1$ orbital in the ground state.[17] Later papers, considering the electronic structure and molecular orbital diagram of the analogous **A** from DFT calculations,

conclude that the formal electronic configuration, when considering relativistic effects, would be $6d^1$.[18]

In 1999 Cloke reported an anionic thorium(III) sandwich complex, **D** $[(COT^{SitBuMe2})_2Th][K(DME)_2]$[14] (**Figure 1.1, D**). Stabilisation of the thermodynamically unstable thorium(III) centre is due to a combination of steric and electronic effects of the COT ligands. The steric effect of the bulky silyl groups protects the anionic thorium(III) centre, and ability of the COT ligands to act as π electron acceptors enables significant stabilisation of the high electron density. This compound was formulated to have a $6d^1$ electronic configuration. An EPR spectrum obtained at 298 K shows a sharp peak at 1.916, which is evidence for a $6d^1$ configuration, as a $5f^1$ electron would be expected to relax too quickly to be observed at room temperature. This is the second fully characterised example of a thorium(III) organometallic compound.

In 2001, Lappert and his group reported a second silyl substituted tris Cp thorium(III) complex[15] where one of the silyl methyl groups from his earlier example depicted in **Figure 1.1, C** was substituted for a tertiary butyl group (**Figure 1.1, E**). This second analogue of Cp differs from the first in that the tertiary butyl groups add additional bulk, and presumably increase the complexes' solubility in non-polar solvents. The crystal structure obtained was broadly similar to that of the **C**. **E** was also reported to be dark blue in colour. The EPR spectra for **C** and **E** were found to contain a sharp peak at 1.910, indicative of a $6d^1$ configuration.

Recently, Evans *et al.* reported upon a further reduction of **C**, leading to the characterisation of $[K(2,2,2\text{-cryptand})][Th(Cp^{SiMe3})_3]$, **F,** and $[K(18\text{-crown-}6)(THF)_2][Th(Cp^{SiMe3})_3]$, **G**, as the first, and to this author's knowledge, only thorium complexes with a formal oxidation state of II (**Scheme 1.2**).[19]

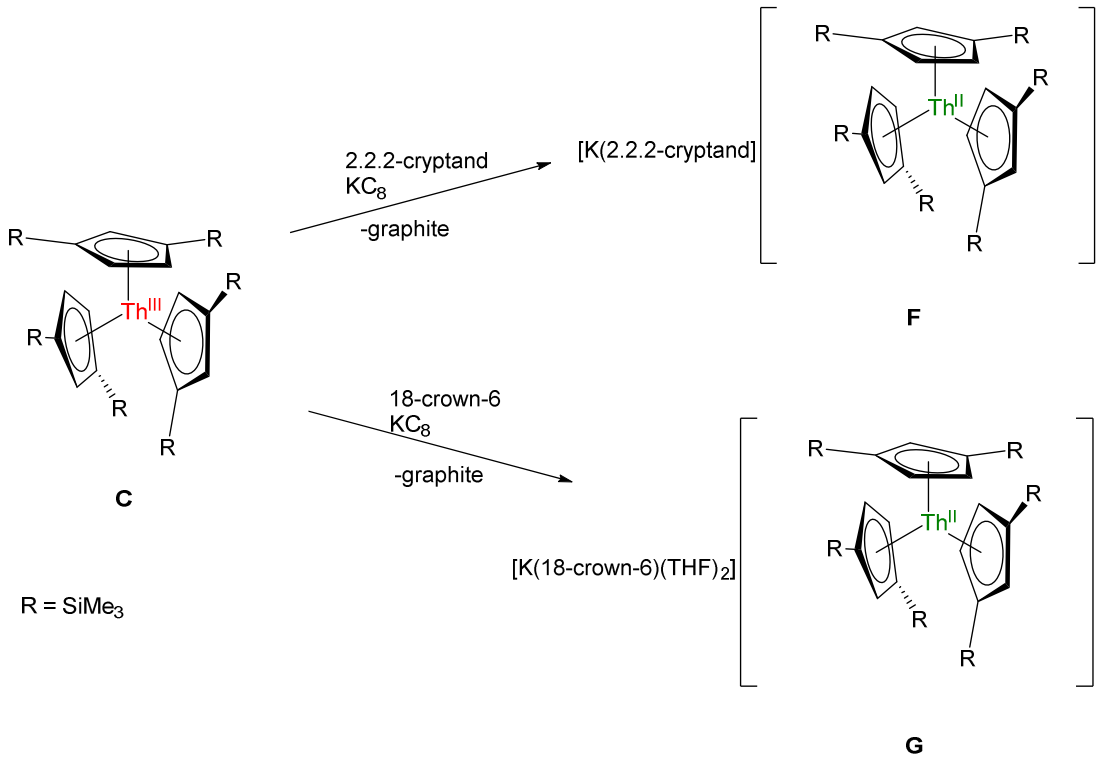

Scheme 1.2: Synthesis of the thorium (II) complexes **F,** [K(2,2,2-cryptand)][Th(Cp^{SiMe3})$_3$] and **G,** [K(18-crown-6)(THF)$_2$][Th(Cp^{SiMe3})$_3$] as reported by Evans *et al*.[19]

The formation of a Th^{2+} complex, which is already problematic given the difficulty in obtaining Th^{3+} complexes, is made more difficult by the estimated redox potential of a Th^{3+}/Th^{2+} pair being – 2.8 V, which when compared with the Th^{3+}/Th^{0} couple of 1.44 V, suggests that formation of thorium metal would be highly favoured.[8] No EPR spectra was observed for complexes **F** or **G**, and the NMR spectra gave resonances in the diamagnetic region. Evans' Method measurements and SQUID measurements on **F** and **G** suggest that the [Th(Cp^{SiMe3})$_3$]$^-$ anion is diamagnetic. The UV/Vis spectra reported absorptions at 650 nm with significantly higher extinction coefficients (ε = 23000 M^{-1} cm^{-1}) of intensely coloured solutions compared to those reported for **C** (ε = 5000 M^{-1} cm^{-1})**.**[19] The solid state structure of the anions in **F** and **G** are very similar to the structure seen for **C**. DFT calculations on **C**, **F** and **G** suggests a $6d^2$ configuration for [Th(Cp^{SiMe3})$_3$]$^-$ and a $6d^1$ configuration for Th(Cp^{SiMe3})$_3$, which agrees with the EPR data for these complexes. Accordingly **F** and **G** represents the first examples of an isolable ion with a $6d^2$ configuration.[19]

In 2010, Evans *et al.*[20] reported an amidinate analogue of the ubiquitous thorium metallocene system, (**Figure 1.2**) **H**, via reduction of a cationic species with a non-co-ordinating anion. The EPR data for **H**, a single sharp peak at 1.871 with no hyperfine coupling, indicates a $6d^1$ configuration and compares well to the data seen for **C**-**E**. In 2013 Evans *et al.*[21] also reported upon the synthesis of $Th(C_5HMe_4)_3$, **I** *via* reduction of the Th(IV) precursor $Th(C_5HMe_4)_3Br$ using potassium graphite. The EPR data of this complex with a g value of 1.92 was also in agreement with a Th^{3+} oxidation state with $6d^1$ configuration, which correlates well with **C**-**F**.

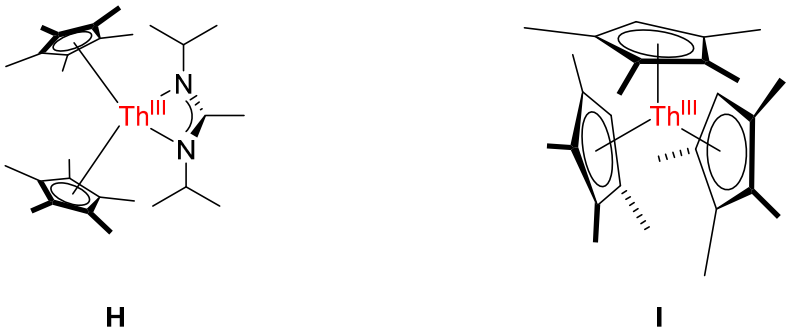

H **I**

Figure 1.2: The structures of **F**, $Th(Cp^*)_2(^iPrNC(H)MeN^iPr)$ and **G**, $Th(C_5HMe_4)_3$ as reported by Evans *et al*.[20, 21]

In 2006, Gambarotta *et al*. group reported ring opening and carbon-nitrogen, and carbon –oxygen bond activation by *in situ* production of reduced thorium compounds.[22] Reduction of $Th\{\kappa^3\text{-}NC_4H_8(2,CPh_2(\text{-}2,[Me][NC_4H_8]\text{-}5,)CPh_2NC_4H_8)Cl_2DME$, **J** (**Figure 1.3**) under different reaction conditions led to differing reactivities.

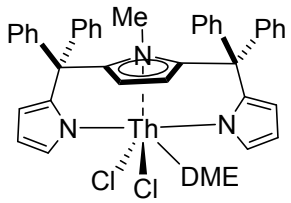

J

Figure 1.3: Structure of **J**, $Th\{\kappa^3\text{-}NC_4H_8(2,CPh_2(\text{-}2,[Me]\{NC_4H_8]\text{-}5,)CPh_2NC_4H_8)Cl_2DME$ as synthesised by Gambarotta *et al*.[22]

In the presence of a dimethoxyethane ligand, potassium reduction of **J** was found to fragment three dimethoxyethane molecules to form the product shown in Equation 1.2. This reduction postulated to progress *via* a transient low oxidation state thorium compound, a claim which was mainly supported by the formation of a dark red colour

in the reaction mixture which slowly vanished over time and the manner in which the ligands were reduced, i.e. through separate one-electron reductions and with C-O bond cleavage. In gas chromatograms of the reaction mixture, evidence of methane and ethane formation was found, further supporting the reduction of DME.

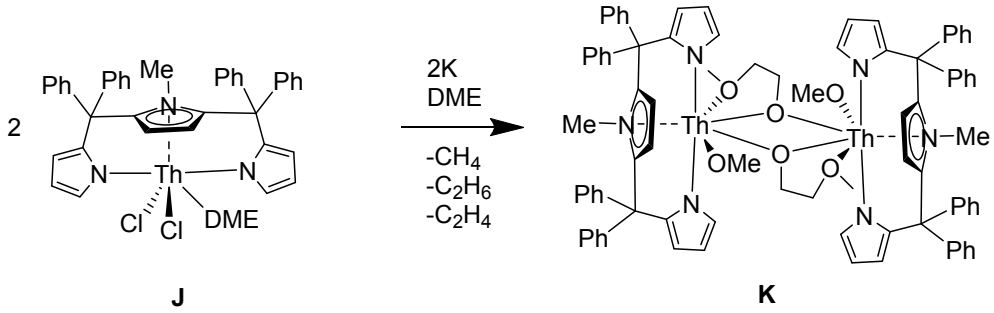

J **K** **(1.2)**

Activation of DME by an in situ generated thorium (III) complex as reported by Gambarotta *et al*.[22]

Carbon nitrogen bond activation and concurrent ring opening was also observed when Th{κ^3-NC_4H_8(2,CPh_2(-2,[Me]{NC_4H_8]-5,)$CPh_2NC_4H_8$)({κ^2-NC_4H_8(2,CPh_2(-2,[Me]{NC_4H_8])Cl, **L,** was subjected to reduction *via* potassium metal (Equation 1.3). This transformation was deemed to proceed *via* the same transient reduced thorium compound that was suggested in the fragmentation of DME, but this time through two one-electron reductions, from both thorium centres to form the bimetallic 'ate' complex. The two one-electron reductions resulted in ring opening of the pyrrolic moiety via C-N bond cleavage. This reaction provides more evidence for the formation of a thorium containing intermediate that carries out the reduction, as a blank reduction of the potassium salt of the dipyrrolic ligand by potassium did not yield a ring opened product. This led to the conclusion that the thorium is key in allowing the ring opening reaction to occur.

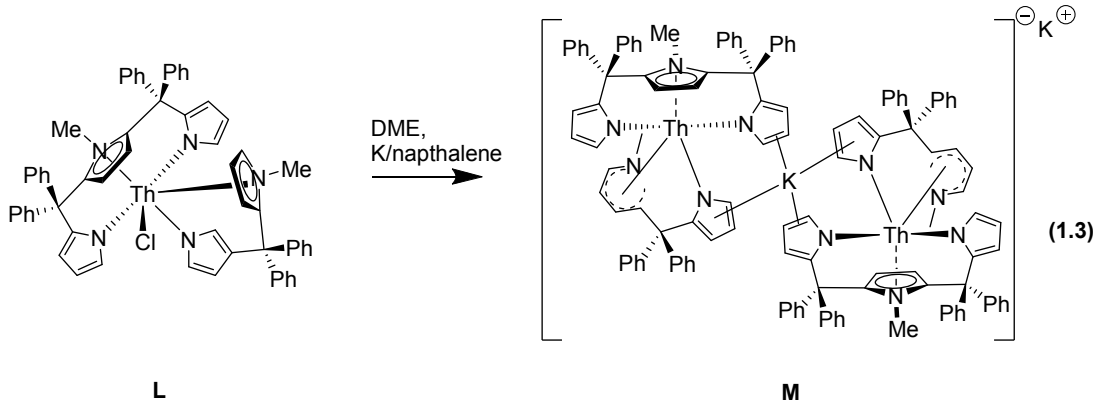

L **M**

Synthetic route to a thorium C-N activation complex as reported by Gambarotta *et al*.[22]

In 2010, Gambarotta reported the preparation of a rare paramagnetic thorium compound, **O** (Equation 1.4).[23] It was expected that reduction of the thorium centre with potassium would yield a deprotonated central phenyl ring. However, this was not observed and instead a simple atom count was suggestive of a thorium(III) centre being generated. Initial evidence for the generation of a thorium (III) centre was that the ^{1}H NMR spectrum was paramagnetic with substantial line broadening, and a magnetic moment calculated to be 1.23μ_B. An EPR spectrum of the paramagnetic complex displayed a broad resonance with no discernible hyperfine coupling, postulated to result from significant spin-orbit coupling at room temperature. This spectrum sharpened greatly when the temperature was reduced to 113.2K. This contrasts with the EPR spectra of **C**-**E** and **H**-**I,** which exhibited a sharp peak. However, the EPR resonance of **O** may have been due to a $5f^1$ configuration which is expected to relax too quickly at room temperature. In an attempt to substantiate whether this reaction was indeed an example of a thorium (III) centre DFT-hybrid calculations were carried out on a simplified form of the complex, as shown in **Figure 1.4**.

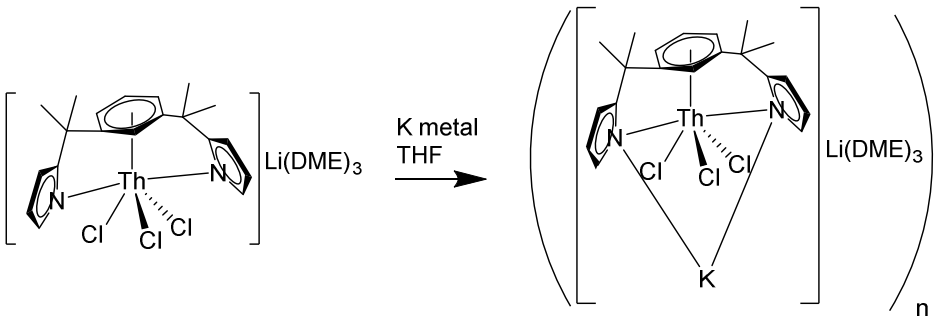

N **O** **(1.4)**

A paramagnetic thorium complex generated from potassium reduction as reported by Gambarotta *et al*.[22]

These calculations found that the unpaired electron responsible for the paramagnetic properties of this complex was associated more strongly with the ligand than with the thorium centre, in such a way that the ligand acts as a radical anion which donates to a thorium(IV) centre with only *circa* 13% contribution to the HOMO coming from the atomic orbitals of thorium.

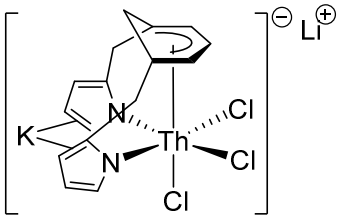

P

Figure 1.4: The simplified model used in DFT calculations[22]

1.3 Thorium hydrides

In 2007 Evans reported upon the reactivity of $Th_2(Cp^*)_4H_2(\mu_2\text{-}H)_2$, **Q**, first synthesised in 1979,[24, 25] that could be used as a multi-electron reductant for a variety of substrates, driven by the evolution of hydrogen gas as a side product.[26] **Q** is based upon the permethylated Cp ligand and the complex is shown in **Figure 1.5.**

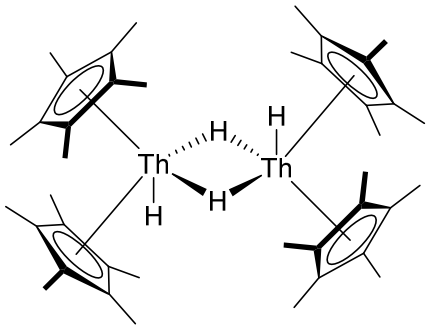

Q

Figure 1.5: Structure of **Q,** $Th_2(Cp^*)_4H_2(\mu_2\text{-}H)_2$ as synthesised by Evans and Marks *et al.* [24-26]

Evans showed that **Q** could be used to effect four and six electron reductions of organic substrates to form new thorium complexes and hydrogen gas. **Scheme 1.3** illustrates the ability of Evans' thorium hydride compound to act as a four electron reductant in a reaction with diphenyl disulphide, resulting in two sulphide ligands being ligated per thorium. **Scheme 1.4** shows how **Q** can act as a six electron reductant in effecting the reduction of three cyclooctatetraene ligands.

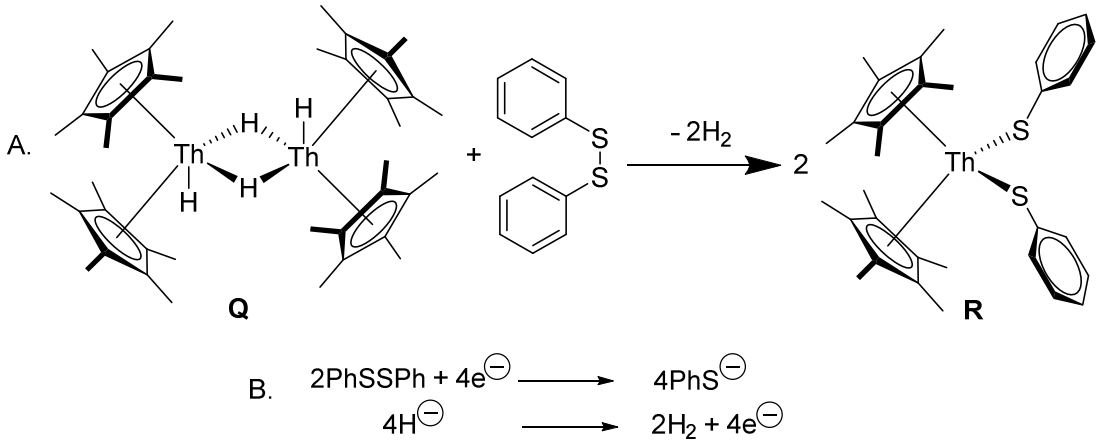

Scheme 1.3: A. Overall scheme of $Th_2(Cp^*)_4H_2(\mu_2\text{-}H)_2$ acting as a four electron reductant

B. redox half equations of formation of $Th(Cp^*)_2(SPh)_2$[26]

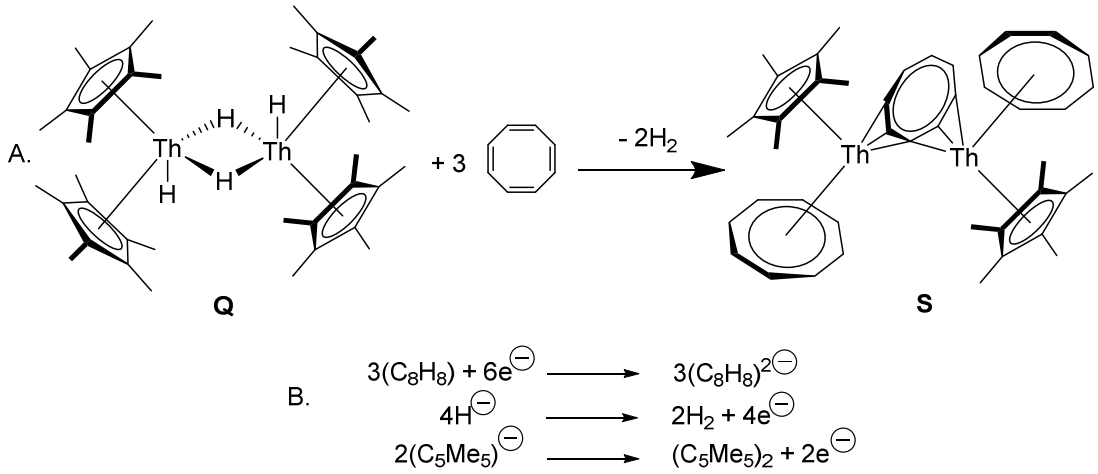

Scheme 1.4: A. Overall scheme of $Th_2(Cp^*)_4H_2(\mu_2\text{-}H)_2$ acting as a six electron reductant

B. redox half equations of formation of $Th(Cp^*)_2(COT)_3$[26]

Over thirty years ago Marks *et al*. reported the migratory insertion of carbon monoxide into thorium hydride bonds to make μ^2-formyl complexes ($Cp^*_2Th(\mu^2\text{-}CO(H))(O^tBu)$) (Equation 1.5).[27] Thereafter, investigation into the formation of thorium hydride complexes increased substantially.

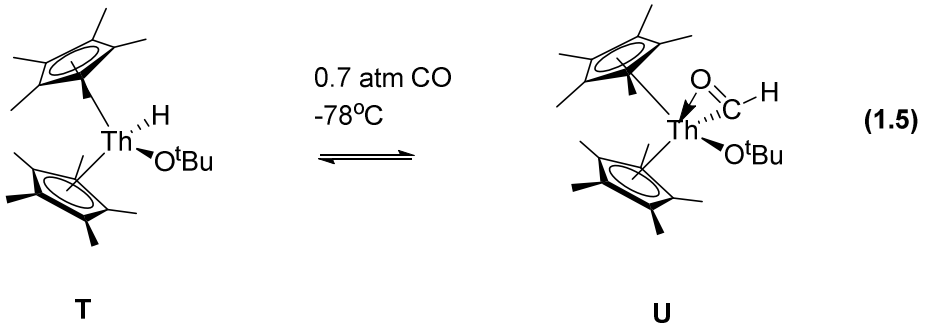

Reversible formation of a formyl thorium complex as reported by Marks *et al*.[27]

The activation of carbon monoxide to formaldehyde is a commercially important reaction and attracted further research into thorium hydrides.

A neutron diffraction structure study of **Q**, published in 1979 by Marks, was one of the first molecular structures to be determined by a neutron diffraction study.[25] It was reported that the thorium to thorium separation is 4.007 Å, which is considerably longer than that observed in elemental thorium (3.60 Å)[28], and slightly longer than the Th-Th distance in ThI_2 of 3.97 Å. ThI_2 contains two electrons in the band gap and has

been proposed to be short enough for some small Th-Th orbital overlap to exist.[29] This led to the suggestion that any interaction between thorium atoms in **Q** is likely to be extremely weak. In 1988 Marks also reported on $Th_2(Cp'SiMe_2Cp')_2(\mu_2\text{-}H)_4$**, W,** [30] in which the Cp ligands were bridged by an *ansa* dimethyl silyl group as shown in Equation 1.6**.**

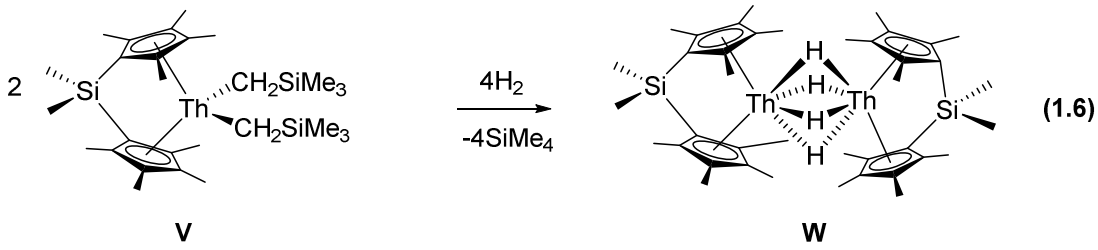

V **W** **(1.6)**

Synthetic route to **W**, $Th_2(Cp'SiMe_2Cp')_2(\mu_2\text{-}H)_4$ as reported by Marks *et al*. [30]

In the solid state structure of **W**, the hydrogen atoms postulated to be bridging hydrides could not be crystallographically defined. However, the Th-Th distance was reported to be 3.632 Å, which is very close to to the sum of the Th(0)-Th(0) van der Vaals radii (3.60 Å)[28] and the typical Th-Th single bond distance (3.44 Å)[31] reported in the literature, indicating that there is a strong interaction constraining the distance between the thorium atoms. This interaction is arguably far stronger than the interaction in **Q**, given the comparative intermetallic distances. A Th-Th bond distance was hypothetically predicted by Marks to have a bond distance *ca*. 3.22 Å.[30] This is significantly shorter than the observed thorium to thorium distance for **W**, which supports the formulated four bridging hydrides as the Th-Th was shorter than that of **Q,** which is only constrained by two bridging hydrides. The rare $(\mu\text{-}H)_4$ was further suggested to be stabilised by the strained, silicon-bridged Cp ligands. There was found to be no evidence to support the existence of terminal hydrides in the IR spectrum due to a lack of observed stretching frequencies observed in the region of 1350 to 1400 cm^{-1}. Stretching frequencies in this region would be expected to correspond to terminal hydride resonances on thorium as has been seen in the example of **Q**, which contained terminal thorium hydride bonds.

Marks also reported upon the catalytic properties of **W** and compared it to **Q** as a catalyst for olefin hydrogenation. **W** was found to be a better catalyst for this conversion than **Q**. Whilst gas chromatography indicated that both formed the desired

alkane in greater than 98% yield, with 98% or greater of the recovered hydride catalysts deemed to have been regenerated by NMR spectroscopy, the turnover number for **Q** was 0.58 per hour, whilst for **W** it was 610 per hour; representing an increase of over 3 orders of magnitude. That **W** was found to be a superior catalyst to **Q**, whilst containing more bridging hydrides and a shorter intermetallic distance it may be postulated that these factors are key to the activity of these catalysts.

In 1995 Watkin *et al.*[32] reported upon a $Th_3(Od^tBup)_3(\mu_2\text{-}H)_4(\mu_3\text{-}H)_2$, **Y**, produced from the reaction of $Th(CH_2SiMe_3)_2(Od^tBup)_2$, **X,** with hydrogen gas as depicted in Equation 1.7.

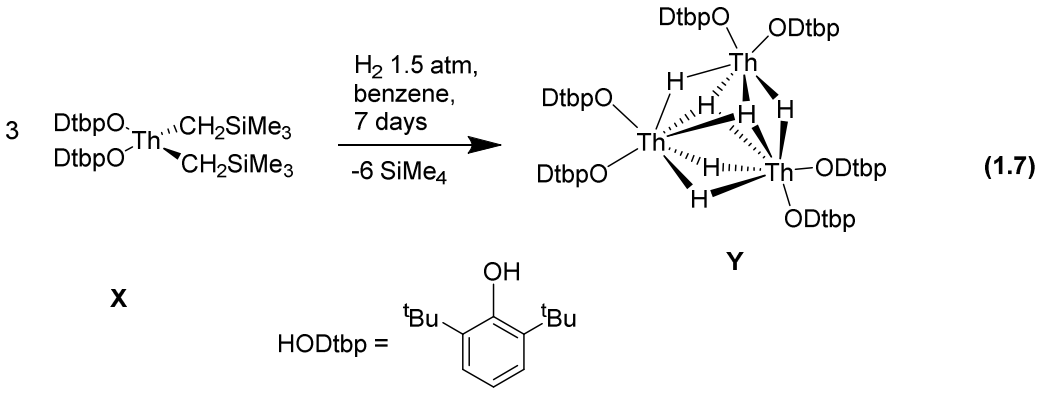

(1.7)

The formation of $Th_3(Od^tBup)_3(\mu_2\text{-}H)_4(\mu_3\text{-}H)_2$ as reported by Watkin *et al.*[32]

The synthesis forms tetramethylsilane as a side product. The structure comprises four $\mu^{2\text{-}}$ bridging hydrides and two μ_3 bridging hydrides all located and refined in the crystal structure. The ^1H NMR spectrum shows a resonance at 20.54 ppm, which is significantly deshielded for a diamagnetic NMR spectrum, and only displayed slight broadening upon cooling to -90°C. This suggests that the hydrides are equivalent on the ^1H NMR timescale, which suggests that a rapid interconversion occurs.

In 2013 Evans *et al.*[21] reported the formation of a poly-thorium hydridic cage structure from the hydrogenation of a thorium alkyl complex, if stabilised by a *bis* metallocene ligand system, $(C_5Me_4H_4)_2ThMe_2$, **Z**, (**Scheme 1.5**). In the formation of the polymetallic polyhydride, $(C_5Me_4H_4)_4[\mu\text{-}\eta^5\text{-}C_5Me_3H(CH_2)\text{-}\kappa C]_2Th_4(\mu_4\text{-}H)_4(\mu_3\text{-}H)_4$, **AB**, a 'tuck-over' moiety *via* metalation of one of the methyl groups of the cyclopentadienyl rings was observed. The formation of **Z** was accompanied by the formation of two equivalents of the ligand redistribution product $(C_5Me_4H_4)_3ThMe$, **AA**.

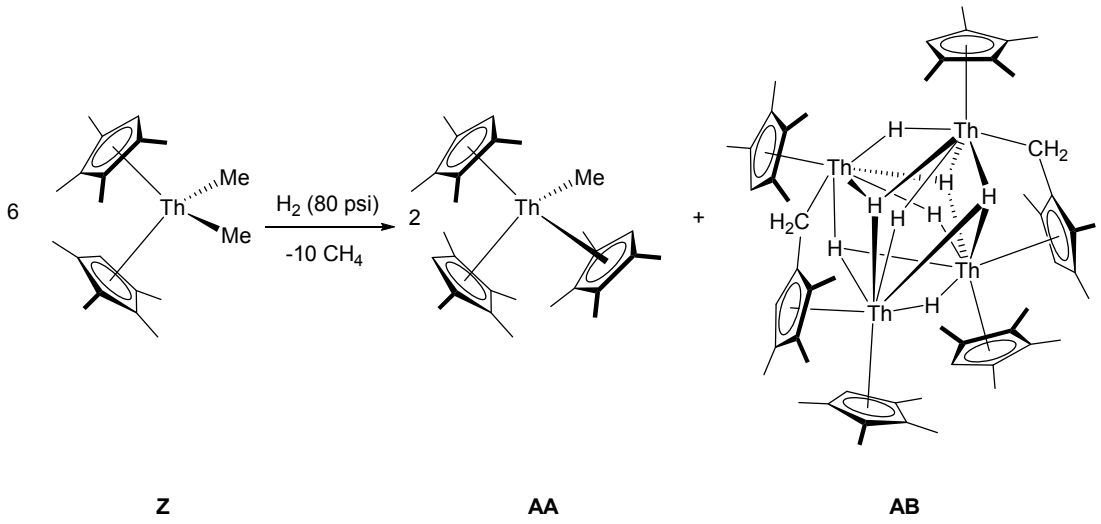

Scheme 1.5: The synthetic route to form a polymetallic polyhydridic cage, **AB**, as reported by Evans *et al*.[21]

In 2001 Parkin reported upon the reactions of $Th(Ind^{Me})_2(Cl)_2$, **AC**, to form $Th(Ind^{Me})_2(BH_4)_2$, **AD**, and $Th(Ind^{Me})_2(Me)_2$, **AE**,[33] displayed in **Scheme 1.6.**

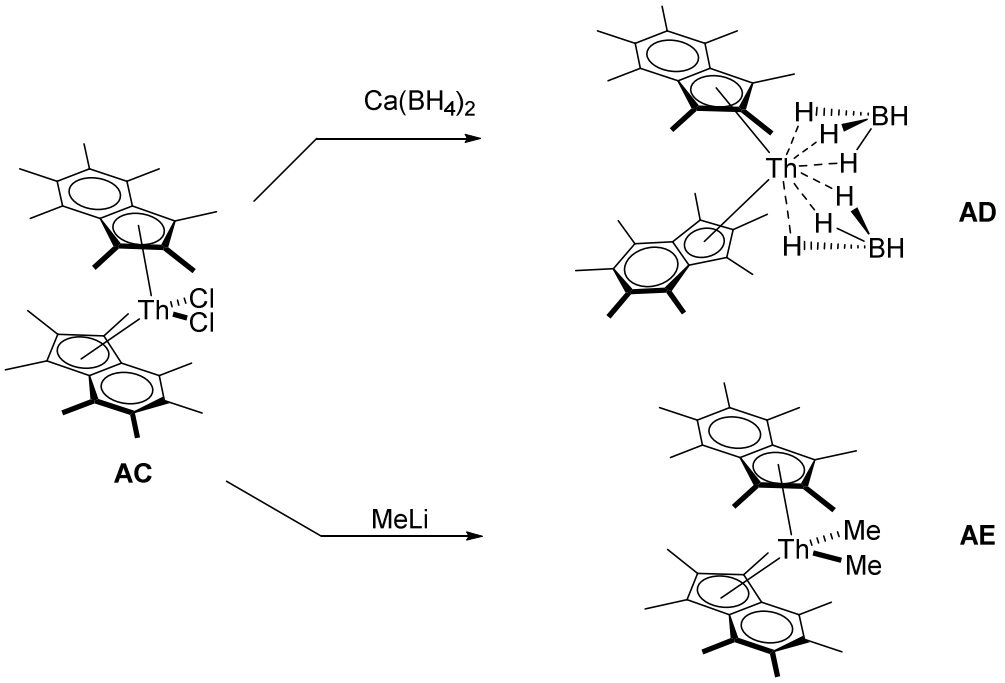

Scheme 1.6: Synthesis of $Th(Ind^{Me})_2(BH_4)_2$ and $Th(Ind^{Me})_2(Me)_2$ as reported by Parkin *et al*.[33]

The borohydrido ligand of **AD** was postulated to bind in a tridentate fashion, as determined by the thorium to boron distance of 2.62(7)Å, which is equivalent within

s.u.s to the bond distance reported in ThN"$_3$(κ^3-BH_4) (N"= N($SiMe_3$)$_2$), **AG,** synthesised by Andersen (**Figure 1.6**)[34] which had a separation of 2.61(3) Å.

The Andersen group were also amongst the earliest to report upon hydride complexes of thorium which primarily consisted of variations upon derivatives of tris N" complexes of thorium.[34-36] The two main complexes reported upon were ThHN"$_3$, **AF,** and **AG,** as shown in **Figure 1.6.**

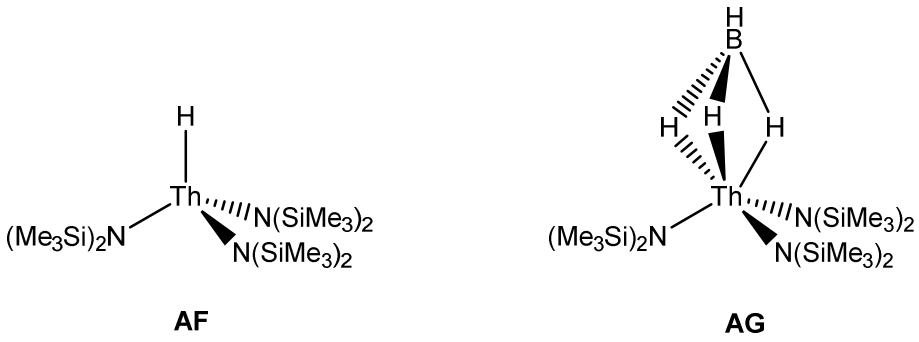

Figure 1.6: The structure of **AF,** ThHN"$_3$ and **AG**, ThN"$_3$(κ^3-BH_4) as reported by Andersen *et al.*[34]

Whilst **AF** and **AG** are interesting due to the formation of actinide hydride bonds, the relatively low lability of the N" ligands limits the chemistry available to these compounds compared to those incorporating the archetypal Cp* based ligand sets. Nonetheless it has been demonstrated that interesting chemistry with these compounds is possible. Andersen showed that it was possible with **AF** to replace the hydride with a chloride or a methyl group by reaction with carbon tetrachloride in the case of chloride substitution and butyl lithium followed by methyl bromide in the case methyl substitution. (**Scheme 1.5**) In the synthesis of **AF** the source of the hydride was postulated to be the solvent, THF.

1.4 Thorium alkyls

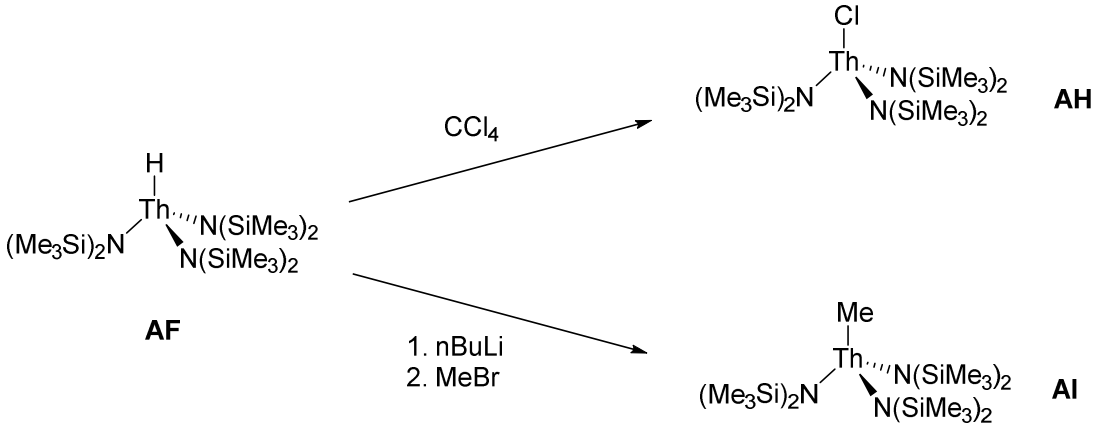

Scheme 1.7: Synthetic route to **AF**, ThClN"$_3$ and **AG**, ThMeN"$_3$ as reported by Andersen *et al*.[34]

The thorium alkyl compound, MeThN"$_3$, **AI,** depicted in **Scheme 1.7** is an example of a another fascinating group of compounds, as the examples that have been reported show high and unusual reactivity. Crucially, thorium alkyls could potentially be used to form Schrock type carbenes, which invoke lower symmetry Th-C bonding (*i.e.* π or δ symmetry). Furthermore, there is a high probability that such compounds would show catalytic activity. Further examples of thorium alkyl compounds are discussed below.

Andersen *et al*. were amongst the earliest research groups to report upon the complexation of benzyl groups to thorium in the compounds **AJ,** Th(Bz)$_2$(Cp)$_2$(DMPE) and **AK,** Th(Bz)$_4$(DMPE) depicted in **Figure 1.7**.[37, 38] **AJ** and **AK** are of particular interest as the benzyl moiety is known for its ability to exhibit η^3 or η^4 bonding modes towards actinide centres.[39]

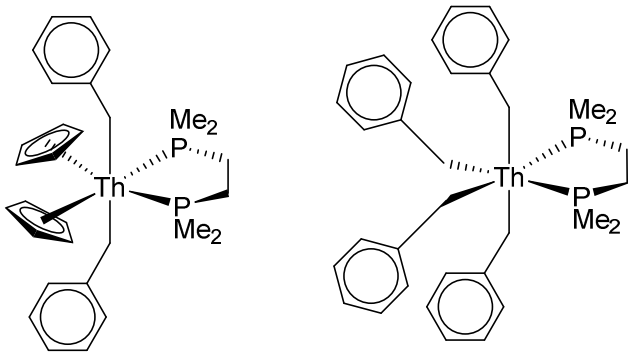

AJ **AK**

Figure 1.7: The structures of **AJ,** $Th(Bz)_2(Cp)_2(DMPE)$ and **AK,** $Th(Bz)_4(DMPE)$as reported by Andersen *et al*.[37, 38]

Examples of other thorium alkyls are quite varied, with Marks particularly prominent in having synthesised thorium benzyl compounds[39-41] and thorium aliphatic alkyl compounds.[40, 42-44] Some of these compounds show cyclometallate formation amongst other interesting reactions.

In 1996, Watkin *et al.* reported on further reactivity of **X**.[45] This reactivity solely concerned the neosilyl to thorium bond, as it was found to be highly reactive. Aside from the general interest of forming a bond between an atom that has a preference for covalency and one with a tendency to form ionic bonds, this is the main reason for the investigation of thorium to carbon bonds, as their high reactivity can lead to unusual reaction products as depicted in **Scheme 1.8**.[32, 45]

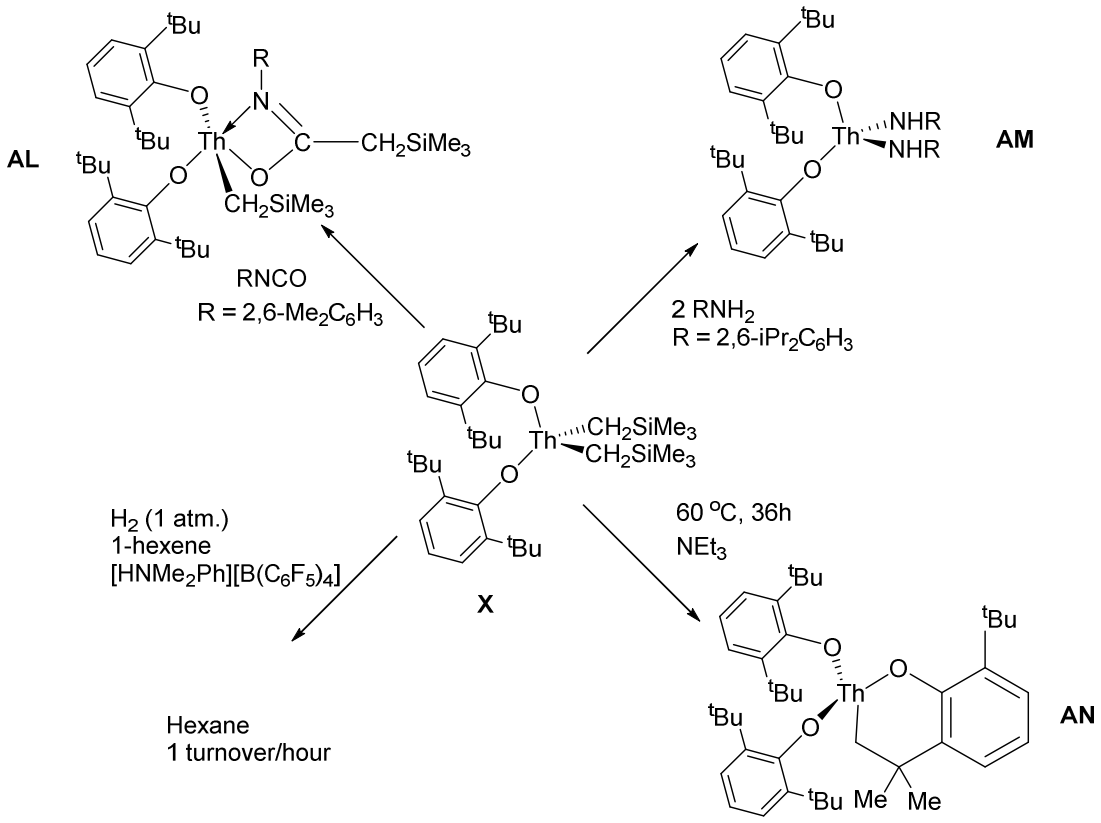

Scheme 1.8: The diverse reactivity of **X**, $Th(CH_2SiMe_3)_2(Od^tBup)_2$ including insertion, **AL**, ligand substitution, **AM**, ligand rearrangement, **AN** and catalysis as observed by Watkin *et al.*[32, 45]

The above scheme illustrates the wide and varied scope and reactivity of this complex, ranging from insertion reactions into the thorium carbon bond, through substitution of ligand, to catalysis and activation of the ligand. The aryloxide moiety has proven to be an excellent ancillary ligand for thorium compounds as varied and controllable reactivity has been observed.

Parkin[33] reported that **AE** undergoes two analogous insertion reactions, notably with CO_2 and CS_2 to form $Th(indenyl^{Me})_2(\kappa^2\text{-}OC(O)CH_3)_2$, **AO**, and $Th(indenyl^{Me})_2(Me)(\kappa^2\text{-}SC(S)CH_3)$, **AP**, shown in **Scheme 1.9.**

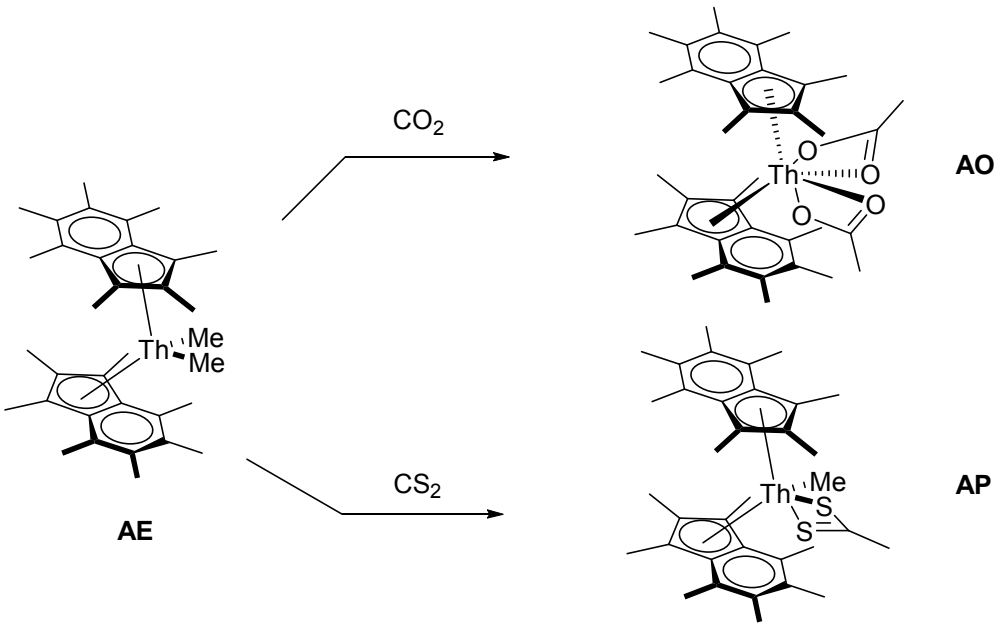

Scheme 1.9: The synthetic route to the synthesis of AO and AP as reported by Parkin *et al*.[33]

Parkin[33] also reported the formation of Th(indenyl^{Me})$_2$(κ^2CH$_2$SiMe$_2$N(SiMe$_3$)$_2$), **AQ**, as a product of reaction of **AC** with one equivalent of the potassium salt of hexamethyldisilylamide, Equation 1.8**.**

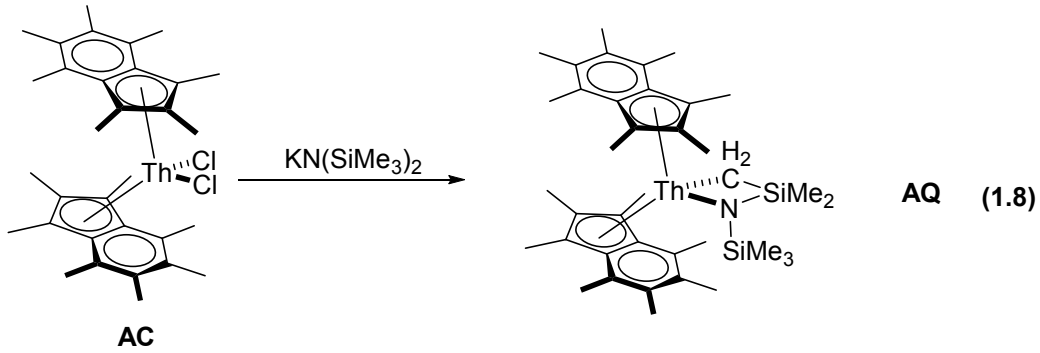

The synthesis of **AQ,** Th(indenyl^{Me})$_2$(κ^2CH$_2$SiMe$_2$N(SiMe$_3$)$_2$) as reported by Parkin *et al*.[33]

AQ contains the same moiety as an earlier reported example by Andersen[35], namely the deprotonated hexamethylsilylamide ligand. It includes a N-Th-C bond angle of 70.9°, which clearly demonstrates the strain on this system.

In 2004, Gambarotta reported an 'ate' complex with C-H aromatic activation,[46] from an attempted reduction using potassium metal and a homoleptic terphenolate complex, Th(OAr)$_4$, **AR** (Ar = 2,6 diphenylbenzene), shown in **Scheme 1.10.**

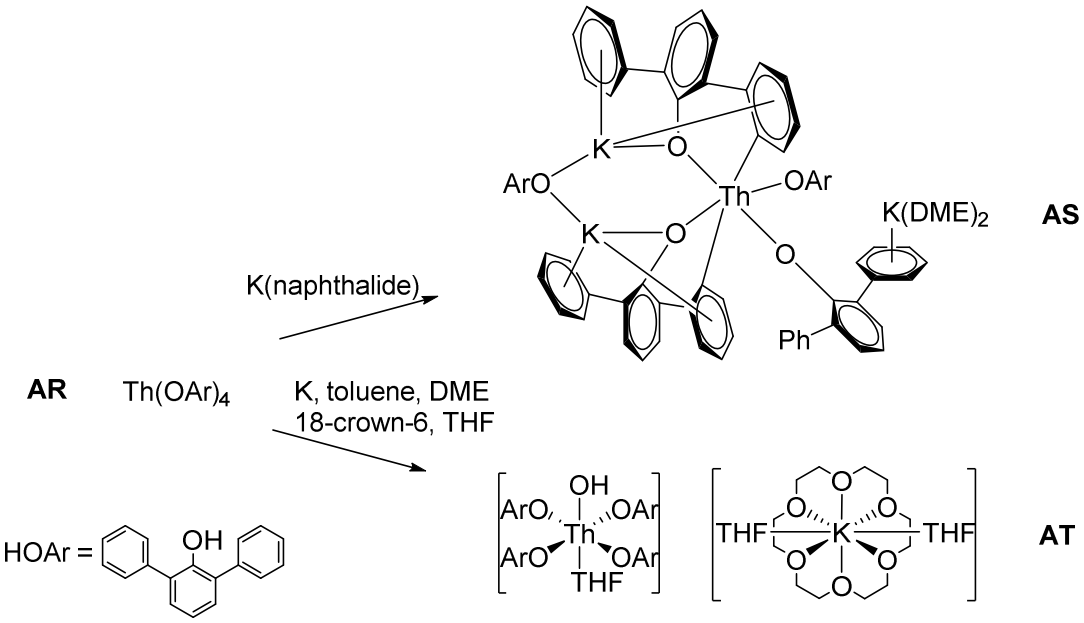

Scheme 1.10: Synthetic route to the reduction products synthesised from $Th(OAr)_4$, **AS** and **AT** as reported by Gambarotta *et al*.[46]

In the reaction producing $K_2Th(OAr)_4(DME)_2$, **AS**, two aromatic C-H bonds have been activated and an 'ate' complex has been formed. However, if the reaction is carried out in toluene and DME with a crown ether to sequester the potassium ions, it appears that C-O activation of a THF molecule occurs. This forms $[(THF)Th(OAr)_4OH][(THF)_2K(18\text{-crown-6})]$, **AT**. These complexes exhibit a striking reactivity, particularly as this reactivity can be tuned by adjusting the reaction conditions, and potentially provide an opportunity to selectively activate certain bonds depending on the solvent system.

In 1987, Rothwell reported on aryloxide supported complexes of thorium which had chelated to dimethyl pyridines via deprotonation of one of the α methyl groups as shown in **Figure 1.8**.[47] **AU**, $Th(ODtbp)_2(py^{Me})_2$ was synthesised by first displacing two chlorides from $ThCl_4$ with $Li(py^{Me})$. This synthetic step was followed by substituting the remaining two chlorido- ligands with the bulky ODtbp aryloxide ligands. The chelate effect of the methyl pyridine ligands combined with steric protection offered by the bulkier aryloxide ligands likely contribute to the stability of the complex.

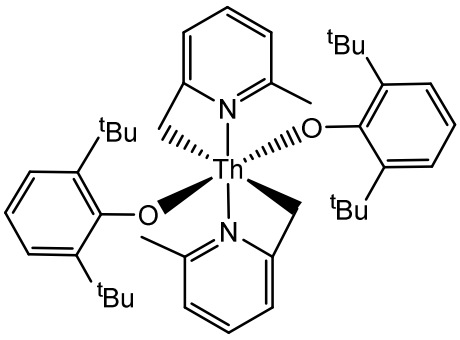

AU

Figure 1.8: The structure of **AU**, Th(ODtbp)$_2$(py^{Me})$_2$ as reported by Rothwell *et al*.[47]

1.5 Thorium complexes with multiply bonded ligands

1.5.1 Carbenes

Thorium compounds containing bonds to a carbon which have double bond character are academically interesting species as they are likely to display high and potentially unusual reactivity. Before starting a discussion of carbenes it is important to clarify whether Schrock or Fischer type carbenes are considered.

Thorium complexes are more likely to form Schrock carbenes, as alkylidenes are commonly known, than Fischer carbenes. These are formally defined (in terms of oxidation state), by the existence of two covalent bonds linking the carbon and the metal. Therefore, to stabilise a thorium containing alkylidene only two other anionic ligands need to be present on the metal centre.

In 2011, Fang *et al*. reported the synthesis and structure of Th{κ^3-C[P(Ph$_2$)S}$_2$DME, **AV,** which contained a thorium-carbon double bond[48] as depicted in **Figure 1.9** .

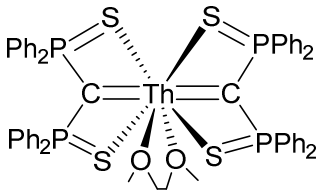

AV

Figure 1.9: The structure of **AV,** Th{κ^3-C[P(Ph$_2$)]S}$_2$DME as reported by Fang *et al*.[48]

X-ray crystallographic studies of **AV** revealed the Th-C$_{carbene}$ bond distances to be 2.485 (7) Å and 2.498 (7) Å, which fall within the range of a Th-C single bond,[49] suggesting that the Th-C$_{carbene}$ π-interaction contributes little to overall bonding, as would be

expected given the vast differences in the sizes of their valence atomic orbitals and energy levels of their frontier orbitals. In such a scenario, a Th-$C_{carbene}$ σ bond would form the majority of the bonding character. The weak π-bond may be better described as the electrons in the *p*-orbital of the sp^2 hybridised carbon being delocalised around the π-orbitals of the ligand and thorium. As such the Th-$C_{carbene}$ bond may be better described as a Th-C single bond, rather than a double bond, if one were to solely base bond order upon bond length. However bond energy is also an important factor in the multiplicity of a bond.

Computational studies carried out on **AV** to elucidate the distribution of the electron density of the Th-$C_{carbene}$ bond found the majority of the electron density to be polarised towards the nucleophilic carbon atom with the NBO calculation showing the Th-C bonds to be 11.0% Th and 89.0 % carbon in character. [48] This was expected from the Pauling electronegativities of the carbon and thorium atoms of 2.50 and 1.11, respectively.[50] The nucleophilicity of the carbene carbon was experimentally confirmed. The reaction with diphenyl ketone, as shown in Equation 1.9**,** which yielded an alkene after the added ketone has been subjected to nucleophillic attack, and subsequent elimination of an oxo-thorium species, reputed to be 'ThO_2', to form the alkene.

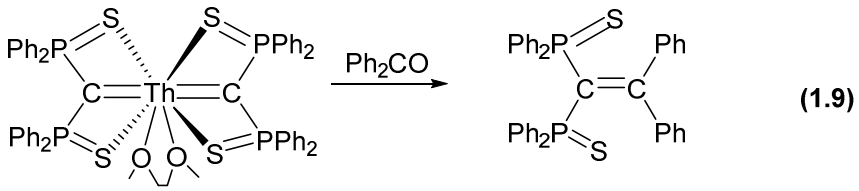

AV **AW** **(1.9)**

Evidence for the nucleophilicity of the carbene carbon as reported by Walter *et al*.[48]

In 2011, Cavell *et al*. reported three complexes of thorium containing a Th-$C_{carbene}$ bond based upon the same ligand framework, illustrated in **Scheme 1.11**.[51]

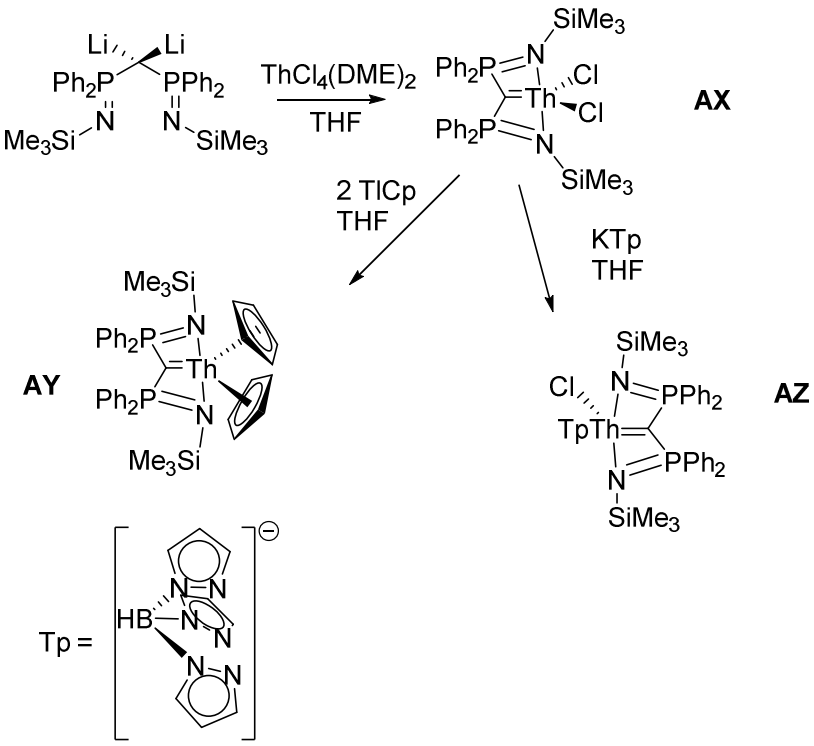

Scheme 1.11: Synthesis of three thorium carbene complexes **AX**, **AY** and **AZ** as reported by Cavell *et al*.[51]

Similarly to **AV**, the carbene complexes **AX** Th{κ³-C[P(Ph₂)N(SiMe₃)]}Cl₂, **AY,** Th{κ³-C[P(Ph₂)N(SiMe₃)]}Cp₂ and **AZ,** Th{κ³-C[P(Ph₂)N(SiMe₃)]}TpCl, synthesised by *Cavell et al.,* exist as a result of a phosphazene pincer ligand.[51] **AX**, **AY** and **AZ** indicate that the chelate effect is crucial in stabilising the Th-$C_{carbene}$ bond. DFT calculations carried out on **AY** and **AZ** found that the HOMO was the individual double bonding Th and $C_{carbene}$ components.[51] NBO calculations revealed that the Th-$C_{carbene}$ bonds contained approximately 7.0% Th to 93.0% carbon character. X-ray crystallographic studies revealed that the Th-$C_{carbene}$ bond distances in these compounds was 2.436(4) Å for the Cp derivative and 2.469(3) Å for the Tp derivative, which are both smaller than the distances reported for **AV**. These bond lengths are shorter than those previously reported for thorium hydrocarbyl complexes of 2.61-2.89 Å[52, 53], strongly suggesting an interaction beyond the single bond. However, the NBO calculation suggest that this is not due to any double bond character, as the π interaction appears to be fairly weak, in this case even weaker than **AV**. It was therefore proposed that the Th-$C_{carbene}$ bond is actually closer to a ylid than an alkylidene in nature, with a single bond between the atoms and an electrostatic interaction between the thorium(IV) and the carbon as

depicted in **Figure 1.10.** This does not consider the very likely delocalisation of the carbon-π electrons around the N-P-C-P-N backbone. If these calculations were irrefutable this would result in a formal change in oxidation state to thorium(III), which would be controversial, especially given that there is no reported EPR data and the diamagnetism of the complex by ^{1}H NMR spectroscopy, which would support the formation of a Th (III) complex. This leads to the conclusion that this supposition is based upon the accuracy of DFT calculations.

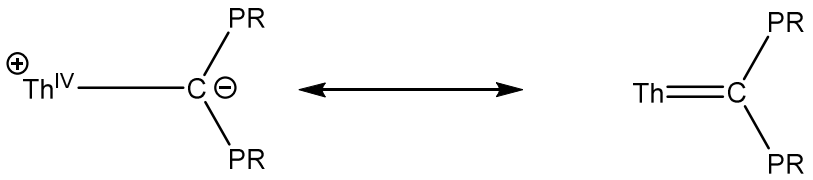

Figure 1.10: A proposed model for the thorium-carbon double bond as a ylid

However, DFT calculations do not definitively prove the makeup of the Th-$C_{carbene}$ bond and the examples, **AV, AX-AZ,** indicate that sterics also play a key role in stabilising thorium-carbene bonds.

Recently, Arnold *et al,* reported upon the formation of some aryloxide-tethered N-heterocyclic carbene complexes of f-elements, amongst them the thorium complex, **BA, Figure 1.11**.[54] Comparison of the Th-$C_{carbene}$ bond distances of the alkylidene type complexes of Cavell and Walter *et al.*, **AV**, **AX-AZ,** with **BA**, finds that **BA** contains bonds that are considerably longer as they lie in the range 2.852(6) to 2.884(5) Å. The Th-C bond distances in **BA** are amongst the longest reported in the literature,[49] underlining the weakness of a thorium Fischer carbene interaction, due to the mismatch in bonding from the 'hard' Lewis acid by the relatively soft Fischer carbene.[54-57] There is also likely to be a significant steric strain within the structure of **BA**, which is also key in explaining the lengthening of the Th-$C_{carbene}$ bond when compared to **AV**, **AX-AZ**. The chemistry of Th-$C_{carbene}$ bonds, has not been researched thoroughly due to the recent nature of the discovery and synthesis of this class of complex. However, complexes containing hetero-atom to thorium double bonds have been investigated and are detailed below.

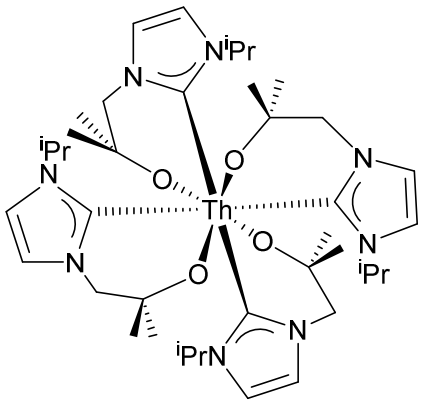

BA

Figure 1.11: The structure of **BA,** an aryloxide tethered homoleptic thorium N-heterocyclic carbene complex, as reported by Arnold *et al*.[54]

1.5.2 Thorium-imido bonds

Almost two decades ago, Eisen *et al.* reported the first crystallographically characterised example of a thorium imido complex.[58] Various thorium imido complexes have been reported, but crystallographic characterisation has not proved facile, mostly due to the reactivity of a thorium imido moiety in solution.[59-61] During Eisen *et al.*'s investigations into hydroamination of terminal alkynes by $ThCp^*_2Me_2$ they managed to isolate an intermediate in the catalytic pathway: $Cp^*_2Th{=}N(2,6\ Me_2Ph)THF$, **BB,** shown in **Figure 1.12.** The Th=N-C bond was found to be near linear (Th-N-C bond angle = 171.5°) and to have a bond length of 2.045(8) Å, which is substantially shorter than that observed for Th=C in the carbene complexes **AV** and **AX-AZ**. This observation is not surprising considering the lack of a chelate effect and the change of the identity from C to N in the Th-X multiple bond.

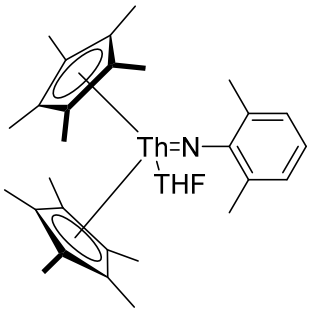

BB

Figure 1.12: The structure of **BB**, $Cp^*_2Th{=}N(2,6\ Me_2Ph)THF$ as reported by Eisen *et al*.[58]

After a fifteen year hiatus, the synthesis and characterisation of this class of compound was resumed, when in 2011, Walter *et al.*[62] reported the synthesis and complete characterisation of two thorium imido complexes, stabilised using modified bis Cp ligands. The structures of $[\eta^5\text{-}1,2,4\text{-}(Me_3C)_3C_5H_2]_2Th{=}NSiMe_3$, **BC**, and $[\eta^5\text{-}1,2,4\text{-}(Me_3C)_3C_5H_2]_2Th{=}NCPh_3$, **BD**, are shown in **Figure 1.13**. The Th-N-C/Si angles in **BC** and **BD**, in similarity to those seen in **AZ,** are nearly linear at 175.8(2)° and 168.3(2)°, respectively. The Th=N bond lengths of 2.035(3) Å, and 2.034(2) Å, for **BC** and **BD**, respectively, are identical within s.u.s to that observed in **BB.**

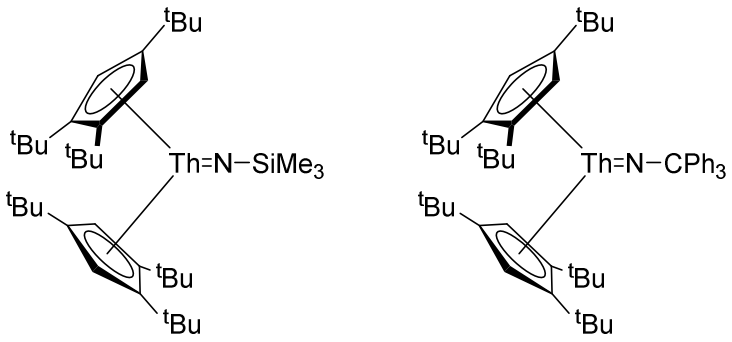

BC **BD**

Figure 1.13: The structures of **BC**, $[\eta^5\text{-}1,2,4\text{-}(Me_3C)_3C_5H_2]_2Th{=}NSiMe_3$, and, **BD**, $[\eta^5\text{-}1,2,4\text{-}(Me_3C)_3C_5H_2]_2Th{=}NCPh_3$ as reported by Walter *et al.*[62]

A common precursor to the synthesis of **BC** and **BD**, $[\eta^5\text{-}1,2,4\text{-}(Me_3C)_3C_5H_2]_2ThCl_2$, **BE**, was found to also be amenable towards the formation of a thorium analogue of Rosenthal's reagent, $Cp_2Zr(THF)(Me_3SiC{\equiv}CSiMe_3)$.[63, 64] Reduction with potassium

graphite, in the presence of diphenyl acetylene led to the formation of [η^5-1,2,4-$(Me_3C)_3C_5H_2]_2Th(\eta^2$-$C_2Ph_2)$, **BF**, as shown in Equation 1.10. **BF** represents a masked thorium (II) reagent as the ease of loss of the C_2Ph_2 moiety or insertion into the Th-C bonds leads to a reactive complex.[63] The formation of a Th-metallocyclopropane was unprecendented to the best of the author's knowledge.[63]

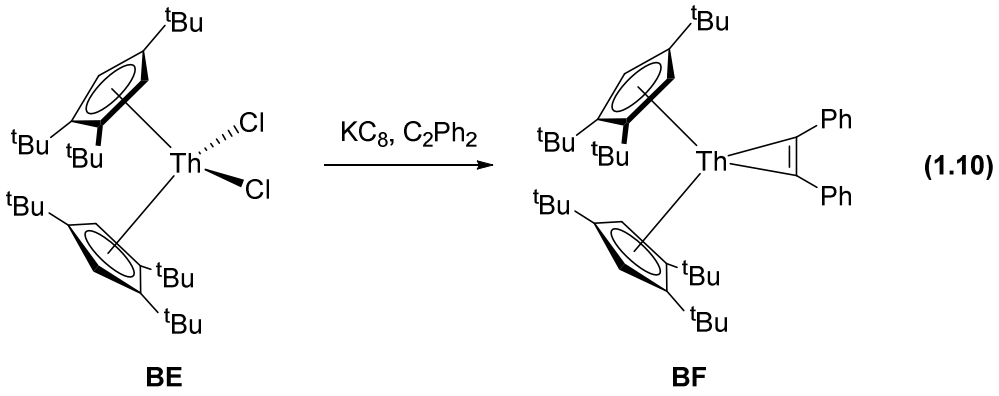

(1.10)

Formation of a thorium analogue of Rosenthal's reagent.[63]

Walter *et al*.[63] showed that **BF** was capable of a variety of insertion reactions, some examples of which are shown in **Scheme 1.12**, which illustrate the synthetic flexibility observed for this complex. Compounds **BG**-**BM** demonstrate the wide range of insertion reactions that are possible using **BF**. Complexes **BJ-BM** show fairly simple insertion products, in which unsaturated carbon-heteroatom substrates inserted into one of the Th-C bonds of the reduced acetylene moiety. The compounds **BG**-**BI** show perhaps the most interesting reactivities. The formation of **BI**, [η^5-1,2,4-$(Me_3C)_3C_5H_2]_2Th\kappa^2$-$[OC(Ph)_2C(Ph)_2O]$, proceeds with the concomitant loss of the C_2Ph_2 acetylene. The loss of this moiety is accompanied by a one-electron reduction of each of the ketones, causing a new C-C bond to form. Complex **BH,** [η^5-1,2,4-$(Me_3C)_3C_5H_2]_2Th\kappa^2$-$[N(SiMe_3)C(Ph)C(Ph)]$ was synthesised using an azide reagent following loss of N2. Isolation of a four-membered thorium-metallocycle, **BG,** [η^5-1,2,4-$(Me_3C)_3C_5H_2]_2Th\kappa^2$-$[CH_2SiMe_2N(CPhCHPh)]$ as a result of *via* a hydrogen migration step following the formation of **BH** was also reported.

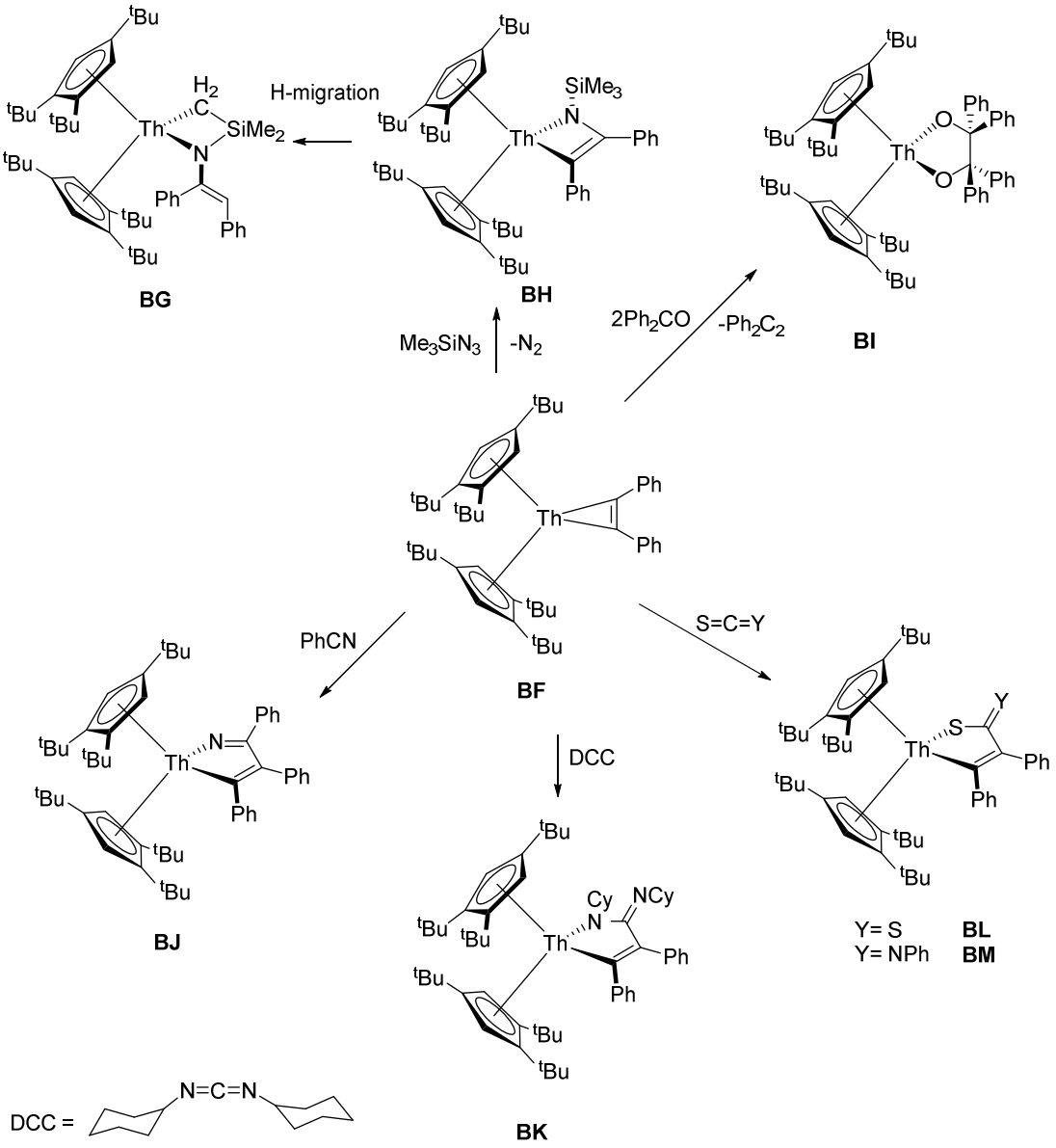

Scheme 1.12: Examples of the diverse insertion chemistry seen for **BF**, [η^5-1,2,4-$(Me_3C)_3C_5H_2]_2Th(\eta^2$-$C_2Ph_2)$as reported by Walter *et al*.[63]

More recently, Arnold *et al.*[65] reported the synthesis of two thorium imido complexes based upon silyl amide ligands, [(N{$SiMe_3$}$_3$)Th=N(1,5-$(CHMe_2)_2(C_6H_3)$][K(18-crown-6)], **BN,** and [(N{$SiMe_3$}$_2$)Th=N(1,5-$(CHMe_2)_2(C_6H_3)_2$][$K_2(THF)_2$], **BO**, shown in **Figure 1.14**. An interesting aspect of **BO** is that it is the first bis(imido) complex of thorium and adopts a *cis* geometry in the solid state, which was confirmed computationally to be the energetically favourable conformation. Compared to bis(imido) complexes of uranium in the literature, the preference for a *cis* geometry is a clear contrast to the *trans* geometry observed for the majority (95%) of literature examples.[65] This is

proposed to be a result of Th complexes being more d-block (which favour *cis* geometries) in character, which can be attributed to its ground state of [Rn]$7s^2$ $6d^2$, than uranium complexes.[65]

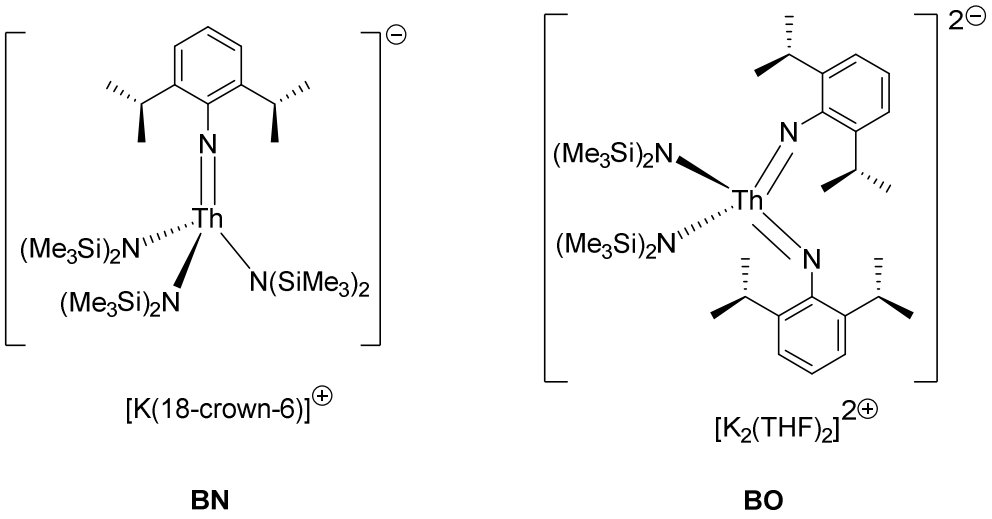

BN **BO**

Figure 1.14: Structures of the thorium-imido complexes, **BN** and **BO** based upon silyl amide ligands, as reported by Arnold *et al*.[65]

1.5.3 Terminal thorium-chalcogen bonds

In 2011, Walter *et al.* reported on the conversion of an analogue of their previously reported imido complexes into terminal oxo- and sulphido complexes.[62] The structures of, and synthetic routes to, η^5-1,2,4-$(Me_3C)_3C_5H_2]_2Th{=}O$, **BQ**, and η^5-1,2,4-$(Me_3C)_3C_5H_2]_2Th{=}S$, **BR**, are depicted in **Scheme 1.13**.

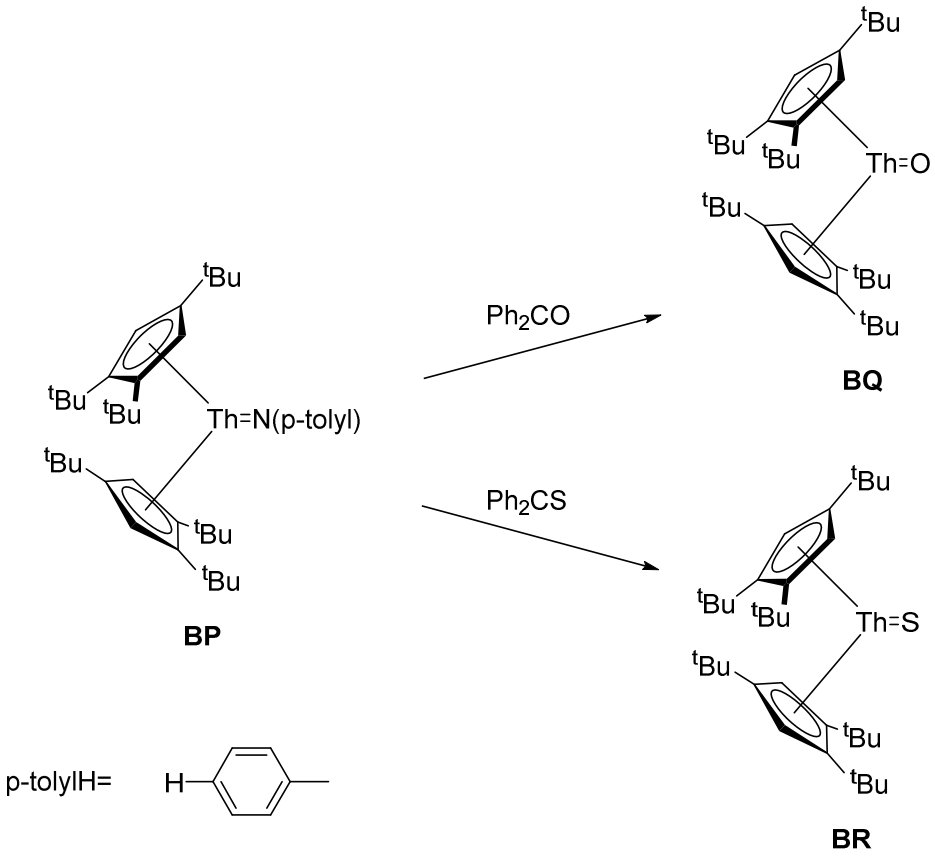

Scheme 1.13: Synthetic route to the formation of **BQ**, η^5-1,2,4-$(Me_3C)_3C_5H_2]_2Th{=}O$ and **BR**, η^5-1,2,4-$(Me_3C)_3C_5H_2]_2Th{=}S$ as reported by Walter *et al.*[62]

The Th=O bond length in **BQ** of 1.929(4) Å, was, at time of publication, found to be the shortest Th-O bond interaction in the literature by a significant distance[62] and was only recently surpassed by **BT** (below).[66] This substantial shortening of the Th-O bond length is good evidence for the substantial multiple bond character of this bond.

Recently, Eisen *et al*,[66] reported the formation of dimethylsilyl bis(aminidate)actinide complexes, with some particularly interesting results observed for the thorium complexes shown in **Scheme 1.14**. If work-up of the reaction was undertaken using dry THF the expected monomeric heteroleptic bis aminidate complex, **BS,** was formed. However, if wet THF was used during the work-up procedure an unusual dimeric complex with *trans*-oriented hydroxyl groups, **BT,** was isolated.

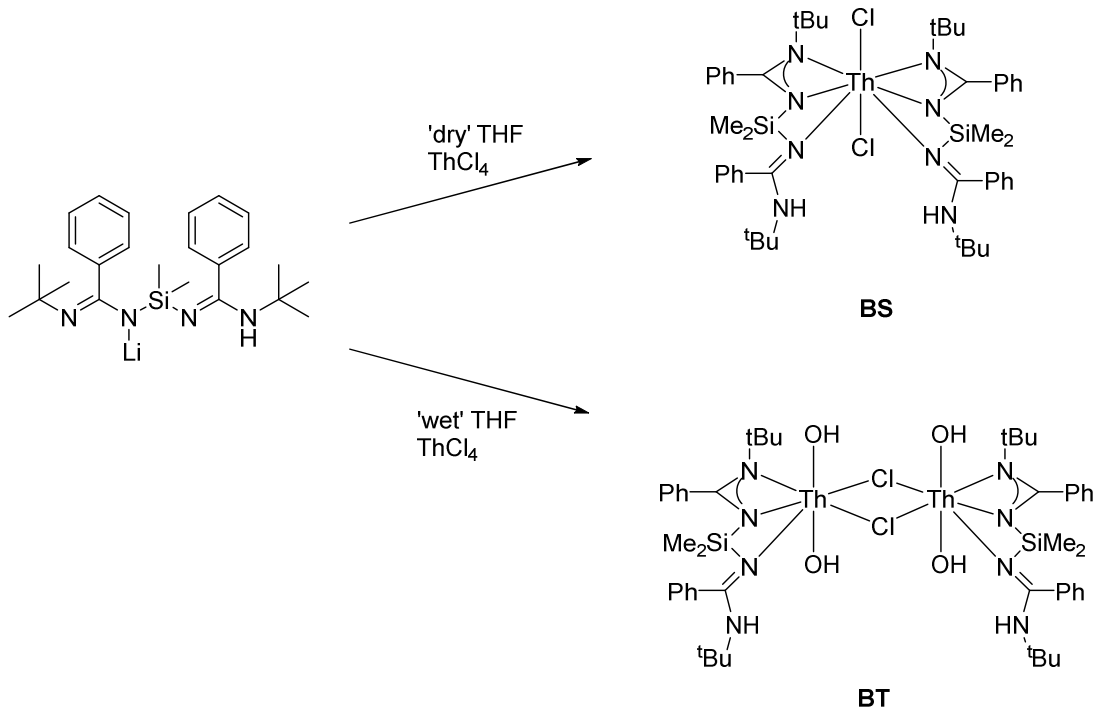

Scheme 1.14: Synthetic routes to the structures of **BS** and **BT** as reported by Eisen *et al*.[66]

The solid state structure of **BT** is of particular interest as the *trans*-oriented hydroxyl groups ligated to the thorium centre have a highly linear O-Th-O bond angle of 176.4(2)°. The combination of this linearity with the extraordinarily short Th-O bond lengths of 1.739(5) Å, which are 0.2 Å shorter than any other Th-O bond reported in the literature,[49] is highly reminiscent of a uranyl type motif, suggesting multiple bond character within the Th-O bond. Even when compared to the terminal Th=O bond in **BP**, these bonds are short, which is highly suggestive of multiple bond character within this system. The astonishing shortness of this bond is further highlighted when considering that with the exception of that in **BP**, no other Th-O bond length has been observed to break the 2.0 Å barrier.[49] The Th-O bond lengths in **BT** are similarly short as the U=O bond lengths of all crystallographically characterised examples of uranyl motifs range from 1.523 to 2.675 Å, with an average of 1.810 Å and the ,ajpority ranging from 1.7 to 2.0 Å .[49] It is interesting to note the difference between the Th-OH bond distances in **BT,** with the Th-OH motif (Th-O = 2.105(13) Å) observed in **AT**, described in *1.4* synthesised by Gambarotta *et al*.[46] This is further evidence supporting the multiple bond character present within the Th-O bonds of **BT**.

1.6 Terphenolate complexes

Previous research indicates that bulky phenolates stabilise thorium complexes as they undergo interesting chemical reactions,[32, 45, 46] making complexes with this class of ligands an attractive target for investigation. The bulky aryloxide ligands that will be used in this project: 2,6 diisopropyl diphenyl terphenol ($Ter^{Dipp}OH$), **BU**, 2,4,6 trisopropyl diphenyl terphenol ($Ter^{Trip}OH$), **BV**, and mesityl terphenol ($Ter^{Mes}OH$), **BW**, are shown in **Figure 1.15** and were first synthesised by Power and Dickie, respectively.[67, 68] They have a history of being able to stabilise compounds displaying unusual chemistry or bonding.[68-76]

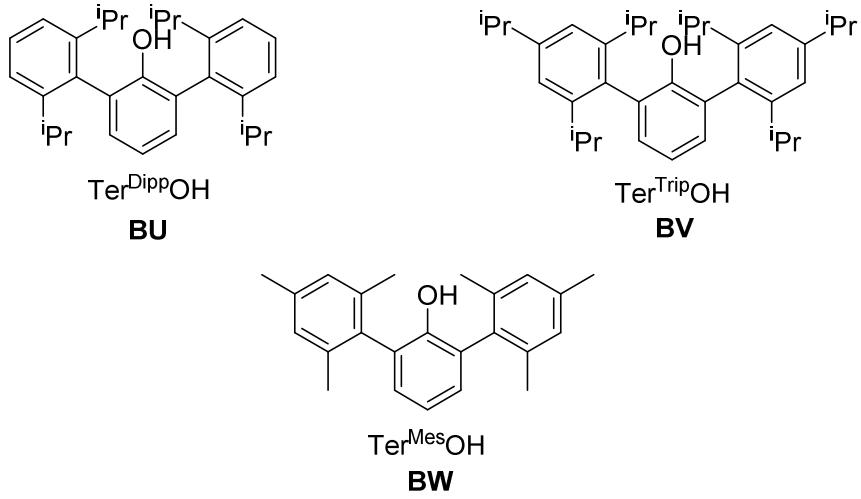

Figure 1.15: Structure of ligands

In the past these ligands have been used to stabilise a zinc zinc singly bonded organometallic complex[70], tin (II) complexes[68, 69], molybdenum[71-73] and tungsten[74] alkylidene complexes and tungsten metallacyclic[75, 76] complexes (**Figure 1.16**), demonstrating that this ligand type has scope to stabilise what would be likely to be otherwise unstable compounds.

Terphenolates should be able to sterically protect a thorium centre and hence aid the formation of interesting species such as low coordinate thorium complexes or thorium alkyls, hydrides and carbenes. Their bulk would sterically hinder and thus prevent nucleophilic attacks that could potentially lead to the decomposition of highly reactive species.

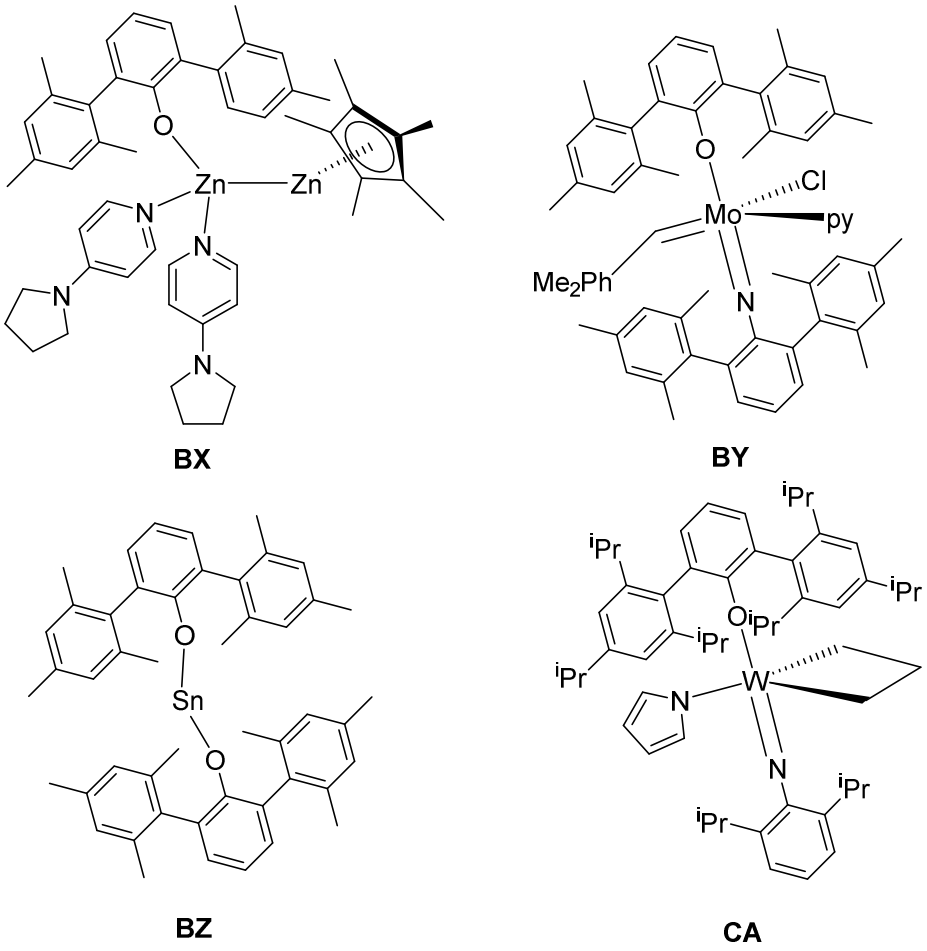

Figure 1.16: Examples of complexes that have been stabilised using terphenolate ligands[69, 70, 72, 75]

An additional property of terphenolate ligands is the presence of a strong σ-donor, in the form of the aryloxide oxygen. This is postulated to provide sufficient electrostatic and ionic bonding interactions (the bond dissociation energy of a Th-O bond being reported to be 854(13) kJ/mol[77]) to result in the formation of actinide aryloxide complexes, that are stable enough to undergo transformation reactions. Due to its high symmetry, the terphenolate motif also produces a fairly distinctive NMR spectra, increasing the ease of characterisation of the formed complexes.

1.7 Aims of project

The excellence of bulky aryloxides, such as ODtbp, as ancillary ligands inspires the thought that research into even bulkier aryloxide derivatives may result in the

discovery of even more diverse and interesting reactivity, which may also lead to an increase in selectivity.

The primary aims of this project are twofold. The initial target is the synthesis of heteroleptic thorium(IV) compounds of terphenolate ligands. These heteroleptic compounds will then be used to act as precursors in the attempted syntheses of thorium hydrides, alkyls and carbenes, as well as attempts to reduce the heteroleptic compounds and form thorium (III) complexes that will be able to activate small molecules.

The secondary aim is to synthesise thorium alkyl compounds, which themselves could act as precursors towards synthesising both thorium hydride compounds and thorium carbene compounds, depending upon which thorium alkyl complexes successfully form and which type of elimination is favoured.

The final aspects of the project is to investigate catalytic activity of generated thorium complexes and to attempt small molecule activations with the thorium(IV) compounds that this project may generate.

1.8 References

1. N. Kaltsoyannis and P. Scott, *The f elements*, Oxford Science Oxford, 1999.
2. J. Kang and F. N. von Hippel, *Science & Global Security*, 2001, 9, 1-32.
3. S. David, E. Huffer and H. Nifenecker, *Europhysics News*, 2007, 38, 24-27.
4. D. LeBlanc, *Nucl. Eng. Des.*, 2010, 240, 1644-1656.
5. F. T. Edelmann, *Coord. Chem. Rev.*
6. H. S. La Pierre, A. Scheurer, F. W. Heinemann, W. Hieringer and K. Meyer, *Angew. Chem., Int. Ed. Engl.*, 2014, 53, 7158-7162.
7. M. R. MacDonald, M. E. Fieser, J. E. Bates, J. W. Ziller, F. Furche and W. J. Evans, *J. Am. Chem. Soc.*, 2013, 135, 13310-13313.
8. S. G. Bratsch and J. J. Lagowski, *J. Phys. Chem.*, 1986, 90, 307-312.
9. S. G. Bratsch, *J. Phys. Chem. Ref. Data*, 1989, 18, 1-21.
10. L. Pauling, *The Nature of the Chemical bond*, Cornell University Press, 3rd Edition edn., 1960.
11. B. Kanellakopulos, E. Dornberger and F. Baumgaertner, *Inorg. Nucl. Chem. Lett.*, 1974, 10, 155-160.
12. J. W. Bruno, D. G. Kalina, E. A. Mintz and T. J. Marks, *J. Am. Chem. Soc.*, 1982, 104, 1860-1869.
13. P. C. Blake, M. F. Lappert, J. L. Atwood and H. Zhang, *J. Chem. Soc., Chem. Commun.*, 1986, 1148-1149.
14. J. S. Parry, F. G. N. Cloke, S. J. Coles and M. B. Hursthouse, *J. Am. Chem. Soc.*, 1999, 121, 6867-6871.
15. P. C. Blake, N. M. Edelstein, P. B. Hitchcock, W. K. Kot, M. F. Lappert, G. V. Shalimoff and S. Tian, *J. Organomet. Chem.*, 2001, 636, 124-129.
16. T. J. M. W.T. Carnall, R.D. Fischer,, *Organometallics of the f-Elements*, Reidel, Dordrecht,, 1979.

17. S. G. Bratsch and J. J. Lagowski, *J. Phys. Chem.*, 1986, 90, 307-312.
18. N. Kaltsoyannis and B. E. Bursten, *J. Organomet. Chem.*, 1997, 528, 19-33.
19. R. R. Langeslay, M. E. Fieser, J. W. Ziller, F. Furche and W. J. Evans, *Chem. Sci.*, 2015, 6, 517-521.
20. J. R. Walensky, R. L. Martin, J. W. Ziller and W. J. Evans, *Inorg. Chem.*, 2010, 49, 10007-10012.
21. N. A. Siladke, C. L. Webster, J. R. Walensky, M. K. Takase, J. W. Ziller, D. J. Grant, L. Gagliardi and W. J. Evans, *Organometallics*, 2013, 32, 6522-6531.
22. A. Arunachalampillai, P. Crewdson, I. Korobkov and S. Gambarotta, *Organometallics*, 2006, 25, 3856-3866.
23. I. Korobkov, B. Vidjayacoumar, S. I. Gorelsky, P. Billone and S. Gambarotta, *Organometallics*, 2010, 29, 692-702.
24. P. J. Fagan, J. M. Manriquez, E. A. Maatta, A. M. Seyam and T. J. Marks, *J. Am. Chem. Soc.*, 1981, 103, 6650-6667.
25. R. W. Broach, A. J. Schultz, J. M. Williams, G. M. Brown, J. M. Manriquez, P. J. Fagan and T. J. Marks, *Science* 1979, 203, 172-174.
26. W. J. Evans, K. A. Miller, S. A. Kozimor, J. W. Ziller, A. G. DiPasquale and A. L. Rheingold, *Organometallics*, 2007, 26, 3568-3576.
27. P. J. Fagan, K. G. Moloy and T. J. Marks, *J. Am. Chem. Soc.*, 1981, 103, 6959-6962.
28. A. F. Wells, *Structural Inorganic Chemistry*, University, Oxford, 1984.
29. E. F. N. P. Freestone, H. Geckeis, L. Gmelin, J. H. Holloway, R. J. Meyer, E. H. E. Pietsch, , *Gmelin handbook of inorganic and organometallic chemistry* Verl. Chemie [u.a.], Berlin [u.a.], 1993.
30. C. M. Fendrick, L. D. Schertz, V. W. Day and T. J. Marks, *Organometallics*, 1988, 7, 1828-1838.
31. L. Pauling and B. Kamb, *Proc. Natl. Acad. Sci. U. S. A.*, 1986, 83, 3569-3571.
32. D. L. Clark, S. K. Grumbine, B. L. Scott and J. G. Watkin, *J. Am. Chem. Soc.*, 1995, 117, 9089-9090.
33. T. M. Trnka, J. B. Bonanno, B. M. Bridgewater and G. Parkin, *Organometallics*, 2001, 20, 3255-3264.
34. H. W. Turner, R. A. Andersen, A. Zalkin and D. H. Templeton, *Inorg. Chem.*, 1979, 18, 1221-1224.
35. S. J. Simpson, H. W. Turner and R. A. Andersen, *Inorg. Chem.*, 1981, 20, 2991-2995.
36. R. A. Andersen, A. Zalkin and D. H. Templeton, *Inorg. Chem.*, 1981, 20, 622-623.
37. A. Zalkin, J. G. Brennan and R. A. Andersen, *Acta Crystallogr., Sect. C: Cryst. Struct. Commun.*, 1987, C43, 421-423.
38. P. G. Edwards, R. A. Andersen and A. Zalkin, *Organometallics*, 1984, 3, 293-298.
39. E. A. Mintz, K. G. Moloy, T. J. Marks and V. W. Day, *J. Am. Chem. Soc.*, 1982, 104, 4692-4695.
40. C. M. Fendrick, E. A. Mintz, L. D. Schertz and T. J. Marks, *Organometallics*, 1984, 3, 819-821.
41. W. Ren, N. Zhao, L. Chen and G. Zi, *Inorg. Chem. Commun.*, 2013, 30, 26-28.
42. H. Lauke, P. J. Swepston and T. J. Marks, *J. Am. Chem. Soc.*, 1984, 106, 6841-6843.
43. J. W. Bruno, G. M. Smith, T. J. Marks, C. K. Fair, A. J. Schultz and J. M. Williams, *J. Am. Chem. Soc.*, 1986, 108, 40-56.
44. X. Yang, W. A. King, M. Sabat and T. J. Marks, *Organometallics*, 1993, 12, 4254-4258.
45. D. L. Clark, S. K. Grumbine, B. L. Scott and J. G. Watkin, *Organometallics*, 1996, 15, 949-957.
46. I. Korobkov, A. Arunachalampillai and S. Gambarotta, *Organometallics*, 2004, 23, 6248-6252.

47. S. M. Beshouri, P. E. Fanwick, I. P. Rothwell and J. C. Huffman, *Organometallics*, 1987, 6, 2498-2502.
48. W. Ren, X. Deng, G. Zi and D.-C. Fang, *Dalton Trans.*, 2011, 40, 9662-9664.
49. F. Allen, *Acta Crystallogr., Sect. B: Struct. Sci*, 2002, 58, 380-388.
50. F. Albert Cotton and G. Wilkinson, *Advanced Inorganic Chemistry: a comprehensive text*, Interscience.
51. G. Ma, M. J. Ferguson, R. McDonald and R. G. Cavell, *Inorg. Chem.*, 2011, 50, 6500-6508.
52. J. A. Pool, B. L. Scott and J. L. Kiplinger, *J. Am. Chem. Soc.*, 2005, 127, 1338-1339.
53. C. N. Carlson, T. P. Hanusa and W. W. Brennessel, *J. Am. Chem. Soc.*, 2004, 126, 10550-10551.
54. P. L. Arnold, T. Cadenbach, I. H. Marr, A. A. Fyfe, N. L. Bell, R. Bellabarba, R. P. Tooze and J. B. Love, *Dalton Trans.*, 2014, 43, 14346-14358.
55. P. L. Arnold and S. T. Liddle, *Chem. Commun.*, 2006, 3959-3971.
56. S. T. Liddle, I. S. Edworthy and P. L. Arnold, *Chem. Soc. Rev.*, 2007, 36, 1732-1744.
57. P. L. Arnold and I. J. Casely, *Chem. Rev.*, 2009, 109, 3599-3611.
58. A. Haskel, T. Straub and M. S. Eisen, *Organometallics*, 1996, 15, 3773-3775.
59. E. J. Schelter, D. E. Morris, B. L. Scott and J. L. Kiplinger, *Chem. Commun.*, 2007, 1029-1031.
60. T. Straub, A. Haskel, T. G. Neyroud, M. Kapon, M. Botoshansky and M. S. Eisen, *Organometallics*, 2001, 20, 5017-5035.
61. I. Korobkov, S. Gambarotta and G. P. A. Yap, *Angew. Chem., Int. Ed. Engl.*, 2003, 42, 814-818.
62. W. Ren, G. Zi, D.-C. Fang and M. D. Walter, *Chem. Eur. J.*, 2011, 17, 12669-12682.
63. B. Fang, W. Ren, G. Hou, G. Zi, D.-C. Fang, L. Maron and M. D. Walter, *J. Am. Chem. Soc.*, 2014, 136, 17249-17261.
64. U. Rosenthal, A. Ohff, W. Baumann, A. Tillack, H. Görls, V. V. Burlakov and V. B. Shur, *Z. Anorg. Allg. Chem.*, 1995, 621, 77-83.
65. N. L. Bell, L. Maron and P. L. Arnold, *J. Am. Chem. Soc.*, 2015.
66. I. S. R. Karmel, T. Elkin, N. Fridman and M. S. Eisen, *Dalton Trans.*, 2014, 43, 11376-11387.
67. C. Stanciu, Marilyn M. Olmstead, Andrew D. Phillips, M. Stender and Philip P. Power, *Eur. J. Inorg. Chem.*, 2003, 2003, 3495-3500.
68. D. A. Dickie, I. S. MacIntosh, D. D. Ino, Q. He, O. A. Labeodan, M. C. Jennings, G. Schatte, C. J. Walsby and J. A. C. Clyburne, *Can. J. Chem.*, 2008, 86, 20-31.
69. C. Stanciu, A. F. Richards, M. Stender, M. M. Olmstead and P. P. Power, *Polyhedron*, 2006, 25, 477-483.
70. M. Carrasco, R. Peloso, A. Rodriguez, E. Alvarez, C. Maya and E. Carmona, *Chem. - Eur. J.*, 2010, 16, 9754-9757, S9754/9751-S9754/9769.
71. L. C. H. Gerber, R. R. Schrock, P. Müller and M. K. Takase, *J. Am. Chem. Soc.*, 2011, 133, 18142-18144.
72. R. R. Schrock, A. J. Jiang, S. C. Marinescu, J. H. Simpson and P. Müller, *Organometallics*, 2010, 29, 5241-5251.
73. E. M. Townsend, R. R. Schrock and A. H. Hoveyda, *J. Am. Chem. Soc.*, 2012, 134, 11334-11337.
74. D. V. Peryshkov, R. R. Schrock, M. K. Takase, P. Müller and A. H. Hoveyda, *J. Am. Chem. Soc.*, 2011, 133, 20754-20757.
75. M. M. Flook, A. J. Jiang, R. R. Schrock, P. Müller and A. H. Hoveyda, *J. Am. Chem. Soc.*, 2009, 131, 7962-7963.
76. S. C. Marinescu, R. R. Schrock, P. Müller, M. K. Takase and A. H. Hoveyda, *Organometallics*, 2011, 30, 1780-1782.

77. J. A. Dean and N. A. Lange, *Lange's handbook of chemistry*, McGraw-Hill, 1992.

Chapter 2: Actinide Catalysis

This chapter comments in part on results that are published in the 2015 Organometallics paper.[1]

2.1 Introduction

Actinide catalysis is an underutilised and underdeveloped area of catalysis, which has been shown to be parallel and complementary to transition metal based catalysis.[2] This is illuminated by alternate reactivities being observed[3-5] (see **Figure 2.1**), for a variety of different metals,[6-19] which can be elucidated in differing stereo or regiochemistries in many instances.[2] Despite the multiple products that are able to be accessed via transition metal catalysis, there remain some problems, particularly in terms of the expense associated with some transition metals, such as rhodium, iridium, platinum and palladium.[20] Additionally, late transition metal catalysts generally enjoy greater functional group tolerance, but they often require acidic conditions and protecting group strategies and may be further afflicted by low efficiency and short catalyst lifetimes.[21-24]

The aim of many small molecule activation studies is to generate a catalytic process which can produce fine or bulk chemicals. Prerequisites for small molecule activation are the ability, sterically and kinetically, and willingness, thermodynamically, of a substrate to bind to a metal centre. Once bound to a metal centre the resulting metal-substrate complex must then have a pathway available whereby a rearrangement occurs in order to activate the small molecule.

Using simple actinide complexes, research can be undertaken to see if small molecule activation can be done catalytically with a comparison to that seen by transition metals in an attempt to provide proof of concept. If the actinide-mediated catalysis is not particularly selective it is hoped that more elegant systems, with more tailored ancillary ligands, may be able to provide greater selectivity.

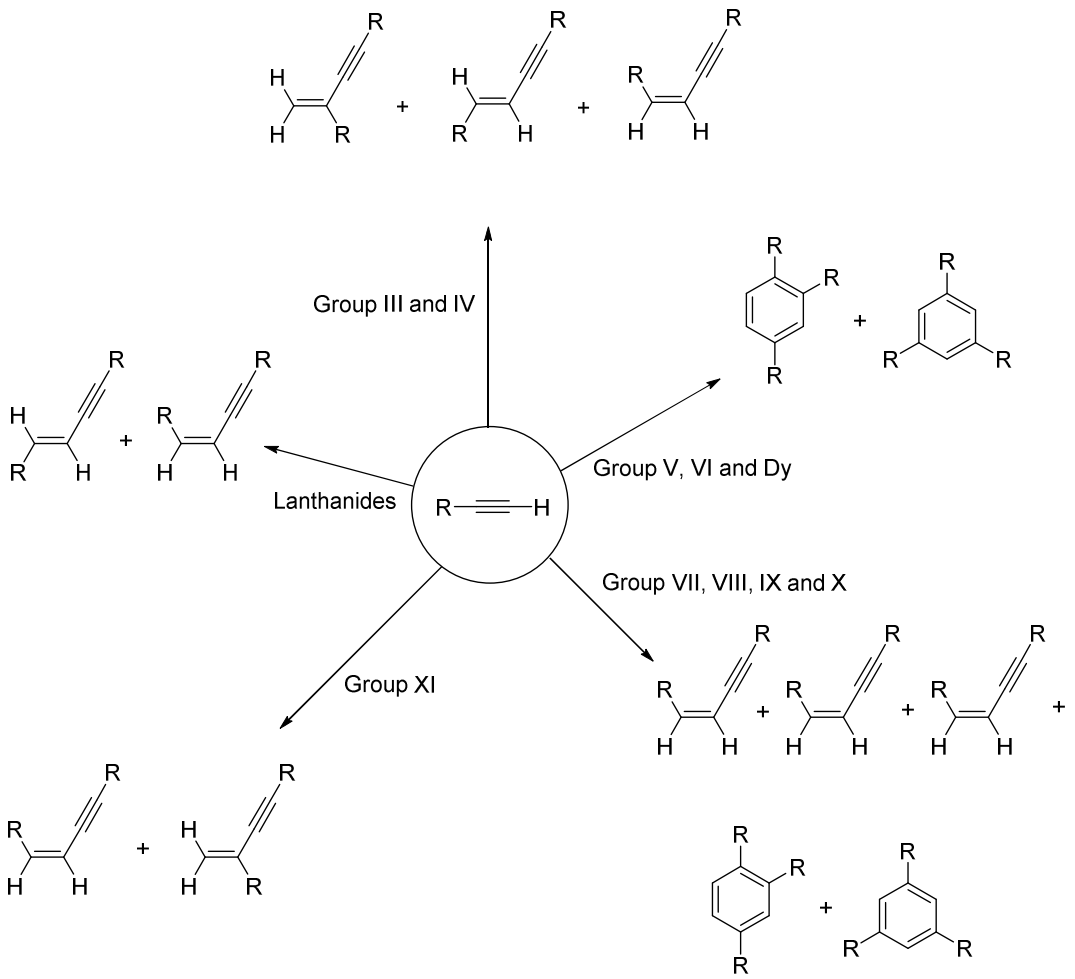

Figure 2.1: the divergent products possible from catalysis using terminal alkynes as substrates[6-19]

Figure 2.1 illustrates the different products that can be formed using transition metal or lanthanide complexes and terminal alkynes as substrates, by changing the identity of the metal to tune the product distribution.

There is literature precedent for activation of terminal alkynes to form more useful products, using the well-studied bis(permethyl cyclopentadienyl) (Cp^*_2) complexes of uranium and thorium (**Figure 2.2**) as catalysts.[25]

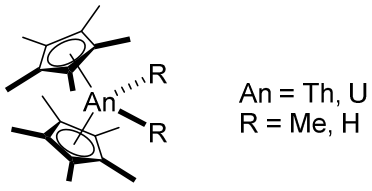

Figure 2.2: $Cp^*_2AnR_2$ complexes used in catalysis[25]

To date, all thorium based catalysed processes can be defined as Lewis acid catalysis and/or σ bond metathesis type catalysis, (see **Scheme 2.1**) where concomitant cleavage of two of the 'bonds' in a four–centred transition state results in the net formation of two new bonds. Thorium is the 'softest' tetravalent ion known, as based on Shannon ionic radii Th^{IV} is the largest tetravalent ion in the Periodic Table. (Th^{IV} has an ionic radius of 105 pm with a co-ordination number of 8, whilst U^{IV}, Pb^{IV} and Sn^{IV} have ionic radii of 100 pm, 94 pm and 81 pm respectively for a co-ordination number of 8).[26, 27]

A good substrate for testing the activity of Lewis acid catalysis must be high in electron density. Terminal acetylenes are high in electron density, given that they contain one σ and two π bonds. Terminal acetylenes may also undergo sigma bond metathesis with a suitable precatalyst (i.e. one that contains an internal base) to form a terminal acetylide. (**Scheme 2.1**). As terminal acetylenes are good substrates for both Lewis acid and sigma bond metathesis mediated catalysis, investigations into the homocoupling of terminal acetylenes were undertaken.

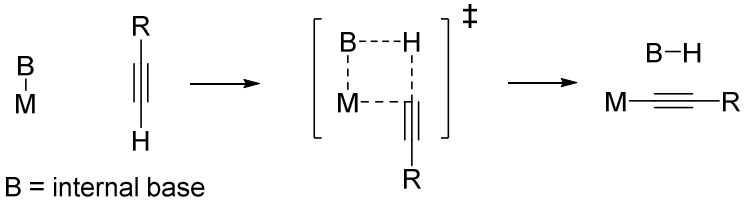

Scheme 2.1: Sigma bond metathesis of a terminal acetylene

2.1.1 Oligomerisation of terminal alkynes

Oligomerisation of terminal alkynes by metal catalysts is of considerable interest, as the products of these catalytic pathways, organic enynes and oligoacetylenes derivatives, are valuable precursors towards the synthesis of natural products and a variety of organic conducting polymers.[28] Actinide-mediated oligomerisation of terminal alkynes has been shown to proceed via insertion into an actinide-acetylide bond, which is regio-selective. From **Scheme 2.2**, it can be seen that the oligomerisation of alkynes by actinide catalysts is dependent upon the formation of a metal- acetylide bond so the actinide precatalyst must contain an internal base capable of deprotonating the terminal hydrogen of the substrate.

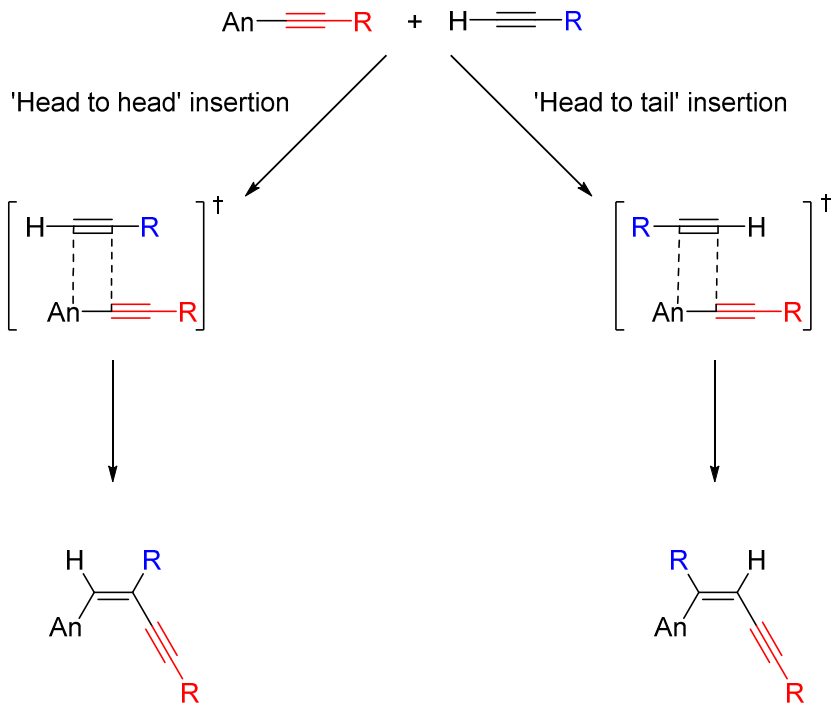

Scheme 2.2: Differing pathways for the insertion of a terminal acetylene into a metal acetylide bond through a *syn* four-centred transition state, resulting in the formation of two regio-isomers.

Alkyl actinide complexes of the form $Cp^*_2AnMe_2$ (An = Th, U) have been shown to catalyse the conversion of *tert*-butylacetylene (^{t}BuCCH) regio-selectively to yield the head-to-tail geminal dimer (Th 99%, U 95%) (**Scheme 2.3**). This contrasts with the use of trimethylsilyl acetylene ($SiMe_3CCH$) which yields the head-to-tail geminal dimer (Th 10%, U 5%) and the head-to-tail-to-head trimer (Th 90%, U 95%) as exclusive products (**Scheme 2.3**).[29] This shows that changes in the electronics of the acetylene substrate, from electron donating in the case of the ^{t}Bu substituent to electron withdrawing in the case of the $SiMe_3$ substituent, can have a drastic affect upon the outcome of the oligomerisation by actinide catalysts. However, other terminal acetylenes such as PhCCH and ^{i}PrCCH produced mixtures of products, with no specific regio- or chemo-selectivity.

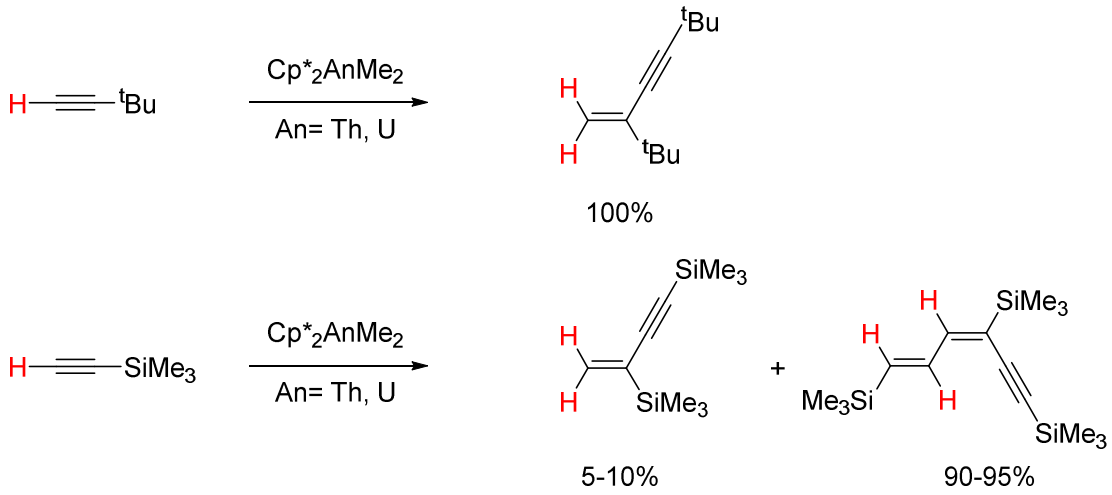

Scheme 2.3: Different products yielding from changing the electron withdrawing and donating properties of the acetylene substrate as described by Eisen *et al*.[29]

2.1.2 Hydroamination

The synthesis of nitrogen-containing products via catalysis has been extensively studied[30] and the production of fine nitrogen-containing chemicals is a well-known target. A possible route into producing nitrogen-containing fine chemicals is hydroamination of alkenes and alkynes, which has been shown to be a clean, atom-efficient process (see **Scheme 2.4**), as well as being an economically efficient and thermodynamically favourable process. However, it is entropically disfavoured, but has previously been declared as one of the 10 most important catalytic challenges.[31]

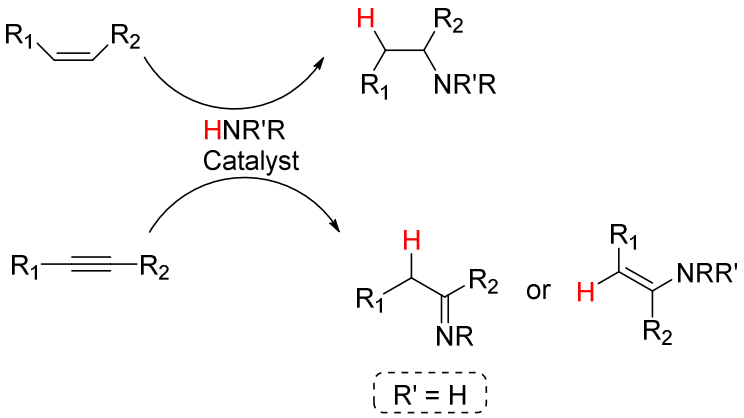

Scheme 2.4: Hydroamination of alkenes and alkynes

Organoactinide catalysts of the form $Cp^*_2AnMe_2$ (An = U, Th) have been shown to be excellent precatalysts for intermolecular hydroaminations of terminal alkynes (both aromatic and aliphatic) in the presence of primary aliphatic amines, to make immines.[25, 32] For the thorium based catalyst, $Cp^*_2ThMe_2$, it was shown that hydroamination of alkynes yielded methyl alkyl-substituted imines in moderate yields, whilst also forming *gem* dimers of the alkyne, whilst the uranium based catalyst, $Cp^*_2UMe_2$, exhibited highly selective regio- and stereo- chemistry towards forming imines with E-regiochemistry. Actinide mediated catalysts have also been shown to catalyse intramolecular hydroaminations.[33 34] This reaction forms heterocyclic rings, which are important targets, because they are structural motifs widely found within many pharmaceutical and biologically important products. Transition metal based catalysts, have so far been shown to have better regioselectivity and require lower catalyst loadings[30] than actinide based catalysis for hydroamination, but this may be a product of more intensive research into transition metal catalysis.

2.1.3 Hydrosilylation

The catalytic insertion of a Si-H bond into a C-C multiple bond is one of the central reactions of organo-silicon chemistry and catalytic hydrosilylation reactions produces components of a variety of commercial products, the most common of which are sealants, caulks, adhesives, and coatings made from silicones. The diverse and abundant chemistry of vinylsilanes, which are of particular interest as synthons in organic synthesis,[35] are important products that can be formed via a hydrosilylation route.[36-38] Hydrosilylation of terminal alkynes generally results in the formation of three different isomers; *cis*, *trans* and geminal (*gem*) (Equation 2.1).

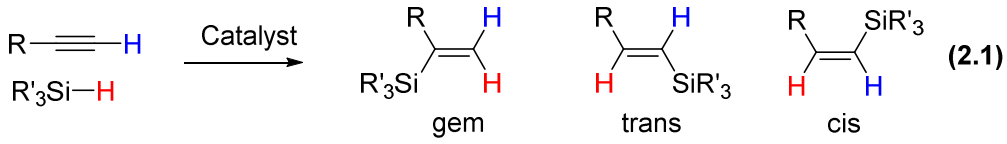

(2.1)

At room temperature the reaction of catalytic quantities of $Cp^*_2AnMe_2$ (An = U, Th) with an excess of terminal alkyne and $PhSiH_3$ affords substituted vinyl silanes, with the *trans* isomer generated exclusively from alkynes with bulky substituents (^{t}Bu, ^{i}Pr).[39] However tuning the electronics of the terminal alkyne, by use of $SiMe_3$ groups, results in divergent reactivity being observed, with the formation of some hetero-coupled acetylene.[39]

2.1.4 Catalytic coupling of isonitriles with terminal alkynes

Isonitriles have been shown to insert into metal acetylide bonds of early or late transition metal complexes under stoichiometric conditions to form 1-aza-1,3-enyne derivatives (see **Scheme 2.5**).[40-42] These products have great potential as organic synthons as they include three complementary reactive centres (a triple bond, a double bond and nitrogen lone pairs), thus enabling investigation of regio-specific reactions.

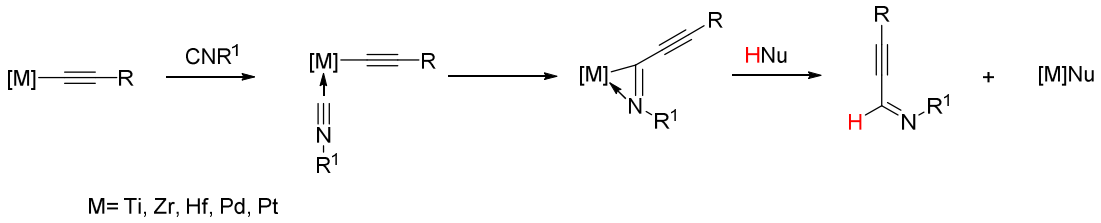

Scheme 2.5: Stoichiometric insertion of an isonitrile moiety into a metal acetylide

Some organo-actinide complexes have been found to be very reactive catalysts for isonitrile and terminal alkyne coupling.[43, 44] Successful coupling was observed for $Cp^*_2AnMe_2$ (An = U, Th) at 90-100 °C. The isonitrile: alkyne ratio has a significant effect upon the product ratio and distribution (**Scheme 2.6**). When using the thorium catalyst, $Cp^*_2ThMe_2$, the major product is the single insertion into the isonitrile (RC≡CC(H)=NR'). However, double insertion of the acetylene into the isonitrile (RC≡CC(H)=C(H)=NR') was observed when using unhindered terminal alkynes, such as isopropyl acetylene. $Cp^*_2UMe_2$ also produced the single insertion of alkyne into isonitrile as the major product (RC≡CC(H)=N^{t}Bu). However, double insertion of isonitrile into the alkyne was also observed(RC≡CC(HC=N^{t}Bu)=N^{t}Bu). The yield of this doubly inserted product can be increased by increasing the ratio of isonitrile to alkyne.[2]

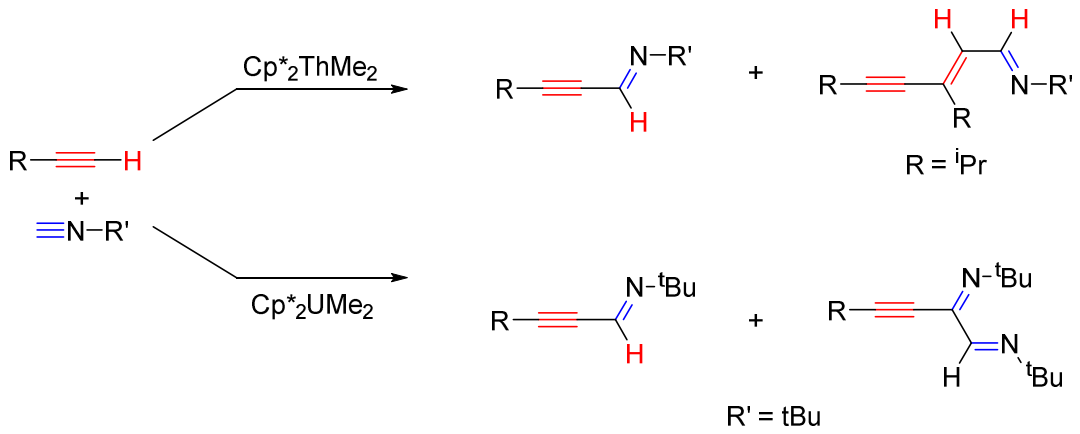

Scheme 2.6: Insertion of an isonitrile into a terminal acetylene catalysed by $Cp^*_2UMe_2$ and $Cp^*_2ThMe_2$ as described by Eisen *et al.*[43, 44]

2.1.5 Hydrogenation

Actinide hydrides of the form $Cp^*_2AnH_2$ (An = U, Th) have been shown to hydrogenate alkenes (**Scheme 2.7**) and acetylenes, under 0.9 atm of H_2, with turnover frequencies of 0.5 h^{-1} (Th) and 7 h^{-1} (U).[45] The hydrogenation of the acetylene was complete, i.e. the corresponding alkane was yielded.[46] The *ansa*- bridged $Me_2Si(C_5Me_4)_2ThH_2$ was a far more active catalyst for hydrogenation giving turnover frequencies 3 orders of magnitude greater than $Cp^*_2ThH_2$ for the hydrogenation of 1-hexene.[47] It should be noted that previously observed actinide hydrogenation catalysts required a hydride ligand in order to be active.

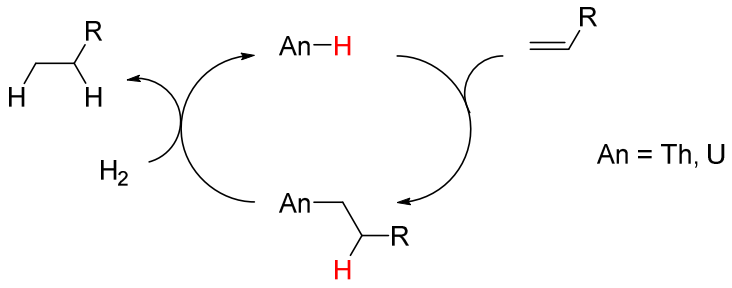

Scheme 2.7: Hydrogenation by actinide hydrides

2.2 Suitability of catalytic method[1]

$N''_2Th^{IV}\{\kappa^2\text{-}N(SiMe_3)SiMe_2CH_2\}$, **2.1** (**Figure 2.3**) was first synthesised by Andersen *et al.*, in 1981[48] and has not been investigated for catalytic activity before this study. In order to probe the possible use of **2.1** as a catalyst, its reactivity in facilitating the

oligomerisation of terminal acetylenes was examined. A key property of **2.1** is the two internal bases, Th-C and Th-N bonds, from either of which metal acetylides could form. As either the Th-C or Th-N bonds could potentially act as the base, this catalytic study provides scope for examining the differing reactivity of Th-C and Th-N bonds. The difference in pKa between HN" and PhCCH in DMSO is small (30 vs 28.7) but significant enough to allow for deprotonation.[49] The bond dissociation energy for a Th-C bond is 484(25) kJ/mol compared to 577.4(21) kJ/mol for a Th-N bond.[27] From these data it would be expected that the Th-C bond would be responsible for a first deprotonation of a terminal acetylene, whilst the Th-N bond would also be capable of affecting this deprotonation when encountering an excess of terminal acetylene.

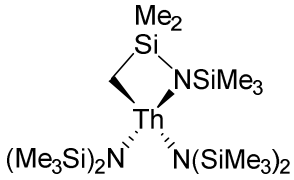

2.1

Figure 2.3: The thorium metallacycle precatalyst used in this study[48]

By careful substrate selection, terminal acetylene oligomerisation is a catalysis which allows for examination of steric and electronic effects upon the activity of the catalyst. The terminal acetylenes used in this study: 1-hexyne (^{n}BuC≡CH), phenyl acetylene (PhC≡CH), trimethylsilyl acetylene ($SiMe_3$C≡CH) and 3,3, dimethyl 1-butyne (^{t}BuC≡CH), have varied sterics and electronics, (See **Table 2.1**) thus allowing an exploration into the robustness of the catalysis.

Table 2.1: A comparison of the sterics and electronics of the terminal acetylenes used in this study.

Substrate	Effective steric factor (ν_{eff})[50]	Relative electronics
^{n}BuC≡CH	0.68	Electron neutral (inductive donator)
PhC≡CH	0.57	Electron-rich
$SiMe_3$C≡CH	1.40 (equivalent to Me (0.52) at α-position)	Electron-poor
^{t}BuC≡CH	1.24	Electron neutral (inductive donator)

To compare the effects of the availability of valence *f*-electrons and variable actinide oxidation state upon the catalysis detailed below comparisons of catalytic activity and selectivity were made with uranium analogues of **2.1**, namely $N''_2U^{IV}\{\kappa^2\text{-}N(SiMe_3)SiMe_2CH_2\}$, **2.2** and UN''_3, **2.3** (**Figure 2.4**).

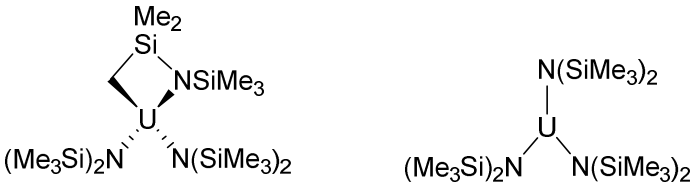

2.2 **2.3**

Figure 2.4 The uranium based precatalysts used in this study[48, 51]

The actinide amido complexes **2.1**-**2.3** react with terminal alkynes to yield dimers, trimers, or trisubstituted benzenes as the major products, with small quantities of alkene being generated in selected experiments (**Figure 2.5**). The distribution of products was found to be strongly dependent on the nature of the metal centre and the reacting alkyne (**Table 2.2**).

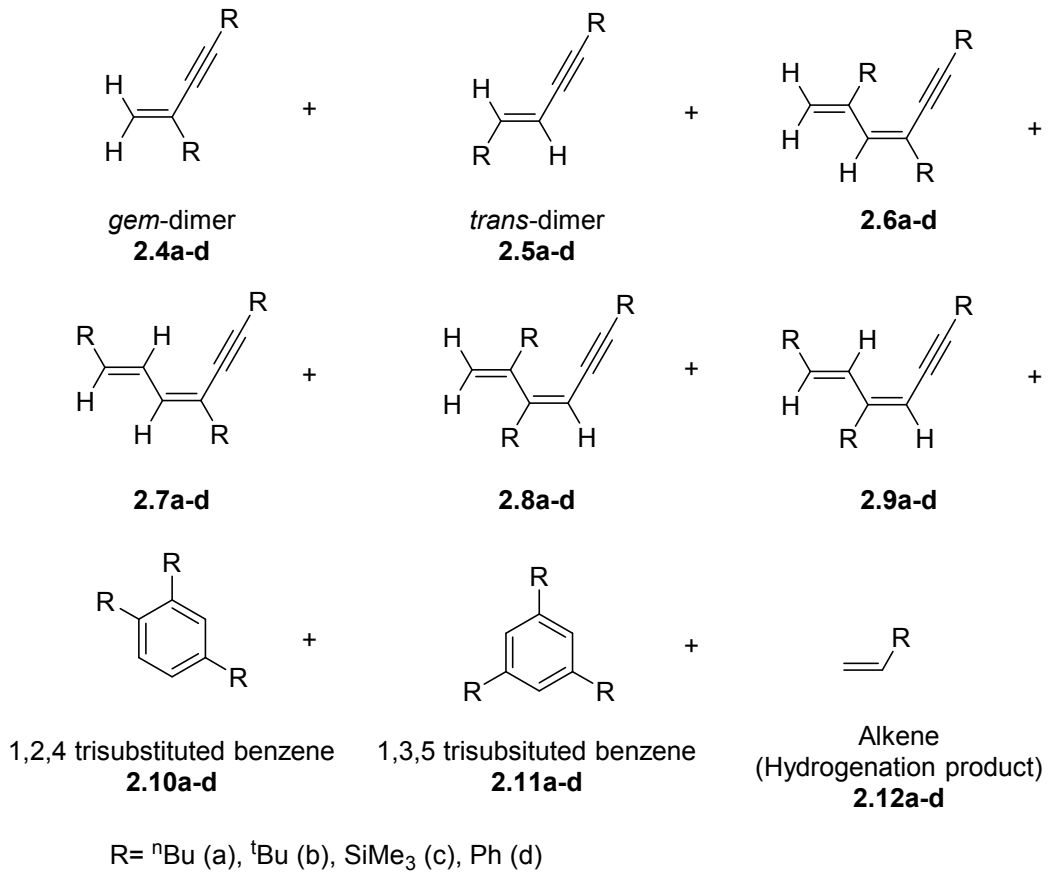

Figure 2.5 Accessible products from the catalytic reaction of terminal alkynes with **2.1-2.3**. The R substituent is *n*-butyl (a), *tert*-butyl (b), trimethylsilyl (c), or phenyl (d).

As can be seen from **Figure 2.5**, a variety of products are yielded from the catalytic reaction of terminal alkynes with the precatalysts **2.1**-**2.3**. The formation of **2.4** and **2.5** follows the mechanism outlined in **Scheme 2.2**, whilst the formation of four trimers (**2.6**-**2.9**) with distinctive regiochemistry is outlined in **Scheme 2.8**. As can be seen from **Scheme 2.8** the formation of a trimer is a result of a double insertion into the actinide-carbon bond of the terminal alkyne, with the regiochemistry of the insertion decided by the conformation of the acetylene before insertion into the Th-C bond.

Table 2.2: Results for the catalytic oligomerisation/cyclotrimerisation of terminal alkynes by complexes 2.1-2.3[a1]

Entry	Catalyst (Loading (mol %))	R[b]	Conversion (%)	Yield (%)								
				2.4	**2.5**	**2.6**	**2.7**	**2.8**	**2.9**	**2.10**	**2.11**	**2.12**
1	**2.1** (1)	^{n}Bu	86	92				7				
2	**2.1** (10)	^{n}Bu	99	93				7				
3	**2.2** (1)	^{n}Bu	88	96				2		1	1	
4	**2.2** (10)	^{n}Bu	100							41	37	22
5[c]	**2.3** (1)	^{n}Bu	88	91				5		2	1	
6	**2.3** (10)	^{n}Bu	100	13						29	42	15
7[c]	**2.1** (1)	^{t}Bu	70	41	43				14			
8	**2.1** (10)	^{t}Bu	97	14	46				39			
9[c]	**2.2** (1)	^{t}Bu	77	60	22			9		3	1	5
10	**2.2** (10)	^{t}Bu	100		54			23		6	2	14
11[c]	**2.3** (1)	^{t}Bu	87	22	40				21	8	1	7
12[c]	**2.3** (10)	^{t}Bu	100		55						22	23
13	**2.1** (1)	$SiMe_3$	64	22	43		35					
14	**2.1** (10)	$SiMe_3$	87	27	32		41					
15	**2.2** (1)	$SiMe_3$	97	32	8	38	19			2	2	
16	**2.2** (10)	$SiMe_3$	100	34	25					23	19	
17[c]	**2.3** (1)	$SiMe_3$	42	50	11					22	17	
18[c]	**2.3** (10)	$SiMe_3$	100							57	41	
19[d]	**2.1** (1)	Ph	99	91	9							
20[d]	**2.1** (10)	Ph	100	77	15							8
21[d,e]	**2.2** (1)	Ph	96	2	17					35	40	
22[d,e]	**2.2** (10)	Ph	100							40	51	
23[d,e]	**2.3** (1)	Ph	92							25	63	
24[d,e]	**2.3** (10)	Ph	100							48	49	

[a]Product percentages are ratios of converted substrate. Reactions were run for 72 h at 75 °C in C6D6. [b]R = substituent of the corresponding RC≡CH. [c]Traces of larger oligomers. [d]Products and distributions determined by HPLC-MS. [e]Remaining product contains dimers up to tetramers.

In the example of **2.6**, this trimer is the result of successive tail to tail insertions. In contrast, **2.7** is the result of a tail to tail insertion followed by a tail-to-head insertion. Conversely, **2.8** is the result of a tail-to-head insertion followed by a tail to tail whilst **2.9** in the result of successive tail-to-head insertions. The sterics of the terminal acetylenes will hence have a rather large impact of the ease of formation of each separate trimer, in both the initial insertion and the secondary insertion step, so it is perhaps expected to see a clearly favoured linear trimer in the results (**Table 2.2**).

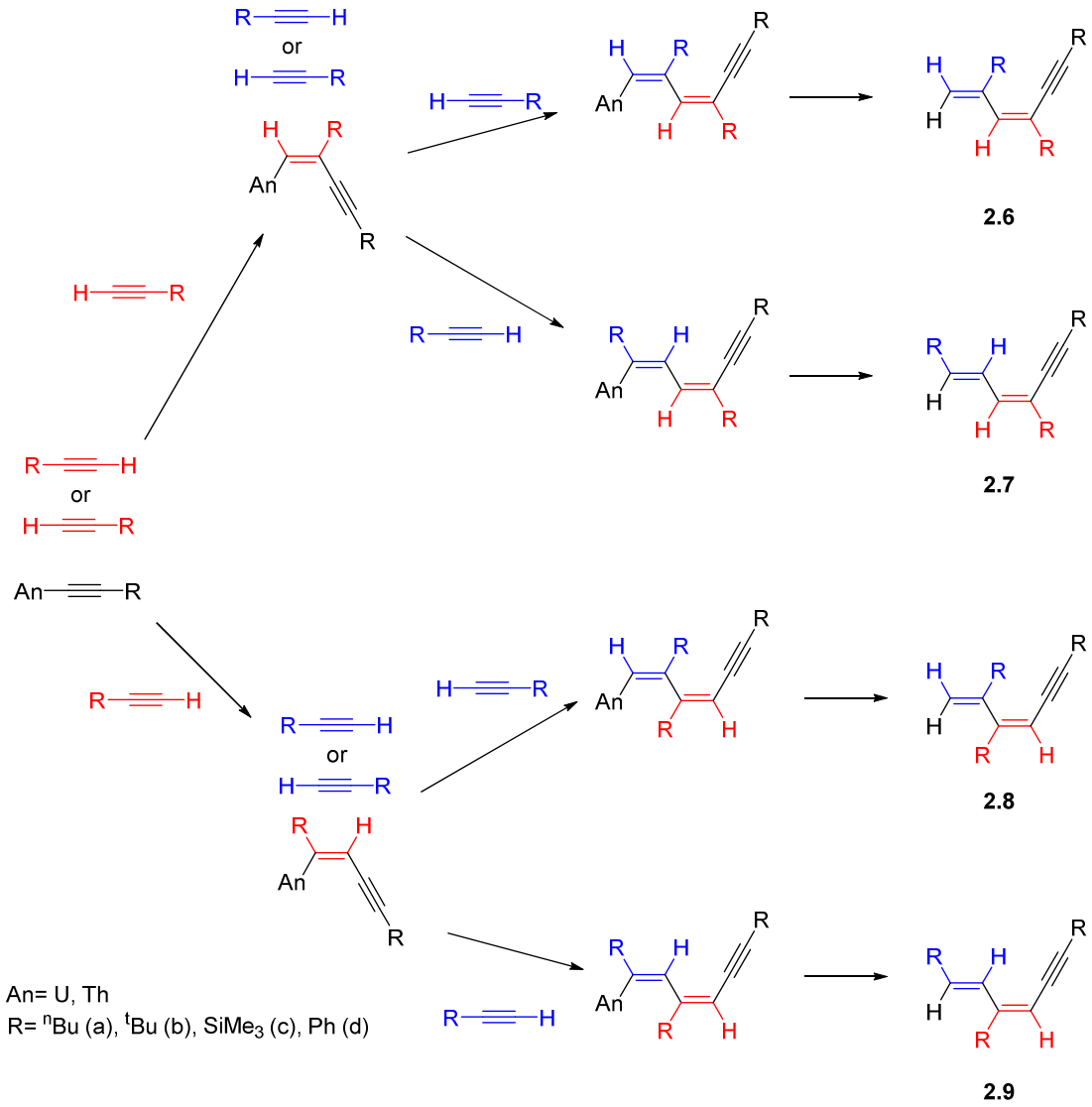

Scheme 2.8: A possible route for the formation of the four observed trimers and their observed regiochemistry. Actinide ligands are omitted and only one side of attack is illustrated for clarity.

One of the most notable results from **Table 2.2**, is the observation that [2 + 2 + 2] cycloaddition is only observed when uranium based precatalysts (**2.2**, **2.3**) are used. This is particularly noteworthy as the observation of cycloaddition of terminal alkynes has mostly been limited to late-transition metal based systems,[52, 53] with a few examples of early transition metal systems mediating this transformation, and no previous precedent for actinide based systems.[54-57] (See **Scheme 2.9**)

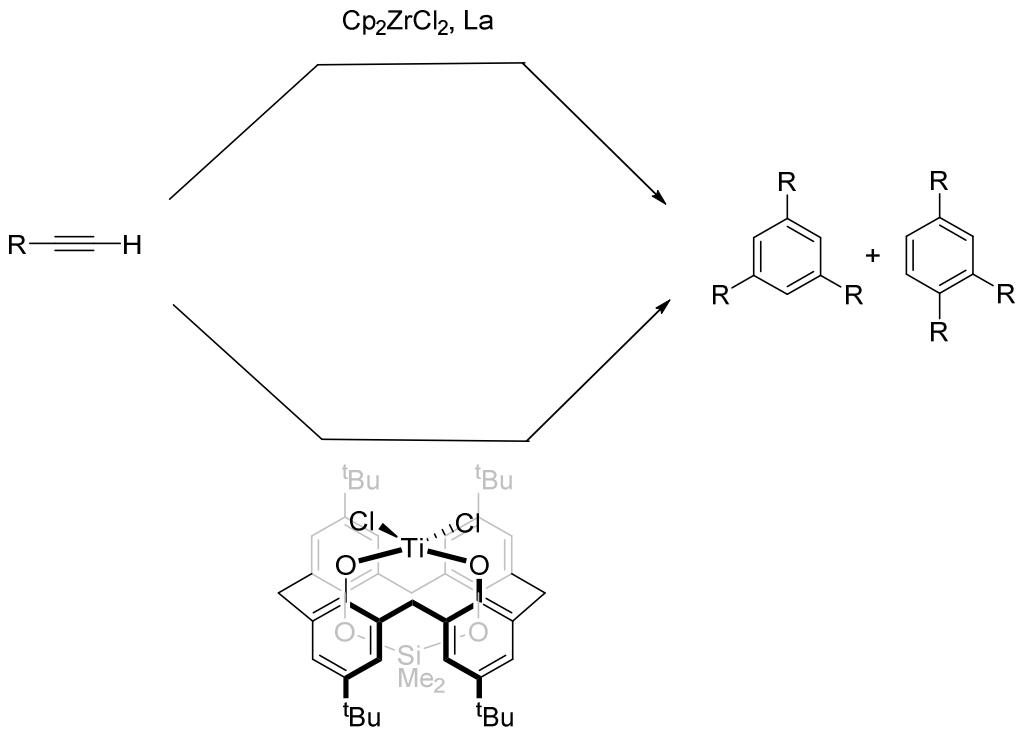

Scheme 2.9: Selected examples of transition-metal-mediated [2+2+2] cycloaddition from terminal alkyne oligomerisation as reported by Ladipo and Szymoniak *et al*.[54, 57]

A further unexpected result seen in **Table 2.1** is the observation of an alkene product, which has presumably formed as a result of reduction of the terminal acetylene by the catalysts. These results are mainly observed for the uranium based precatalysts **2.2** and **2.3**. As a result, the reductant is this reaction is proposed to be an *in situ* generated uranium hydride (See Equation 2.2).

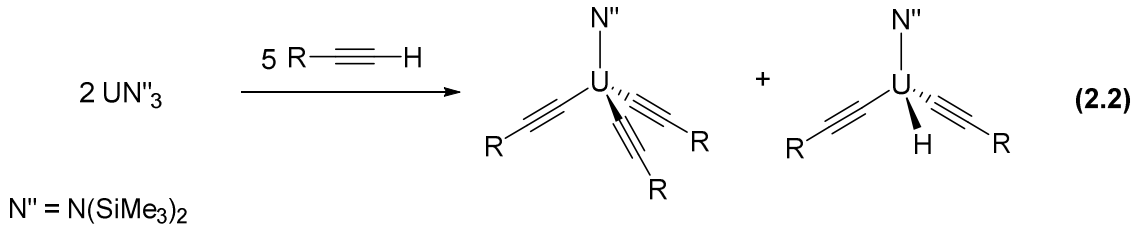

(2.2)

2.3 Oligomerisation and cyclotrimerisation of 1-hexyne by 2.1-3[1]

At low precatalyst loadings (1%, entries 1, 3 and 5) a common observation for all three precatalysts **2.1**-**3**, is the excellent conversion (>85%) of 1-hexyne (>90%) almost exclusively to the *geminal*-dimer (**2.4a**) as a result of tail-to-tail insertion into the Th-C bond. This is accompanied by some formation of linear trimer **2.8a** (The product of tail-

to-head insertion followed by a subsequent tail to tail insertion) and in the case of uranium precatalysts (**2.2** and **2.3**) the formation of a small amount of trisubstituted benzenes (<4%) as a result of cyclic trimerisation.

At higher loadings (10%, entry 2) for **2.1** increased conversion is observed (99 vs 86%) with almost identical product distributions between the *gem*-dimer **2.4a** and the linear trimer **2.8a** with no evidence of cyclic trimer formation. Conversely, when at higher loadings (10%) for the uranium based precatalysts (**2.2** and **2.3**, entries 4 and 6) a change in selectivity is observed, with the major products being the trisubstituted benzenes. For **2.2** (entry 4) quantitative conversion to the cyclic trimers as major products is observed with no significant preference between the different isomers (41% **2.10a**, 37% **2.11a**). Additionally, and surprisingly, these products were accompanied by the formation of 22 % of the reduction product 1-hexene, **2.12a**. In similarity to **2.2**, **2.3** (entry 6) also showed quantitative conversion to give predominately cyclic trimer products. In contrast to **2.2**, **2.3** exhibited formation of the *gem*-dimer (**4a**, 13%) whilst showing a slight preference for the 1,3,5 trisubstituted benzene product (**2.11a,** 42%) over the 1,2,4 derivative (**2.10a**, 29%). There was also evidence of the hydrogenation product 1-hexene (**2.12a**, 15%).

The formation of the linear trimer **2.8a**, which is formed *via* the same proposed intermediate as in the formation of **2.4a** is suggestive of a preference for tail-to-tail insertion for **2.1**-**2.3** when catalysing the oligomerisation of 1-hexyne. This can be explained by the minimal steric hindrance that can be affected by an *n*-butyl moiety, thus allowing the C-$H_{acetylene}$ group to adopt a position within the co-ordination sphere of the metal that favours the thermodynamically favoured regioselectivity of insertion of tail-to-tail.[58]

At low catalyst loadings (1%) for **2.1**-**2.3** the substantially higher yield of the *gem*-dimer, **2.4a**, when compared to the linear trimer, **2.8a**, indicates that migratory insertion of a terminal acetylene into an actinide-vinyl bond (An(R)C=CR'(R'')) is disfavoured when compared to protolytic cleavage. However, for **2.2**-**2.3** at higher catalyst loadings (10%) the formation of trisubstituted benzenes is favoured, whilst for **2.1**, the selectivity remains the same as at lower loadings, leading to a conclusion that perhaps valence electrons that can form π- or higher symmetry interactions with one or more substrates are key in the formation of cyclic trimers in this system.

A particularly noteworthy observation, in terms of mechanism, of the formation of 1,3,5 cyclic trimers (**2.11a**) is that these products can only be the result of successive head-to-tail insertions by the proposed mechanism. The 1,2,4 cyclic trimers have three possible intermediates in the proposed mechanism as they only require a tail-to-tail insertion step in either of the two insertion steps. The greater degree of cyclisation at higher loadings is suggested to result from a bimetallic process, hence the increased favourability at higher catalyst loadings due to increased catalyst concentrations in solution. The process for forming cyclic trimers is proposed as being bimetallic as the *sp* hybridised carbon atoms of the starting terminal acetylene molecules have all been converted to sp^2 hybridisation upon formation of the cyclic trimer. It is thought that the cyclisation would require two metal centres in order to favour the geometry required for this process to occur (**Scheme 2.10**).

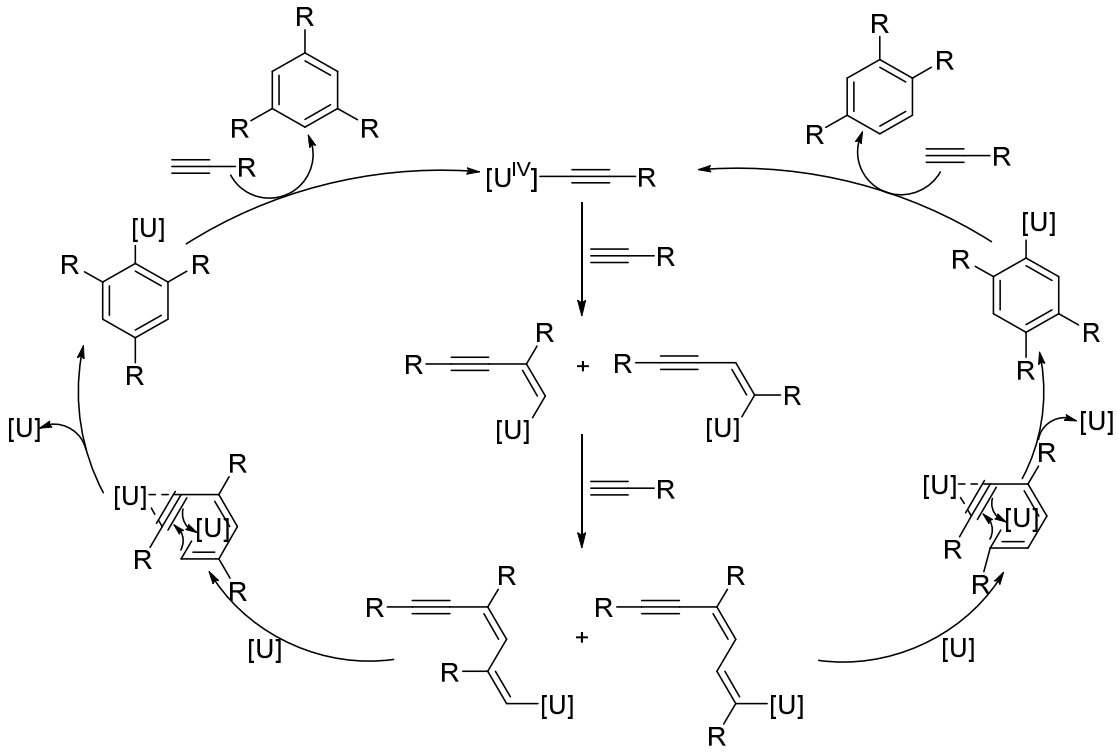

Scheme 2.10: proposed bimetallic mechanism for the cyclotrimerisation of terminal alkynes by complexes **2.2** and **2.3**.

Catalysis by **2.2** was found to favour 1,2,4 cyclic trimers over 1,3,5 cyclic trimers, hence possibly favouring a tail-to-tail migratory insertion step, however the ratio of **2.10a**:**2.11a** was smaller than the expected 3:1 ratio if the probability of formation of all of the linear trimer intermediates was equivalent (i.e statistical distribution).

Catalysis by **2.3** was found to show a slight preference for the formation of 1,3,5 cyclic trimers, which given the 3:1 proposed statistical distribution shows a clear preference for successive head-to-tail insertions. The difference in the activity of precatalysts **2.2** and **2.3**, despite their structural similarity, is suggestive of different structures of the active catalysts.

2.4 Oligomerisation and cyclotrimerisation of ^{t}Bu acetylene by 2.1-3[1]

An investigation into tuning of the sterics of the terminal acetylene used in this study, without greatly changing the electronics of the substrate, determined that *tert*-butylacetylene would be the obvious contrast to 1-hexyne (ν_{eff} = 1.24 for ^{t}Bu vs 0.68 for ^{n}Bu),[50] in attempting to ascertain the effect of sterics upon the observed reactivity.

At low precatalyst loadings (1%), good conversion (>70%) was observed for all three precatalysts, **2.1**-**2.3.** However, unlike the results examined in for 1-hexyne, selectivity for the three precatalysts differed at low loadings.

For **2.1** (entry 7), the major products at low precatalyst loading were the dimers, with no significant preference for *gem* or *trans*- dimer, **2.4b** and **2.5b** respectively, observed (41 vs 43 % respectively). The formation of linear trimer, **2.9b** (14%), the result of successive head-to-tail migratory insertions, was also observed. The formation of **2.9b** is proposed to proceed through a common intermediate to the formation of **2.5b**, hence suggesting a preference for head-to-tail insertion over the thermodynamically favoured tail-to-tail insertion as was seen for 1-hexyne. This is likely due to the difference in sterics between ^{t}Bu acetylene and 1-hexyne causing a preference for tail-to-head insertion to avoid steric clashes.

For **2.2** (entry 9), the major product at low precatalyst loading was the *gem*-dimer, **2.4b** (60%), with the *trans* dimer, **2.5b**, a relatively minor product (22%). There was also evidence of the linear trimer **2.8b** (9%), as well as the formation of some cyclic trimers **2.10b** and **2.11b** (<5%) and hydrogenation product **2.12b** (5%). The formation of **2.4b** as a major product, shows **2.2** has a clear preference for tail-to-tail insertions at low loadings, which is in direct contrast to the metallacyclic analogue **2.1** at low precatalyst loadings. This is likely due to the difference in size of a thorium and uranium cation in addition to the role of f-electrons in bonding within this catalytic pathway.

For **2.3** (entry 11), the major product at low precatalyst loading was the *trans*-dimer, **2.5b** (40%), with roughly equivalent amounts of *gem*-dimer, **2.4b**, and linear trimer, **2.9b**, produced (22 and 21% respectively). Accompanied by these products were cyclic trimers **2.10b** and **2.11b** (<10%) and hydrogenation product **2.12b** (7%) as minor products. An 8:1 ratio of **2.10b** to **2.11b** was observed, indicating a clear preference for the 1,2,4 trisubstituted benzene derivative. The high yields of formation of **2.5b** and **2.9b**, by **2.3**, in agreement with **2.1**, suggests a preference for tail-to-head insertion a low precatalyst loadings due to the steric effects of the ^{t}Bu functional group.

At higher precatalyst loadings (10%) excellent conversion is observed for **2.1**-**3** (>96%) with a clear preference for formation of the *trans*-dimer, **2.5b**, by all three precatalysts as a result of tail-to-head migratory insertion. For **2.1** (entry 8), the preference for the formation of **2.5b** (46%), is accompanied by formation of almost equimolar amounts of linear trimer **2.9b** (39%), with *gem*-dimer **2.4b** a minor product (14%). This shows a clear preference for **2.1** for head to tail insertion with ^{t}Bu acetylene at high and low loadings to prevent steric clashes.

For **2.2** (entry 10), at higher precatalyst loadings (10%), the favoured formation of **2.5b** (54%), is complemented by the formation of linear trimer **2.8b** (23%), drawing parallels to the results of the lower loading experiment. The formation of cyclic trimers **2.10b** and **2.11b** (<10%) and the hydrogenation product **2.12b** (14%) were also observed. This result is particularly notable as it illustrates a change in observed regioselectivity upon change of catalyst loading, which is unprecedented in f-element and transition metal based catalysis. This change in regioselectivity hints at the migratory insertion step of the terminal alkyne into the uranium acetylide bond being a reversible process. The variable regioselectivity based on variable catalyst loading is proposed to result from favourable formation at high concentrations of the sterically challenging ^{t}Bu acetylene substrate, of a π-alkynyl complex such as those described by Eisen *et al* (**Figure 2.6**).[59] The formation of a π-alkynyl complex would be expected to favour tail-to-head insertion and it should be noted that in Eisen's initial description of π-alkynyl complexes, isolation was only possible for the ^{t}Bu acetylene analogue.

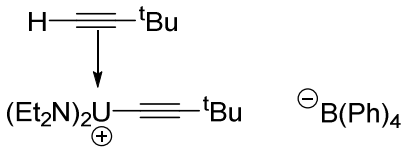

Figure 2.6: An uranium π-alkynyl complex as described by Eisen *et al*.[59]

For **2.3** (entry 12), at higher precatalyst loadings, in addition to the favoured formation of **2.5b** (54%) roughly equimolar amounts of cyclic trimer **2.11b** (22%) and hydrogenation product **2.12b** (23%) were produced. The formation of **2.11b**, the 1,3,5 substituted benzene derivative, can form the proposed mechanism only proceed via successive tail-to-head migratory insertion steps and when combined with the favoured formation of **2.5b**, which shares a common intermediate to **2.11b**, is evidence of a preference of tail-to-head insertion as would be expected for the sterically challenging ^{t}Bu group. The difference in favoured products between **2.2** and **2.3** again underlines the notion that despite their similar precatalyst starting structures, the active catalyst is substantially different structurally. The absence of linear trimers **2.6-8b**, which share a common intermediates with **2.11b** from the products is highly suggestive of the cyclisation of this common intermediate favouring cyclisation over protolytic cleavage.

The lower conversions, comparatively, observed for ^{t}Bu acetylene compared to 1-hexyne, indicate that the steric bulk of ^{t}Bu acetylene has an inhibitory effect upon the rate of migratory insertion or substrate co-ordination during the catalytic cycle. It also has the effect of reversing the observed regioselectivity seen for 1-hexyne in the majority of cases. The presence of the product of hydrogenation **2.12b**, in the catalytic products for **2.2** and **2.3**, in higher concentrations than the uranium based precatalysts, suggests that whilst the formation a uranium hydride species may occur upon activation of the precatalyst, there must exist an alternative pathway to regenerate the uranium hydride species to enable the catalytic formation of the corresponding alkene from the alkyne.

2.5 Oligomerisation and cyclotrimerisation of trimethylsilyl acetylene by 2.1-3[1]

The trimethylsilyl functional group has been determined, experimentally and computationally, to be of equivalent sterics to a methyl group at the α-position.[60-63] This allows for the comparison with catalytic products of 1-hexyne to be considered mostly

in terms of the change in electronics. Due to the inductive effects of a Si-C bond and its subsequent stabilisation of α-carbanions and β-carbocations[64-66] it was expected that tail-to-tail insertion would be favoured (**Figure 2.7**). The increased electron density within the alkyne bond of $SiMe_3C{\equiv}CH$ is also expected to favour the formation of a π-alkynyl complex, which is also expected to favour cyclisation.

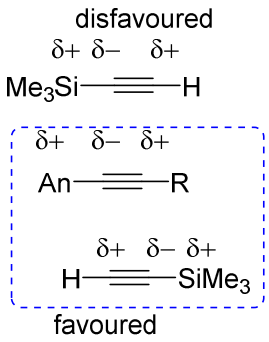

Figure 2.7: The polarisation of the Si-C bond leads to tail-to-head insertion being favoured on grounds of electrostatic attraction.

A common observation to all three precatalysts **2.1-2.3** is that the lowest catalytic conversions were observed when $SiMe_3C{\equiv}CH$ was the substrate (entries 13-18). This is likely a result of the favourable formation of the π-alkynyl complex raising the enthalpic activation barrier towards migratory insertion, which is also thought to be responsible for the increased amounts of cyclic trimers observed for precatalysts **2.2** and **2.3**.

At low precatalyst loading, **2.1** (entry 13), shows moderate conversion (64%) of the $SiMe_3C{\equiv}CH$ substrate to form the trans dimer, **2.5c** (43%), as the major product, accompanied by the formation of the linear trimer **2.7c** (35%) and formation of the *gem*-dimer **2.4c** (22%). The formation of **2.7c**, according to the mechanism illustrated in **Scheme 2.9** is proposed to be the result of a tail-to-tail insertion followed by a tail-to-head insertion. This product distribution appears to be indicative of multiple competing reaction pathways being present within this catalytic reaction at low precatalyst loadings.

For **2.2** (entry 15) at low precatalyst loading an excellent conversion (97%) was observed. However, the selectivity for this catalytic reaction was low. The major products, produced in roughly equimolar amounts were the *gem*-dimer **2.4c** (32%) and the linear trimer as a result of consecutive tail-to-tail insertions **2.6c** (38%). Both of

these major products show a preference for tail-to-tail insertions. The minor products were predominantly made up of the linear trimer as a result of tail-to-tail followed by tail-to-head insertion **2.7c** (18%), the *trans*-dimer **2.5c** (8%), and the cyclic trimers **2.10c** (2%) and **2.11c** (2%). The distribution of products shows that only 10% of products did not involve a tail-to-tail migratory insertion step, clearly indicating that this step is favoured for **2.2** at low catalyst loadings, which is unsurprising given the theory espoused surrounding the polarisation of a Si-C bond.

For **2.3** (entry 17) at low precatalyst loading, a rather poor conversion of 42% was observed which the lowest conversion that was observed in this study. The selectivity showed a strong preference towards the thermodynamically favoured product; the *gem*-dimer **2.4c**, which was formed as the major product (50%). The minor products were dominated by the cyclic trimers **2.10c** (22%) and **2.11c** (17%), accompanied by the formation of some *trans*-dimer **2.5c** (11%). The cyclic trimers showed a slight preference for the 1,2,4 cyclic trimer, **2.10c**.

At higher catalyst loadings (10%), the catalytic oligomerisation of trimethylsilyl acetylene by **2.1** (entry 14) shows good conversion (87%) with a similar product distribution as seen for the lower loading experiment. However, in this case the major product is the linear trimer **2.7c** (41%)**,** with the rest of the products consisting of the *gem*- **2.4c** (27 %) and *trans*-dimers **2.5c** (32%). This continues the indication that many competing reaction pathways are present in the catalytic reaction of **2.1** with trimethylsilyl acetylene. These results show a marginal preference for tail-to-tail insertion.

At higher catalyst loadings (10%), the catalytic oligomerisation of trimethylsilyl acetylene by **2.2** (entry 16) shows quantitative conversion with low selectivity of products. The major product was found to be the thermodynamically favoured product; the *gem*-dimer **2.4c** (34%). Roughly equimolar amounts of *trans*-dimer **2.5c** (25%) and 1,2,4 **2.10c** (23%) and 1,3,5 **2.11c** (19%) cyclic trimers were also produced. The lack of formation of linear trimers is suggestive of formation of a π-alkynyl complex which was proposed to favour the formation of cyclic trimers. The roughly equimolar amounts of cyclic trimers **2.10c** and **2.11c** suggest a preference for tail-to-tail insertion.

At higher catalyst loadings (10%), the catalytic oligomerisation of trimethylsilyl acetylene by **2.3** (entry 18) shows quantitative conversion with a narrow product

distribution observed. The products were exclusively found to be the cyclic trimers **2.10c** and **2.11c**. A slight preference was observed for the 1,2,4 trimer **2.10c** (57%) over the 1,3,5 trimer **2.11c** (43%). The sole formation of cyclic trimers is highly suggestive of the proposed π-alkynyl complex formation favouring cyclisation. The formation of **2.11c** requires successive tail-to-head insertions according to the proposed mechanism, whilst **2.10c** only requires one of the two migratory insertions to be tail-to-tail. As such if the formation of cyclic trimers followed a statistical distribution there should be a 3:1 ratio of **2.10c** to **2.11c** in the products. As this ratio is closer to 1:1, this indicates a favouring of the tail-to-head migratory insertion.

2.6 Oligomerisation and cyclotrimerisation of phenyl acetylene substrate by 2.1-3[1]

The most electron poor substrate studied here is phenyl acetylene. The electron deficiency of the alkyne (**Figure 2.8**) was expected to result in a preference for cyclisation due to increased π-backbonding. The electron deficient alkyne should also show a preference for tail-to-tail insertion. The phenyl ring is expected to impart minimal steric hindrance ($\nu_{Ph} = 0.57$)[50] so the steric barrier for tail-to-tail insertion is expected to be minimal.

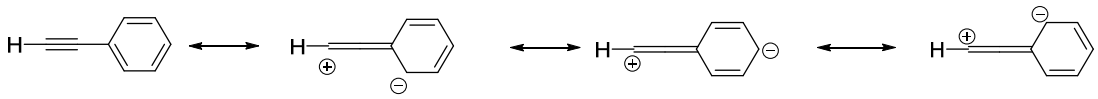

Figure 2.8: The electron deficient nature of Ph acetylene is due to its ability to adopt three canonical forms with a positive charge based upon the α-carbon of the terminal acetylene

A common observation for all (**2.1-2.3**) catalytic reactions with phenyl acetylene as a substrate in this study is that excellent conversions are observed (>91%).

At low precatalyst loading for **2.1** (entry 19), in addition to the excellent conversion of 99%, excellent regioselectivity was also observed with near quantitative conversion to the *gem*-dimer **2.4d** (91%) with the minor product being the *trans*-dimer, **2.5d.** This is indicative of a clear preference for tail-to-tail insertion. This also represents the highest selectivity observed in this study.

At low precatalyst loading for **2.2** (entry 21), an excellent conversion (96%) of was observed. The major products of this reaction were found to be the cyclic trimers **2.10d** (35%) and **2.11d** (40%) with the *gem*- **2.4d** (2%) and *trans*-dimers **2.5d** (17%) seen as

minor products. The slight preference of formation of the 1, 3, 5 cyclic trimer, **2.11d**, illustrates a clear favouring for tail-to-head migratory insertion as the 1, 3, 5 cyclic trimer can only form via successive head-to-tail insertions.

For **2.3** (entry 23), at low catalyst loading, was also observed to result in an excellent conversion (92%), and in common with **2.2**, cyclic trimers **2.10d** (25%) and **2.11d** (63%) were found to be the major products of the reaction. The remainder of the products of this reaction were higher oligomers. The relatively high yield of **2.11d**, is again clear evidence of a preference for tail-to-head migratory insertion, which was not the anticipated result.

At high precatalyst loading, **2.1** (entry 20), was found to result in quantitative conversion of phenyl acetylene with the *gem*-dimer **2.4d** (77%) again found to be the major product, however with lower selectivity than in the lower precatalyst loading experiment. The minor products were found to be the *trans*-dimer (15%) (**2.5d**) and unexpectedly the hydrogenation product **2.12d** (8%). The preference for formation of the **2.4d** is a clear indication of the expected inclination for tail-to-tail insertion. The formation of **2.12d** is surprising as it is the only example in this study of the thorium-based precatalyst, **2.1**, causing this formation. Its formation is sub-stoichiometric compared to the precatalyst loading, which means that **2.12d** may form as a result of degradation of the active catalyst. This degradation could result in the formation of a thorium-hydride complex (**Figure 2.9**) that could cause the formation of a hydrogenation product.

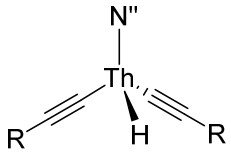

Figure 2.9 Possible identity of thorium hydride complex formed as a result of catalyst degradation

At high precatalyst loading, **2.2** (entry 22), quantitative conversion of phenyl acetylene was observed. The major products, in common with the lower precatalyst loading, were found to be the cyclic trimers **2.10d** (40 %) and **2.11d** (51%). The remainder of the minor products were higher oligomers, also in line with the results seen at lower precatalyst loadings. The preference for forming the 1,3,5 cyclic trimer **2.11d**, shows a

preference for tail-to-head insertion for catalysis by **2.2** at both low and high precatalyst loadings.

At high precatalyst loadings, **2.3** (entry 24), in common with **2.1-2** shows quantitative conversion of phenyl acetylene. The formation of cyclic trimers was again found to be highly favourable, with **2.10d** (48%) and **2.11d** (49%) forming the vast majority of the products (97%). A slight preference for the formation of the 1,3,5 trimer **2.11d** was observed, which represents a clear preference for tail-to-head insertion, which goes against the anticipated result.

The results of the catalytic reaction of phenyl acetylene thus follow two divergent regioselectivities dependent, seemingly, upon the identity of the actinide cation in the precatalyst. For the uranium based catalysts; **2.2**-**3**, a clear preference for tail-to-head insertion was observed at both low and high precatalyst loadings. Contrastingly for **2.1**, the thorium based precatalyst, the expected preference for tail-to-tail insertions was observed. This unexpected deviation from the theoretically predicted regioselectivity for the uranium based catalysts may hint at the role of valence electrons capable of forming π- or higher symmetry interactions with one or more unsaturated substrates in deciding the regioselectivity of terminal acetylene oligomerisation/ cyclotrimerisation, perhaps particularly when the terminal acetylene has (relatively) reduced electron density. However it is also likely that differences in ionic radii between uranium and thorium will have an effect upon the catalysis.

2.7 Conclusions and Summary[1]

In this investigation, it has been seen that actinide amide precatalysts **2.1-3** allow for a manipulation of regioselective oligomerisation or cyclotrimerisation of terminal alkynes. The [2 + 2 + 2] cycloaddition process, discussed in section *2.3*, is unprecedented in actinide catalysis. This is perhaps unexpected when considering that the formation of an aromatic system is likely to be thermodynamically favourable. In terms of oligomerisation, a combination of regioselective migratory insertions and protolytic cleavages are proposed to comprise the catalytic cycle.

The electron-deficient and -rich alkynes phenylacetylene and (trimethylsilyl)acetylene, respectively, show a strong preference toward cyclization when either uranium-based precatalyst (**2.2**-**3**) are used. The thorium based precatalyst, **2.1**, is observed to show a high degree of regioselectivity for all studied terminal acetlyenes. For 1-hexyne and

phenylacetylene two products are observed, with a high degree of selectivity (>75%) observed at all loadings towards the major product. When *tert*-butylacetylene and (trimethylsilyl)acetylene were used as substrates it was observed that 3 products were formed, with seemingly no preference for a major product for these substrates at all loadings.

Despite the similarity between precatalysts **2.2** and **2.3**, the results of this study suggest that there is a different active catalyst present in each case. This supposition is based upon the different chemo- and regio-selectivities observed for both cyclotrimerisation and oligomerisation products within this study for catalysis by **2.2** and **2.3**. The observed difference in products between **2.1** and **2.2-3**, i.e. that cyclotrimerisation products were only observed when **2.2-3** were the catalyst is highly suggestive of the significant role of actinide valence electrons capable of participating in π- interactions or higher symmetry with one or more unsaturated substrates in stabilising certain transition states and intermediates the structure, bonding and reactivity.

2.9 References

1. R. J. Batrice, J. McKinven, P. L. Arnold and M. S. Eisen, *Organometallics*, 2015, 34, 4039-4050.
2. T. Andrea and M. S. Eisen, *Chem. Soc. Rev.*, 2008, 37, 550-567.
3. B. M. Trost, M. T. Sorum, C. Chan and G. Rühter, *J. Am. Chem. Soc.*, 1997, 119, 698-708.
4. B. M. Trost, C. Chan and G. Ruhter, *J. Am. Chem. Soc.*, 1987, 109, 3486-3487.
5. W. Reppe, Schweckendiek, W. J., *Justus Liebigs Ann Chem*, 1948, 560, 104-116.
6. B. R. Galan and T. Rovis, *Angew. Chem., Int. Ed. Engl.*, 2009, 48, 2830-2834.
7. X. Bu, Z. Zhang and X. Zhou, *Organometallics*, 2010, 29, 3530-3534.
8. A. K. Dash and M. S. Eisen, *Org. Lett.*, 2000, 2, 737-740.
9. G. Hilt, T. Vogler, W. Hess and F. Galbiati, *Chem. Commun.*, 2005, 1474-1475.
10. R. H. Platel and L. L. Schafer, *Chem. Commun.*, 2012, 48, 10609-10611.
11. K. H. Den Haan, Y. Wielstra and J. H. Teuben, *Organometallics*, 1987, 6, 2053-2060.
12. C. J. Schaverien, *Organometallics*, 1994, 13, 69-82.
13. C. G. J. Tazelaar, S. Bambirra, D. van Leusen, A. Meetsma, B. Hessen and J. H. Teuben, *Organometallics*, 2004, 23, 936-939.
14. B. M. Trost and G. Kottirsch, *J. Am. Chem. Soc.*, 1990, 112, 2816-2818.
15. L. S. Meriwether, E. C. Colthup and G. W. Kennerly, *J. Org. Chem*, 1961, 26, 5163-5169.
16. C. Bianchini, P. Frediani, D. Masi, M. Peruzzini and F. Zanobini, *Organometallics*, 1994, 13, 4616-4632.
17. S. Ogoshi, M. Ueta, M.-a. Oka and H. Kurosawa, *Chem. Commun.*, 2004, 2732-2733.
18. X. Chen, P. Xue, H. H. Y. Sung, I. D. Williams, M. Peruzzini, C. Bianchini and G. Jia, *Organometallics*, 2005, 24, 4330-4332.

19. I. P. Kovalev, K. V. Yevdakov, Y. A. Strelenko, M. G. Vinogradov and G. I. Nikishin, *J. Organomet. Chem.*, 1990, 386, 139-146.
20. J. Dong, Q. Wu and J. You, *Tetrahedron Lett.*, 2015, 56, 1591-1599.
21. B. D. Stubbert and T. J. Marks, *J. Am. Chem. Soc.*, 2007, 129, 6149-6167.
22. A. L. Odom, *Dalton Trans.*, 2005, 225-233.
23. K. C. Hultzsch, *Adv. Synth. Catal.*, 2005, 347, 367-391.
24. K. C. Hultzsch, D. V. Gribkov and F. Hampel, *J. Organomet. Chem.*, 2005, 690, 4441-4452.
25. T. Straub, A. Haskel, T. G. Neyroud, M. Kapon, M. Botoshansky and M. S. Eisen, *Organometallics*, 2001, 20, 5017-5035.
26. R. D. Shannon, *Acta Crystallographica Section A*, 1976, 32, 751-767.
27. J. A. Dean and N. A. Lange, *Lange's handbook of chemistry*, McGraw-Hill, 1992.
28. E. Barnea and M. S. Eisen, *Coord. Chem. Rev.*, 2006, 250, 855-899.
29. T. Straub, A. Haskel and M. S. Eisen, *J. Am. Chem. Soc.*, 1995, 117, 6364-6365.
30. M. Nobis and B. Drießen-Hölscher, *Angew. Chem., Int. Ed. Engl.*, 2001, 40, 3983-3985.
31. J. Haggin, *Chem. Eng. News*, 1993, 17, 23.
32. A. Haskel, T. Straub and M. S. Eisen, *Organometallics*, 1996, 15, 3773-3775.
33. B. D. Stubbert, C. L. Stern and T. J. Marks, *Organometallics*, 2003, 22, 4836-4838.
34. C. E. Hayes, R. H. Platel, L. L. Schafer and D. B. Leznoff, *Organometallics*, 2012, 31, 6732-6740.
35. I. Fleming, J. Dunogues and R. Smithers, *Org. React. (Hoboken, NJ, U. S.)*, 1989, 37, No pp. given.
36. N. Asao, T. Sudo and Y. Yamamoto, *J. Org. Chem.*, 1996, 61, 7654-7655.
37. M. A. Esteruelas, O. Nuernberg, M. Olivan, L. A. Oro and H. Werner, *Organometallics*, 1993, 12, 3264-3272.
38. R. Takeuchi and N. Tanouchi, *J. Chem. Soc., Perkin Trans. 1*, 1994, 2909-2913.
39. A. K. Dash, J. Q. Wang and M. S. Eisen, *Organometallics*, 1999, 18, 4724-4741.
40. W. Ahlers, G. Erker and R. Fröhlich, *J. Organomet. Chem.*, 1998, 571, 83-89.
41. F. Takei, K. Yanai, K. Onitsuka and S. Takahashi, *Chem. Eur. J.*, 2000, 6, 983-993.
42. A. M. Martins, J. R. Ascenso, C. G. de Azevedo, A. R. Dias, M. T. Duarte, J. F. da Silva, L. F. Veiros and S. S. Rodrigues, *Organometallics*, 2003, 22, 4218-4228.
43. E. Barnea, T. Andrea, M. Kapon, J.-C. Berthet, M. Ephritikhine and M. S. Eisen, *J. Am. Chem. Soc.*, 2004, 126, 10860-10861.
44. E. Barnea, T. Andrea, J.-C. Berthet, M. Ephritikhine and M. S. Eisen, *Organometallics*, 2008, 27, 3103-3112.
45. P. J. Fagan, J. M. Manriquez, E. A. Maatta, A. M. Seyam and T. J. Marks, *J. Am. Chem. Soc.*, 1981, 103, 6650-6667.
46. R. G. Bowman, R. Nakamura, P. J. Fagan, R. L. Burwell and T. J. Marks, *J. Chem. Soc., Chem. Commun.*, 1981, 257-258.
47. R. D. Gillespie, R. L. Burwell and T. J. Marks, *Langmuir*, 1990, 6, 1465-1477.
48. S. J. Simpson, H. W. Turner and R. A. Andersen, *Inorg. Chem.*, 1981, 20, 2991-2995.
49. F. G. Bordwell, G. E. Drucker, N. H. Andersen and A. D. Denniston, *J. Am. Chem. Soc.*, 1986, 108, 7310-7313.
50. M. Charton, *J. Am. Chem. Soc.*, 1975, 97, 1552-1556.
51. R. A. Andersen, *Inorg. Chem.*, 1979, 18, 1507-1509.
52. S. Saito and Y. Yamamoto, *Chem. Rev.*, 2000, 100, 2901-2916.
53. M. Lautens, W. Klute and W. Tam, *Chem. Rev.*, 1996, 96, 49-92.
54. A. Joosten, M. Soueidan, C. Denhez, D. Harakat, F. Hélion, J.-L. Namy, J.-L. Vasse and J. Szymoniak, *Organometallics*, 2008, 27, 4152-4157.

55. P. Andrews, C. M. Latham, M. Magre, D. Willcox and S. Woodward, *Chem. Commun.*, 2013, 49, 1488-1490.
56. R. Srinivasan and M. F. Farona, *J. Mol. Catal.*, 1989, 53, 203-208.
57. O. V. Ozerov, B. O. Patrick and F. T. Ladipo, *J. Am. Chem. Soc.*, 2000, 122, 6423-6431.
58. M. Sharma, T. Andrea, N. J. Brookes, B. F. Yates and M. S. Eisen, *J. Am. Chem. Soc.*, 2011, 133, 1341-1356.
59. J. Q. Wang, A. K. Dash, J. C. Berthet, M. Ephritikhine and M. S. Eisen, *Organometallics*, 1999, 18, 2407-2409.
60. Y. Apeloig, R. Biton and A. Abu-Freih, *J. Am. Chem. Soc.*, 1993, 115, 2522-2523.
61. A. D. Allen, R. Krishnamurti, G. K. S. Prakash and T. T. Tidwell, *J. Am. Chem. Soc.*, 1990, 112, 1291-1292.
62. Y. Apeloig and A. Stanger, *J. Am. Chem. Soc.*, 1985, 107, 2806-2807.
63. J. Frey, E. Schottland, Z. Rappoport, D. Bravo-Zhivotovskii, M. Nakash, M. Botoshansky, M. Kaftory and Y. Apeloig, *J. Chem. Soc., Perkin Trans. 2*, 1994, 2555-2562.
64. J. B. Lambert, G. T. Wang, R. B. Finzel and D. H. Teramura, *J. Am. Chem. Soc.*, 1987, 109, 7838-7845.
65. J. B. Lambert, *Tetrahedron*, 1990, 46, 2677-2689.
66. J. B. Lambert, Y. Zhao, R. W. Emblidge, L. A. Salvador, X. Liu, J.-H. So and E. C. Chelius, *Acc. Chem. Res.*, 1999, 32, 183-190.

Chapter 3: Actinide terphenolate complexes with chlorides as ancillary ligands

This chapter comments in part on results that are published in the 2014 Dalton Transactions paper.[1]

3.1 Introduction

The development of small molecule activation using actinide terphenolate complexes began with attempts to characterise and synthesise chlorido- starting materials with the aim of these being good precursors for synthesising complexes which may facilitate small molecule activation.

It is of particular interest to know how much steric bulk was required in order to stabilise these potentially unstable molecules, whilst optimising the reactivity of the metal centre and causing steric hindrance to potential further reactivity. This would ideally be achieved with ligands that make isolation of potentially reactive complexes more facile. However, traditional methods to measure ligand sterics, such as Tolman cone angles,[2-4] are not a good measure of steric bulk in this case, as phenolates are much more two dimensional in nature than phosphines, possess a high degree of rotational freedom, and in many cases do not have linear M-O-C bond angles. To remedy this, percentage buried volume (PBV) calculations were carried out.[5, 6] These give the percentage that a ligand will fill in a 3.5 Å sphere surrounding the metal centre of a complex, assuming that the bond length donor atom to the metal is 2 Å . These calculations were carried out on terphenolates and other selected bulky actinide ligands and the results are displayed in **Figure 3.1**.

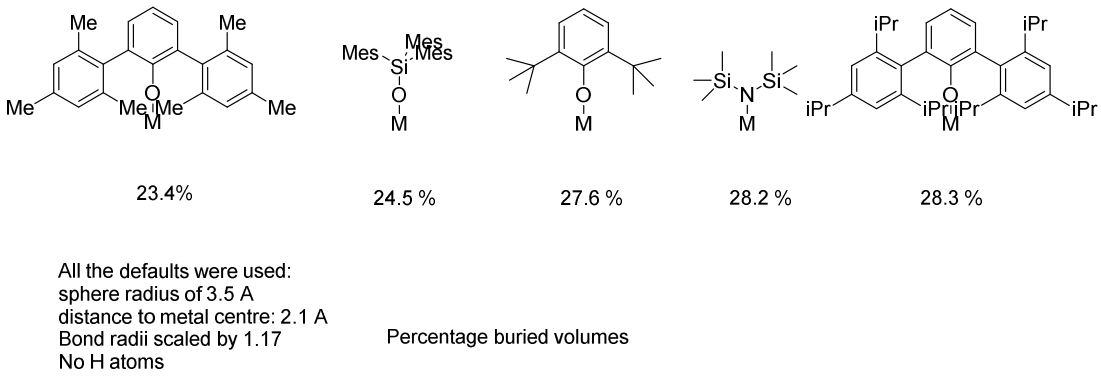

Figure 3.1: Values of percentage buried volume calculations for selected ligands (from left to right: $Ter^{Mes}OM$, Mes_3SiOM, d^tBupOM, $(Me_3Si)_2NM$ and $Ter^{Trip}OM$)

As can be seen from **Figure 3.1** the steric effect of the terphenolates range from a single ligand filling 23% of the space of the hypothetical 3.5 Å sphere for the least bulky (Me substituted) variety to 28% for the most bulky form of the ligand (iPr substituted). Initially, this seems indicative of the ligands investigated being bulky and suggests that in terms of bulk the triisopropyl form of the ligand is comparable to the N". However, there are some problems with these calculations which call into question the validity of the obtained results.

For alkoxide ligands the primary limitation is that the oxygen binding to the metal centre has only one other atom bonded to it. This means that the software for calculating the percentage buried volume is unable to calculate the bulk for alkoxides from the oxygen atom as it requires this atom to have at least two bonds to other atoms. In order to calculate the PBV for alkoxides, the metal was modelled to be bonded to the carbon (or silicon) atom attached to the oxygen and the two adjacent carbons to this atom were used as the basis for calculating the bulk of the ligand. This, however, resolves into two further problems; the metal carbon distance is assumed to be 2 Å, when in reality it is closer to 3.5 Å, causing the calculation to vastly overestimate the amount of bulk close to the metal centre. In addition, the M-O-C bond angle is usually bent in solid state structures. This fact is not explicitly taken into account by the PBV calculation. However, due to the distance between M-C being shorter than the sum of M-O and C-O , some of the effect of the metal oxygen carbon bend upon the sterics of the ligands is taken into account. As such the validity of this calculation is reduced to a more qualitative rather than quantitative measure. As a result no information gained

other than the already assumed understanding that an ^{i}Pr moiety will create more steric bulk than a Me moiety has been gained from this calculation.

Whilst qualitative, the result of the PBV calculations tentatively suggest that a Ter^{Mes}OH ligand is less sterically demanding than a d^{t}BupOH ligand, whilst a Ter^{Trip}OH ligand is more sterically challenging. Work on tertiary butoxide complexes of thorium has previously been carried out within the group, so the further investigation into the terphenolate complexes of thorium is an aim of this project.[7]

Complexes incorporating the Ter^{Mes}O^{-} ($C_6H_3$2,6-[$C_6H_2$2,4,6-Me]$_2$O^{-}) moiety have previously been synthesised via the known compound LiOTer^{Mes} ($C_6H_3$2,6-[$C_6H_2$2,4,6-Me]$_2$OLi).[8-12] However, due to actinide complexes' well-precedented predilection towards the formation of 'ate' salts, especially in the presence of LiCl,[13-26] it was decided to attempt to synthesise heteroleptic terphenolate complexes of thorium in a 'lithium-free' manner. This was achieved through the use of the potassium analogue, KOTer^{Mes} ($C_6H_3$2,6-[$C_6H_2$2,4,6-Me]$_2$OK), which can be generated *in situ* by reaction of KN" (KN(SiMe$_3$)$_2$) with HOTer^{Mes} ($C_6H_3$2,6-[$C_6H_2$2,4,6-Me]$_2$OH) (Equation 3.1). The solid state structure of KOTer^{Mes}, **3.3** is displayed in **Figure 3.4**.

3.2 Synthesis of thorium terphenolate chlorido- complexes

The products in the synthesis of terphenolate chlorido-complexes of thorium were found to be dependent upon the identity of the base used to deprotonate Ter^{Mes}OH, and perhaps more significantly the solvent that the reaction was performed in. As can be seen from the summary of these results in **Scheme 3.1**, two divergent products, ThCl$_2$(OTer^{Mes})$_2$(H_2O)$_3$, **3.1**, and ThCl$_2$(OTer^{Mes})$_2$(DME), **3.2**, were formed depending upon the solvent and base used. A description of the synthesis and characterisation of **3.1** will be followed by that of **3.2**.

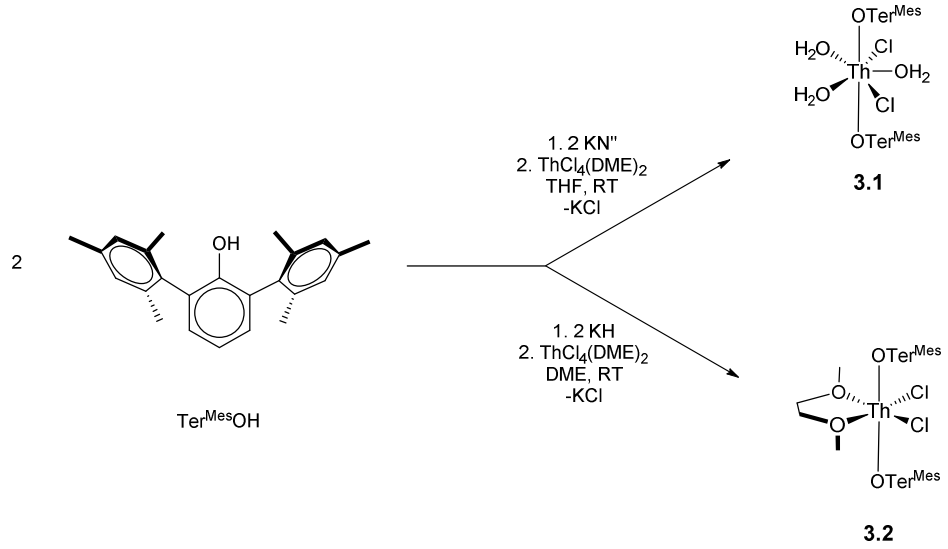

Scheme 3.1: Divergent products dependent upon solvent of heteroleptic terphenolate complexes of thorium

3.2.1 Synthesis of $ThCl_2(OTer^{Mes})_2(H_2O)_3$

The reaction between $ThCl_4(DME)_2$ and two equivalents of *in situ* generated $KOTer^{Mes}$, in THF affords $[Th(OTer^{Mes})_2Cl_2(H_2O)_3]$, **3.1**, as an off- white solid in 60 % yield after workup (**Scheme 3.1**). Single crystals suitable for X-ray diffraction of **3.1** were grown from a saturated toluene solution at -30°C; the solid state structure is shown in **Figure 3.2**. Selected bond angles and distances in the solid state structure of **3.1** are shown in **Table 3.1**.

The solid state structure of compound **3.1** displays a pseudo- pentagonal bipyramidally co-ordinated thorium cation, with the two *trans*-oriented $Ter^{Mes}O^-$ ligands adopting axial positions with a near linear O_1-Th-O_2 bond angle (178.3(1)°). This is atypical and presumably a consequence of the steric bulk of the aryloxides as for seven co-ordinate thorium complexes this is the most linear O-Th-O angle.[27] The Th1-O1,2 distances of **3.1** are 2.194(4) Å, which are amongst the shortest reported Th-O single bonds, although they are significantly longer than the Th=O bond length of the hitherto only reported thorium oxo-complex of 1.929(4) Å as is to be expected.[28] Molecular single Th-O bonds in the CSD range from 1.739(5) to 3.051 Å.[27, 29, 30] The shortest reported Th-O single bond,[30] contained within a bis hydroxyl compound that has been compared to the uranyl moiety as it is proposed to have multiple bond character,[30] is 0.2 Å shorter than any other Th-O interaction. The average of the Th1-O3,4,5 bond distances in **3.1** is

2.64(1) Å and this is atypical as this is long for any Th-O bond. When the comparison is restricted to Th-OH_2 bond distances, **3.1** contains Th-O distances equivalent to the longest Th-OH_2 bonds in the literature, which range from 2.400 to 2.621(7) Å.[27, 31] Th(IV) hydration in aqueous solutions is well studied experimentally and theoretically and it has been ascertained that that the Th-water first hydration shell distance is 2.45-46 Å. [32-35] When only considering the longest two Th-OH_2 bonds within **3.1** (Th1-O3,4 2.664(6), 2.645(6) Å) it becomes clear that these represent the longest known Th-OH_2 bonds.

Within **3.1** the thorium centre is seven co-ordinate. It is unique within the literature for a thorium complex with more than one aquo-ligand ligated to the metal centre to have a co-ordination number as low as seven. All other thorium complexes, characterised crystallographically, with more than one aquo ligand ligated have a co-ordination number of at least eight. The fact that these Th-OH_2 bond lengths are long, despite this low co-ordination number, which would be expected to favour shorter Th-O bonds becomes more surprising. This is further evidence as to the steric bulkiness of the aryloxides as three-fold aqua-co-ordination in 7 co-ordinate thorium complexes is unprecedented. It is also unprecedented for any aqua ligation to a thorium complex with co-ordination number less than 8.

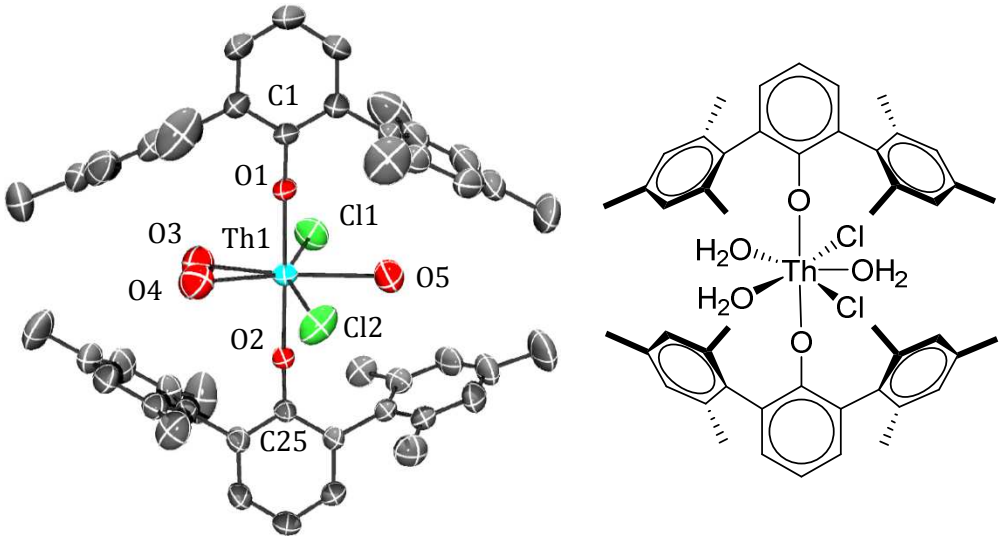

Figure 3.2: Displacement ellipsoid drawing of the solid-state molecular structure of [Th($OTer^{Mes}$)$_2$$Cl_2$($H_2O$)$_3$], **3.1** (50 % probability ellipsoids). Hydrogen atoms are omitted for clarity.

In the solid state structure of **3.1**, the chlorido- and aqua ligands occupy the equatorial plane, with the chlorido- ligands adopting a near *trans* orientation (Cl_1-Th_1-Cl_2 angle is 148.71(7)°). This Cl-Th-Cl bond angle is typical. The H_2O-Th-OH_2 angle of the adjacent aqua ligands (O3 and O4) is 68.4(2)° which is fairly typical for what would be expected for a the internal angles of a pentagon (ideal angle is 72°), and this remains the same for the Cl1-Th1-O5, Cl1-Th1-O3, Cl2-Th1-O5 and Cl2-Th1-O4 angles which are 74.60(17), 72.64(17), 74.23(18) and 72.74(17) respectively. As would be expected from their relative sizes the chloride ligands occupy more space than the aquo ligands as shown by the wider angles involving the chloride ligands in the equatorial plane than the ones involving only oxygen atoms.

The C1-O1-Th1 and C25-O2-Th1 angles of **3.1**, in the solid state are 172.5(4) and 165.2(3)° respectively, indicating that these angles tend towards the linear, which is perhaps a function of their steric bulk meaning that minimising their proximity is favourable.

A slightly unusual aspect of the equatorial plane is that the homoleptic ligating atoms appear to adopt different planes with the thorium cation. The Th1-Cl1-Cl2 plane deviates from the Th1-O3-O4-O5 plane by an angle of 17.01° meaning that what has been referred to as the equatorial plane is distorted, possibly as an effect of incorporating 5 ligands around thorium in this geometry. The ligation of aquo ligands arise is presumed to arise as a result of the 'dry' THF that was used not being completely water-free.

Another unusual aspect of this structure is the combination of the Th-OAr and Th-OH_2 moieties being in proximity to one another without the complex degrading into 2HOAr and Th-$(OH)_2Cl_2.H_2O$, with perhaps the only driving force that prevents this from occurring being the high affinity of thorium towards high co-ordination numbers. Thorium is purported to be the metal cation that can accommodate the highest co-ordination number within the literature.[36]

Upon ligation of an aquo-ligand to a metal centre, the protons of an aquo-ligand become more acidic, due to a loss of electron density from the O-H bonds due to donation by the highly electronegative oxygen's into the metal's orbitals and subsequent weakening of the O-H bonds. The effect of the metal on the acidity of the O-H protons of ligated water molecules are then primarily twofold; the charge and size of the metal cation. An

increased charge, as in the case of Th^{IV} results in increased electrostatic attraction, thus increasing donation and making the O-H protons more acidic. Increased size of cation, as is also the case for Th^{IV}, which is the largest tetravalent cation in the periodic table,[37] results in less polarisation of the Th-O interaction, resulting in a relatively less acidic O-H proton compared to smaller cations of the same charge. When considering these two affects, it would be expected that the charge of the cation would predominate and that thorium aquo-ligated complexes would exhibit fairly high acidity of the O-H protons. However, most of the acidity of metal-aquo complexes depends upon the identity of the solvent, so it is proposed that in relatively non-polar solvents, such as toluene or THF, this expected acidity of the O-H proton is not observed. The acidity of this proton could be determined by calculating the pKa of this proton by a potentiometric titration of a known concentration of a solution of **3.1** against an analyte.

The ^{1}H NMR spectrum of **3.1**, shows three resonances assigned to aromatic environments and two resonances assigned to alkyl environments as would be expected form the $Ter^{Mes}OH$ ligand. The aqua ligands appear as a singlet resonance at -0.41 ppm, perhaps indicating the shielding effect of the thorium cation, which has an electronegativity value of 1.3, upon the aqua ligands.[38]

The IR spectrum of **3.1**, shows a broad peak at 2960 cm^{-1} assigned to the stretching frequency of the O-H bonds of the aqua ligands, although significant overlap with the C-H stretching frequency is observed as a shoulder of this peak at 2920 cm^{-1}. This is a shift from organic O-H type stretching frequencies (*circa* 3600 cm^{-1}) which is expected given the mass difference of a thorium atom to a carbon atom.

The suitability of **3.1** towards small molecule activation is compromised by the presence of three aqua ligands, which are likely to quench any reactivity that may be observed. To attempt to confirm the presence of $Th\text{-}OH_2$ ligation some deprotonation reactions were carried out with an excess of reagent in an attempt to not only remove the aquo ligands, but also transform the chlorido ligands. The results of these reactions are presented in **3.3.2** and **3.3.4**

Table 3.1: Selected distances and angles for **3.1**

Atoms	Distance (Å) / angle (°)
Th1-O1, Th1-O2, Th1-Cl1, Th1-Cl2	2.197(3), 2.191(4), 2.7616(18), 2.7601(18)
Th1-O3, Th1-O4, Th1-O5	2.664(6), 2.645(6), 2.605(6)
C1-O1, C25-O2	1.348(6), 1.333(6)
O1-Th1-O2, Cl1-Th1-Cl2	178.31(13), 148.71(7)
Th1-O1-C1, Th1-O2-C25	172.5(4), 165.2(3)
Cl1-Th1-O1, Cl1-Th1-O2	89.25(12), 92.21(11)
Cl2-Th1-O1, Cl2-Th1-O2	94.31(11) , 84.88(11)
Cl1-Th1-O3, Cl1-Th1-O4, Cl1-Th1-O5	72.64(17), 138.39(17), 74.60(17)
Cl2-Th1-O3, Cl2-Th1-O4, Cl2-Th1-O5	137.40(17), 72.74(17) , 74.23(18)
O1-Th1-O3, O1-Th1-O4, O1-Th1-O5	81.14(18) , 96.35(19), 91.55(16)
O2-Th1-O3, O2-Th1-O4, O2-Th1-O5	97.21(17), 83.29(19), 89.65(16)
O3-Th1-O4, O3-Th1-O5, O4-Th1-O5	68.4(2) , 145.5(2), 146.1(2)

3.2.2 Synthesis of $ThCl_2(OTer^{Mes})_2DME$

As seen in *3.2.1*, the formation of **3.1**, with the presence of three aqua ligands, was not the ideal precursor for the formation of alkyl or hydrido- complexes that may take part in small molecule activation. To remedy this, the decision was made to alter the reaction conditions that formed **3.1**, in order to access an aqua-free complex, which may prove more amenable towards small molecule activation processes. A change of base for deprotonating $Ter^{Mes}OH$ and a change of solvent proved to be fruitful alterations to the synthetic procedure of **3.1**. The use of potassium hydride as a base also allows for an excess to be used, whilst reducing the possibility of it acting as a nucleophile towards the generated complex, which can act as a drying agent for the solvent, thus reducing the possibility of aqua-ligated complexes forming.

The reaction of $ThCl_4DME_2$ and two equivalents of $KOTer^{Mes}$, generated *in situ* by reaction of $HOTer^{Mes}$ with KH, with DME as a solvent affords $[Th(OTer^{Mes})_2Cl_2(DME)]$, **3.2**, as an off-white solid in 66 % yield after workup (**Scheme 3.1**). Single crystals suitable for X-ray diffraction of **3.2** were grown from a saturated solution of toluene at -30°C; the solid state structure is shown in **Figure 3.3**. Selected bond angles and distances calculated from the solid state structure of **3.2**, are shown in **Table 3.2**.[1]

The solid state molecular structure of **3.2**, shown in **Figure 3.3**, displays pseudo-octahedral geometry around the thorium cation, with two *trans*-oriented $Ter^{Mes}O^-$ ligands and a nearly linear O1-Th1-O2 bond angle (179.1(2)°). This is atypical, and presumably a result of the steric bulk of the aryloxides as it is the most linear O-Th-O observed in six co-ordinate thorium aryloxide complexes.[27] This bond angle is identical within s.u.s to the analogous bond angle in **3.1**. The Th-O1,2 bonds of **3.2** are 2.180(3) Å, amongst the shortest reported Th-O single bonds, and are identical within s.u.s to the analogous bonds in **3.1**.When compared to **3.1**, the solid state structure of **3.2**, exhibits a lower co-ordination number, which is likely due to the chelate effect of the DME solvent compared to three aqua ligands meaning the ligation of a further solvent molecule would be sterically challenging. This is seen by the shorter Th1-O2 bond distances in **3.2** (2.519(3) Å) compared to the Th1-O3,4,5 bond distances seen in **3.2.1** for **3.1** (2.664(6), 2.645(6), 2.605(6) Å). The shorter Th-$O^{solvent}$ bond distance means that the steric bulk of the DME molecule is closer to the thorium cation, thus proving more of a hindrance to further ligation. The Th1-Cl1 bond distances in **3.2**, are significantly shorter than the analogous distances in **3.1**, (2.6645(13) Å for **2** versus 2.7616(18), 2.7601(18) Å for **3.1**). This observation is likely due to the change is co-ordination number between **3.1** and **3.2**, especially in the equatorial plane, as this pronounced difference in bond length is not seen for the axial ligands. The lower co-ordination number would result in the chloride ligands binding to thorium through more favourable orbital mixing thus producing potentially stronger and shorter bonds. The shortening of the Th-Cl bond may also be a result of the change in Cl-Th-Cl bond angle from 148.71(7)° in **3.1** to 127.28(7)° in **3.2,** resulting in reduced *trans* influence by the chlorides upon one another. The predominant effect upon the adoption of this *cis* geometry by the chloride ligands is likely to be the chelate effect of the co-ordinated DME molecule and its subsequent effects upon the structure, such as exerting a reduced *trans* effect upon the chloride ligands in comparison to a chloride ligand. The C1-O1 bond distances for **3.1** and **3.2** are identical within s.u.s.

The ^{1}H NMR spectrum of **3.2** in C_6D_6 at room temperature exhibits three resonances in the aromatic region assigned to the aromatic protons of the $Ter^{Mes}O^-$ ligand. It also shows two resonances attributed to the methyl group protons of the $Ter^{Mes}O^-$ ligand which show 0.1 ppm shifts from the free ligand. The largest shifts for the ^{1}H NMR spectrum of **3.2** are the resonances assigned to the ligated DME molecule, where the $\mathit{CH_3}OCH_2CH_2O\mathit{CH_3}$ resonances shift by 0.2 ppm upfield, whilst the $CH_3O\mathit{CH_2CH_2}OCH_3$

resonances shift by 1.1 ppm upfield. This is likely due to the reduced degrees of freedom these protons experience upon binding of the DME molecule to the thorium cation, resulting in greater shielding.

In theory, **3.2**, is a far more favourable and suitable precursor for the formation of thorium- alkyl and hydrido complexes which should be able the effect chemical transformations towards the activation of small molecules than **3.1**. This is due to there being no ligating aqua ligands, which are highly likely to prevent the formation of alkyl or hydrido complexes via protonation of the alkylating agent or hydride source. **3.2** is unlikely to affect Lewis acid based small molecule activations due to the steric hindrance of the ligands preventing access of any potential substrate to the metal centre and due to the fact that there is a lack of an reactive bond in this complex which limits the potential of a small molecule to insert into bonds. The remainder of this chapter will mainly focus upon the attempted transformation of **3.2**, into complexes which may affect small molecule activations.

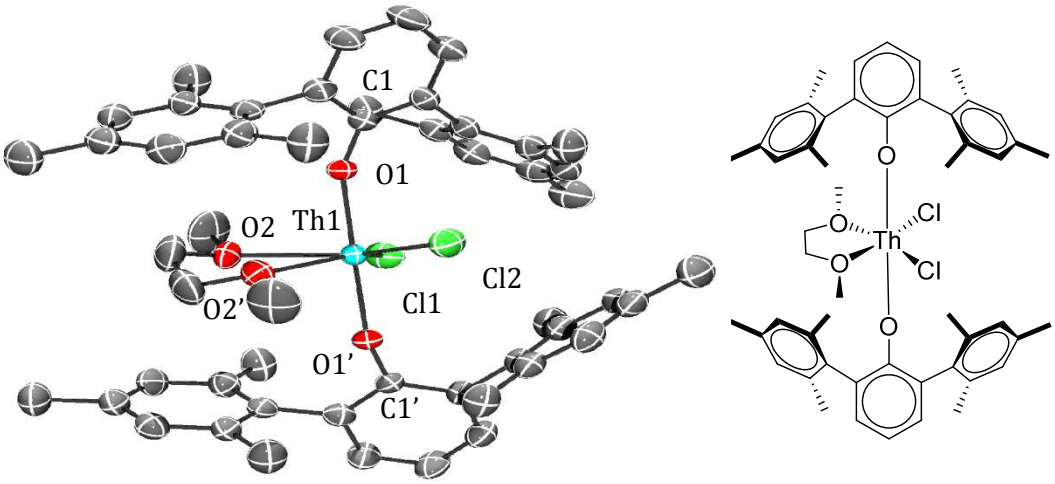

Figure 3.3: Displacement ellipsoid drawing of the solid-state molecular structure of [Th(OTer^{Mes})$_2$Cl$_2$(DME)], **3.2** (50 % probability ellipsoids). Hydrogen atoms, solvent molecules and disorder in DME molecule are omitted for clarity.

Table 3.2: Selected distances and angles for **3.2**

Atoms	Distance (Å) / angle (°)
Th1-O1	2.180(3)
Th1-O2	2.519(3)
C1-O1	1.352(5)
Th1-Cl1	2.6645(13)
O1-Th1-O1'	179.10(15)
Th1-O1-C1	152.5(3)
Cl1-Th1-Cl1'	127.28(7)
Cl1-Th1-O1	93.76(9), 85.84(9)
Cl1-Th1-O2	146.65(9), 85.40(9)
O2-Th1-O2'	63.51(17)
O1-Th1-O2	95.35(12), 85.41(12)

3.3 Reactivity of thorium terphenolate chlorido- complexes

The terphenolate ligand used in this chapter, $Ter^{Mes}O^-$, is a strong σ-donor, and as a result will experience strong electrostatic attractions to electropositive metals. This is a benefit when attempting to initially ligate the terphenolate ligand to the electropositive thorium atom (The electronegativity of Th is 1.3 compared to 0.98 for Li, 0.82 for K and 1.31 for Mg)[38], as was seen in *3.2*. However, upon attempting to transform **3.1** or **3.2**, using classical group I or group II based reagents, a competition for the strongly σ-donating ligand exists, which shall be shown in *3.3*, mostly results in transmetallation occurring. It is assumed that this is due to the 'hardness' and oxophilicity of the group I and II reagents causing the formation of group I and II terphenolate salts to be favourable. The potential reducing nature of Group I organometallics was also likely to result in the observed reactivity. As a result of these findings, attempts to transform **3.2,** with 'softer' reagents will also be described.

3.3.2 Group I transmetallation

The use of alkali metal transfer reagents to form actinide hydrido- and alkyl complexes is well precedented.[39-47] It therefore seemed prudent to begin in the targeting the formation of novel hydrido- and alkyl complexes by salt metathesis reactions using alkali metal transfer reagents.

*3.3.2.1 Synthesis of [(THF)K(μ²- OTer^{Mes})]$_2$, **3.3***

An attempted reduction of **3.2,** using potassium graphite, to transform the thorium centre to a +3 oxidation state by abstraction of a chloride in a salt elimination reaction to form KCl is depicted in Equation 3.1.

$$\underset{\textbf{3.2}}{ThCl_2(OTer^{Mes})_2DME} + KC_8 \not\longrightarrow ThCl(OTer^{Mes})_2DME + KCl + C_8 \qquad \textbf{(3.1)}$$

Attempted reduction of $ThCl_2(OTer^{Mes})_2DME$

This reaction occurred at room temperature and discolouration of the potassium graphite from bronze to black was almost immediately apparent. However, the reaction depicted in Equation 3.1 did not occur as after work-up and crystallisation from hexane, crystals of [(THF)K(μ²- OTer^{Mes})]$_2$, **3.3** were grown. Due to the rarity of Th(III) complexes, [48-52] it is not surprising that the observed reactivity was divergent from the formation of a thorium(III) species. The solid state structure of **3** is depicted in **Figure 3.4**. Selected bond angles and distances calculated from the solid state structure of **3.3**, are shown in **Table 3.3**.

The solid state molecular structure of **3.3** shows the two potassium-atoms bridging between the two oxygen-atoms of the terphenolates forming a four-membered ring. This causes the formation of a non-planar K-O-K-O bimetallacyclic ring with a torsion angles ranging from 20.6-20.9° between the four atoms in the ring. Another characteristic of this structure is that the potassium-bound THF molecules are almost orthogonal to the K-O-K-O ring with torsion angles of 94.6° and 86.4°. This may be due to the steric hindrance of the bulky mesityl groups in the plane of the ring. It may also be the case that their presence in the plane of the ring may inhibit the potassium π-interactions with the aryl rings.

In **3.3** the K-O^{terphenolate} distances of 2.628(2) Å, 2.591(2), Å 2.594(2) Å and 2.613(2) Å are typical of bridging K-O-K bond distances within the literature which range from 1.940- 3.584 Å.[27] This may be indicative of the oxygen to potassium bonds in this compound being relatively stronger than that of the average potassium oxygen bond, which may help to explain the observed transmetallation reactivity.

As can be seen from the solid state molecular structure in **Figure 3.4**, the potassium atoms undergo π-interactions with the phenyl rings of the mesityl rings of the

terphenolate. Both of the potassium atoms (K1 and K2) show an η^2 interaction with one phenyl ring and η^3 with another phenyl ring. The K-C bond distances (ranging from 3.121(3) to 3.393(3) Å) from the π-interactions with the phenyl rings are fairly typical for this type of interaction.[27] The C-O bond distances in the terphenolate molecules of 1.302(3) and 1.300(3) Å are relatively short amongst those reported within the literature for terphenolate complexes of metals.[27]

The ^{1}H NMR spectrum at room temperature in C_6D_6 for this reaction showed a few small shifts from **3.2** and the obvious (due to the resonances having different multiplicities) appearance of bound THF molecules replacing the DME resonances.

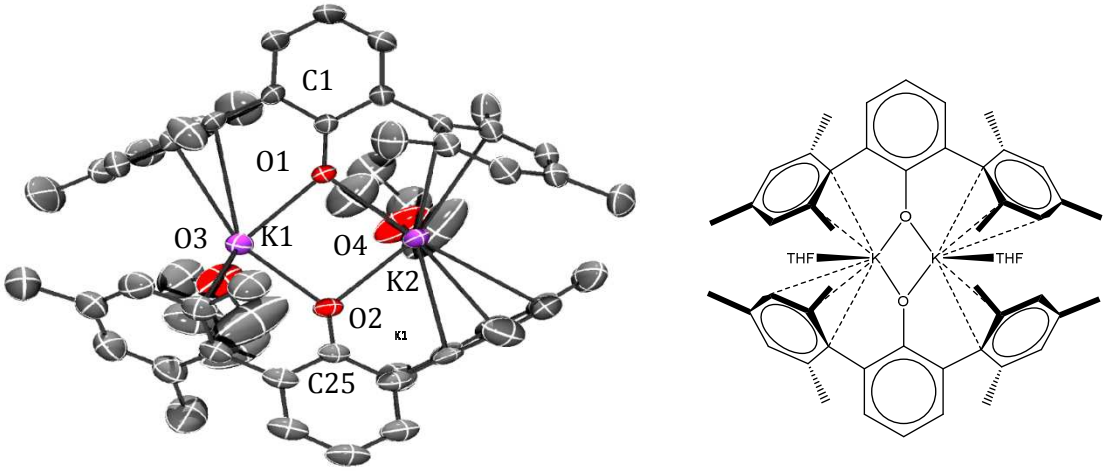

Figure 3.4: Displacement ellipsoid drawing of the solid-state molecular structure of [(THF)K(μ^2- OTer^{Mes})]$_2$, **3.3** (50% probability ellipsoids). Hydrogen atoms are omitted for clarity.

Table 3.3: Selected distances and angles for **3.3**

Atoms	Distance (Å) / angle (°)
K1-O1, K2-O1	2.628(2), 2.594(2)
K1-O2, K2-O2	2.591(2), 2.613(2)
K1-O3, K2-O4	2.751(3), 2.656(19)
C1-O1, C25-O2	1.302(3), 1.300(3)
K1-C16, K1-C17, K1-C40	3.123(3), 3.270(3), 3.168(3)
K1-C41, K1-C42	3.393(3), 3.228(3)
K2-C7, K2-C8,	3.338(3), 3.297(4)
K2-C31, K2-C32, K2-C33	3.277(3), 3.331(4), 3.121(3)
K1-O1-K2, K1-O2-K2	92.66(6), 93.09(6)
O2-K1-O1, O2-K2-O1	83.20(6), 83.45(6)
C1-O1-K1, C1-O1-K2	137.76(19), 127.54(19)
C25-O2-K1, C25-O2-K2	128.59(17), 136.20(17)

3.3.2.2 Synthesis of [(THF)Li(μ²- OTer^{Mes})]$_2$, ***3.4***

The rationale behind this reaction was to attempt to substitute the chloride ligands of **3.2** with neosilyl groups by a salt elimination reaction to form LiCl as shown in Equation 3.2.

$$\underset{\textbf{3.2}}{ThCl_2(OTer^{Mes})_2DME} + 2LiCH_2SiMe_3 \xrightarrow{X} Th(OTer^{Mes})_2(CH_2SiMe_3)_2DME + 2LiCl \quad \textbf{(3.2)}$$

Attempted nucleophillic substitution with neosilyl lithium

This reaction took place at room temperature, so it may be the case that this reaction is temperature sensitive and the reactivity discussed below is a result of decomposition. Whilst decomposition may be expected in formation of the majority of actinide alkyls at room temperature, there is some literature precedent for successful actinide alkylations forming heteroleptic complexes being performed at room temperature.[42] The reaction mixture was a yellow THF solution and the crystals obtained from a saturated hexane solution held at a temperature of -30°C, following work-up of this reaction were colourless and characterised as [(THF)Li(μ²- OTer^{Mes})]$_2$, **3.4** (**Figure 3.5**).

Selected bond angles and distances calculated from the solid state structure of **3.4**, are shown in **Table 3.4**.

The ^{1}H NMR spectra, measured in C_6D_6, in great similarity with **3.3** showed a few small shifts from the spectra of **3.2**, with the exception of the obvious replacement of DME by THF molecules, as could be easily seen by the multiplicity of the resonances.

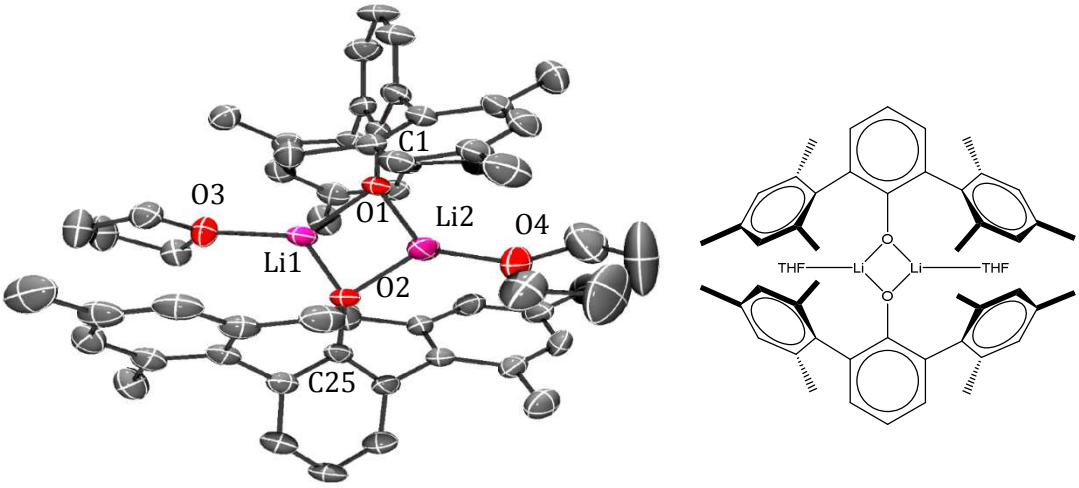

Figure 3.5: Displacement ellipsoid drawing of the solid-state molecular structure of $[(THF)Li(\mu^2\text{- }OTer^{Mes})]_2$, **3.4** (50% probability ellipsoids). Hydrogen atoms are omitted for clarity.

This is a novel crystal structure, as although the lithium salt of the mesityl ligand, has been used before,[8-12] the crystal structure database shows no structure of the THF bound adduct. The solid state molecular structure of **3.4** shows the two lithium-atoms bridging between the two oxygen-atoms of the terphenolates forming a four-membered ring. This causes the formation of a near planar Li-O-Li-O bimetallacyclic ring with a torsion angles ranging from 2.1-2.2° between the four atoms in the ring. This is in contrast to the potassium analogue, **3.3,** where the 4-membered ring is not planar and is likely due to the relative sizes of the lithium and potassium cations rather than any electronic effects.

Another characteristic of this structure is that the lithium-bound THF molecules are almost parallel to the Li-O-Li-O ring with torsion angles of 172.4° and 169.0°. This is contrasting to **3.2** where the THF molecules where orthogonal to the central bimetallic ring system. This may be another effect due to the relative sizes of the lithium and potassium cations. It is also observed that the central phenyl rings of the terphenolate ligands are orthogonal to one another which is in contrast to the structure of **3.1**, **3.2**

and **3.3**. This is again likely due to the relative sizes of a lithium cation against a potassium or thorium cation affecting the sterical considerations of the bulky terphenolate ligands.

It is proposed that lithium π-interactions with phenyl rings being less favoured than potassium π-interactions with the aryl rings results in the THF molecules being able to bind in a higher symmetry mode. Selected examples illustrating the different co-ordination modes exhibited by potassium and lithium atoms to identical ligands are displayed in **Scheme 3.2**.[53, 54]

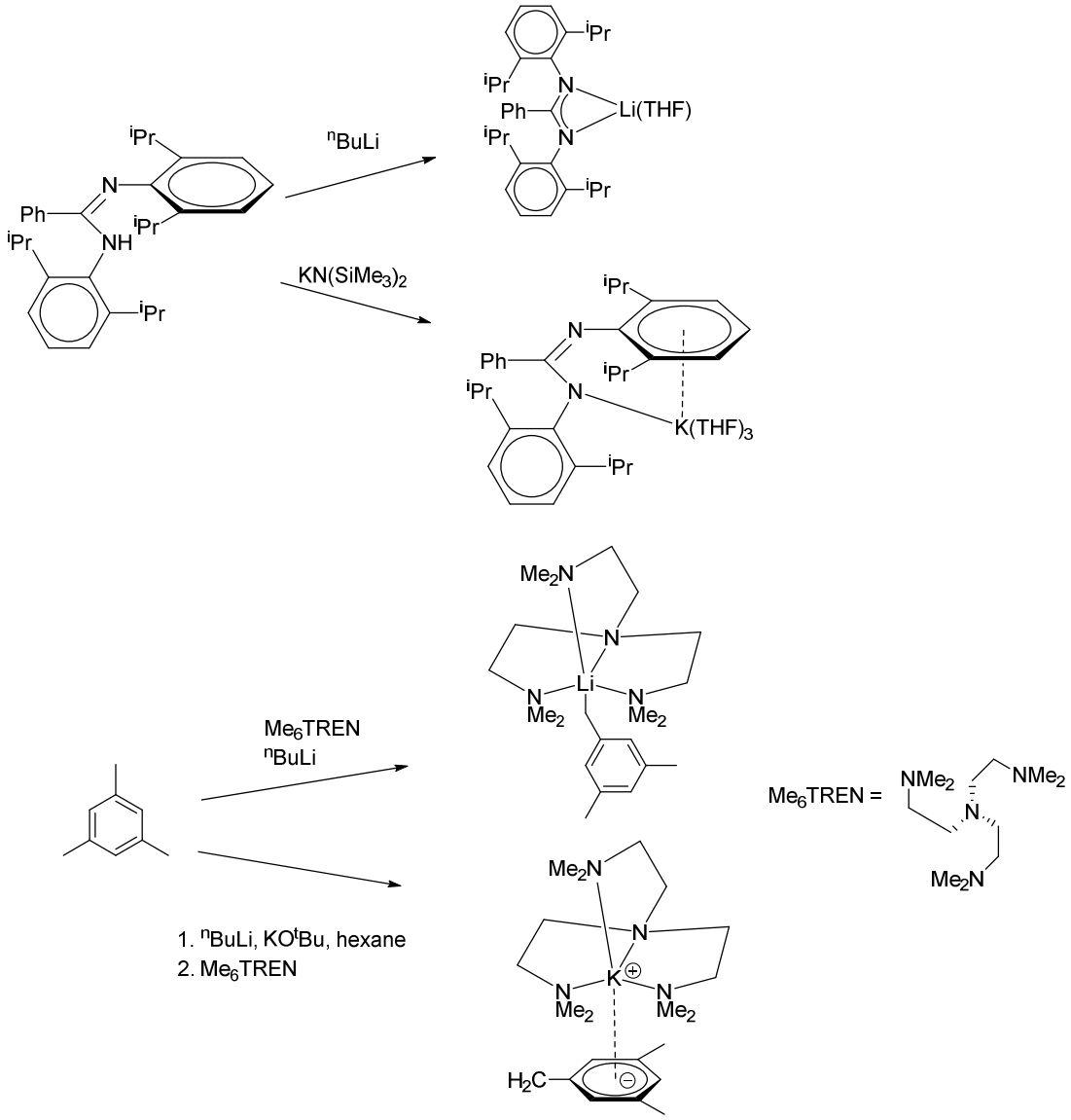

Scheme 3.2: Selected examples of differential binding modes by lithium and potassium to the same ligand[53, 54]

The Li1-O1,2 bond distances of 1.857(6), 1.804(5), 1.841(5) and 1.849(5) Å are all relatively short compared to those reported within the literature.[27] When comparison is limited to 3-co-ordinate lithium atoms with oxygen interactions this bond distance becomes typical.[27] These bond distances are far shorter than those seen in **3.3** and this is most likely due to the size of the lithium cation relative to the potassium cation increasing the electrostatic attraction between the oxygen and metal atom. As is to be expected the neutral Li-O^{THF} bond distances are longer than the bridging Li-$O_{terphenolate}$ distances.

The C-O bond distances of 1.324(3) and 1.331(3) Å in the terphenolate moiety are typical for this class of compounds.[27] These bond distances are slightly longer than those seen in **3.3**.

The result of this reaction may stem from similar arguments as those seen in **3.3.1**. Lithium organometallic reagents are known to be able to act as reducing agents. As such the most significant consideration in explaining the formation of **3.4** is redox transmetallation, with reduction of the thorium centre, accompanied by the lithium requiring a negative charge to compensate and abstracting a terphenolate ligand. It may be expected that the formation of the highly thermodynamically stable lithium chloride ($\Delta_f G°_{LiCl}$ = -408.6 KJ mol^{-1})[38] would be favoured however, it is unlikely that the identity of the ligand has a significant role in the formation of the products of this reaction.

Table 3.4: Selected distances and angles for **3.4**

Atoms	Distance (Å) / angle (°)
Li1-O1, Li2-O1	1.857(6), 1.804(5)
Li1-O2, Li2-O2	1.841(5), 1.849(5)
Li1-O3, Li2-O4	1.899(6), 1.898(5)
Li1-Li2	2.416(9)
C1-O1, C25-O2	1.319(4), 1.328(4)
Li1-O1-Li2, Li1-O2-Li2	82.4(2), 81.6(2)
O2-Li1-O1, O2-Li2-O1	97.1(3), 98.7(2)
C1-O1-Li1, C1-O1-Li2	139.6(2), 133.8(2)
C25-O2-Li1, C25-O2-Li2	131.4(2), 145.3(2)

*3.3.2.3 Synthesis of μ^3-(Ter^{Mes}O)μ^3-(CH_2SiMe_3)$_3Li_4$, **3.5***

As covered in **3.2.1** the structure of **3.1** suggested that small molecule activation would be unlikely as formation of alkyl and hydride complexes of thorium was not likely to be facile or perhaps even possible. Despite this attempts were made to attempt to synthesise an alkyl terphenolate complex of thorium using this complex with the aim of in desired product being potentially able to facilitate small molecule activations.

$$\underset{\textbf{3.1}}{ThCl_2(OTer^{Mes})_2(H_2O)_3} + 5LiCH_2SiMe_3 \xrightarrow{\times} Th(OTer^{Mes})_2(CH_2SiMe_3)_2 + 2LiCl + 3\ LiOH + 3\ CH_3SiMe_3 \quad \textbf{(3.3)}$$

Attempted reaction of **3.1** with five equivalents of neosilyl lithium

Reaction of five equivalents of neosilyl lithium ($LiCH_2SiMe_3$) and **3.1**, in a toluene solution at room temperature, resulted in the isolation of a crystalline material after workup. The desired product of this reaction (see Equation 3.3) was not synthesised but rather a distorted cubane type structure, μ^3-(Ter^{Mes}O)μ^3-(CH_2SiMe_3)$_3Li_4$, **3.5**, the solid structure of which is displayed in **Figure 3.7**. Selected bond angles and distances calculated from the solid state structure of **3.5**, are shown in **Table 3.5**.

The solid state structure of **3.5** consists of a central Li_4 tetrahedron, with the three neosilyl and one terphenolate ligand capping each face of the tetrahedron, thus binding to 3 separate lithium atoms in the cluster. Two of the neosilyl ligands participate in agostic interactions between one of the C-H bonds of the $SiMe_3$ groups and a neighbouring lithium cation.

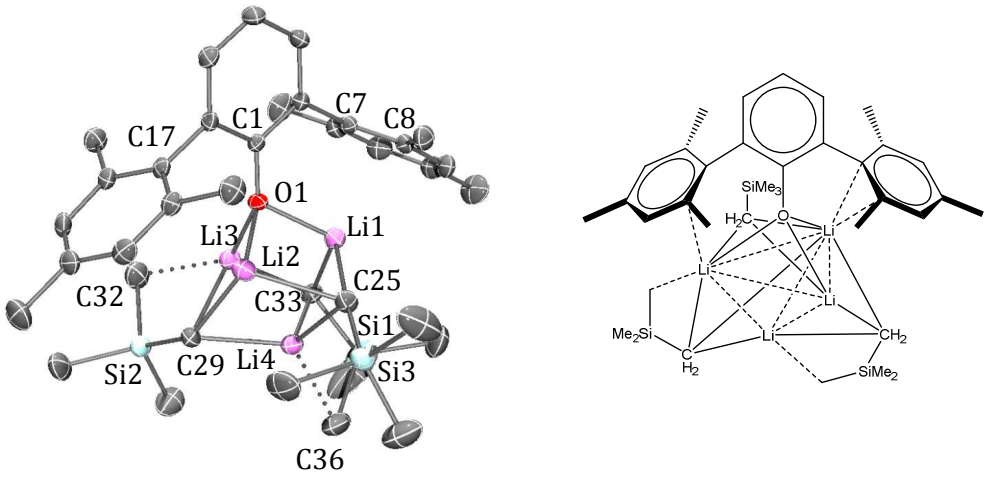

Figure 3.7: Displacement ellipsoid drawing of the solid-state molecular structure of μ^3-($Ter^{Mes}O$)μ^3-$(CH_2SiMe_3)_3Li_4$, **3.5** (50% probability ellipsoids). Hydrogen atoms are omitted for clarity.

The internal Li-Li-Li angles of the Li_4 tetrahedron do not deviate greatly from the idealised internal tetrahedral angle of 60°. The distances between the Li atoms is around 2.5 Å for all distances apart from the Li1-Li2 interaction which is longer at 2.689 Å, representing a 0.2 Å increase on the other Li-Li interactions. The reason for the Li1-Li2 distance being longer than the other Li-Li interactions within the structure of **3.5**, may result from these cations not undergoing γ-agostic interactions with a carbon of the $SiMe_3$ groups. The Li-Li distances are typical for all Li-Li interactions.[27] These distances remain typical when only considering Li-Li distances within cubane-type structures.[27] The sum of the covalent radii of two lithium centres is 3.04 Å,[38] which is considerably longer than the Li-Li distances in **3.5**. However, the sum of ionic radii for 4-co-ordinate lithium cations (1.18Å)[38] is much smaller than the Li-Li distances observed in **3.5**. This is suggestive of the interactions within this cluster being extremely weak, if not non-existent.

Each lithium atom in the solid state structure of **3.5**, binds to three atoms in the cubane structure, thus bridging η^3. In the case of Li1,2,3 this involves ligating to two carbon atoms and one oxygen atom, whereas Li4 η^3 bridges three carbon atoms. Each one of these cubane corner atoms (O1, C25, C29 and C33) also η^3 bridge to three lithium cations, which is fairly common in lithium cluster chemistry.[27] The bond lengths of the

η^3 Li-C bonds in **3.5** are in the range of 2.20 to 2.27 Å, which is typical for the bond lengths seen for these interactions in the literature.[27]

The Li-O distances of **3.5**, are longer than those seen in **3.4**, which is to be expected due to the oxygen bridging three lithium centres in **3.5** compared to two in **3.4.** The Li3-O1 is around 0.05 Å shorter than the Li2-O1 and Li1-O1 bonds and this is likely due to the more obtuse C1-O1-Li3 angle of 147.25(14)°, which is around 30° wider than those observed for C1-O1-Li1,2. A factor in this slight distortion is the agostic interaction experienced by Li3, which Li1 and Li2 do not experience. A further factor is that Li1 and Li2 are observed to experience aryl interaction with carbons of the mesityl rings of the terphenolate ligand. Li1 undergoes an aryl interactions with C7 and C8, whilst Li2 undergoes an aryl interaction with C17. These η^2 and η^1 type interactions are fairly typical for lithium aryl interactions. The bond distances of 2.602(3), 2.589(3) and 2.666(3) Å for Li1-C7, Li1-C8 and Li2-C17 respectively are typical for aryl lithium interactions. The C-O bond distance in **5**, of 1.3385(18) Å, is within s.u.s of the C-O bond distance in **3.4**, whilst being longer than the analogous bond in **3.3**, but in similarity with **3.4**, not massively so. A comparison of the C-O bond distances in **3.1** and **3.2**, to **3.5** finds that these bond distances are also within s.u.s.

There is a clear difference in the geometry of the three bridging neosilyl groups in **3.5,** with two distinctive geometries. The first geometry is adopted by C25-Si1 neosilyl group, whilst the second geometry is adopted by the C29-Si2 and C33-Si3 neosilyl groups. The difference in geometry of the neosilyl groups arises from whether a carbon of the $SiMe_3$ group undergoes agostic interactions with adjacent lithium cations or not. In the case of the C25-Si1 neosilyl group there is no agostic interaction, as borne out by the Li1-C25-Si1 bond angle of 175.27(13)° which is far more linear than any of the other Li-C-Si angles within **3.5**. The Li2-C29-Si2 and Li3-C33-Si3 bond angles of 147.23(13) and 149.77(13)° respectively, indicate a far more bent bond which is required in order for the agostic interactions to occur. The agostic interactions themselves are shown by Li-C bond distances of around 2.50 Å for Li3-C32 and Li4-C36 which are longer than interactions where the agostic interaction has progressed to the point of lithiation, (2.333 Å) as is the case in **A**[55] shown in **Figure 3.6.** This is to be expected as the Li-C interaction has progressed to the point of deprotonation in **A**, which is not the case in **3.5**.

A side effect of the geometric rearrangement of the $SiMe_3$ groups in order to incorporate the agostic interactions to Li3 and Li4 is a substantial shortening, of 0.5 Å, of the Li-Si distance compared to Li1 and Li2. Li3-Si2 and Li4-Si3 have bond distances of 2.818(3) and 2.829(3) Å respectively, whereas Li1-Si3 and Li2-Si1 have respective bond distances of 3.492(3) and 3.397(3) Å. Li4-Si1 is also substantially longer than the 'agostic' silicon to lithium bond distance. The 'agostic' Li-Si bond distances are short for all β-Li-C-Si interactions, perhaps suggesting that there is an interaction between the lithium and silicon atoms as well as the agostic interactions between the C-H bonds.

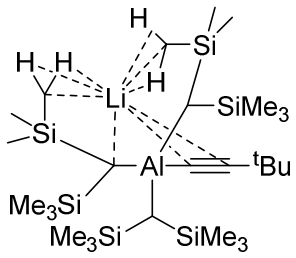

A

Figure 3.6: An example of lithiation of trimethylsilyl groups[55]

The room temperature ^1H NMR spectrum of a C_6D_6 solution of **3.5** shows that the solid state structure of **3.5** is not maintained on an NMR timescale in solution. This is due to all of the neosilyl groups appearing as the same resonances, and is not unexpected due to the presumed fluxionality of **3.5** in solution. The CH_2 groups appear as a singlet at -2.54 ppm, whilst the $SiMe_3$ groups appear as a broad singlet at 0.12 ppm. The resonances assigned to the $Ter^{Mes}O$ ligands do not show any great shift from the spectra of **3.1-3.4**.

Table 3.5: Selected distances and angles for **3.5**

Atoms	Distance (Å) / angle (°)
Li1-O1, Li2-O1, Li3-O1, C1-O1	1.930(3), 1.934(3), 1.876(3), 1.3385(18)
Li1-C25, Li2-C25, Li4-C25	2.271(4), 2.265(4), 2.229(4)
Li2-C29, Li3-C29, Li4-C29	2.245(3), 2.254(4), 2.229(3)
Li1-C33, Li3-C33, Li4-C33	2.199(3), 2.244(3), 2.246(4)
Li2-C17, Li1-C7, Li1-C8	2.666(3), 2.602(3), 2.589(3)
Li1-Li2, Li1-Li3, Li1-Li4	2.689(4), 2.495(4), 2.523(4)
Li2-Li3, Li2-Li4, Li3-Li4	2.488(4), 2.467(4), 2.508(4)
Li4-Si1, Li2-Si1, Li3-Si2, Li1-Si3, Li4-Si3	3.360(4), 3.397(3), 2.818(3), 3.492(3), 2.829(3)
Li3-C32, Li4-C36	2.493(4) , 2.500 (4)
Li1-Li2-Li3, Li1-Li2-Li4, Li1-Li3-Li4, Li1 Li4 Li3	57.45(11), 58.39(11), 60.57(12), 59.45(12)
Li2- Li3- Li1, Li2-Li3-Li4, Li2-Li4-Li1, Li2-Li1-Li4	65.33(12), 59.18(12), 65.21(12), 59.98(12)
Li2-Li1-Li3, Li2-Li1-Li4, Li4-Li2-Li3, Li2-Li4-Li3	57.22(12), 56.40(11), 60.80(12), 60.01(12)
Li1-C25-Si1, Li2-C25-Si1 ,Li4-C25-Si1	175.27(13), 111.57(11), 111.28(11)
Li2-C29-Si2, Li3-C29-Si2, Li4-C29-Si2	147.23(13), 86.34(10), 121.77(12)
Li1-C33-Si3, Li3-C33-Si3, Li4-C33-Si3	119.67(12), 149.77(13), 87.16(10)
C1-O1-Li1, C1-O1-Li2, C1-O1-Li3	119.43(13), 120.78(13), 147.25(14)

3.3.3 Group I, group III mixed metal transmetallation systems

3.3.3.1 Synthesis of $LiAlH_2(\mu^2\text{- }OTer^{Mes})_2$, ***3.6***

The rationale behind this reaction was to attempt to substitute the chloride ligands of **3.2** with hydride ligands by a salt elimination reaction to form $LiAlH_3Cl$ (Equation 3.4).

$$ThCl_2(OTer^{Mes})_2DME + 2LiAlH_4 \not\longrightarrow ThH_2(OTer^{Mes})_2DME + 2LiAlH_3Cl \qquad (3.4)$$

3.2

Attempted hydride formation using $LiAlH_4$

This reaction was carried out at room temperature, so it may be the case that this reaction is temperature sensitive and the reactivity discussed below is a result of decomposition. The product mixture was a colourless solution, with a shiny metallic mirror formed on the surface of the glassware. Following work-up of this reaction

colourless crystals were grown from the hexane solution and characterised as $LiAlH_2(\mu^2$- $OTer^{Mes})_2$, **3.6** (**Figure 3.8**). Selected bond angles and distances calculated from the solid state structure of **3.6**, are shown in **Table 3.6**.

The ^{1}H NMR spectrum of a solution of **3.6** in C_6D_6, showed a resonance at -0.4 ppm, which was assigned to the aluminium hydride resonances. The terphenolate resonances did not shift by more than 0.1 ppm compared to the starting materials. It also clearly showed the formation of hydrogen gas, suggesting that $LiAlH_4$ was acting as a reducing agent, which when combined with the metallic mirror suggests that thorium was reduced to its elemental form. (Equation 3.5)

$$\underset{\textbf{3.2}}{ThCl_2(OTer^{Mes})_2DME} + 2LiAlH_4 \longrightarrow \underset{\textbf{3.6}}{LiAlH_2(OTer^{Mes})_2} + Th + 2H_2 + LiAlCl_2H_2 + DME \quad \textbf{(3.5)}$$

This is a novel crystal structure, and the solid state structure **3.6** is shown with a Li-O-Al-O bimetallacyclic ring which is nearly planar with torsion angles of 1.1° within the four membered ring. This is in contrast to **3.3** in **Figure 3.4** (*3.3.2*) where the 4-membered ring was not planar. However, this agrees with **3.4** in **Figure 3.5**, (*3.3.3*) which also showed a highly planar ring system.

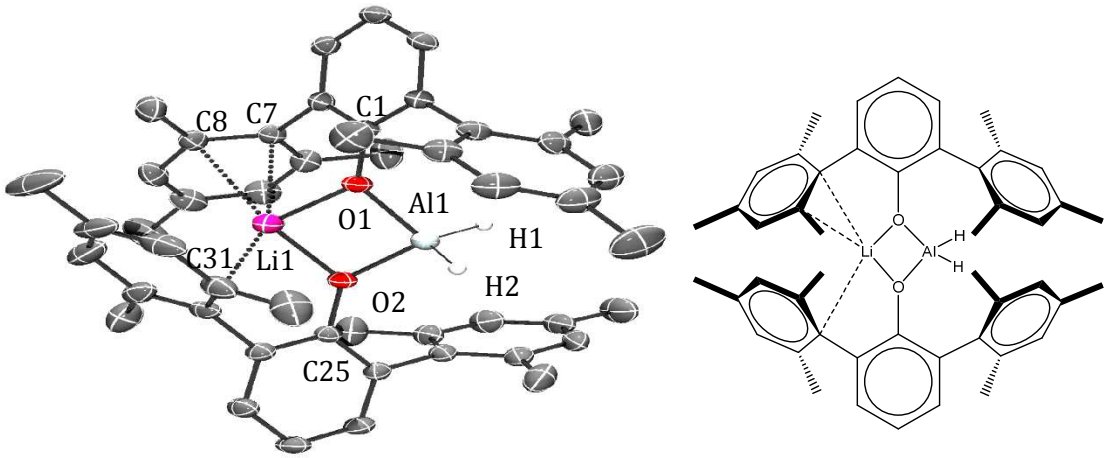

Figure 3.8: Displacement ellipsoid drawing of the solid-state molecular structure of $LiAlH_2(\mu^2$-$OTer^{Mes})_2$, **3.6** (50% probability ellipsoids). Hydrogen atoms are omitted for clarity.

The lithium in **3.6** is donor-solvent free and as such the lithium atom experiences π-interactions with the two phenyl rings. Donor-solvent free lithium 'ate' systems as monomers are rare as usually polymeric chains are formed.[56] The inability of this

system to polymerise is likely due to the steric bulk of the ligands being too great for this to be favourable hence allowing the π-interactions with the two phenyl rings to occur. It is η^1 co-ordinated to one phenyl ring and η^2 co-ordinated to another, precedent for which is limited to three examples in the literature, of which only one does not contain terphenolate ligands.[57]

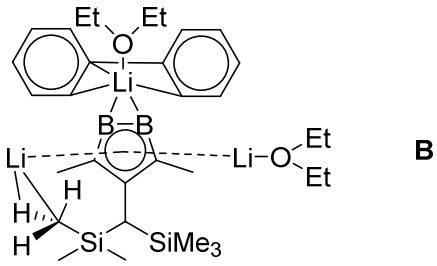

Figure 3.9: Precedent for a lithium atom undergoing η^1 and η^2 co-ordination to separate phenyl rings[57]

In **B** (**Figure 3.9**) the Li-C distances are much shorter than in **3.6** with distances of 2.261(7) Å, 2.713(6) Å and 2.306(7) Å, respectively. None of these distances are statistically equivalent to the distances of 2.585(4), 2.670(3) and 2.675(4)Å, in the solid state structure and with the exception of the second quoted distance the Li-C distances in **3.6** are considerably longer. There are two further examples (**C** and **D**) within the literature of a phenyl ring η^2 bound to a lithium atom[58, 59] (**Figure 3.10**) with Li-C distances of 2.45(2) Å, 2.54(2) Å and 2.289(7) Å, 2.497(6) Å respectively. These distances are also substantially different from the distances within the solid state structure of **3.6** and again the Li-C distances within the solid state structure of **3.6** are considerably longer than those quoted within the literature.

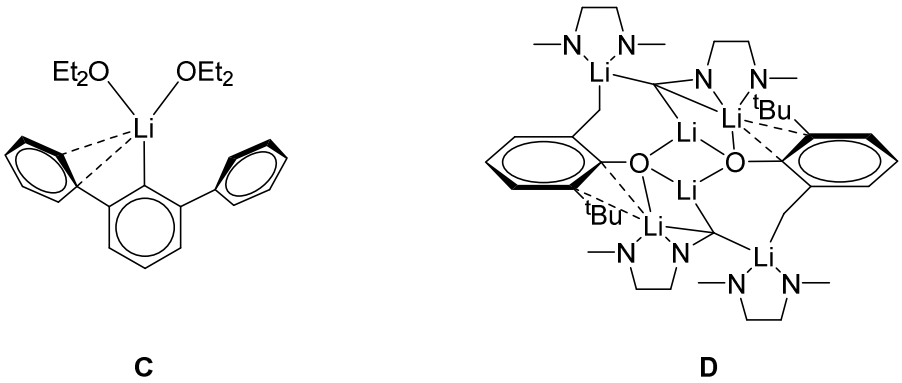

Figure 3.10: Literature examples of η^2 ligation to a phenyl ring by lithium cations[58, 59]

In comparison with **3.5**, the Li-aryl interactions of **3.6**, are very similar. The bond distance of the η^1 Li-C interaction of **3.5** is 2.666(3) Å, which is identical to the analogous distance in **3.6** of 2.675(4) Å within s.u.s. The bond distances of the η^2 Li-C interactions of **3.5** are 2.602(3) and 2.589(3) Å, which are similar to the analogous distances in **3.6** of 2.585(4) and 2.670(3) Å with the shorter distance identical within s.u.s. The Li-C distances of $LiAlH_2(OTer^{Mes})_2$ when considering all of the literature values for a phenyl ring carbon interacting with a lithium atom are long[27] and are very comparable in length to the bond lengths reported in two similar terphenyl systems.[60] These similar terphenyl systems were also bimetallic, and contained calcium, **E,** and strontium **F**. (**Figure 3.11**)

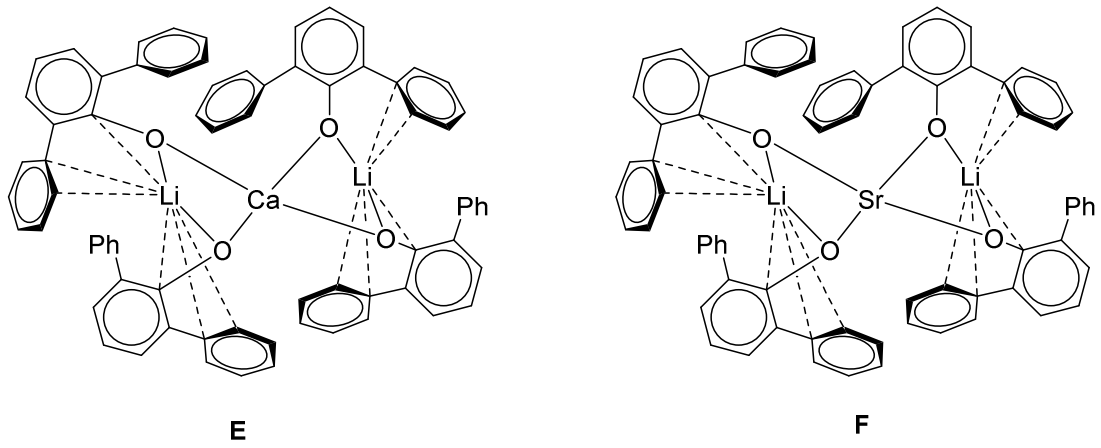

Figure 3.11: Precedent for terphenolate complexes with η^1 and η^2 co-ordination to separate phenyl rings[60]

The aluminium hydride atoms were located crystallographically and the resultant Al-H distances of 1.52(3) Å and 1.54(3) Å fall within the expected distances for terminal aluminium hydride bonds as 70 % of all aluminium hydride bonds distances fall within the range of 1.4 to 1.7 Å in length.[27]

The Li-O bond lengths in **3.6**, of 1.897(3), 1.919(3) Å are longer than those seen for **3.4**, and comparable to those seen for **3.5**, this lengthening of the Li-O bond compared to **3.4** is likely due to the effect of the increased oxophilicity of aluminium when compared to lithium (Standard enthalpy of formation of Al-O is 512(4) KJ/mol compared to 341(6) KJ/mol for Li-O)[38] and the aryl interactions which lithium participates in potentially weakening the Li-O bond. The Al-O bond distance in **3.6** are typical for all

aluminium oxygen interactions.[27] The Al-Li distance is also typical for all oxygen bridged aluminium lithium species.[27]

Table 3.6: Selected distances and angles for **3.6**

Atoms	Distance (Å) / angle (°)
Li1-O1, Li1-O2	1.897(3), 1.919(3)
Al1-O1, Al1-O2	1.8173(12), 1.8122(12)
Al1-H1, Al1-H2	1.54(3), 1.52(3)
C1-O1, C25-O2	1.3678(17), 1.3609(17)
Li1-C7, Li1-C8, Li1-C31	2.585(4), 2.670(3), 2.675(4)
Li1-Al1	2.741(3)
Li1-O1-Al1	95.04(10), 94.45(10)
H1-Al1-H2	116.8 (1)
O2-Li1-O1	82.59(13)
O2-Al1-O1	87.89(5)
C1-O1-Li1, C25-O2-Li1	126.50(13), 125.26(13)
C1-O1-Al1, C25-O2-Al1	128.38(10), 133.27(10)

3.3.4 Group II transmetallation

*3.3.4.1 Synthesis of $MgCl(OTer^{Mes})(THF)_2$, **3.7***

As covered in *3.2.1* and *3.3.2.3* the structure of **3.1** suggested that small molecule activation would be unlikely as formation of alkyl and hydride complexes of thorium was not likely to be facile or perhaps even possible. Despite this further endeavours were made to attempt to synthesise an alkyl terphenolate complex of thorium using this complex with the aim of in desired product being potentially able to facilitate small molecule activations.

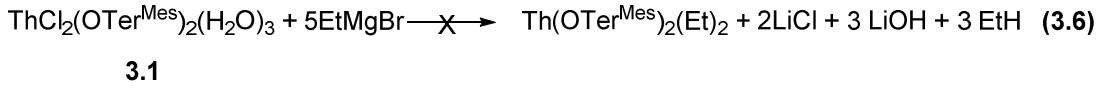

Attempted reaction of 3.1 with five equivalents of ethyl magnesium bromide

Equation 3.6 shows the attempted reaction of five equivalents of ethyl magnesium bromide with **3.1**. This reaction required five equivalents to reach the desired product as the ethyl magnesium bromide reagent can act as both a nucleophile and a base and

the presence of the aqua ligands with acidic protons is likely to present a reaction with alternate pathways, which is not desirable.

Reaction of five equivalents of ethyl magnesium bromide in THF solution (EtMgBr) and **3.1**, in a deuterated benzene solution at room temperature, after workup resulted in the isolation of a crystalline material. The desired product of this reaction (see Equation 3.8) was not synthesised but rather the product of ligand and halide redistribution, $MgCl(OTer^{Mes})(THF)_2$, **3.7, Figure 3.12**. Selected bond angles and distances calculated from the solid state structure of **3.7**, are shown in **Table 3.7**.

The solid state structure of **3.7** displayed in **Figure 3.12**, shows near tetrahedral geometry around the magnesium cation, with an expected steric distortion from the idealised internal tetrahedral angles by the chloride and terphenolate ligands (O1-Mg1-Cl1 126.9(6)°) due to their relative sizes compared to the THF ligands. The Mg1-Cl1 bond distance of 2.450(9) Å, is typical for Mg-Cl bond distances in the literature.[27] The Mg1-O1 bond distance (1.851(17) Å) is shorter than metal-O1 distances seen for **3.1-3.3** and **3.5-3.6.** In the case of **3.1** and **3.2** this is due to the relative sizes of a magnesium and thorium cation. In the case of **3.3**, **3.5** and **3.6**, the Mg-O bond is shorter as it is not bridging two or more metal centres. The $Mg\text{-}O_{terphenolate}$ bond distance is short for all Mg-O bond distances.[27] It is also short for Mg-O bonds in which the oxygen atom is not bridging and for magnesium alkoxide bonds.[27] The $Mg\text{-}O_{THF}$ distance is longer than that seen for lithium in **3.4**, and shorter than that seen for potassium in **3.3**, as is to be expected. The C1-O1 bond distance is fairly imprecise in comparison to those seen for **3.1-3.6**, which is a function of this being the poorest crystal data (R_1= 0.1243 wR^2= 0.3378) presented thus far. However, it is amongst the shortest observed so far, with only **3.3** having a comparable $C\text{-}O_{terphenolate}$ bond distance.

The room temperature ^1H NMR spectrum of a C_6D_6 solution of **3.7**, shows very small shifts in the resonances assigned to $Ter^{Mes}O$ from free ligand or compounds **3.1-3.6**.

This result indicates that the only reactivity that **3.1** was likely to undergo would have been transmetallation and as such represented a synthetic dead end. To this end, further reactivity studies upon **3.1** were halted and focus was trained upon the reactivity of **3.2.**

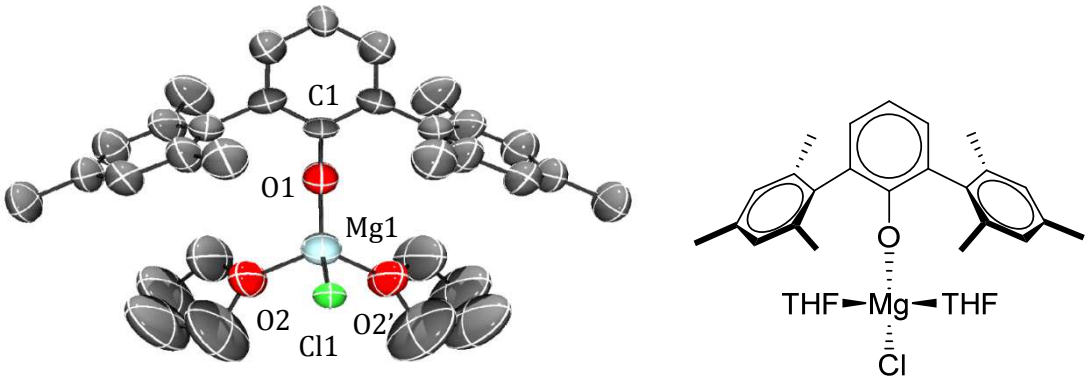

Figure 3.12 Displacement ellipsoid drawing of the solid state molecular structure of $MgCl(OTer^{Mes})(THF)_2$ **3.7**. Hydrogen atoms are omitted for clarity.

Table 3.7: Selected distances and angles for **3.7**

Atom	Distance (Å) / angle (°)
Mg1-Cl1	2.450(9)
Mg1-O1, Mg1-O2	1.851(17), 2.012(13)
C1-O1	1.31(2)
C1-O1-Mg1	162.0(14)
O1-Mg1-Cl1, O1-Mg1 -O2	126.9(6), 108.0(5)
O1-Mg1-O2', O2-Mg1-O2', O2-Mg1-Cl1	108.0(5), 101.3(9), 104.9(5)

*3.3.4.2 Synthesis of $MgBr(OTer^{Mes})(THF)_2$, **3.8***

Reaction of two equivalents of bromo-magnesium acetylide in THF solution (BrMgCCH) and **3.2**, in a toluene solution at room temperature, after workup resulted in the isolation of a crystalline material. The desired product of this reaction (see Equation 3.7) was not synthesised but rather the product of transmetallation, $MgBr(OTer^{Mes})(THF)_2$, **3.8, Figure 3.13** . Selected bond angles and distances calculated from the solid state structure of **3.8**, are shown in **Table 3.8**.

$$\underset{\textbf{3.2}}{ThCl_2(OTer^{Mes})_2(DME)} + 2BrMgCCH \xrightarrow{X} Th(OTer^{Mes})_2(CCH)_2 + 2BrMgCl \quad \textbf{(3.7)}$$

Attempted reaction of **3.1** with five equivalents of ethyl magnesium bromide

The solid state structure of **3.8** displayed in **Figure 3.13,** shows near tetrahedral geometry around the magnesium cation, with an expected steric distortion from the

idealised internal tetrahedral angles by the bromide and terphenolate ligands (O1-Mg1-Br1 124.80(6)°) due to their relative sizes compared to the THF ligands. This distortion is very similar to the one observed in the chloride analogue, **3.7**. However, the effect of this distortion upon the THF ligands is greater in **3.8** than in **3.7**. There is greater distortion from the idealised tetrahedral angle in **3.8** than in **3.7**, as shown by the angles in **Table 3.8**. This greater distortion may have resultant affects upon the structure of **3.7.**

The Mg1-Br1 bond distance of 2.4381(8) Å, is slightly shorter than the Mg-Cl distance seen in **3.7,** which given that a bromide anion is larger than a chloride anion, appears slightly unusual (181 pm is the ionic radius of chloride whilst the ionic radius of bromide is 196 pm).[38] However, this observation is likely due to packing effects as the geometry of **3.8** is not a direct analogue of **3.7**. This non-direct analogy between **3.7** and **3.8** is borne out by the difference in lattice system between **3.7** and **3.8**, as **3.7** was solved in the orthorhombic crystal system, whilst **3.8** was solved in the monoclinic crystal system. The Mg-Br bond is also short for all Mg-Br bonds.[27]

The Mg1-O1 bond distance in **3.8**, of 1.8620(15) Å is identical within s.u.s to that seen in **3.7**, and as such is shorter than those seen in **3.1-3.3** and **3.5-3.6** for the same reasons that were covered in *3.3.4.1*. The Mg-O_{THF} distances (Mg1-O2,3) are also identical to those seen in **3.7** within s.u.s. The C1-O1 bond distance in **3.8**, in unsurprising similarity to **3.7**, is amongst the shortest observed in this work so far with only **3.3**, exhibiting a shorter distance.

A further difference in the structures between what may have assumed to be halogen analogues of **3.7** and **3.8** are the differences in angles around the central magnesium cation. In the solid state structure of **3.8**, the deviation from the idealised internal tetrahedral angle is greater than that observed in the solid state structure of **3.7**. This is likely to be a result of the increased size of a bromide ion compared to a chloride causing a distortion in the ligation sphere, as well as due to packing effects due to the aforementioned differences in crystal system between **3.7** and **3.8**.

In similarity to **3.7**, the room temperature ^{1}H NMR spectrum of **3.8** shows very small shifts in the resonances assigned to $Ter^{Mes}O$ from free ligand or compounds **3.1-3.6**.

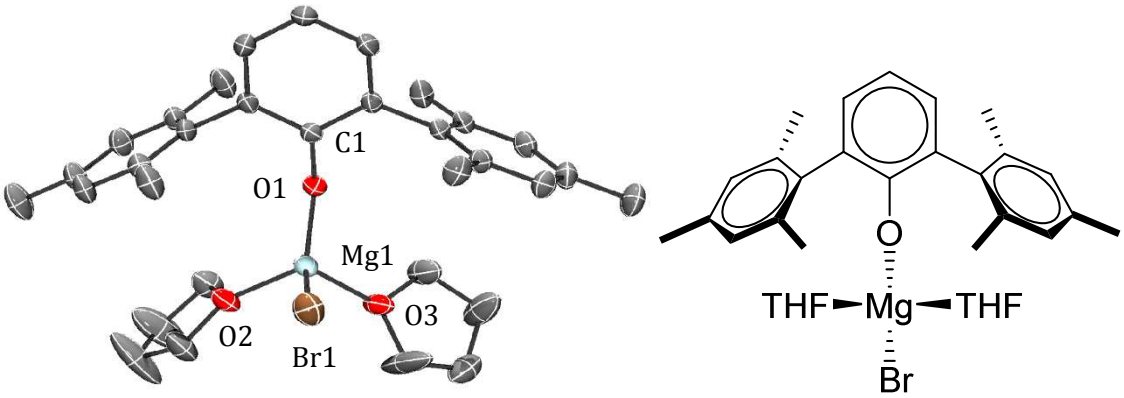

Figure 3.13 Displacement ellipsoid drawing of the solid state molecular structure of $MgBr(OTer^{Mes})(THF)_2$, **3.8**. Hydrogen atoms are omitted for clarity.

Table 3.8: Selected distances and angles for **3.8**

Atom	Distance (Å) / angle (°)
Mg1-Br1	2.4381(8)
Mg1-O1, Mg1-O2, Mg1-O3	1.8620(15), 1.9901(17), 1.9953(17)
C1-O1	1.322(2)
C1-O1-Mg1	137.68(13)
O1-Mg1-Br1, O1-Mg1 -O2	124.80(6), 104.17(7),
O1-Mg1-O3, O2-Mg1-O3	110.87(7), 100.83(8)
O2-Mg1-Br1, O3-Mg1-Br1	106.97(6), 106.55(5)

3.3.5 Transition metal transmetallation

*3.3.5.1 Synthesis of $Fe(OTer^{Mes})_2(py)_2$, **3.9***

The use of group I, II or III transfer reagents in an attempt to form dihydride or dialkyl bis terphenolate thorium complexes resulted in transmetallation (refer to **3.3.3**-**3.3.4** for details). As a result it was proposed that the use of a transition metal transfer reagent may result in the desired products being synthesised. For this purpose an iron alkyl (**Scheme 3.3**) was hoped to afford the target Th^{IV} alkyl.

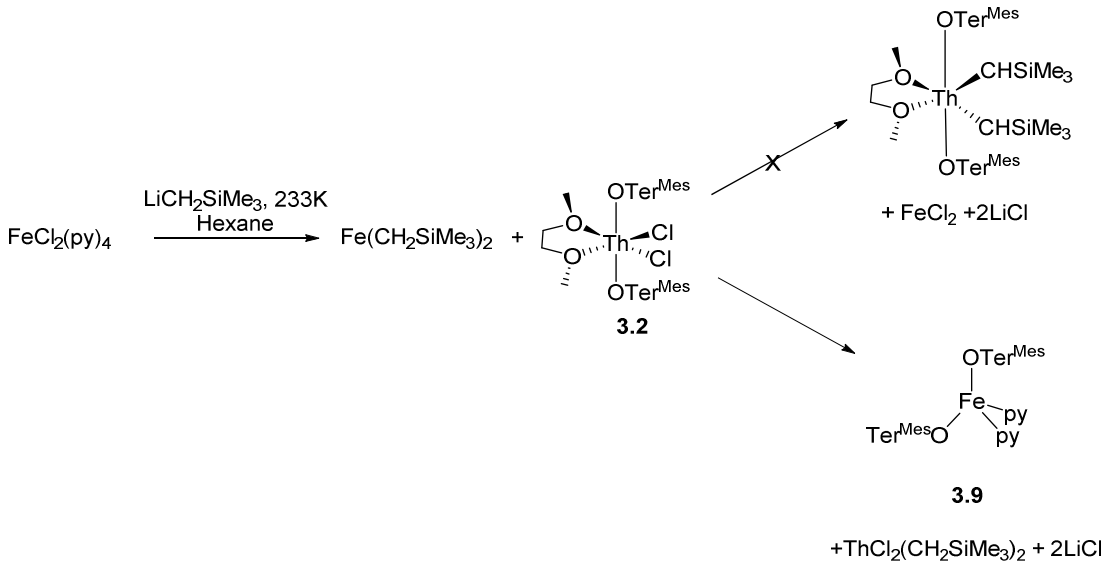

Scheme 3.3: the intended and actual products of using an *in situ* generated iron alkyl as a transfer reagent

It was proposed that iron would be a more suitable transfer reagent for alkyl moieties onto a thorium atom, as it is a 'softer' reagent compared to previously attempted transfer reagents and would perhaps be less like to take part in transmetallation reactions that abstract the terphenolate ligands. Iron organometallic chemistry has been assiduously investigated,[61-63] with alkyl complexes observed to be important intermediates in the extensive field of iron-catalysed cross coupling. Considering this, it was expected that any further alkyl transfer reagents would have the benefit of increased ease of preparation.

However, the reaction of $ThCl_2(OTer^{Mes})_2DME$ and two equivalents of $Fe[CH_2Si(CH_3)_3]_2$ generated *in situ* by reaction of $FeCl_2(py)_4$ with two equivalents of $LiCH_2Si(CH_3)_3$ at -80 °C affords $Fe(OTer^{Mes})_2(py)_2$, **3.9**, as an orange powder in 50% yield after workup (**Scheme 3.3**). Single crystals suitable for X-ray diffraction were grown from a saturated solution of hexane at -30°C; the solid state structure of which is displayed in **Figure 3.18**. Selected bond angles and distances calculated from the solid state structure of **3.9**, are shown in **Table 3.9**.

The solid state structure of **3.9**, shown in **Figure 3.18**, shows a four co-ordinate iron(II) centre bonded in a *pseudo*-tetrahedral fashion to two pyridine molecules and two mesityl terphenolate molecules. The largest distortion of this tetrahedral geometry is

the O1-Fe1-O2 bond angle of 148.87°, which is presumably to accommodate the steric bulk of the terphenolate ligands.

There are six crystallographically characterised examples of iron terphenolate complexes, two of which are four co-ordinate iron(II) terphenolate complexes, **G** and **H**,[64] (see **Figure 3.14**) one which is pyridine ligated, whilst the other is THF ligated.

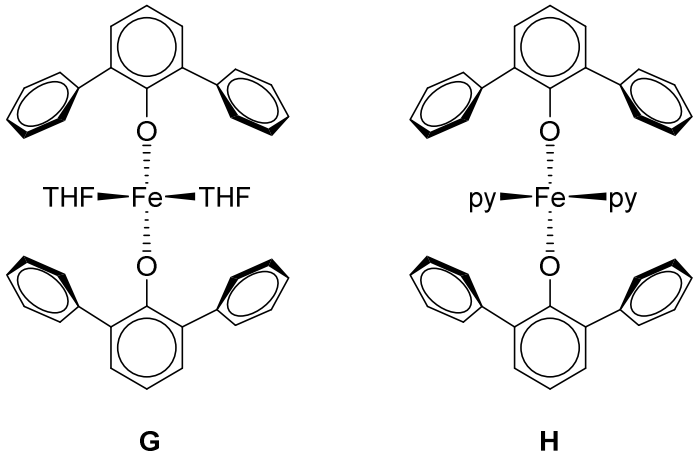

G **H**

Figure 3.14: four co-ordinate iron (II) bis terphenolate complexes in the literature[64]

The other crystallographically characterised iron terphenolate complexes include two mono terphenolate complexes, **I** and **J**,[65, 66] an iron (III) tris terphenolate complex, **K,**[64] (see **Figure 3.15**) and a two-co-ordinate iron (II) complex from Ni and Power, **L**[67] (see **Figure 3.16**).

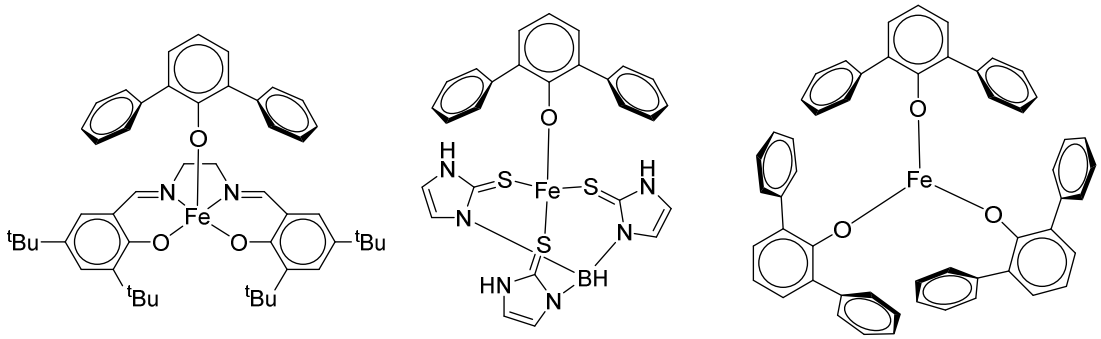

I **J** **K**

Figure 3.15: Other iron (II) terphenolate complexes in the literature[64-66]

In the solid state structure of **3.9**, the Fe-O and Fe-N distances of 1.89(3) Å and 2.12(4) Å respectively, are typical for this type of complex. The Fe-O distances are slightly longer than in **L**, (**Figure 3.16**) as is to be expected.[67] **3.9** is different from previously

reported examples of iron (II) bis terphenolate complexes as it has not been synthesised via the oxidation of a terphenyl iron complex.

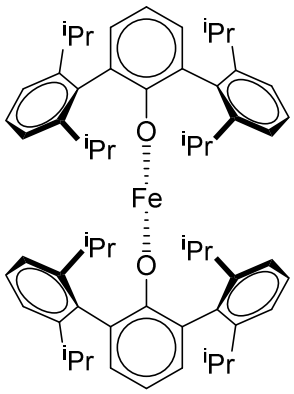

L

Figure 3.16: A two co-ordinate iron (II) terphenolate complex[67]

The formation of **3.9**, represents an unusual example of transition metal transmetallation, which was unexpected especially given that the relative bond dissociation energies of a Th-O and Fe-O bond are 854(13) and 409(13) kJ/mol respectively.[38] Due to the paramagnetism of Fe(II) complexes, no assignable NMR spectra could be obtained.

The results of this reaction are most likely explained by transmetallation of the terphenolate ligand from thorium onto iron. The simplest process by which this occurs is direct transmetallation. However this may not be the process that is most favoured. A multipart process by which the observed reactivity occurs could be a result of catalysis by LiCl in pyridine, (**Scheme 3.4**) or a slight excess of $LiCH_2SiMe_3$ within solution.

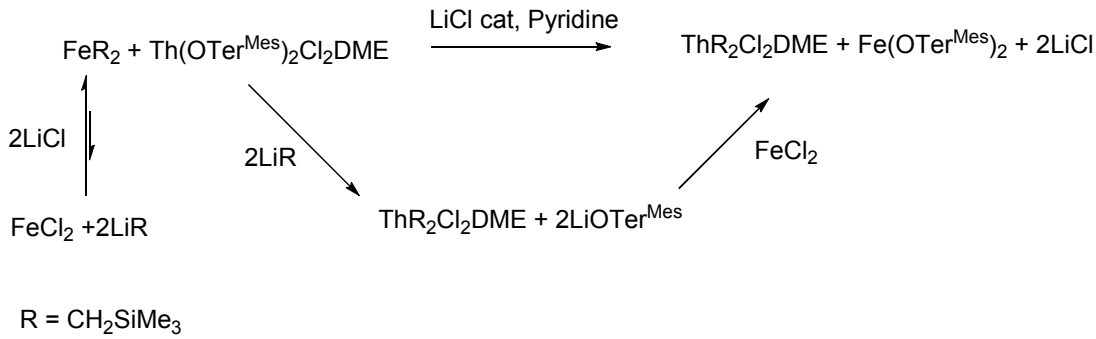

Scheme 3.4: Possible catalytic process by LiCl in pyridine to form **3.9**

The solid state structure of **3.9**, allows for comparison in the geometry of the $Ter^{Mes}O^-$ between the more electrostatic interactions that occur in bonding with thorium and the

greater covalent character of bonding to transition metals. The increased electrostatic character of a bonding interaction in aryloxides should, in theory, result in greater linearity of the M-O-C bond in order to minimise the electrostatic repulsion between the α-carbon and the metal cation (see **Figure 3.17**).[68]

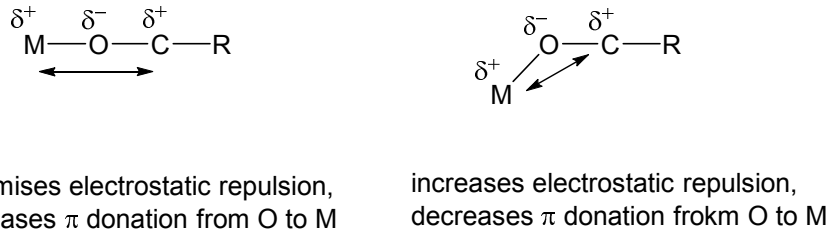

Figure 3.17: The effect of the linearity of aryloxides on electrostatic interaction with the α-carbon

The C1-O1-Fe1 and C25-O2-Fe1 bond angles in **3.9**, are 148.0(3) and 143.9(3)°, respectively. This is substantially more bent than the corresponding C1-O1-M angles in **3.1-3.2**, which appears to support the theory that increased linearity reduces electrostatic repulsion.

Table **3.9**: Selected distances and angles for **3.9**

Atoms	Distance (Å) / angle (°)
Fe1-O1, Fe1-O2	1.894(3), 1.887(4)
Fe1-N1, Fe1-N2	2.127(4), 2.124(4)
C1-O1, C25-O2	1.324(6), 1.327(6)
C25-O2-Fe1, C1-O1-Fe1	143.9(3), 148.0(3)
N1-Fe1-O1, N1-Fe1-O2, N1-Fe1-N2	104.79(17), 97.67(17), 94.26(16)
N2-Fe1-O1, N2-Fe1-O2,	95.21(17), 104.43(17)
O1-Fe1-O2	148.87(15)

As can be seen from the transmetallation result of this reaction, transition metal transfer reagents, and in particular iron transfer reagents were not compatible with this ligand system to transform **3.2** into a desired complex, as such even softer alternatives were examined as to their suitability as shall be seen in *3.3.6.*

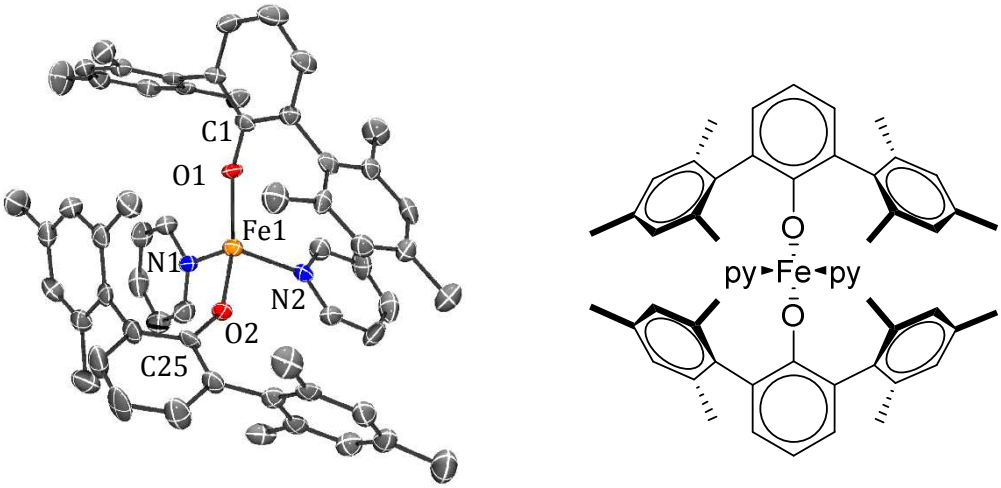

Figure 3.18: Displacement ellipsoid drawing of the solid state molecular structure of **3.9,** $Fe(OTer^{Mes})_2(py)_2$. Hydrogen atoms are omitted for clarity.

3.3.6 Main group reactivity

*3.3.6.1 Reaction of **3.2** with tetra allyl tin*

In the search for softer transfer reagent to avoid the transmetallation chemistry that has dogged the chemistry in this chapter it was decided to attempt to soften both the metal that was transferring the alkyl and the alkyl moiety itself. The use of *tetra* allyl tin satisfied both of these aims. The allyl moiety is softer than the majority of other alkylating reagents attempted due to its ability to adopt η^3 ligation and hence delocalise the charge, whilst tin is, in addition to being a main group metal, fairly heavy, and as such has many electrons in its valence shell, so should be able to be polarised fairly easily. Additionally, the use of a tin reagent introduces an additional NMR handle into the reaction, mostly as a means to ascertain whether the reaction has progressed to completion or not.

The reaction of two equivalents of **3.2** with one equivalent of tetra allyl tin, yielded no reaction according to ^{1}H and ^{119}Sn NMR spectroscopy, with a clear resonance in the ^{119}Sn spectrum indicating unreacted tetra allyl tin. The reaction mixture was left to stir for two months upon which time it was observed that a precipitate had formed. After workup it was found that free ligand had been reformed by NMR spectroscopy. Heating the reaction mixture also resulted in no reaction occurring.

3.3.7 Alternative routes to thorium alkyls

As seen in 3.3.1-3.3.6 traditional routes towards the formation of heteroleptic terphenolate alkyl complexes of thorium were nixed by transmetallation being the prevalent reaction pathway for a variety of metals. In an attempt to work around this obstacle towards the formation of alkyl complexes it was decided to attempt to reverse the order of transformations, i.e. place alkyl ligands on the thorium centre initially and then make this alkyl complex undergo a reaction with the free terphenolate ligand.

*3.3.7.1 Synthesis of $Li_2(OTer^{Mes})_2(THF)$, **3.10***

The reaction of three equivalents of $Ter^{Mes}OH$ with *in situ* generated $Li[Th(CH_2SiMe_3)_5]$ in a THF suspension resulted in the initial isolation of a crystalline substance, determined to be $Li_2(OTer^{Mes})_2(THF)$, **3.10**. The solid state structure of **3.10** is shown in **Figure 3.19**. Selected bond angles and distances calculated from the solid state structure of **3.10** are shown in **Table 3.10**.

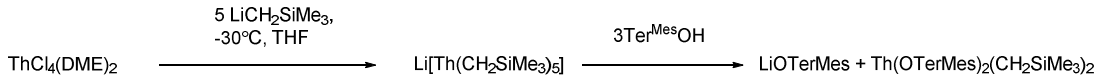

Scheme 3.5: Proposed formation of a heteroleptic thorium alkyl from an alternative route

The lithium salt of ligand was expected to be a product of this reaction (**Scheme 3.5**). However, what was not expected was that only one of the lithium atoms in the solid state structure would bear a THF molecule, but rather the solid state structure of **3.4**. However, as can be seen from **Figure 3.18** this is not the case. This may be due to the thorium containing product requiring THF molecules to ligate in order to satisfy its need for high co-ordination numbers. Attempts to isolate the thorium containing species have so far been unsuccessful.

The Li-Li distance in **3.10**, is comparable to those seen in **3.4** and **3.5**, whilst the Li-O distances are shorter than those seen in **3.5**, probably due to the terphenolate ligands only bridging two lithium atoms in **3.10**, whilst bridging three lithium atoms in **3.5**. The Li-O distances in **3.4** are almost identical to those seen in **3.10**. The Li-C aryl interactions are longer than those seen in **3.6**, but not considerably so. The ^1H NMR spectrum of **3.10**, shows the resonances assigned to the terphenyl mesityl ligand in a two to one ratio with the resonances attributed to the bound THF molecule.

Table **3.10**: Selected distances and angles for **3.10**

Atom	Distance (Å) / angle (°)
Li1-O1, Li1-O2, Li2-O1,Li2-O2	1.845(7), 1.838(6), 1.835(7), 1.830(7)
Li2-O3	1.882(7)
Li1-Li2	2.463(9)
Li1-C7, Li1-C40	2.705(7), 2.638(7)
C1-O1, C25-O2	1.331(4), 1.323(4)
Li1-O1-Li2, Li1-O2-Li2	84.4(3), 84.0(3)
O2-Li1-O1, O2-Li2-O1	95.5(3), 96.1(3)
C1-O1-Li1, C1-O1-Li2,	126.7(3), 143.5(3)
C25-O2-Li1, C25-O2-Li2	128.1(3), 136.4(3)

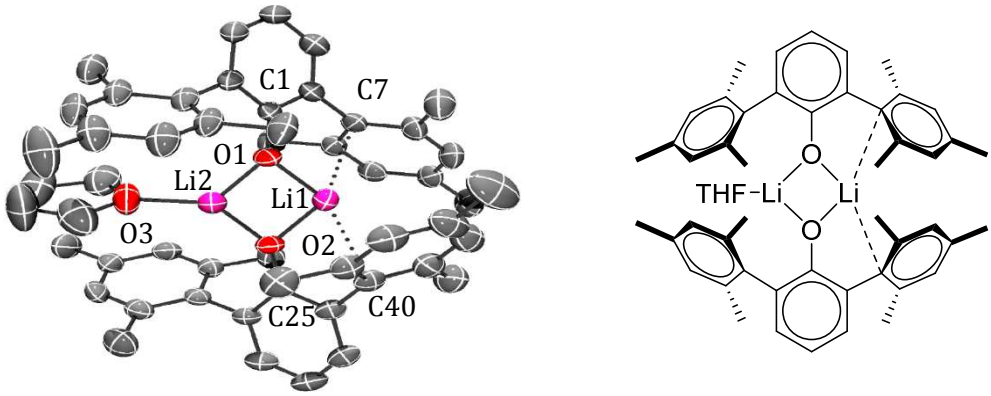

Figure 3.19: Displacement ellipsoid drawing of the solid state molecular structure of **3.10,** $Li_2(\mu^2\text{-}OTer^{Mes})_2(THF)$. Hydrogen atoms are omitted for clarity.

3.3.8 Group II reactivity

As seen in *3.3.6* the attempts to use a 'softer' metal and a potentially 'softer' alkyl moiety were found to result in no immediate reaction; however, the use of 'softer' alkyl species with 'harder' metals had not yet been investigated. Considering this it was decided to attempt to carry out a salt metathesis reaction using a commercially available allyl Grignard reagent; 2-methyl allyl magnesium chloride. However, this commercially available product was observed to contain dispersed magnesium so first the results of a reaction with 2-methyl allyl chloride synthesised according to literature procedures will be presented.[69]

The reaction between **3.2** and two equivalents of the 2-methylallyl Grignard C_4H_7MgCl[69] affords **3.11**, characterised as the dinuclear Th^{IV} allyl hydride {Th(η^3-C_4H_7)($OTer^{Mes}$)}$_2$(μ-η^3:η^3-C_4H_7)(μ-H)(μ- $MgCl_3(THF)_2$), and the by-products Mg($OTer^{Mes}$)$_2$(THF)$_2$ **3.12**, magnesium chloride, and other organic byproducts, equation 3.8. Complex **3.11** is isolated as a colourless powder in 47 % yield after workup, and its identity confirmed by single crystal X-ray crystallography studies after crystallisation from a hexane solution. Complex **3.12** can be isolated by fractional crystallisation from a hexane solution in a 20 % yield. Single crystals of **3.12** suitable for X-ray diffraction were grown from a saturated hexanes solution at -30°C; the solid state structure is shown in **Figure 3.21**. Selected bond angles and distances calculated from the solid state structure of **3.12**, are shown in **Table 3.12**.

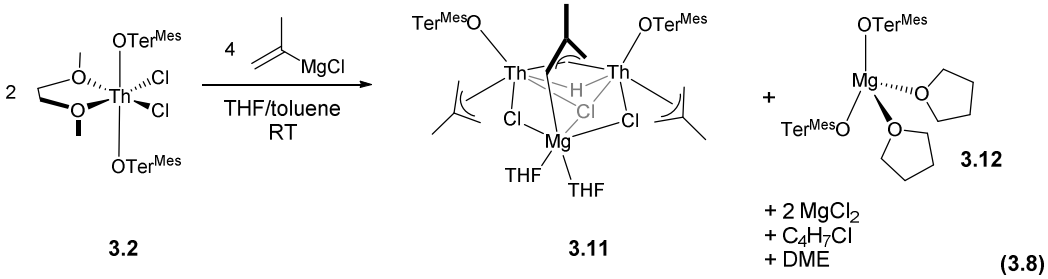

Equation 3.8 shows that the formation of **3.11** and **3.12** may proceed via a reduction by the Grignard reagent, in that the 2-methyl allyl chloride may be regenerated in the process of forming a bridging hydride in **3.11**. It is proposed that 2 equivalents of 2-methyl allyl chloride act in a nucleophilic fashion, with removal of $MgCl_2$ to cause the addition of the terminal methyl allyl groups to thorium. A third equivalent of 2-methyl allyl magnesium chloride is then incorporated into the structure by bridging between the two thorium centres in an atom-efficient way. The final equivalent of magnesium allyl chloride then causes a two electron reduction of the thorium dimer, causing the formation of a hydride from the bridging 2-methyl allyl ligand, whilst making the mono-anion into a dianion. The oxidised species is the 2-methyl allyl moiety which changes from a mono-anionic species to a 'cationic' or at least δ positive species in forming 2-methyl allyl chloride (see **Scheme 3.5**). The magnesium atom concomitantly removes two $Ter^{Mes}O^-$ ligands thus causing the formation of **3.12** as a separate species. Due to the size of the $Ter^{Mes}O^-$ ligands it is likely that this reduction and abstraction of the ligands is favoured for sterical reasons.

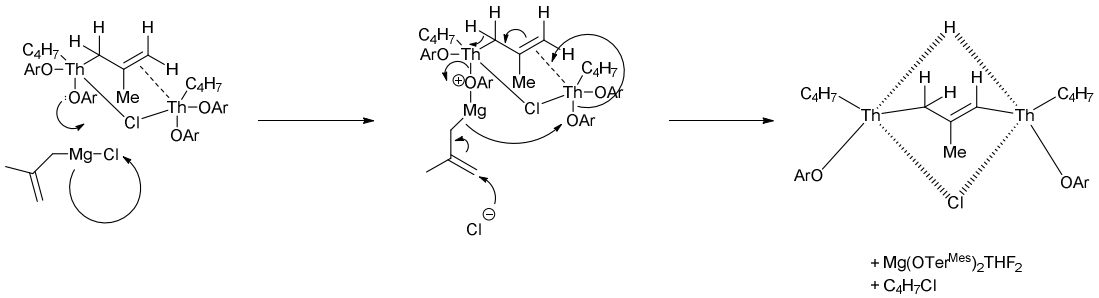

Scheme 3.5 : Possible reduction mechanism pathway causing the formation of **3.11** and **3.12**. Magnesium chloride and ligated THF ligands are omitted for clarity.

The reaction of **3.2** with two equivalents of commercially available C_4H_7MgCl affords $[MgTh_2Cl_3(OTer^{Mes})_2(C_4H_7)_3]$, **3.11**, as a yellow powder in a 52 % yield after workup, with no evidence of formation of **3.12** (Equation 3.9). Single crystals of **3.11** suitable for X-ray diffraction were grown from a saturated hexane solution at -30°C; the solid state structure is shown in **Figure 3.20**. Selected bond angles and distances calculated from the solid state structure of **3.11**, are shown in **Table 3.11**.

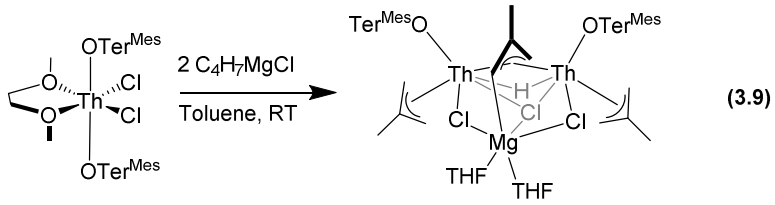

The absence of the formation of **3.12** in the synthesis of **3.11** using commercially available 2-methyl allyl chloride reagent is instructive as it hints at the role of suspended magnesium within the reaction. This observation is suggestive that suspended magnesium acts as reducing agent in equation 3.9, whilst in equation 3.8, once the suspended magnesium has been excluded from the reaction mixture an equivalent of 2-methyl allyl is proposed to act as the reducing agent.

The solid state structure of **3.12**, **Figure 3.21**, shows magnesium, in analogy to the solid state structures of **3.7** and **3.8** adopting a *pseudo*-tetrahedral geometry. The greatest deviation from the idealised tetrahedral angles, unsurprisingly involves the sterically challenging $Ter^{Mes}O^-$ ligands, which distort towards the linear so as to minimise steric repulsions. This is shown by the O1-Mg1-O2 angle of 138.51(9)° which indicates a far larger distortion from the tetrahedral than for any of the angles observed for **3.7** and **3.8**.

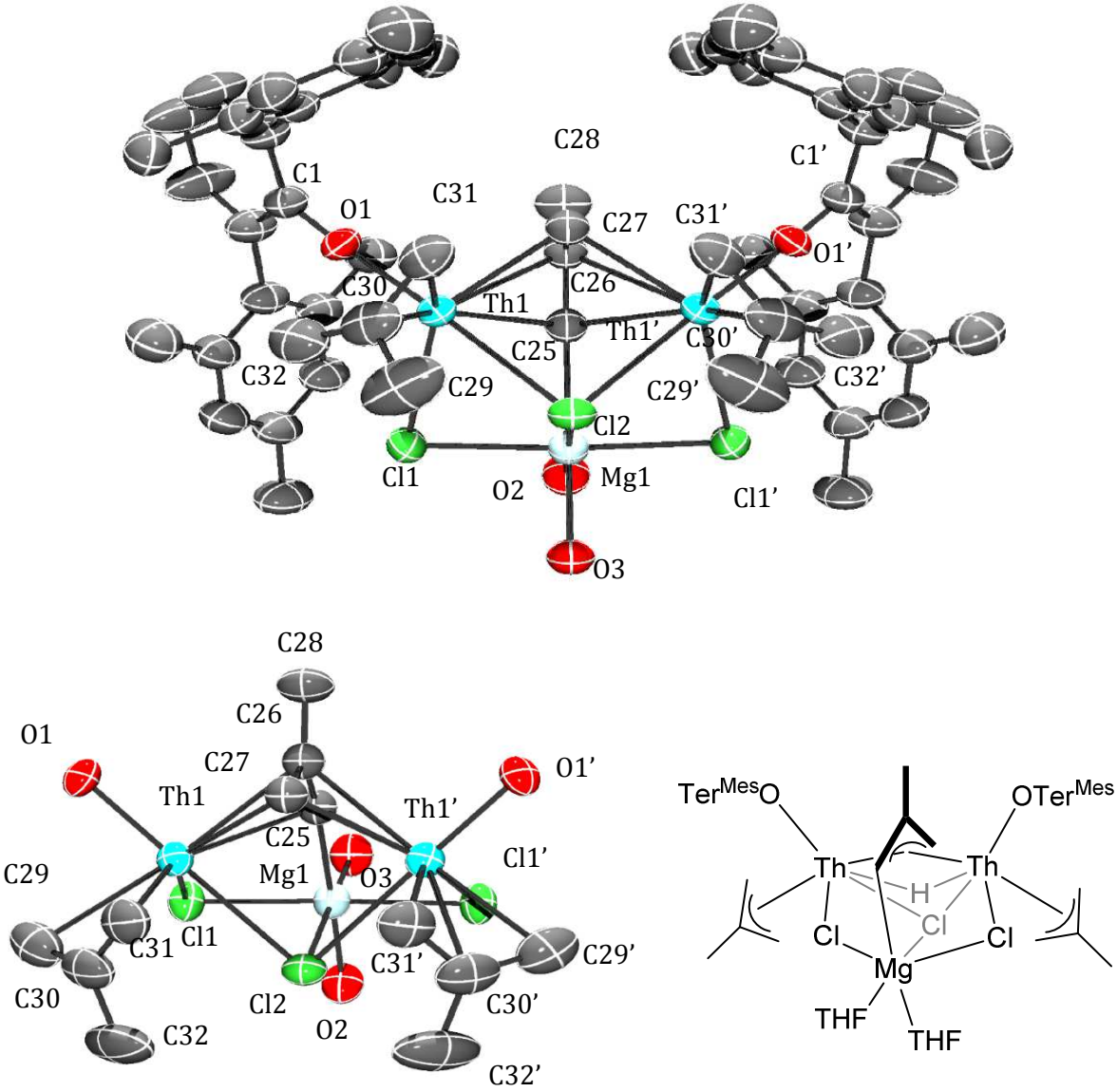

Figure 3.20 Top: Displacement ellipsoid drawing of the solid state molecular structure of **3.11,** $[MgTh_2\mu^2\text{-}Cl_2\mu^3\text{-}Cl(OTer^{Mes})_2(C_4H_7)_2\mu\text{-}\eta^3\text{:}\eta^3(C_4H_7)H]$. Hydrogen atoms and carbon atoms of ligating THF molecules are omitted for clarity. Bottom left: Displacement ellipsoid drawing of the core of the solid state structure of **3.11**. Hydrogen atoms, terphenolate ligands and carbon atoms of ligating THF molecules are omitted for clarity

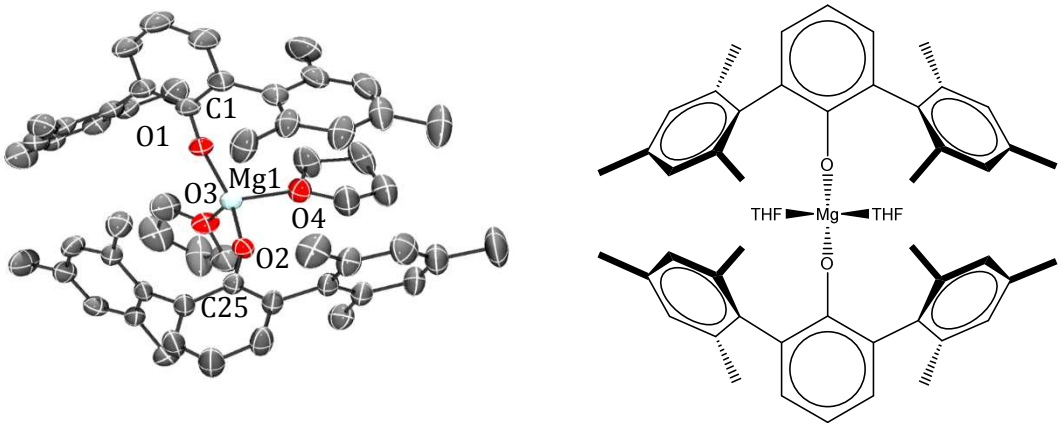

Figure 3.21 A displacement ellipsoid drawing of the solid state molecular structure of **3.12**, $Mg(OTer^{Mes})_2(THF)_2$. Hydrogen atoms are omitted for clarity.

In the crystal structure of **3.11** a mirror plane passing through the bridging allyl ligand and the Mg atom renders the two Th centres identical. The solid state structure of **3.11**, shown in **Figure 3.20**, consists of a dimeric thorium complex, bridged by one μ^2-chloride (Cl2) and one 2-methylallyl ligand (C25, C26, C27, C28) binding in an unusual fashion of μ-η^3:η^3. Incorporated into this structure is a unit of magnesium dichloride accompanied by two THF molecules which ligate to the magnesium centre. The incorporated magnesium atom undergoes an η^1 interaction with C25 of the bridging allyl ligand of bond length 2.339(9) Å, which is equal to the longest Mg-C bond in the literature.[70] (**Figure 3.29**) μ-η^3:η^3 bridging allyl complexes between metal centres are rare, especially when there are not any group I salts contained within the structure[71-79] with only one previously crystallographically characterised non- group I containing example in the literature, **M**.[80] (**Figure 3.22**)

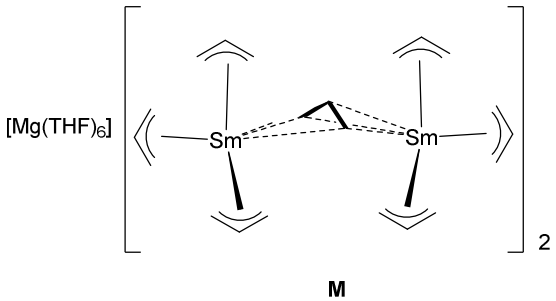

M

Figure 3.22 Bochmann's example of a μ-η^3:η^3 bridging allyl moiety[80]

M is a homoleptic allyl complex, $Mg(THF)_6[Sm_2(C_3H_5)_7)_2$, meaning that **3.11** is the first heteroleptic bridging allyl species to contain the μ-η^3:η^3 moiety. It is also the first

example of the 2-methylallyl ligand bridging in this way for any complex. **3.11** is also the first actinide complex to contain this type of moiety.

By electron counting, the solid state structure of **3.11** suggests that the thorium centres are Th^{3+}. However, this is not consistent with the NMR spectra, which indicate a diamagnetic complex. The two remaining solutions to satisfy the electron count of the solid state structure are that the thorium centres have an interaction that may be termed a bond, or perhaps the most likely explanation for the solid state structure is the presence hydride anions, which due to their proximity to the thorium centres could not be located by X-ray crystallography. The Th1-C28 and Th1-C32 distance of 3.957(7) and 3.851(9) Å respectively, precludes the formation of a trimethylene methane dianion moiety as seen by Evans *et al* in the samarium complex $(Cp^*_2Sm)_2[C_4H_6]$, **N**.[81, 82] (**Figure 3.23**) This is indicative of the 2-methylallyl ligand is not acting as a dianion in a way that has previously been precedented within the literature. This is due to the range of bond lengths of M-C_{allyl} in $(Cp^*_2Sm)_2[C_4H_6]$ being 2.734(4)-2.799(4) Å, which is two orders of magnitude smaller a range than that seen in **3.11.**

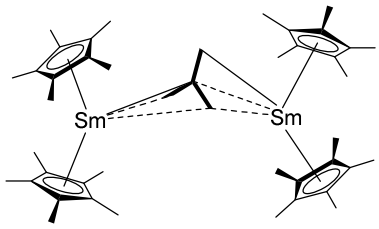

N

Figure 3.23: A complex containing the trimethylene methane dianion[81, 82]

The Th-C distances of **3.11** differ greatly for the bridging and terminal 2-methylallyl groups. For the terminal 2-methylallyl group, **3.11** contains Th1-C bond distances of 2.706(7) (C29), 2.811(7) (C30) and 2.676(7) (C31) Å, whilst for the bridging 2-methylallyl group the Th1-C bond distances are 2.654(5) (C25), 2.766(6) (C26) and 2.487(5) (C27) Å. The Th1-C30 bond is a significantly longer Th-C bond, 2.811(7) Å, compared to Th1-C29,31 and this is to be expected from allyl-type ligation as the *exo*-carbons have a pincer-type interaction with the metal centre. The bridging 2-methylallyl displays a similar Th1-C26 bond length to Th1-C30, but more drastic differences can be seen between the *exo*-carbon to thorium bond distances. Th1-C25 has a bond distance that is slightly shorter than Th1-C26,30 but similar to the Th1-C29,31 bond distances, whereas Th1-C27 has a significantly shorter distance at 2.487(5) Å. The Th-C27 bond length of 2.487(5) Å is short for Th-C interactions, which

range from 2.376(6)[83, 84] to 3.435(6) Å.[27, 85]It should be noted that C25 undergoes a η^1 interaction with magnesium, which is equivalent to the longest η^1 Mg-C allyl distance in the literature, **O**.[70] (**Figure 3.24**)

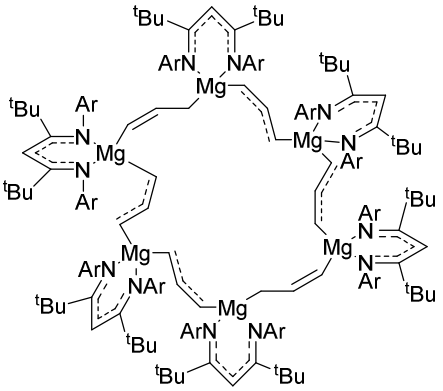

O

Figure 3.24: A complex with η^1 Mg-C allyl bond distance of the same length as **3.11**[70]

This legislates for the discrepancy between the *exo*-carbons of the bridging 2-methylallyl ligand. However it does not account for the shortness of the Th-C27 bond. The Th-C27 bond length of 2.487(5) Å is short for Th-C interactions. However when restricting the Th-C bonds distances to being single bonds, the Th-C27 bond becomes typical in length. This is to be expected as the Th-C27 bond would incorporate a significant amount of π character and hence would be longer than bonds with greater σ character. However, the shortness of the bond compared to all Th-C interactions is unusual. The Th-C25 bond distance is typical for Th-C single bond distances. The other Th-C bond distances are long for Th-C single bond distances, which is to be expected as there is significant π character within these bonds, so they would be expected to be longer in comparison to Th-C bonds with greater σ character. When comparing the Th-C bond lengths to previously crystallographically characterised thorium allyl complexes, **T-V**,[86, 87] (**Figure 3.26-7**), the Th-C bond distances of which range from 2.617(5) to 2.892(5) Å, it can be seen that the bond distances of Th-C25-26,29-31 are comparable, whilst Th-C27 is significantly shorter. The Th-C27 bond distance is statistically the second shortest Th-C bond distance observed from the small pool of carbon bridged thorium dimers (**P-S**) (see **Figure 3.25**).[88 89-91]

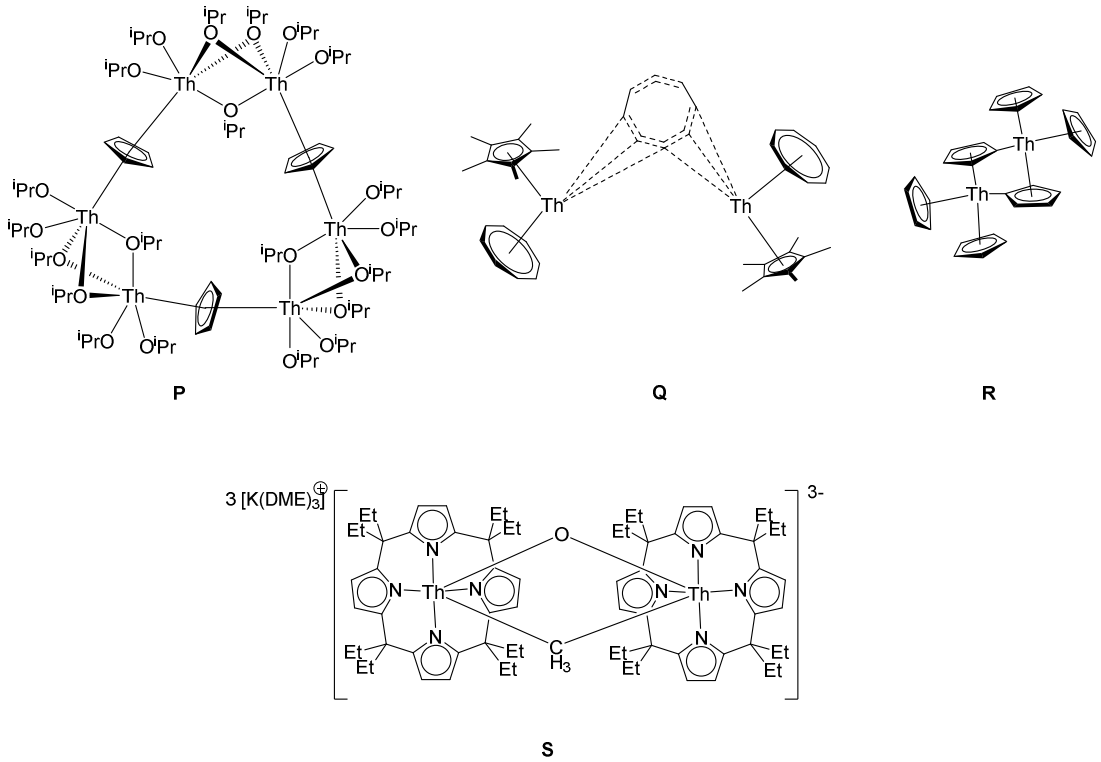

Figure 3.25: Crystallographically characterised poly-thorium complexes bridged by carbon atoms[88-91]

The shortest Th-C distance for a bridging carbon, is shown within compound **S** (bridging methyl group) which has an average Th-C bond distance of 2.467(3) Å, which is slightly shorter than that seen for Th1-C27 in **3.11.** However, it should be noted that it is also bridged by an oxo ligand, which is likely to cause the thorium atoms to become closer, hence reducing the bonding distance to the bridging carbon. The shortness of this bond perhaps raises the possibility that C27 has lost a proton as a hydride, which is now bridging between the thorium atoms. This would mean that the bridging 2-methyl allyl moiety is now acting as a dianion. This would satisfy the valency of two Th^{IV} centres. If this were the case it would be expected to see a discrepancy in the bond lengths of the C-C bonds of the 2-methyl-allyl ligands of **3.11**.

From the solid state structure of **3.11,** it can be seen that there is a difference between C27 and C25 from its bonding to the central carbon in the methyl allyl moiety. C25-C26 has a bond length of 1.399(11) Å whilst C26-C27 has a bond length of 1.448(11) Å showing a clear and expected lengthening of the C-C bond that would be expected to bear a greater negative charge. This lengthening becomes more apparent when comparing the C-C distances to the terminal bridging allyl moiety, which has C29-C30 and C30-C31 bond lengths of 1.390(12) and 1.395(11) respectively. When taking into

account all 2-methyl allyl complexes crystallographically characterised within the literature it is seen that the bond lengths C25-C26, C29-C30 and C30-C31 are all typical for these complexes whilst C26-C27 is long, suggesting that the theory of additional negative charge being present at this position is more likely. This $[\mu\text{-}\eta^3\text{:}\eta^3]^{2-}$ moiety represents a novel and hitherto unseen binding mode for allyl ligands.

Comparison of the Th-C27 bond distance in **3.11** to the Th-C_{alkyl} bond distance in $Th(Cp^*)Me_2$ of 2.475(9),[92] results in the conclusion that these two bond lengths are identical within s.u.s. The conclusion that a terminal Th-methyl bond would have an equivalent bond length to a bridging allyl Th-C is surprising and unexpected and gives credence to an increased electrostatic attraction between this carbon and the thorium centres, suggestive of an additional charge being present. This observation is strengthened when it is noted that the Th-C27 bond distance in **3.11** is shorter or statistically equivalent to the bond lengths of all neutral terminal Th-Me complexes,[27] which would be a very unusual occurrence if the allyl group remained mono-anionic.

The FTIR spectrum of **3.11** displays absorptions in the region expected for an actinide hydride stretch of 1456, 1418, 1378, 1245, 1080, 1015 cm^{-1}. For comparison $[(C_5Me_5)_2ThH_2]_2$ has Th−H absorptions at 1406, 1361, 1215, and 1114 cm^{-1},[93] whilst $(C_5Me_4H)_4[\mu\text{-}\eta^5\text{-}C_5Me_3H(CH_2)\text{-}\kappa\text{-}C]_2Th_4(\mu\text{-}H)_4(\mu^3\text{-}H)_4$ has a Th−H absorption at 1108 cm^{-1}.[51] (See **Figure 3.24**) However, this may not be evidence of Th-H as because of the 2-methylallyl ligands the resonances in this region may also be due to C-C or C-H stretches and bending, thus clouding the conclusions that can be drawn. The room temperature ^{1}H NMR spectrum of a benzene solution of **3.11**, perhaps due to the highly fluxional nature of the 2-methylallyl ligands appears as a series of overlapping signals in the aromatic region (7.2-6.5 ppm) and the alkyl region (2.5-1.7 ppm). In an attempt to characterise **3.11**, variable temperature experiments were undertaken. The ^{1}H NMR spectrum of a toluene solution of **3.11** at 323 and 343K, shows some coalescing of the resonances, resulting in smoother, but still unassignable overlapping multiplets. The ^{1}H NMR spectrum of a benzene solution of **3.11** at 223K, shows sharpening of the resonances, but there is still significant overlapping of the resonances, meaning any conclusions drawn from the data are limited. The highly fluxional nature of thorium bound allyl groups on the NMR timescale due to $\eta^3 \leftrightharpoons \eta^1$ ligand rearrangements were also found for the homoleptic thorium complexes.[86, 94] Combined with the dianionic

nature of the bridging 2-methyl allyl ligand, it is proposed that a bridging hydride exists to allow for charge balancing of the thorium centres.

3.11 is the fourth crystallographically characterised example of a thorium complex containing the allyl moiety, with two of the other complexes being homoleptic with bulky silyl substituents.[86] (see **Figure 3.26**).

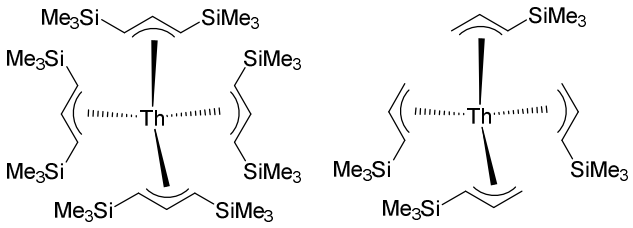

Figure 3.26: Previously crystallographically characterised homoleptic thorium allyl complexes[86]

The third crystallographically characterised example of a thorium allyl complex was published recently by Evans and was stabilised by Cp* ligands.[87] As can be seen from **Figure 3.27**, the solid state structure exhibits differential binding modes for the two allyl ligands, with one undergoing η^1 ligation whilst the other undergoes η^3 ligation.

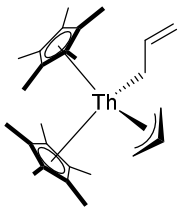

Figure 3.27: The singular crystallographically characterised example of the solid state structure of a heteroleptic thorium allyl complex[87]

In addition to **3.11** being the second example of a heteroleptic thorium allyl complex it is also the second thorium allyl complex to exhibit different binding modes for the allyl moiety within the same complex. Other metals have been shown to bind to more than one allyl ligand in differing fashions within the same complex, some selected examples of which are shown in **Figure 3.28**. [95-102]

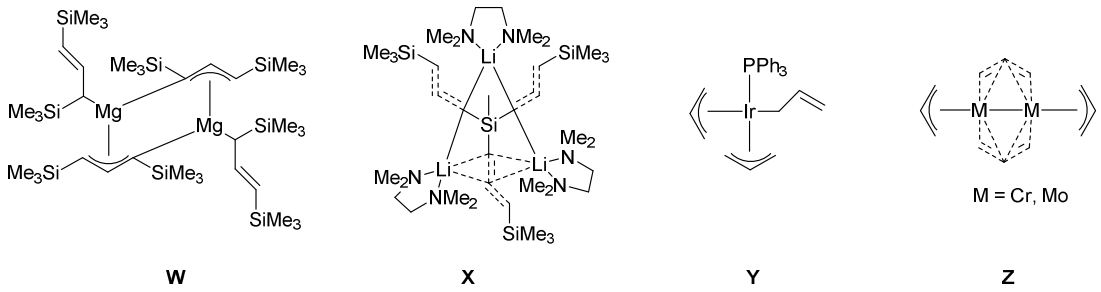

Figure 3.28: Selected examples of allyl complexes with different binding to metals within the same complex

The examples of differential binding to metals within the same complex by allyl complexes within **Figure 3.28** show four distinct types of system, which the other literature examples will fall into. Examples of these four systems are **W**, η^1, μ-η^1:η^3 ; **X,** η^1, μ-η^2:η^2 ; **Y**, η^3, η^1 and **Z**, η^3, μ-η^3:η^2.

The metals that favour these sorts of system are clear given a survey of the literature. The **W** and **X** classes only, to this author's knowledge, exists in the systems shown above and as such would appear to be favoured by group II and I metals respectively.[95, 100] The **Y** class is by far the most populated and include mainly the noble metals (i.e. Rh, Ir, Ru)[97, 99] but also has examples from Group III (Sc) and Group IV (Zr)[101, 102], whilst the **Z** class is solely the precinct of group VI metals which favour metal to metal bonding. There is also the additional class presented earlier of **M**: the μ-η^3:η^3 moiety (**Figure 3.20**). The trends that can be observed from these systems are that transition metals, tend to prefer bridging allyl ligation, presumably to follow the eighteen electron rule, whilst group I and II systems prefer more classical η^1 ligation. Having observed this it should come as no surprise that in **3.11**, the 'hard' magnesium cation interacts with the bridging allyl in an η^1 fashion, whilst the 'softer' and more transition metal-like thorium undergoes η^3 interactions with the allyl ligands in the solid state.

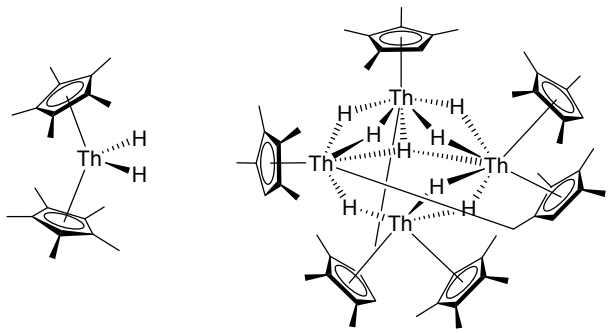

AA **AB**

Figure 3.29: Selected examples of thorium hydride complexes with reported IR spectra[51, 93]

Examining the possibility of a Th-Th interaction begins with the Th1-Th1' distance of 3.9150(3) Å, which is fairly short amongst thorium to thorium intramolecular distances. However, many of these complexes with shorter distances are bridged by multiple hydrides [103, 104], or oxygen based bridging species [28, 88, 105-109], (see **Figure 3.30**) whilst some species bridged by these types of moieties have longer intramolecular Th-Th distances than **3.11**.[27]

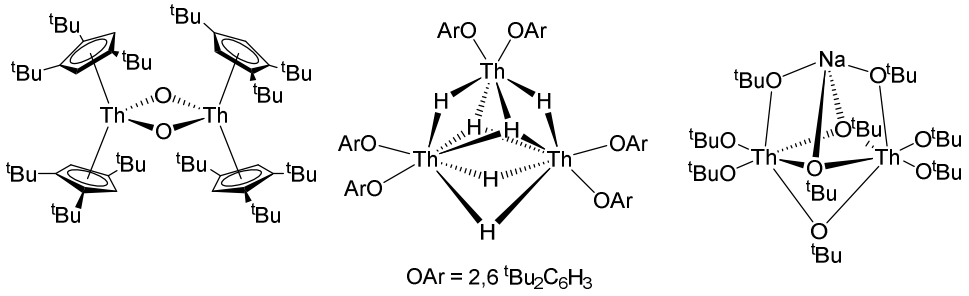

AC **AD** **AE**

Figure 3.30: Selected examples of bimetallic thorium complexes containing short inter-thorium distances[28, 103, 107]

When comparing **3.11** to intramolecular thorium species bridged by halides, **3.11** contains the fourth shortest Th-Th intramolecular distance, with two complexes, **AF** and **AG**, containing three bridging fluorides being the shortest in the literature.[110, 111] (**Figure 3.31**)

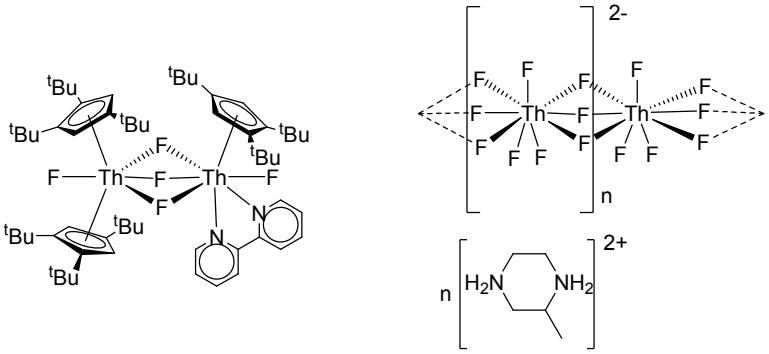

AF AG

Figure 3.31: Bimetallic thorium complexes bridged by fluorides with shorter inter-thorium distances than **3.11**[70, 71]

When restricting the comparison of **3.11** to intramolecular thorium species bridged by chlorides it contains the second shortest Th-Th distance. The complex containing a Th-Th intramolecular distance that is bridged by chlorides that is shorter than **3.11**, **AH** is also bridged by oxygen atoms of aryloxides.[16] (see **Figure 3.32**)

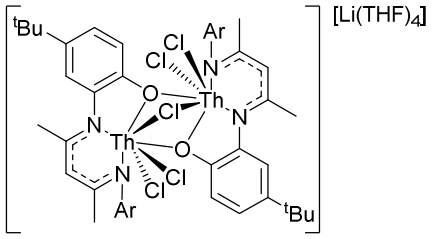

AH

Figure 3.32: A Bimetallic thorium complex bridged by a chloride with a shorter inter-thorium distances than **3.11**[16]

The Th-Th distance of thorium metal is 3.60 Å [112],which is not much smaller that the intermolecular distance seen in **3.11**. The Th-Th distance in ThI_2 is 3.97 Å, which contains two electrons in the band gap, and has been proposed to be short enough for some small Th-Th orbital overlap to exist[113] is longer than that of **3.11**, so there is the potential for some Th-Th overlap in **3.11**.

The Mg1-Th1 distance in **3.11** of 3.499(2) Å, is significantly shorter than the two other crystallographically characterised examples of magnesium-thorium clusters.[84, 114] (see **Figure 3.32**)

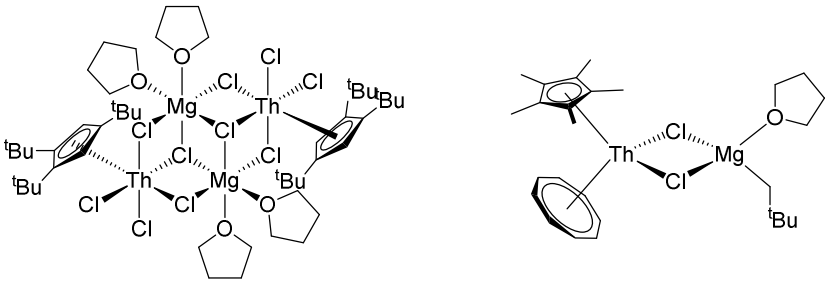

AI **AJ**

Figure 3.33: Crystallographically characterised magnesium-thorium complexes[84, 114]

The complexes in **Figure 3.33** have Th-Mg bond distances of 4.159(4) and 3.962(5) Å respectively, meaning that **3.11** contains the shortest Mg-Th distance by over 0.4 Å. This shortness is likely due to the increased number of bridging atoms between the thorium and magnesium atoms in **3.11**, compared to **AI** and **AJ** rather than any bonding interaction between magnesium and thorium. A further factor in the shortness of the Th-Mg bond in **3.11**, is the presence of the η^1 C25-Mg1 interaction. The geometry around the magnesium cation in **3.11** is almost octahedral, as shown by the angles shown in **Table 3.11** being roughly 90°. The octahedral geometry is typical for magnesium complexes. The Th-O bond distance of **3.11**, is identical within s.u.s to that seen for **3.2**, but is shorter than that observed for **3.1**. This is suggestive of the thorium atom requiring slightly more electron density per oxygen atom in **3.11** than in **3.1**. This may be due to there being more oxygen donors for thorium in **3.1**, thus reducing the pull for electron density from the terphenolate ligand.

Table 3.11: Selected distances and angles for **3.11**

Atom	Distance (Å) / angle (°)
Th1-O1, Th1-Cl1, Th1-Cl2	2.163(4), 2.9563(14), 2.8105(13)
Mg1-O2, Mg1-O3	2.073(7), 2.053(7)
Mg1-Cl1, Mg1-Cl2	2.631(3), 2.4577(14)
Th1-Th1', Mg1-Th1	3.9150(3), 3.499(2)
Th1-C25, Th1-C26, Th1-C27	2.654(5), 2.766(6), 2.487(5)
Th1-C29, Th1-C30, Th1-C31	2.706(7), 2.811(7), 2.676(7)
Mg1-C25, Th1-C28, Th1-C32, C1-O1	2.339(9), 3.957(7), 3.851(9), 1.340(7)
C25-C26, C26-C27, C29-C30, C30-C31	1.399(11), 1.448(11), 1.390(12), 1.395(11)
C1-O1-Th1	177.2(4)
O2-Mg1-O3, O2-Mg1-C25, O3-Mg-C25	88.6(3), 175.3(3), 96.2(3)
O2-Mg1-Cl2, O3-Mg1-Cl2, Cl2-Mg1-Cl2'	91.15(8), 93.41(7), 172.85(14)
Cl2-Mg1-Cl1, Mg1-C25-Th1	86.61(7), 88.8(2)

Table 3.12: Selected distances and angles for **3.12**

Atom	Distance (Å) / angle (°)
Mg1-O1, Mg1-O2	1.8546(18), 1.8565(18)
Mg1-O3, Mg1-O4	2.014(2), 2.015(2)
C1-O1, C25-O2	1.322(3), 1.323(3)
C1-O1-Mg1, C25-O2-Mg1	159.05(17), 160.58(18)
O1-Mg1-O2, O1-Mg1-O3, O1-Mg1-O4	138.51(9), 101.71(8), 107.74(8)
O2-Mg1-O3, O2-Mg1-O4, O3-Mg1-O4	105.02(9), 102.17(8), 102.17(8)

3.4 Reactivity of 3.11

The synthesis of a compound with nine Th-C bonds was in theory a good step towards activating small molecules as there was the possibility of insertion of molecules into these reactive Th-C bonds. *3.4* will focus upon the attempts to activate small molecules using **3.11**

3.4.1 Suitability of 3.11 for small molecule activation chemistry

3.11 would appear to have some properties that are tailor-made to facilitate the activation of small molecules, the most obvious being the presence of multiple, presumably reactive Th-C and Th-H bonds. These bonds should allow for insertion

reactions to take place. η^3 allyl complexes have been shown to facilitate small molecule activations in the past for transition metal systems and it was hoped that the same would remain true for actinide complexes.[115, 116] Additionally the steric protection afforded by the bulky $Ter^{Mes}O^-$ ligands may impart some selectivity upon these insertion reactions.

However, the system may be too sterically protected to allow for small molecule activations, or may have too many active bonds that a substrate may insert into thus resulting in uncontrolled and undefined reactivity, so it may be more suitable to have a more open possible co-ordination site or a lesser number of reactive bonds in order to favour more selective or controlled activation.

3.4.2 Insertion reactions

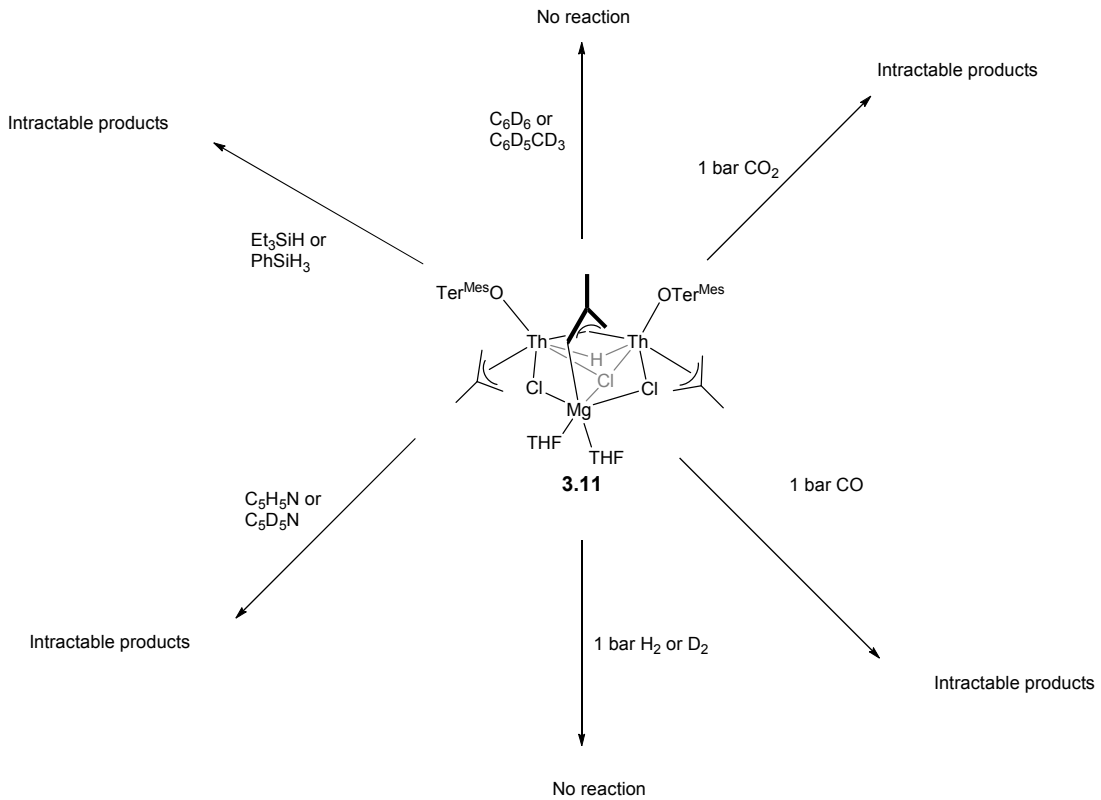

Scheme 3.6: A summary of attempts to activate small molecules using **3.11**

*3.4.2.1 Reaction of **3.11** with CO_2*

The reaction of **3.11** with 1 bar of CO_2 appeared by ^1H NMR spectroscopy to result in a reaction occurring as evidenced by small shifts in the resonances assigned to **3.11**, with

the most obvious shift being those assigned to the ligating THF molecules. The ^{13}C NMR spectroscopy, other than shifts in the THF resonances, proved inconclusive. After addition of CO_2 decolourisation of the solution and a small amount of precipitate was observed but the products proved to be intractable.

*3.4.2.2 Reaction of **3.11** with CO*

The reaction of **3.11** with 1 bar of CO appeared by ^{1}H NMR spectroscopy to result in a reaction occurring as evidenced by small shifts in the resonances assigned to **3.11**. There was evidence of formation of H_2 gas, by the formation of a resonance at 4.47 ppm.[117] The ^{13}C NMR spectroscopy of the products of this reaction, did not prove conclusive. After addition of CO a slight darkening of the solution and formation of a micro-crystalline precipitate was observed but unfortunately none of the products were tractable.

3.4.3 Hydride exchange reactions

*3.4.3.1 Reaction of **3.11** with H_2*

The reaction of **3.11** with 1 bar pressure of H_2 appeared by ^{1}H NMR spectroscopy to result in a reaction occurring as it was observed that there was a shift in the resonances of **3.11**. After the addition of a H_2 atmosphere a lightening of the solution and a small amount of precipitate was observed. However, no product was able to be isolated from the solution and the NMR spectra remained difficult to assign and interpret given the fluxional nature of hydrides and 2-methyl allyl ligands, leaving the results of this reaction unknown.

*3.4.3.2 Reaction of **3.11** with D_2*

To attempt to ascertain the results of the reaction of H_2 with **3.11,** a reaction of **3.11** with 1 bar pressure of D_2 was attempted, in the hope that an additional NMR handle may aid the characterisation of the unknown product. It was found that the reaction does not result in hydride exchange, as no HD was observed in the ^{1}H or ^{2}H spectra. This suggests that no reaction occurred and the observed reactivity with H_2 was most likely due to product degradation.

*3.4.3.3 Reaction of **3.11** with deuterated solvents*

Reaction of **3.11** in deuterated solvents (C_6D_6 and $CD_3C_6D_5$) does not yield deuterium-hydrogen exchange products. However, reaction with pyridine (perdeuterated or per-proteo) results in a reaction being observed, although the products were intractable.

*3.4.3.4 Reaction of **3.11** with Et_3SiH and $PhSiH_3$*

Reaction of **3.11** with Et_3SiH and $PhSiH_3$ was found to result in a reaction occurring, however the products produced were intractable.

3.5 Attempts to transform or remove DME from $Th(OTer^{Mes})_2Cl_2(DME)$

3.2 is not the best suited complex towards small molecule activation as it lacks the presence of active bonds in which substrates may be able to insert, and due to the size of the $Ter^{Mes}O^-$ ligands and solvated DME molecule, lacks a vacant co-ordination site upon which substrates could bind in Lewis-acid based activation. Attempts were made to transform **3.2** into a complex more suited towards small molecule activation and catalysis by substituting or removing the chelating DME molecule.

3.5.1 Alternative solvates of $Th(OTer^{Mes})_2Cl_2DME$

3.5.1.1 Pyridine

The reaction of **3.2** with pyridine resulted in shifts in the resonances of **3.2**, consistent with the substitution of the DME chelating molecule by ^1H NMR spectroscopy, see Equation 3.13. However, attempts to isolate this product were not successful.

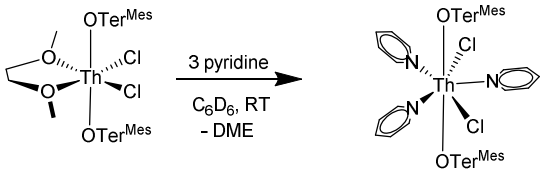

3.2 (3.13)

Proposed product of reaction with pyridine

3.5.1.2 4,4' bipyridine[1]

Treatment of **3.2** with two equivalents of 4,4' bipyridine successfully displaces the coordinated DME to afford a co-ordination polymer $[Th(OTer^{Mes})_2(Cl)_2(4,4'\text{-bipyridyl})_{1.5}]_\infty$, **3.13,** which crystallises readily and easily out of the reaction mixture as

colourless needles, **Equation 3.14**. The solid state structure of a single repeat unit of **3.13** is displayed in **Figure 3.35**. Selected bond angles and distances calculated from the solid state structure of **3.13**, are shown in **Table 3.13**.

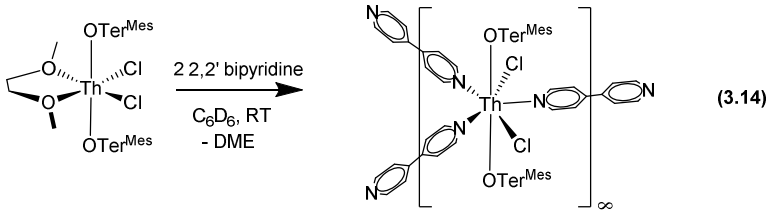

3.2 (3.14)

In **3.13** the Th^{IV} centre adopts a *pseudo*-pentagonal bipyramidal structure with 3 N-donor bipyridyl ligands and two chloride ligands in the equatorial plane whilst retaining the two *trans* disposed $OTer^{Mes}$ ligands with a highly linear angle of 177.78(11)°. This is slightly less linear than the analogous angles seen in **3.1** and **3.2**.

In **3.13** the Cl-Th-Cl angle of 159.24(4)° is wider when compared to the *pseudo*-octahedral **3.2**, presumably to enable the ligation of three donor ligands in the equatorial plane. In comparison to the also pseudo- pentagonal bipyramidal **3.1**, **3.13** is also wider, which is to be expected as it is highly likely that aqua-ligands occupy less space than bipyridyl ligands. In **3.13** the equatorial ligands do not occupy one plane, with the chloride and bipyridyl ligands occupying different planes. This is shown by the angle O_1-Th_1-X (where X is the bonding atom in the plane.) The O_1-Th_1-Cl bond angles of 94.96(10) and 86.44(10)° are near to the perpendicular and this contrasts strongly with the O_1-Th_1-N angles of 103.94(12), 78.34(12) and 88.20(15)°, which indicate a substantial tilt from the perpendicular.

In **3.13** there are three Th_1-Th_1-Th_1 bond angles of 144.97(9), 150.32(9) and 64.66(9)°. The first two of these angles are comparable to each other, whilst the third is far narrower and results in the formation of a 2-D polymer in the form of containing hexagonal motifs (**Figure 3.34**). The formation of two-dimensional co-ordination polymers with use of the 4,4'-bipyridine ligand is well established.[118, 119] In **3.13** the two $OTer^{Mes}$ central aryl groups are, in direct contrast to **3.1** and **3.2**, orthogonal to each to other, and this is likely due to minimising the interactions with the bipyridine ligands. This orthogonal geometry of the central aryl groups has only previously been seen in **3.4 i**n this chapter, and this was due to the small size of the lithium cations causing steric repulsions within the dimer by reducing the distance between the ligands.

The Th1-O1,2 bonds, of 2.221(3) and 2.232(3) Å, are longer than those seen in **3.1**, **3.2** and **3.11**, but remain short for Th-O bonds. This slight lengthening is to be expected from the increased electron donation that a third N-donor ligand provides, increasing the electron density on thorium, and thus reducing the electrostatic interaction with the $OTer^{Mes-}$ ligand. The Th-N bond distances in **3.13**, of 2.695(4), 2.667(5) and 2.677(4) Å are typical. The Th-Cl bond distances in **3.13**, of 2.698(2), 2.710(2) Å, are also typical. The Th-Cl distances are, as is to be expected, shorter than the Th-Cl distances observed in **3.11**, due to them not bridging between metal centres. The Th-Cl distances are also shorter than those seen for **3.1**, which is perhaps a result of there being three nitrogen donors rather than three oxygen donors in the solid state structure of **3.13**. **3.13** has longer Th-Cl distances than the lower co-ordination number **3.2**, which is to be expected.

The distances between the thorium atoms in **3.13** of 12.437(3), 12.460(2) and 12.486(3) Å are typical for thorium clusters bridged by organic ligands. **13.2** could possibly be used as a means for purifying or extracting thorium residues, given that once the polymeric form has been synthesised the crystallisation of this polymer is almost immediate.

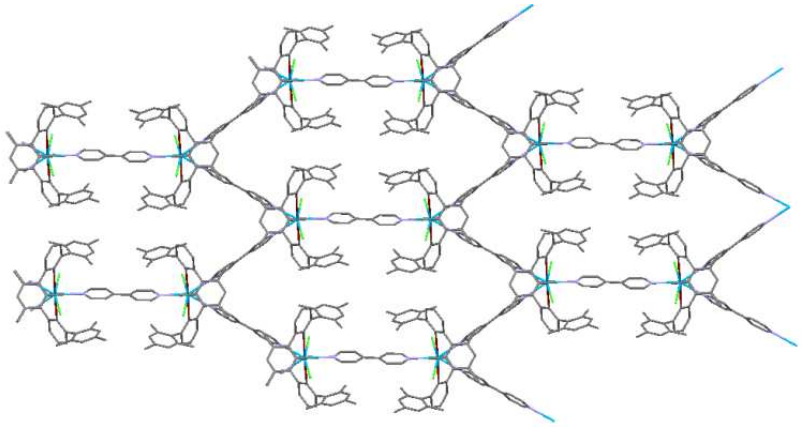

Figure 3.34: The 2-D polymeric structure of 3.13. Hydrogen atoms and lattice benzene and bipyridine molecules removed for clarity.

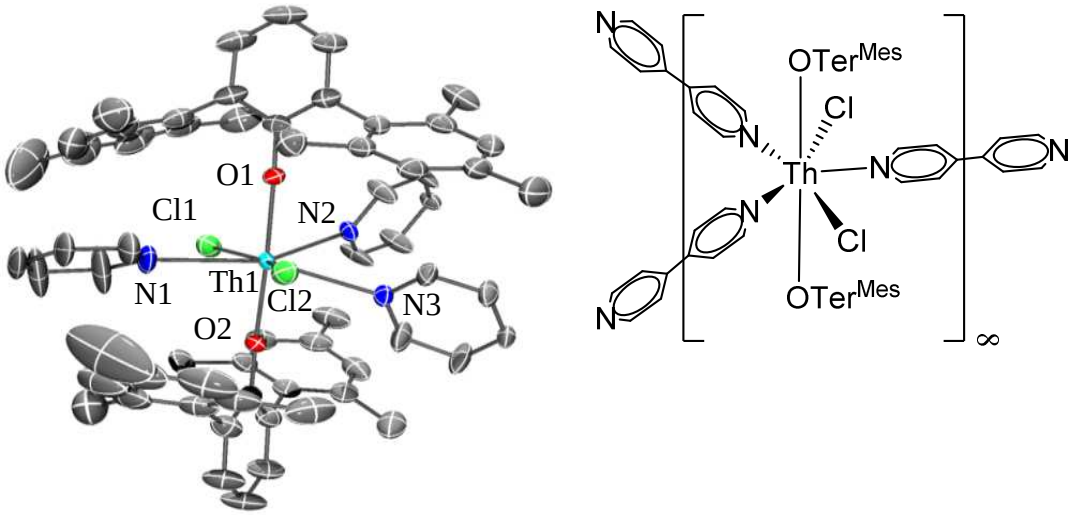

Figure 3.35: Displacement ellipsoid drawing of the solid-state molecular structure of the monomeric unit of **3.13** (50 % probability ellipsoids). Hydrogen atoms and lattice benzene and bipyridine molecules removed for clarity.

Table 3.13: Selected distances and angles for **3.13**

Atoms	Distance (Å) / angle (°)
Th1-O1, Th1-O2	2.221(3), 2.232(3)
Th1-N1, Th1-N2, Th1-N3	2.695(4), 2.667(5), 2.677(4)
Th1-Cl1, Th1-Cl2	2.6976(16), 2.7101(16)
Th1-Th1', Th1-Th1'', Th1-Th1'''	12.437(3), 12.460(2), 12.486(3)
C1-O1	1.362(6)
C1-O1-Th1, C25-O2-Th1	173.6(3), 174.6(3)
O1-Th1-O2, O1-Th1-N1, O1-Th1-N2, O1-Th1-N3	177.78(11), 103.94(12), 88.20(15), 78.34(12)
O1-Th1-Cl1, O1-Th1-Cl2, O2-Th1-N1, O1-Th1-N2	94.96(10), 86.44(10),
Th1-Th1'-Th1'', Th1-Th1''-Th1', Th1'-Th1-Th1''	144.97(9), 150.32(9), 64.66(9)

3.5.2 Attempts to remove bound solvent from [Th(OTer^{Mes})$_2$Cl$_2$(DME)]

In an attempt to open up a co-ordination site to allow for Lewis-acid based activation, some reactions were attempted to remove the chelating DME molecule.

3.5.2.1 Reaction with Al(iPr)$_3$ and AlMe$_3$

Attempts to remove the chelating DME molecule from **3.2** by use of trimethyl or tri-isopropyl aluminium (Equation 3.12) resulted in no reaction being observed by ^{1}H NMR spectroscopy.

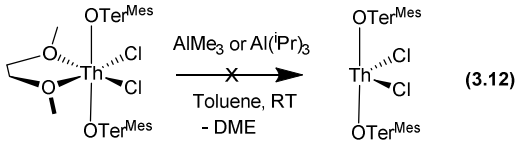

(3.12)

3.2

3.6 Reaction of uranium salts with Ter^{Mes}OH

3.6.1 Uranium (IV) halides

3.6.1.1 Reaction of UCl$_4$ with in situ generated Ter^{Mes}OK

Reaction of two equivalents of in situ generated Ter^{Mes}OK, from reaction of KN" and Ter^{Mes}OH in toluene, with a green solution of UCl_4 with THF results in the initial formation of a brown-orange solution. This solution was observed to progress to a red-orange suspension. After extraction into hexane crystalline material was isolated suitable for X-ray crystallographic studies and was determined to be $U_4K_2Cl_8(2\mu^3\text{-}O)(Ter^{Mes}O)_6$, **3.14**, the solid state structure of which is displayed in **Figure 3.36**. Selected bond angles and distances calculated from the solid state structure of **3.14** are shown in **Table 3.14**.

Due to the poor quality of the crystal data for **3.14**, with an observed R_1 of 0.186 and observed wR_2 of 0.360, the only conclusions that can be made firmly concern the connectivity of this complex in the solid state, although speculations about the meaning of some selected bond lengths will form part of the discussion of this complex.

The solid state structure of **3.14** shows the formation of a molecular cage, with incorporation of two equivalents of KO^{Ter}Mes salt into the structure. The four uranium atoms are arranged in a plane with four chloride atoms (Cl1, Cl4, Cl1' and Cl4') and two oxygen atoms (O4, O4') the latter of which bridge between three of the uranium centres each. U2 and U2' also form a puckered 'butterfly' shaped planar motif with the potassium atoms (K1, K1') and four chloride atoms (Cl2, Cl3, Cl2' and Cl3'). The Ter^{Mes}O

ligands adopt terminal positions, capping the cations within the cluster. In the case of the $Ter^{Mes}O$ ligands associated with the uranium atoms, linear geometries are observed, whilst in the case of the TerMesO ligand associated with the potassium atoms, there is a substantial bend in the K1-O3-C49 angle of 134(4)° which is due to the potassium undergoing aryl interactions with the ortho mesityl group of the $Ter^{Mes}O$ ligand. The uranium centres within this cluster have a clear difference in co-ordination number as U1 is five co-ordinate, whilst U2 is six co-ordinate. This difference in co-ordination extends to the identity of the atoms ligating to the uranium centres; whilst U1 ligates to three oxygen atoms (O1, O4, O4') and two chlorides (Cl4, Cl4'), U2 ligates to two oxygen atoms (O2, O4) and 4 chlorides(Cl1, Cl2, Cl3, Cl4). In the solid state structure of **3.14** an inversion centre lying at the centre of the U1-O4-U1'-O4' plane renders both sides of the molecular cage as identical.

Further discussion upon the structure of **3.14**, due to the quality of the crystal data, can only comment on the connectivity. The differences in coordination number of the uranium centres is perhaps suggestive of a difference in formal oxidation state between the two centres. The bridging oxygen motif, which presumably comes from the splitting of adventitious molecular oxygen during synthesis may be responsible for the change in oxidation state.

Due to the adventitious nature of synthesis of **3.14,** the repeatability of this reaction was not possible and as such NMR data for the crystalline material is not available. However, NMR data for the crude reaction material was obtained and it was observed to contain a series of paramagnetic resonances that could be assigned to a paramagnetically shifted terphenolate ligand.

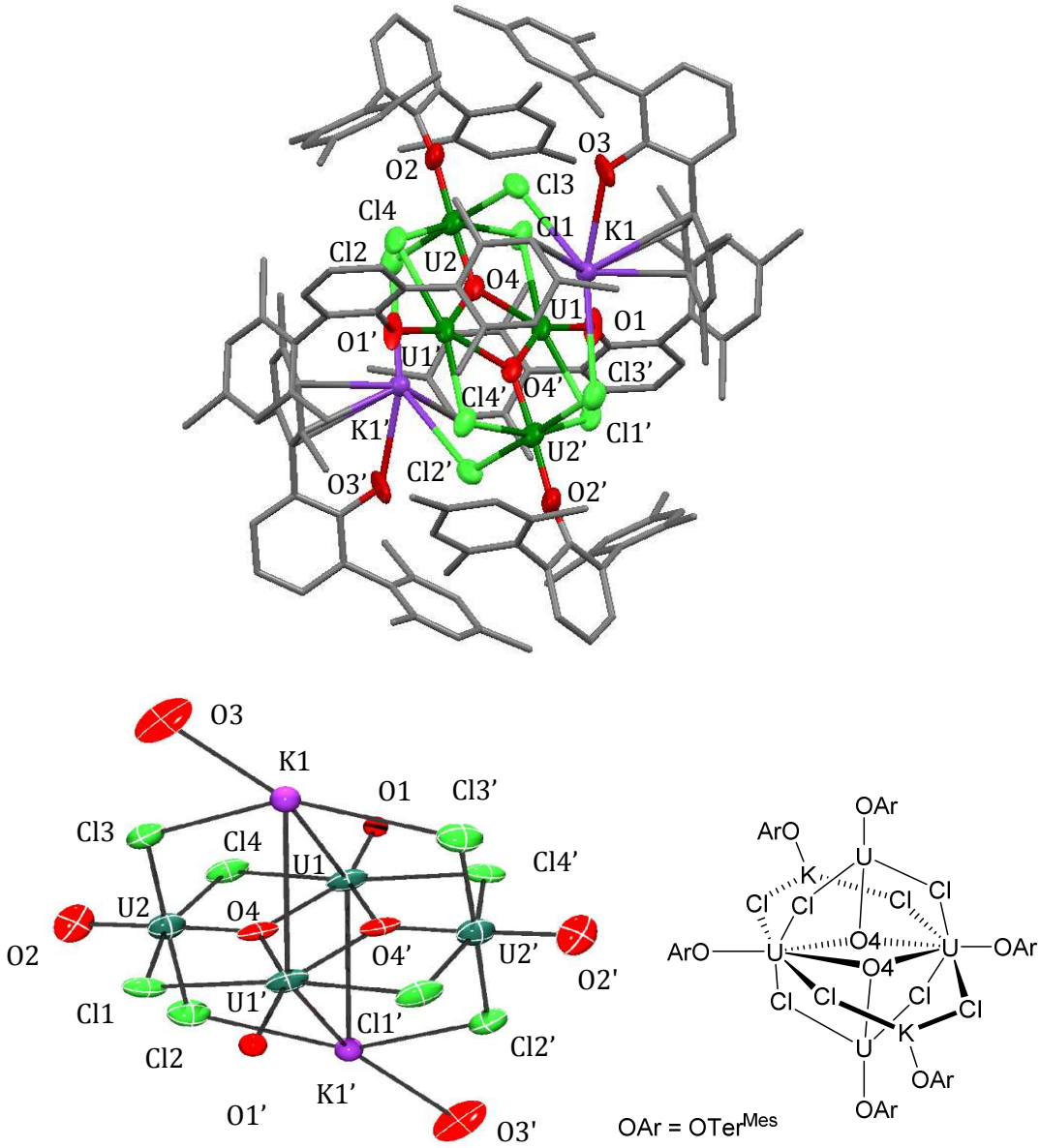

Figure 3.36: Top: Displacement ellipsoid drawing of the solid state molecular structure of **3.14,** $U_4K_2Cl_8(\mu^3\text{-})O_2(Ter^{Mes}O)_6$, with carbon atoms set to capped sticks and hydrogen atoms omitted for clarity. Bottom right: A view of the core of **3.14** with hydrogen and carbon atoms omitted for clarity.

Table **3.14** : Selected X-ray crystallographic data for **3.14**

Bond	Bond distance (Å) / angle (°)
U1-U1', U1-U2, U2-U2'	4.179(2), 3.866(7), 6.490(2)
K1-U1, K1-U2	4.26 (2), 4.93(2)
C1-O1, C25-O2, C49-O3	1.31(7), 1.23(6), 1.37(5)
U1-O2, U1-O2, U2-O4, U1-O4	1.99(6), 2.36(7), 1.94(5), 2.49(7)
U1-O2, U1-O4	2.36(7), 2.49(7)
K1-O3, K1-Cl2, K1-Cl3	2.95(5), 3.37(3), 3.44(3)
U1-Cl1, U1-Cl4, U2-Cl1, U2-Cl2, U2-Cl3, U2-Cl3	2.86(2), 2.83(2), 2.64(3), 2.595(18), 2.571(19)
U1-O1-C1, U2-O2-C25, K1-O3-C49	171(5), 151(4), 134(4)
O4-U1-O4', U1-O4-U1', O4-U2-O1, O4-U1-O2	65(2), 115(2), 175(2), 148(3)
Cl3-K1-Cl2, Cl4-U2-Cl1, Cl2-U2-Cl3, Cl2-U2-Cl4	140.8(7), 160.5(6), 178.3(3), 90.5(6)
Cl2-U2-Cl1, Cl1-U2-Cl3,Cl4-U2-Cl3, Cl1-U1-Cl4	89.2(6), 91.3(7) 88.5(7), 158.8(6)
O2-U1-Cl1, O2-U1-Cl4	80(1), 79(1)

3.6.1.2 Reaction of $UI_4(dioxane)_2$ with in situ generated $Ter^{Mes}OK$

Reaction of two equivalents of *in situ* generated $Ter^{Mes}OK$, from reaction of KH and $Ter^{Mes}OH$ in toluene, with a THF solution of $UI_4(dioxane)_2$ resulted in a reaction occurring. The ^1H NMR spectrum of the products of this reaction show one major set of paramagnetic resonances that can be assigned to a symmetric product containing two $Ter^{Mes}O^-$ ligands of the form $(Ter^{Mes}O)_2UI_2$. Attempts to isolate and characterise this paramagnetic product did not prove successful.

3.6.2 Uranium (III) salts

3.6.2.1 Reaction of UI_3 with in situ generated $Ter^{Mes}OK$

Reaction of two equivalents of *in situ* generated $Ter^{Mes}OK$, from reaction of KH and $Ter^{Mes}OH$ in toluene, with a THF solution of UI_3 resulted in a reaction occurring. The ^1H NMR spectrum of the products of this reaction show twenty two paramagnetic resonances suggesting multiple products. Attempts to isolate or characterise these products were not successful.

3.6.2.2 Reaction of $U(BH_4)_3(THF)_2$ with in situ generated $Ter^{Mes}OK$

Reaction of two equivalents of *in situ* generated $Ter^{Mes}OK$, from reaction of KH and $Ter^{Mes}OH$ in toluene, with a THF solution of $U(BH_4)_3(THF)_2$ resulted in a reaction occurring. The ^1H NMR spectrum of the products of this reaction show twenty eight paramagnetic resonances suggesting multiple products. Attempts to isolate or characterise these products were not successful.

3.7 Conclusions and Summary

In summary, we have the successful synthesis of a heteroleptic thorium terphenolate chlorido complex, which has shown some reactivity. This represents a resolution of one of the primary aims of this project as outlined in *Chapter One*. Unfortunately the majority of reactivity has resulted in transmetallation, with the loss of the terphenolate ligands from the thorium centre, leading to the conclusion that Group I transfer reagents are too 'hard' for this system to result in the desired reactivity. When switching to Group II transfer reagents transmetallation was seen in the majority of cases, but was not seen to go to completion in the case of softer ligand moieties. The isolation of **3.14**, a uranium cluster with potentially ambiguous formal oxidation states was described. However, due to poor crystal data and the indefinite pathway to its synthesis further characterisation was not possible. The formation of **3.11**, a complex containing nine Th-C bonds, signifies a partial resolution of the secondary aims of this project; to synthesis a complex with Th-C bonds that may facilitate small molecule activation. Attempts to activate small molecules using **3.11** did not result in isolable products, whilst attempts to transform **3.2** with simple substitution reactions to help facilitate small molecule activations did not prove successful. In the next chapter investigations into what changing the ancillary ligands of heteroleptic terphenolate complexes has upon reactivity will be presented.

3.8 References

1. J. McKinven, G. S. Nichol and P. L. Arnold, *Dalton Trans.*, 2014, 43, 17416-17421.
2. C. A. Tolman, *J. Am. Chem. Soc.*, 1970, 92, 2956-2965.
3. C. A. Tolman, W. C. Seidel and L. W. Gosser, *J. Am. Chem. Soc.*, 1974, 96, 53-60.
4. C. A. Tolman, *Chem. Rev.*, 1977, 77, 313-348.
5. H. Clavier and S. P. Nolan, *Chem. Commun.*, 2010, 46, 841-861.
6. A. Poater, B. Cosenza, A. Correa, S. Giudice, F. Ragone, V. Scarano and L. Cavallo, *Eur. J. Inorg. Chem.*, 2009, 2009, 1759-1766.

7. S. M. Mansell, N. Kaltsoyannis and P. L. Arnold, *J. Am. Chem. Soc.*, 2011, 133, 9036-9051.
8. S. C. Marinescu, V. W. L. Ng, A. G. Lichtscheidl, R. R. Schrock, P. Müller and M. K. Takase, *Organometallics*, 2012, 31, 6336-6343.
9. L. C. H. Gerber, R. R. Schrock, P. Müller and M. K. Takase, *J. Am. Chem. Soc.*, 2011, 133, 18142-18144.
10. D. V. Peryshkov, R. R. Schrock, M. K. Takase, P. Müller and A. H. Hoveyda, *J. Am. Chem. Soc.*, 2011, 133, 20754-20757.
11. D. V. Peryshkov and R. R. Schrock, *Organometallics*, 2012, 31, 7278-7286.
12. A. G. Lichtscheidl, V. W. L. Ng, P. Müller, M. K. Takase and R. R. Schrock, *Organometallics*, 2012, 31, 2388-2394.
13. F. M. Chadwick and D. M. O'Hare, *Organometallics*, 2014, 33, 3768-3774.
14. C. E. Hayes, D. E. Gill, M. L. Brown and D. B. Leznoff, *Eur. J. Inorg. Chem.*, 2014, 2014, 3690-3700.
15. J. T. Golden, D. N. Kazul'kin, B. L. Scott, A. Z. Voskoboynikov and C. J. Burns, *Organometallics*, 2003, 22, 3971-3973.
16. F. Dulong, P. Thuéry, M. Ephritikhine and T. Cantat, *Organometallics*, 2013, 32, 1328-1340.
17. C. Villiers, P. Thuery and M. Ephritikhine, *Chem. Commun.*, 2007, 2832-2834.
18. K. C. Jantunen, F. Haftbaradaran, M. J. Katz, R. J. Batchelor, G. Schatte and D. B. Leznoff, *Dalton Trans.*, 2005, 3083-3091.
19. O. J. Cooper, D. P. Mills, W. Lewis, A. J. Blake and S. T. Liddle, *Dalton Trans.*, 2014, 43, 14275-14283.
20. M. A. Edelman, M. F. Lappert, J. L. Atwood and H. Zhang, *Inorg. Chim. Acta*, 1987, 139, 185-186.
21. P. C. Blake, E. Hey, M. F. Lappert, J. L. Atwood and H. Zhang, *J. Organomet. Chem.*, 1988, 353, 307-314.
22. I. Korobkov, S. Gorelsky and S. Gambarotta, *J. Am. Chem. Soc.*, 2009, 131, 10406-10420.
23. I. Korobkov, B. Vidjayacoumar, S. I. Gorelsky, P. Billone and S. Gambarotta, *Organometallics*, 2010, 29, 692-702.
24. T. M. Trnka, J. B. Bonanno, B. M. Bridgewater and G. Parkin, *Organometallics*, 2001, 20, 3255-3264.
25. C. A. Secaur, V. W. Day, R. D. Ernst, W. J. Kennelly and T. J. Marks, *J. Am. Chem. Soc.*, 1976, 98, 3713-3715.
26. J.-C. Tourneux, J.-C. Berthet, T. Cantat, P. Thuéry, N. Mézailles, P. Le Floch and M. Ephritikhine, *Organometallics*, 2011, 30, 2957-2971.
27. F. Allen, *Acta Crystallogr., Sect. B: Struct. Sci*, 2002, 58, 380-388.
28. W. Ren, G. Zi, D.-C. Fang and M. D. Walter, *J. Am. Chem. Soc.*, 2011, 133, 13183-13196.
29. E. Barnea, T. Andrea, M. Kapon and M. S. Eisen, *J. Am. Chem. Soc.*, 2004, 126, 5066-5067.
30. I. S. R. Karmel, T. Elkin, N. Fridman and M. S. Eisen, *Dalton Trans.*, 2014, 43, 11376-11387.
31. K. E. Knope, R. E. Wilson, M. Vasiliu, D. A. Dixon and L. Soderholm, *Inorg. Chem.*, 2011, 50, 9696-9704.
32. R. E. Wilson, S. Skanthakumar, P. C. Burns and L. Soderholm, *Angew. Chem., Int. Ed. Engl.*, 2007, 46, 8043-8045.
33. N. Torapava, I. Persson, L. Eriksson and D. Lundberg, *Inorg. Chem.*, 2009, 48, 11712-11723.

34. H. Moll, M. A. Denecke, F. Jalilehvand, M. Sandström and I. Grenthe, *Inorg. Chem.*, 1999, 38, 1795-1799.
35. R. Spezia, C. Beuchat, R. Vuilleumier, P. D'Angelo and L. Gagliardi, *J. Phys. Chem. B*, 2012, 116, 6465-6475.
36. S. R. Daly, P. M. B. Piccoli, A. J. Schultz, T. K. Todorova, L. Gagliardi and G. S. Girolami, *Angew. Chem., Int. Ed. Engl.*, 2010, 49, 3379-3381.
37. R. D. Shannon, *Acta Crystallogr. Sect. A*, 1976, 32, 751-767.
38. J. A. Dean and N. A. Lange, *Lange's handbook of chemistry*, McGraw-Hill, 1992.
39. E. Lu, O. J. Cooper, J. McMaster, F. Tuna, E. J. L. McInnes, W. Lewis, A. J. Blake and S. T. Liddle, *Angew. Chem., Int. Ed. Engl.*, 2014, 53, 6696-6700.
40. J. A. Higgins, F. G. N. Cloke and S. M. Roe, *Organometallics*, 2013, 32, 5244-5252.
41. P. L. Arnold, T. Cadenbach, I. H. Marr, A. A. Fyfe, N. L. Bell, R. Bellabarba, R. P. Tooze and J. B. Love, *Dalton Trans.*, 2014, 43, 14346-14358.
42. W. J. Evans, M. K. Takase, J. W. Ziller and A. L. Rheingold, *Organometallics*, 2009, 28, 5802-5808.
43. B. S. Newell, A. K. Rappé and M. P. Shores, *Inorg. Chem.*, 2010, 49, 1595-1606.
44. B. S. Newell, T. C. Schwaab and M. P. Shores, *Inorg. Chem.*, 2011, 50, 12108-12115.
45. A. Zalkin, J. G. Brennan and R. A. Andersen, *Acta Crystallogr., Sect. C: Cryst. Struct. Commun.*, 1987, C43, 421-423.
46. J. W. Bruno, T. J. Marks and V. W. Day, *J. Organomet. Chem.*, 1983, 250, 237-246.
47. A. R. Fox, S. E. Creutz and C. C. Cummins, *Dalton Trans.*, 2010, 39, 6632-6634.
48. J. S. Parry, F. G. N. Cloke, S. J. Coles and M. B. Hursthouse, *J. Am. Chem. Soc.*, 1999, 121, 6867-6871.
49. P. C. Blake, M. F. Lappert, J. L. Atwood and H. Zhang, *J. Chem. Soc., Chem. Commun.*, 1986, 1148-1149.
50. P. C. Blake, N. M. Edelstein, P. B. Hitchcock, W. K. Kot, M. F. Lappert, G. V. Shalimoff and S. Tian, *J. Organomet. Chem.*, 2001, 636, 124-129.
51. N. A. Siladke, C. L. Webster, J. R. Walensky, M. K. Takase, J. W. Ziller, D. J. Grant, L. Gagliardi and W. J. Evans, *Organometallics*, 2013, 32, 6522-6531.
52. B. Kanellakopulos, E. Dornberger and F. Baumgaertner, *Inorg. Nucl. Chem. Lett.*, 1974, 10, 155-160.
53. C. Loh, S. Seupel, H. Görls, S. Krieck and M. Westerhausen, *Eur. J. Inorg. Chem.*, 2014, 2014, 1312-1321.
54. D. R. Armstrong, M. G. Davidson, D. Garcia-Vivo, A. R. Kennedy, R. E. Mulvey and S. D. Robertson, *Inorg. Chem.*, 2013, 52, 12023-12032.
55. W. Uhl, E. Er and M. Matar, *Z. Anorg. Allg. Chem.*, 2006, 632, 1011-1017.
56. D. R. Armstrong, E. Brammer, T. Cadenbach, E. Hevia and A. R. Kennedy, *Organometallics*, 2013, 32, 480-489.
57. D. Scheschkewitz, M. Menzel, M. Hofmann, P. v. R. Schleyer, G. Geiseler, W. Massa, K. Harms and A. Berndt, *Angew. Chem., Int. Ed. Engl.*, 1999, 38, 2936-2939.
58. R. A. Bartlett, H. V. R. Dias and P. P. Power, *J. Organomet. Chem.*, 1988, 341, 1-9.
59. S. Harder and M. Lutz, *Organometallics*, 1994, 13, 5173-5176.
60. M. F. Zuniga, G. B. Deacon and K. Ruhlandt-Senge, *Inorg. Chem.*, 2008, 47, 4669-4681.
61. T. J. Kealy and P. L. Pauson, *Nature*, 1951, 168, 1039-1040.
62. S. A. Miller, J. A. Tebboth and J. F. Tremaine, *J. Chem. Soc.,*, 1952, 632-635.
63. G. Wilkinson, M. Rosenblum, M. C. Whiting and R. B. Woodward, *J. Am. Chem. Soc.*, 1952, 74, 2125-2126.
64. T. J. Boyle, L. A. M. Ottley, C. A. Apblett, C. A. Stewart, S. M. Hoppe, K. L. Hawthorne and M. A. Rodriguez, *Inorg. Chem.*, 2011, 50, 6174-6182.

65. J. S. Figueroa, J. G. Melnick and G. Parkin, *Inorg. Chem.*, 2006, 45, 7056-7058.
66. D. J. Darensbourg, C. G. Ortiz and D. R. Billodeaux, *Inorg. Chim. Acta*, 2004, 357, 2143-2149.
67. C. Ni and P. P. Power, *Chem. Commun.*, 2009, 5543-5545.
68. M. R. Russo, N. Kaltsoyannis and A. Sella, *Chem. Commun. (Cambridge, U. K.)*, 2002, 2458-2459.
69. K. V. Baker, J. M. Brown, N. Hughes, A. J. Skarnulis and A. Sexton, *J. Org. Chem*, 1991, 56, 698-703.
70. P. J. Bailey, S. T. Liddle, C. A. Morrison and S. Parsons, *Angew. Chem., Int. Ed.*, 2001, 40, 4463-4466.
71. T. J. Woodman, M. Schormann and M. Bochmann, *Organometallics*, 2003, 22, 2938-2943.
72. C. K. Simpson, R. E. White, C. N. Carlson, D. A. Wrobleski, C. J. Kuehl, T. A. Croce, I. M. Steele, B. L. Scott, V. G. Young, T. P. Hanusa, A. P. Sattelberger and K. D. John, *Organometallics*, 2005, 24, 3685-3691.
73. P. K. Eckert, B. Schnura and C. Strohmann, *Chem. Commun.*, 2014, 50, 2532-2534.
74. K. T. Quisenberry, C. K. Gren, R. E. White, T. P. Hanusa and W. W. Brennessel, *Organometallics*, 2007, 26, 4354-4356.
75. T. J. Woodman, M. Schormann, D. L. Hughes and M. Bochmann, *Organometallics*, 2003, 22, 3028-3030.
76. C. H. McMillen, C. K. Gren, T. P. Hanusa and A. L. Rheingold, *Inorg. Chim. Acta*, 2010, 364, 61-68.
77. K. T. Quisenberry, R. E. White, T. P. Hanusa and W. W. Brennessel, *New J. Chem.*, 2010, 34, 1579-1584.
78. S. A. Sulway, R. Girshfeld, S. A. Solomon, C. A. Muryn, J. Poater, M. Solà, F. M. Bickelhaupt and R. A. Layfield, *Eur. J. Inorg. Chem.*, 2009, 2009, 4157-4167.
79. S. A. Solomon, C. A. Muryn and R. A. Layfield, *Chem. Commun.*, 2008, 3142-3144.
80. L. F. Sanchez-Barba, D. L. Hughes, S. M. Humphrey and M. Bochmann, *Organometallics*, 2005, 24, 5329-5334.
81. W. J. Evans, J. M. Perotti and J. W. Ziller, *J. Am. Chem. Soc.*, 2005, 127, 1068-1069.
82. W. J. Evans, T. M. Champagne, J. W. Ziller and N. Kaltsoyannis, *J. Am. Chem. Soc.*, 2006, 128, 16178-16189.
83. G. M. Smith, M. Sabat and T. J. Marks, *J. Am. Chem. Soc.*, 1987, 109, 1854-1856.
84. W. Ren, G. Zi, D.-C. Fang and M. D. Walter, *Chem. Eur. J.*, 2011, 17, 12669-12682.
85. C. A. Cruz, D. J. H. Emslie, C. M. Robertson, L. E. Harrington, H. A. Jenkins and J. F. Britten, *Organometallics*, 2009, 28, 1891-1899.
86. C. N. Carlson, T. P. Hanusa and W. W. Brennessel, *J. Am. Chem. Soc.*, 2004, 126, 10550-10551.
87. R. R. Langeslay, J. R. Walensky, J. W. Ziller and W. J. Evans, *Inorg. Chem.*, 2014, 53, 8455-8463.
88. I. Korobkov, S. Gambarotta and G. P. A. Yap, *Angew. Chem., Int. Ed. Engl.*, 2003, 42, 814-818.
89. E. C. Baker, K. N. Raymond, T. J. Marks and W. A. Wachter, *J. Am. Chem. Soc.*, 1974, 96, 7586-7588.
90. W. J. Evans, K. A. Miller, S. A. Kozimor, J. W. Ziller, A. G. DiPasquale and A. L. Rheingold, *Organometallics*, 2007, 26, 3568-3576.
91. D. M. Barnhart, R. J. Butcher, D. L. Clark, J. C. Gordon, J. G. Watkin and B. D. Zwick, *New J. Chem.*, 1995, 19, 503-508.
92. K. C. Jantunen, C. J. Burns, I. Castro-Rodriguez, R. E. Da Re, J. T. Golden, D. E. Morris, B. L. Scott, F. L. Taw and J. L. Kiplinger, *Organometallics*, 2004, 23, 4682-4692.

93. J. M. Manriquez, P. J. Fagan and T. J. Marks, *J. Am. Chem. Soc.*, 1978, 100, 3939-3941.
94. T. P. Hanusa and C. N. Carlson, in *Encyclopedia of Inorganic Chemistry*, John Wiley & Sons, Ltd, 2006.
95. S. C. Chmely, C. N. Carlson, T. P. Hanusa and A. L. Rheingold, *J. Am. Chem. Soc.*, 2009, 131, 6344-6345.
96. C. Lichtenberg, T. P. Spaniol, L. Perrin, L. Maron and J. Okuda, *Chem. Eur. J.*, 2012, 18, 6448-6452.
97. K. D. John, K. V. Salazar, B. L. Scott, R. T. Baker and A. P. Sattelberger, *Chem. Commun.*, 2000, 581-582.
98. F. A. Cotton and J. R. Pipal, *J. Am. Chem. Soc.*, 1971, 93, 5441-5445.
99. R. S. P. Turbervill and J. M. Goicoechea, *Chem. Commun.*, 2012, 48, 6100-6102.
100. R. A. Layfield, F. Garcia, J. Hannauer and S. M. Humphrey, *Chem. Commun.*, 2007, 5081-5083.
101. G. Erker, K. Berg, K. Angermund and C. Krueger, *Organometallics*, 1987, 6, 2620-2621.
102. S. Standfuss, E. Abinet, T. P. Spaniol and J. Okuda, *Chem. Commun.*, 2011, 47, 11441-11443.
103. D. L. Clark, S. K. Grumbine, B. L. Scott and J. G. Watkin, *J. Am. Chem. Soc.*, 1995, 117, 9089-9090.
104. R. J. Butcher, D. L. Clark, S. K. Grumbine, B. L. Scott and J. G. Watkin, *Organometallics*, 1996, 15, 1488-1496.
105. Y.-J. Hu, K. E. Knope, S. Skanthakumar and L. Soderholm, *Eur. J. Inorg. Chem.*, 2013, 2013, 4159-4163.
106. A. Mishra, K. A. Abboud and G. Christou, *Inorg. Chem.*, 2006, 45, 2364-2366.
107. D. L. Clark and J. G. Watkin, *Inorg. Chem.*, 1993, 32, 1766-1772.
108. U. Casellato, P. Guerriero, S. Tamburini, P. A. Vigato and A. Graziani, *Inorg. Chim. Acta*, 1987, 134, 165-174.
109. C. Hennig, S. Takao, K. Takao, S. Weiss, W. Kraus, F. Emmerling and A. C. Scheinost, *Dalton Trans.*, 2012, 41, 12818-12823.
110. J.-Y. Kim, A. J. Norquist and D. O'Hare, *Chem. Commun.*, 2002, 2198-2199.
111. W. Ren, H. Song, G. Zi and M. D. Walter, *Dalton Trans.*, 2012, 41, 5965-5973.
112. B. R. Galan and T. Rovis, *Angew. Chem., Int. Ed. Engl.*, 2009, 48, 2830-2834.
113. E. F. N. P. Freestone, H. Geckeis, L. Gmelin, J. H. Holloway, R. J. Meyer, E. H. E. Pietsch, , *Gmelin handbook of inorganic and organometallic chemistry* Verl. Chemie [u.a.], Berlin [u.a.], 1993.
114. T. M. Gilbert, R. R. Ryan and A. P. Sattelberger, *Organometallics*, 1989, 8, 857-859.
115. K. M. Krebs, J. Wiederkehr, J. Schneider, H. Schubert, K. Eichele and L. Wesemann, *Angew. Chem., Int. Ed. Engl.*, 2015, 54, 5502-5506.
116. A. R. Martin, D. J. Nelson, S. Meiries, A. M. Z. Slawin and S. P. Nolan, *Eur. J. Org. Chem.*, 2014, 2014, 3127-3131.
117. G. R. Fulmer, A. J. M. Miller, N. H. Sherden, H. E. Gottlieb, A. Nudelman, B. M. Stoltz, J. E. Bercaw and K. I. Goldberg, *Organometallics*, 2010, 29, 2176-2179.
118. H. W. Roesky and M. Andruh, *Coord. Chem. Rev.*, 2003, 236, 91-119.
119. S. A. Barnett and N. R. Champness, *Coord. Chem. Rev.*, 2003, 246, 145-168.

Chapter 4: Terphenolate complexes with borohydrides as ancillary ligands

This chapter comments in part on results that are published in the 2014 Dalton Transactions paper.[1]

4.1 Introduction

In *Chapter Three*, it has been established that heteroleptic *bis* terphenolate *bis* chlorido- complexes of thorium have a tendency to lose terphenolate ligands through unwanted transmetallation reactions with reagents. It was hoped that replacing the Cl^- ligands with BH_4^- would enable alternative reactive pathways.

Borohydride ligands, BH_4^-, are frequently considered as isolobal to halide, particularly chloride, ligands. This, however, is not the case. For ligands to be isolobal to one another they must satisfy certain principles as notably outlined by Hoffman in his Nobel lecture of 1982.[2] In this lecture he states that ligands are isolobal if "The number, symmetry, properties, approximate energy and shape of the frontier orbitals and the number of electrons in them are similar".[2] Borohydrido- and chlorido- ligands are therefore not isolobal, even though they display the same charge within a structure, especially when considering actinide complexes. It has been shown that a BH_4^- ligand has greater π-bonding character compared to the Cl^- ligand,[3] meaning that the symmetry and shape of the frontier orbitals are not similar. The capacity of a BH_4^- ligand for different bonding modes[4] means that assumptions surrounding the number of the frontier orbitals bonding to the metal become less certain.

A benefit of using borohydride ligands is that there exists an additional NMR active nucleus with any complex that is formed. This additional handle will make the subsequent characterisation more facile.

4.2 Synthesis of thorium terphenolate borohydrido- complexes

As reviewed in *Chapter One*, formation of crystallographically characterised thorium borohydride complexes is comparatively rare. Methods towards their formation involve reactions of $LiBH_4$ and $Ca(BH_4)_2$ with chlorido- complexes.[5, 6] As $LiBH_4$ was

discounted due to likely formation of transmetallation products, e.g. LiOTer^{Mes}, attempts to transform $ThCl_2(OTer^{Mes})_2DME$ into a borohydride complex used $Ca(BH_4)_2$ as a transfer reagent.

4.2.1 Reaction of $ThCl_2(OTer^{Mes})_2DME$ with $Ca(BH_4)_2(THF)_2$[1]

A salt elimination reaction between $ThCl_2(OTer^{Mes})_2DME$, **3.2** and $Ca(BH_4)_2(THF)_2$ in toluene generates [Th(OTerMes)$_2$((μ-H)$_3$BH)$_2$(DME)], **4.1** as colourless crystals in 63 % yield after workup (Equation 4.1). The use of $Ca(BH_4)_2(THF)_2$ as a metathesis precursor for forming thorium borohydride complexes has precedent.[6] The solid state structure of **4.1** is displayed in **Figure 4.4**. Selected bond angles and distances calculated from the solid state structure of **4.1**, are shown in **Table 4.1.**

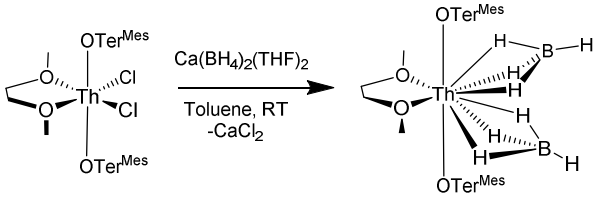

(4.1)

Heteroleptic thorium terminal borohydride complexes are rare, with only three other reported fully characterised examples, [Th(N(SiMe$_3$)$_2$)$_3$((μ-H)$_3$BH)], **A**, [Th(Ind*)$_2$((μ-H)$_3$BH)$_2$], **B**, (Ind* = permethylated indenyl) and Th((μ-H)$_3$BH)$_2$) ($H_3BNMe_2BH_3$)$_2$, **C,** the structures of which are shown in **Figure 4.1**.[5-7] The BH_4 groups are readily identified in the NMR spectra as a broad shoulder beneath one of the DME proton resonances at 3.03 ppm in the ^{1}H NMR spectrum, and a poorly resolved pentet at -12.42 ppm in the ^{11}B NMR spectrum, which is resolved as a singlet upon proton decoupling. This is consistent with an averaged BH4 proton environment on the NMR time scale. No boron NMR spectroscopic data were reported for other heteroleptic thorium borohydrides; for comparison the homoleptic [Th(BH_3CH_3)$_4$], **D**, (**Figure 4.2**) has a ^{11}B NMR spectral chemical shift at -19.3 ppm appearing as a quartet.[8] The FTIR spectrum of **4.1** displays weak absorptions consistent with (μ-H)$_3$BH binding:[4] ν(B–H$_t$) 2473 and 2455 cm^{-1} and ν(B–H$_\mu$) 2225 and 2164 cm^{-1}. Single crystals suitable for x-ray diffraction of **4.1** were grown from a saturated solution in toluene at -30°C.

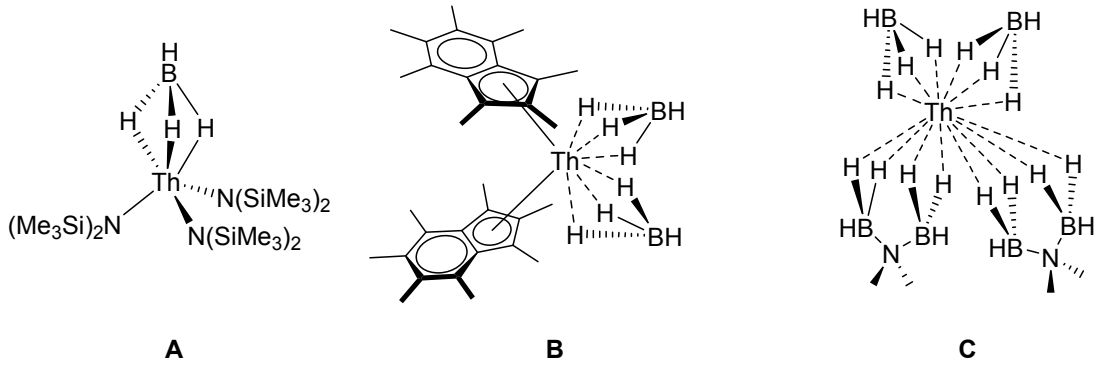

Figure 4.1: Previously crystallographically characterised thorium borohydride complexes as reported by Andersen, Parkin and Girolami *et al*.[5-7]

The solid-state molecular structure of **4.1**, **Figure 4.2**, is essentially the same as that of **3.2** ($ThCl_2(OTer^{Mes})_2DME$,), although the O1-Th1-O2 angle of 158.5(2)° is now significantly more bent than in **3.2.** There is also a notable difference between the Cl1-Th1-Cl1 angle in **3.2**, 127.28(7)°, and the B1-Th1-B2 bond angle in **4.1**, 95.8(3)°, presumably a result of the greater steric demand of the tridentate borohydride ligand and perhaps due to the greater π-bonding character of the BH_4- ligand compared to the Cl^- ligand, and its capacity for different bonding modes.[3, 4] The Th-O1 bond distance of 2.191(4) Å in **4.1**, is identical within s.u.s. to the analogous bond distance in **3.2** of 2.180(3) Å.

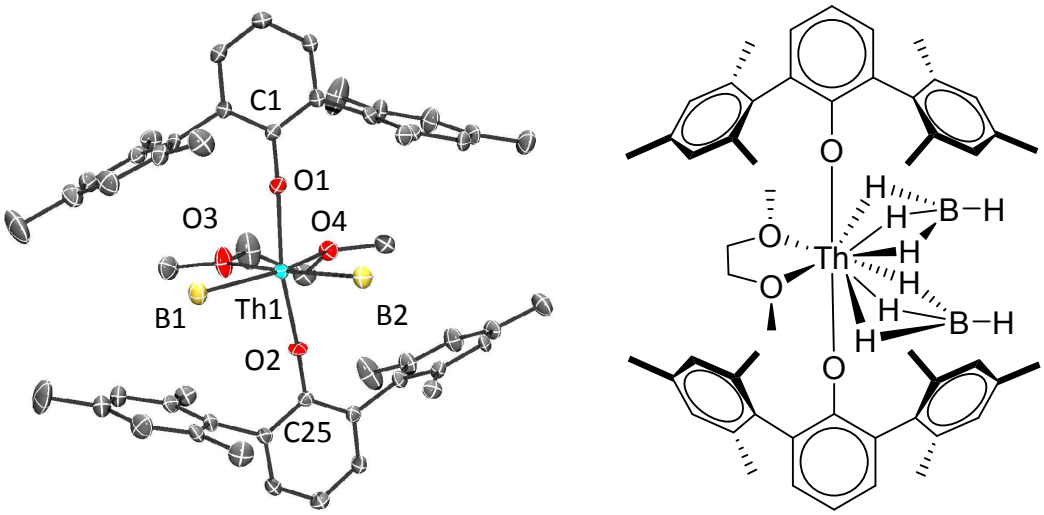

Figure 4.2: Displacement ellipsoid drawing of the solid-state molecular structure of $[Th(OTer^{Mes})_2(BH_4)_2(DME)]$, **4.1** (50 % probability ellipsoids). Hydrogen atoms and toluene solvent molecules are omitted for clarity.

The Th-B1,2 distances in **4.1** are 2.624(9) and 2.67(1) Å, respectively. Compared to the three previously reported thorium borohydride complexes, whose Th-B distances range from 2.583(10) to 2.624(3) Å, the Th1-B2 distance is slightly longer, whilst the Th1-B1 distance falls within this range. Zalkin *et al.* reported upon related methyl substituted Th-BH_4 complexes;[8, 9] $Th(BH_3Me)_4$, **D**, and its solvated analogues $Th_2(BH_3Me)_6(\mu^2\text{-}(BH_3Me))_2(Et_2O)$, **E** and $Th_2(BH_3Me)_6(\mu^2\text{-}(BH_3Me))_2(THF)_2$, **F,** (**Figure 4.3**). The terminal Th-B distances in these complexes ranged from 2.49(6) to 2.71(7) Å, whilst the bridging Th-B distances ranged from 2.91(2) to 3.107(8) Å.[8, 9]

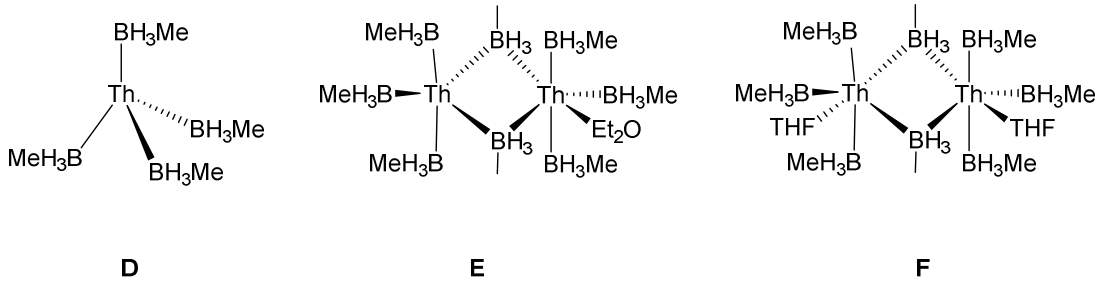

D **E** **F**

Figure 4.3: Examples of substituted homoleptic thorium borohydride complexes as reported by Zalkin *et al*.[8, 9]

The capacity of thorium to accommodate high co-ordination numbers, as shown most pertinently by $Th(H_3BNMe_2BH_3)_4$, **G**, shown in **Figure 4.4** which has a Werner co-ordination number of 15,[7] is thought to be the cause of the favourability of forming a borohydrido- complex from the corresponding chlorido-complex. Given the steric congestion of complex **G** it is unsurprising that the Th-B distances are longer than for those observed for complexes **A**-**F** and **4.1,** ranging from 2.882(3) to 3.193(5) Å.[7]

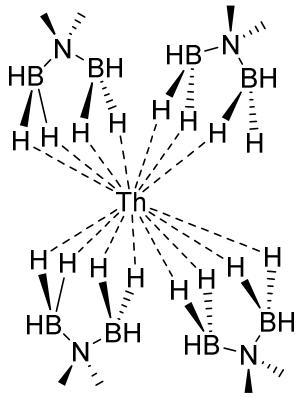

G

Figure 4.4: The only example of a 15-co-ordinate complex by Werner co-ordination number as reported by Girolami *et al*.[7]

The C-$O_{terphenolate}$ bond distances of **4.1** are 1.365(8) and 1.362(8) A, which is considerably longer than most of those observed for the majority of the complexes discussed in *Chapter Three*. While **3.1-2**, **3.6, 3.11** and **3.13** are identical within s.u.s (1.348(6), 1.352(5), 1.3678(17), 1.340(7) and 1.362(6) Å respectively) the transmetallation products of Group I and II and transition metals, **3.3-5**, **3.7-10** and **3.12,** display substantially shorter C-O bonds. It is notable that the structures containing longer C-O interactions either contain a Th(IV) centre or an Al(III) centre, both of which have high charge density. This can be attributed to the increased charge of the thorium (and aluminium) centre compared to alkali and alkali earth metals, which results in an increased electrostatic repulsion of the δ positive α carbon.

Table 4.1: Selected distances and angles for **4.1**

Atom	Distance (Å) / angle (°)
Th1-O1, Th1-O2	2.190(4), 2.191(5)
Th1-O3, Th1-O4	2.553(7), 2.507(5)
Th1-H1B, Th1-H2B, Th1-H3B	2.27(8), 2.31(8), 2.33(8)
Th1-H5B, Th1-H6B, Th1-H7B	2.21(7), 2.34(8), 2.50(8)
Th1-B1, Th1-B2	2.624(9), 2.67(1)
C1-O1, C25-O2	1.365(8), 1.362(8)
C1-O1-Th1, C25-O2-Th1	172.7(5), 172.4(5)
O1-Th1-O2, O1-Th1-O3, O1-Th1-O4	158.51(16), 84.6(2), 79.39(19)
O2-Th1-O3, O2-Th1-O4, O3-Th1-O4	84.3(2), 79.20(18), 63.7(2)
B1-Th1-B2	95.8(3)

4.3 Reactivity of thorium terphenolate borohydrido-complexes

The formation of the borohydride analogue, **4.1**, of the DME solvated chlorido-complex, **3.2,** was a breakthrough in this project. Complexes with borohydrides as ancillary ligands have the potential to exhibit differing reactivity to that seen for those with chlorido- ligands in *Chapter Three*. This makes them promising precursors in the search for complexes suitable for facilitating small molecule activation. As such, the key transformations targeted from the formation of **4.1** were twofold: Firstly, ligand substitution to replace the borohydrido- ligands with moieties known to enable small molecule activation, i.e. hydrides or alkyls; secondly, remove the solvating DME molecule, thereby increasing the ease of access to vacant orbitals of the co-ordination sphere of the thorium centre and thus allowing the approach of potential substrates.

4.3.1 Reaction of $Th((\mu\text{-}H)_3BH)_2(OTer^{Mes})_2DME$ with $AlMe_3$ or Al^iPr_3[1]

A variety of experiments were undertaken with the aim of of removing the coordinated DME solvent from **4.1** similar to those described for its chlorido-ligated analogue **3.2** as detailed in *Section 3.X* . The application of dynamic vacuum (10^{-3} mbar over 12 hours) or heating in non-coordinating solvents (benzene, toluene, hexane) had no effect. The treatment of **3.2** with trimethyl aluminium or tri-isopropyl aluminium in toluene, as described in section *3.5.2.1* also yielded no reaction, but in the case of **4.1** resulted in the abstraction of DME to afford $AlMe_3$.DME and the unusually low-coordinate $Th(OTer^{Mes})_2((\mu\text{-}H)_3BH)_2$, **4.2**, as colourless needles in a 50 % yield after workup (Equation 4.2). The solid state structure of **4.2** is displayed in **Figure 4.6**. Selected bond angles and distances calculated from **4.2** are shown in **Table 4.3.**

The contrast in reactivity between **3.2** and **4.1** can be attributed to the slight difference in Lewis acidity of the thorium centres. The $[Th^{IV}Cl_2]$ is a slightly harder, and stronger Lewis acid unit than the $[Th^{IV}(BH_4)_2]$ fragment, enabling the Al^{III} centre to out-compete the Th^{IV} centre for the O donor solvent DME in the latter case. As the initial rationale behind this reaction was to induce a transformation of the borohydrido ligands to the corresponding alkyl moiety, as indicated in Scheme **4.1**, the desolvation of the chelating DME molecule was unexpected.

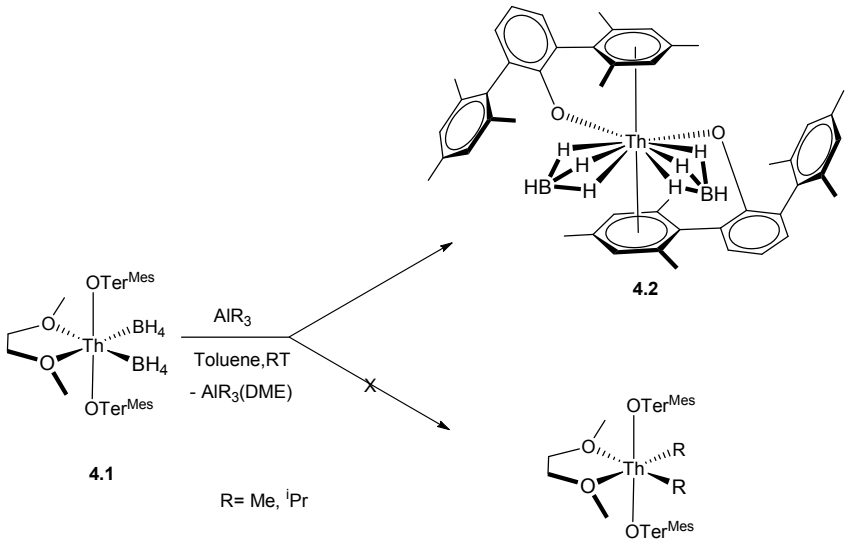

Scheme 4.1: Synthetic route to the formation of **4.2**

Single crystals suitable for X-ray diffraction were grown by allowing a C_6D_6 solution of **4.2** to evaporate to dryness. As can be seen in **Figure 4.6** one mesityl ring of each terphenolate ligand now participates in a η^6-interaction with the thorium ion, presumably to balance the effect of lowering the co-ordination number due to the loss of the chelating DME ligand. The Th^{IV} cation is *pseudo*-octahedral, with the two η^6-aryl interactions in *trans geometry*, forming a weakly sandwiched thorium bis(arene) fragment. The Th^{IV}-arene centroid angle, Ct-Th-Ct, is close to linear, at 172.9(9)°. The distance to one of the arenes is very long, and presumably a very weak interaction, characterised by a Th-Ct1 distance of 4.05(1) Å, while the other is short, with a Th-Ct2 distance of 2.815(3) Å. This, however, is still relatively long compared with the few other examples of Th-η^6-arene interactions in previously reported structures H-M, which are shown in **Figure 4.5**. A survey of the CSD found that neutral η^6-Th-Ct distances in the literature range from 2.706 to 2.950 Å.[10-13] This suggests that **4.2** should be considered to be a mono-arene complex with switchable ligation between the arene that ligates.

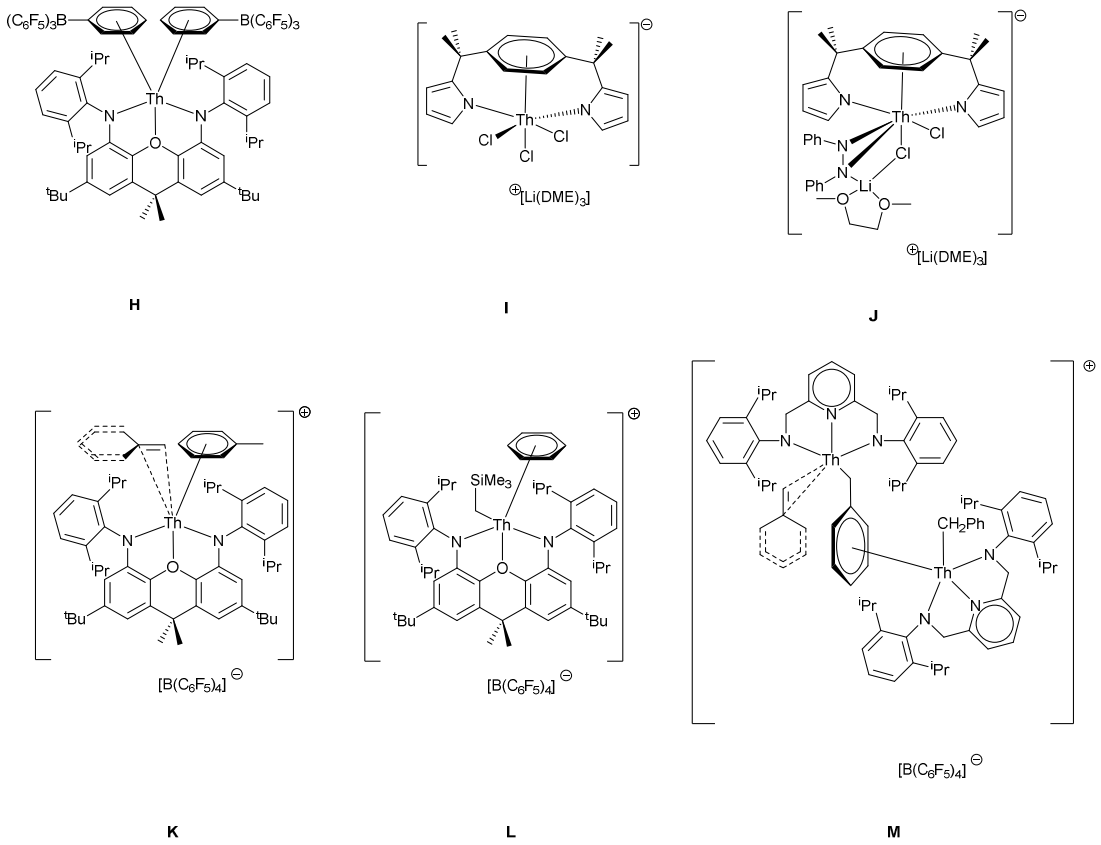

Figure 4.5: Examples of Th-η^6-aryl interactions as reported by Emslie and Gambarotta *et al*.[11-13]

As can be seen from **Figure 4.5**, **4.2** is, after **H**, only the second case of a thorium complex undergoing two η^6 –aryl interactions.[11] In addition **4.2** is also the second fully characterised example of a Th-η^6 –aryl interaction within neutral species as the thorium containing moieties in **I-J** are anionic, whilst for **K-M** they are cationic. Moreover, the Th-η^6 –aryl interactions in **4.2** represent the first to be observed in complexes not supported by chelating or macrocyclic ligands. The thorium-centroid (Th-Ct) distances in **4.2** are longer than the aryl *bis* pyrollide observed in the anionic thorium containing moieties in **I** and **J,** by Gambarotta *et al*.[12] Comparison of the Th-Ct distances in **4.2** to those observed in the cationic thorium containing moieties **K**-**M** finds that for **K** and **L** these interactions are longer than for those observed in **4.2**,[13] as would be initially expected. In **M**, however, the Th-Ct bond distance is shorter than that seen in **4.2** which is likely due to a steric effect of the bridging benzyl moiety stemming from the need to accommodate both thorium centres. A summary of the Th-Ct distances of Th-aryl complexes is displayed in **Table 4.2**. The η^6-aryl interactions in **4.2** deviate from co-planarity by 24.49°. This *trans* arrangement contrasts greatly with that seen for the *cis* geometry adopted within **H**. This is likely a function of the geometry adopted by the

supporting ligands.[11] The two O atoms and two B atoms are approximately co-planar, (Th1, B1 B2 and O1 have a torsion angle of -166.3°) with a deviation of the weaker Th-arene interaction, O_2Ter^{Mes-}, of 28.54° out of the plane. The $Ter^{Mes}O^-$ ligands are *cis*-disposed as evidenced by the O1-Th1-O2 bond angle of 89.0(3)° which is substantially smaller than the corresponding angle in **4.1**. The 92.9(7)° B1-Th1-B2 bond angle observed for **4.2** is also contracted compared its analogue in compound **3.2**.

Table 4.2: A summary of Th-Ct bond distances in Th-aryl complexes.

Complex	Th-Ct distance (Å)
H	2.728(5), 2.738(5)
I	2.701(8)
J	2.732(7)
K	2.935(6)
L	2.950(6)
M	2.798(5)
4.2	2.815(3), 4.05(1)

The room-temperature ^{1}H NMR spectrum of a benzene solution of **4.2** contains a single environment for the $Ter^{Mes}O^-$ protons, suggesting a dynamic equilibrium is present on the NMR timescale that interconverts the free and Th-bound Mes groups. Similarly to **4.1**, the BH_4^- groups appear as a broad resonance at -0.39 ppm in the ^{1}H NMR spectrum and as a poorly resolved triplet at -10.08 ppm in the ^{11}B NMR spectrum, resolving into a singlet upon proton decoupling. The FTIR spectrum of **2** displays weak absorptions characteristic of a (μ-H)$_3$ binding mode (2500–2200 cm^{-1}).[4] ν(B–H$_t$) 2474 cm^{-1} and ν(B–H$_\mu$) 2216 and 2149 cm^{-1}.

Hydrogen atoms of the borohydride moieties were not located in the solid-state structure of **4.2** (**Figure 4.6**). The Th-B bond distances in **4.1** and **4.2** (Th1-B1 = 2.671(19) Å, Th1-B2= 2.660(17) Å) are identical within s.u.s. The C-O bond distances of the terphenolate ligands in **4.2** (C-$O_{terphenolate}$ = 1.361(13) Å, 1.359(13) Å) are identical within s.u.s to those seen in **4.1**, and the other thorium containing complexes; **3.1-2**, **3.11** and **3.13**. In analogy to **4.1**, these C-O bond distances are longer than those seen for the potassium salt analogue, **3.3,** the greater uncertainty in the bond distances of **4.2,** however, renders the C-$O_{terphenolate}$ identical within s.u.s to the remainder of the complexes discussed in *Chapter Three*. Complex **4.2** is found to be fairly thermally

stable with only 5% decomposition observed upon refluxing a deuterated benzene solution of **4.2** for two weeks.

The solid state structure of **4.2,** combined with the ^{1}H NMR spectroscopic data in particular, indicates that the aryl interactions being fairly labile in solution. This suggests that **4.2** is likely to react with a given substrate, if it is a donor than the *ortho*-aryl rings of the Ter^{Mes}O^{-} ligand. Results of investigations into the suitability of **4.2** towards small molecule activation and catalysis are described in section *4.4 and 4.5*.

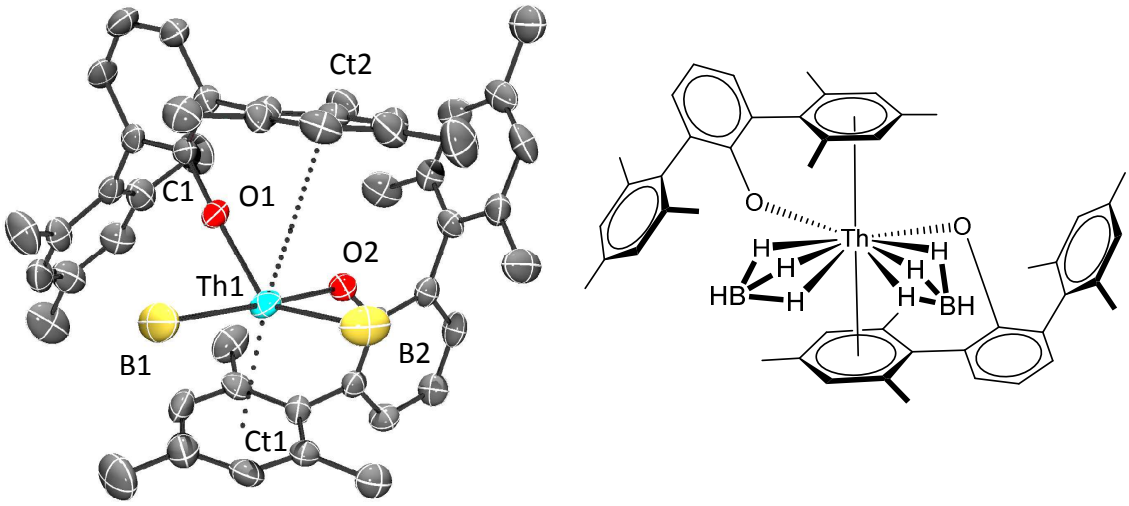

Figure 4.6: Displacement ellipsoid drawing of the solid-state molecular structure of Th(OTer^{Mes})$_2$((μ-H)$_3$BH)$_2$, **4.2** (50 % probability ellipsoids). Hydrogen atoms are omitted for clarity.

Table 4.3: Selected distances and angles data for **4.2**

Atom	Distance (Å) / angle (°)
Th1-O1, Th1-O2	2.213(8), 2.132(8)
Th1-B1, Th1-B2	2.671(19), 2.660(17)
C1-O1, C25-O2	1.361(13), 1.359(13)
Th1-Ct1, Th1-Ct2	4.05(1), 2.815(3)
Ct1-Th1-Ct2	172.9(7)
C1-O1-Th1, C25-O2-Th1	141.4(7), 156.5(7)
O1-Th1-O2	89.0(3)
O1-Th1-B1, O1-Th1-B2	90.8(5), 176.2(6)
O2-Th1-B1, O2-Th1-B2	132.5(5), 87.8(5)
B1-Th1-B2	92.9(7)

4.3.2 Reaction of $Th(OTer^{Mes})_2((\mu\text{-}H)_3BH)_2DME$ with 4,4 bipyridine[1]

Following from the abstraction of the DME ligand of **4.1**, reactivity with Lewis bases was studied. (*cf. 3.5.1*)

Treatment of **4.1** with two equivalents of 4,4'-bipyridine successfully displaced the coordinated DME to afford a co-ordination polymer $[Th(OTer^{Mes})_2(\mu\text{-}H_3BH)_2(4,4'\text{-}NC_5H_4C_5H_4N)]_\infty$, **4.3**, which crystallised readily and cleanly out of the reaction mixture as yellow crystals, equation 4.3. The solid state structure of a single repeat unit of **4.3** is displayed in **Figure 4.11**. Selected bond angles and distances calculated from the solid state structure of **4.3**, are shown in **Table 4.4**.

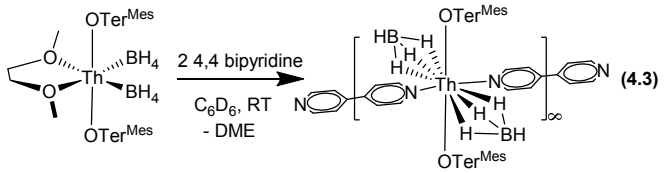

4.1 **4.3**

In the solid state structure of **4.3** the pseudo-octahedral Th^{IV} centre still has two *trans*-disposed $OTer^{Mes}$ ligands with the same angle (179.00(6)°) within s.u.s as its **3.1**-**2** analogues. The two BH_4 ligands, however, are now mutually *trans*, as evidenced by a B1–Th1–B1 angle of 167.33(10)°, allowing the *trans*-4,4'-bipyridine ligation to generate nearly linear 1-D polymeric chains in the solid state as shown in **Figure 4.10**.

The Th1–Th1'–Th1'' angle of 152.40(5)° shows that there is a significant undulation in the polymeric chain. The two OTer^{Mes} central aryloxide C_6 planes are now orthogonal, whereas in **3.1**, **3.2**, **3.13** and **4.1** they are parallel, presumably to reduce interactions with the coordinated bipyridine. A similar observation was made for the lithium complexes **3.4** and **3.10** discussed in Sections 3.3.2.2 and 3.3.7.1. While in those cases the relative size of the lithium cation was proposed to be the determining factor, in this case the reduction of steric strain with the bipyridine ligands appears to be the far more probable reason. The Th–O bonds are both short, 2.168(2) and 2.210(2) Å, with Th–O1 being shorter, perhaps due to a π-stacking interaction between one of the mesityl rings on O1Ter^{Mes} and the 4,4'-bipyridyl ligand (Ct1–Ct2 distance 3.74(7) Å).

The stacking leads to part of the terphenolate moiety being more proximal to the equatorial plane of the thorium cation, hence leading to a shortening of the Th-$O_{terphenolate}$ bond. Both Th– O bond lengths remain short for Th–O bonds, similar to those observed for **3.1-2, 3.11, 3.13** and **4.1-2**. The Th–N bond distances of 2.626(2) and 2.644(2) Å are typical.[10] The Th–B bond lengths in **4.3**, of 2.666(3) and 2.673(3) Å, are identical within s.u.s to those seen in **4.1-2**. The C-O bond distances of the terphenolate ligands in **4.3**, (Average C-O bond distance = 1.348(5) Å) are in analogy to **4.1-2** equivalent within s.u.s to the thorium containing complexes **3.1-2**, **3.11**, **3.13** and **4.1-2**.The $[BH_4]^-$ group is observed as a broad resonance at 3.28 ppm in the ^{1}H NMR spectrum and as a broad singlet at −6.42 ppm in the ^{11}B NMR spectrum, which sharpens upon proton decoupling, consistent with an averaged BH_4 proton environment on the NMR timescale. The FTIR spectrum of **4.3** contains weak absorptions in the 2500–2200 cm^{-1} region, consistent with a (μ-H)$_3$ binding mode; ν(B–H$_t$) 2454 cm^{-1} and ν(B–H$_\mu$) 2237 and 2171 cm^{-1}.

A clear and immediate contrast between the structures of the analogous co-ordination polymers **3.13** and **4.3** is that **3.13** forms a 2-D polymer, whilst **4.3** forms a 1-D polymer. The increased number of donor ligands in the solid state structure of **3.1.3** compared to that of **4.3** in the equatorial plane is likely the reason why this structural divergence is observed. The increased number of donor ligands in **3.13** also responsible for the three Th1-Th1'-Th1'' bond angles of 144.97(9), 150.32(9) and 64.66(9)°, in **3.13** compared to only one such angle existing in **4.3** (152.40(5)°). The first two angles found in **3.13** are comparable to the analogous angle observed for **4.3**,

whilst the third is less than half, resulting in the formation of a 2-D polymer in the form of sheets.

As a donor, 4,4'-bipyridine has been used extensively to bridge two metal centres to form co-ordination polymers, particularly for transition metals.[14] There are six known actinide compounds containing 4,4'-bipyridine as a bridging ligand and almost all involve uranium. The five previously fully characterised uranium examples, as shown in **Figure 4.7, N-R**[15-17] have been based upon either 'acac' type complexes of uranyl moieties or U(III) systems bearing three substituted cyclopentadienyl ligands, which are ubiquitous in low oxidation state actinide chemistry,.

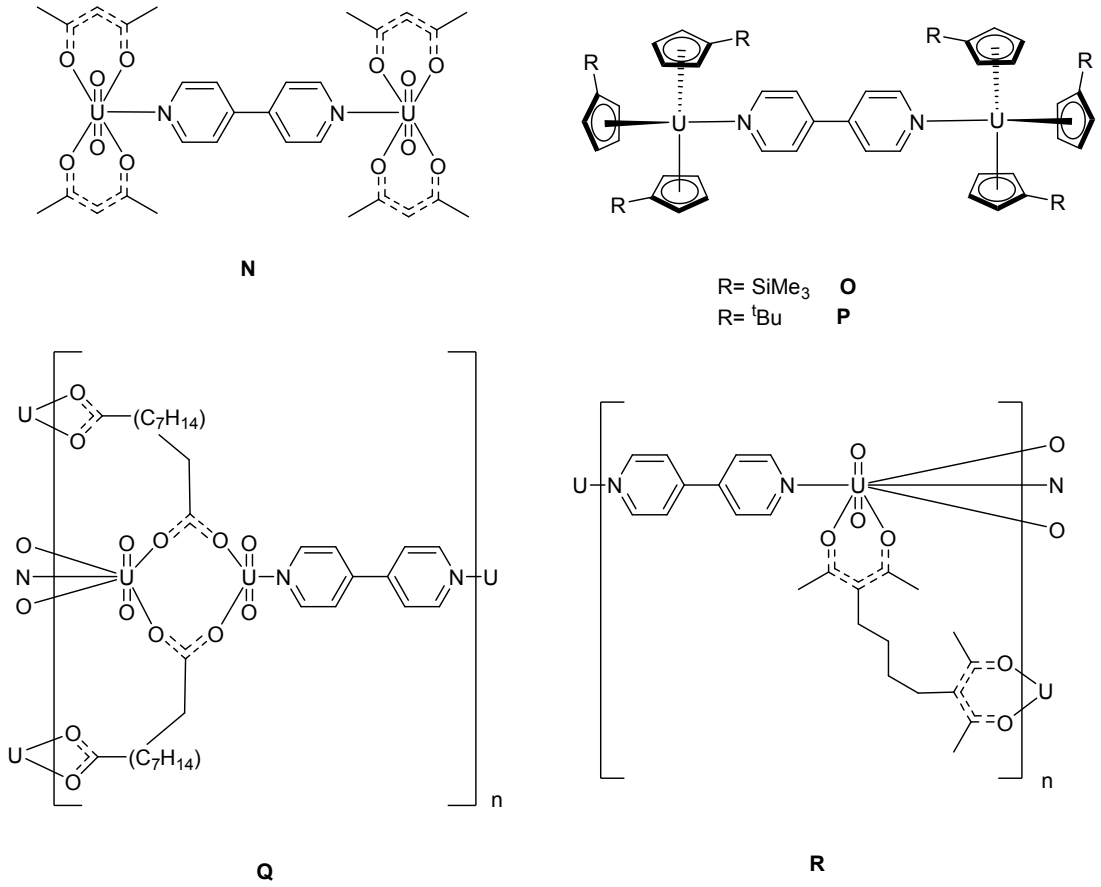

Figure 4.7: Examples of actinide complexes bridged by 4,4' bipyridine as reported by Kitazawa, Cahill and Ephritikhine *et al*.[15-17]

The U-N bond distances in complexes **N-R,** ranging from 2.543 to 2.664 Å, are very similar to the Th-N bond distances of 2.6263(19) and 2.6442(19) Å in **4.3**. These bond distances are significantly shorter than those observed in **3.13** (Th-N **=** 2.695(4), 2.667(5) and 2.677(4) Å). The primary reason for this shortening is likely the lower co-ordination number of **4.3**, with a secondary effect originating from the differing

electronics and sterics of the borohydrido-ligands compared to chlorido-ligands. At this time, **3.13** and **4.3** are the only complexes in the literature in which two thorium centres are bridged by 4,4'-bipyridine; and only the second and third examples of 4,4-bipyridine acting as a ligand towards thorium.[18] Complex **4.3** has considerably shorter Th-N bond distances than the first reported example, [Th(η^8-C_8H_8)$_2$(4,4'-bipyridyl)], **T**, (2.707(2) Å) the structure of which is shown in **Figure 4.8**.[18] This is likely due to a combination of the differences in the coordination number and the electronics of the ancillary ligands between these complexes.

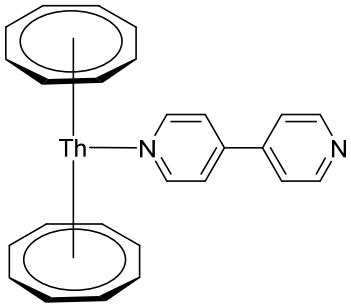

T

Figure 4.8: Precedent for 4,4'bipyridine ligation to a thorium centre as reported by Ephritikhine *et al*.[18]

In the process of characterising **4.3** it was noted that **4.3** is soluble in benzene and non-co-ordinating solvents. This is unusual for co-ordination polymers which, at the minimum, need a suitable additional donor to terminate the oligomer ends or fully break up the polymer. It is proposed that the demonstrated ability of the terphenolate arene groups to bind to the metal centres, as shown for **4.2**, provides a route for the polymeric structure to be re-dissolved and form monomers in such low polarity solvents.

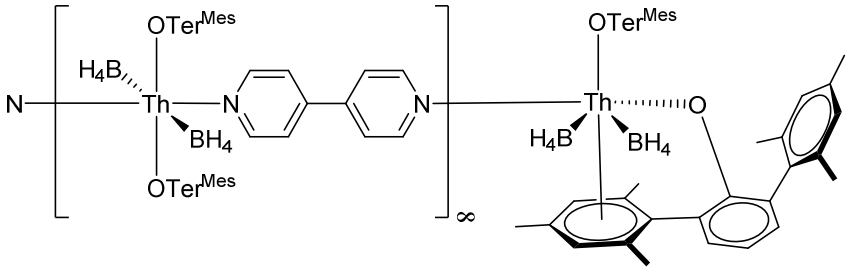

Figure 4.9: Proposed structure of thorium-terminated polymer.

The number of bipyridine ligands coordinated to the thorium centre appears to be directly responsible for the solid state structure of the complexes. While two *trans*-

oriented 4,4'-bipyridine molecules in **4.3** led to a (1D) chain structure, three molecules in a pentagonal equatorial plane, as observed for **3.13,** led to a (2D) sheet structure. Perhaps as a result, **3.13** contains voids of pore radius size 1.2 Å (similar to the radii of hydrogen gas) which makes up 6.3% of the unit cell volume, whilst **4.3** does not contain any voids of this size. This void volume of a structure is not atypical, given that MOF type structures regularly contain void volumes of around 50%.[19]

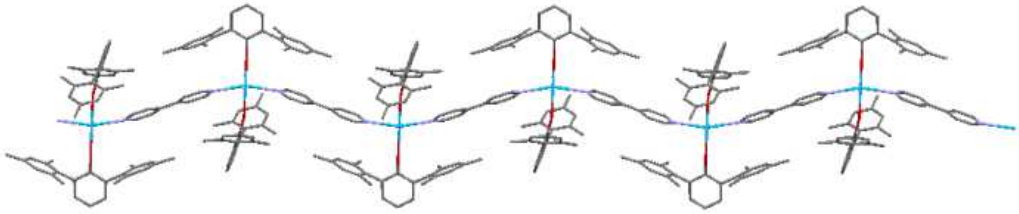

Figure 4.10: The 1-D polymeric chain structure of $[Th(OTerMes)_2((\mu\text{-}H)_3BH)_2(4,4'\text{-}NC_5H_4C_5H_4N)]_\infty$, **4.3**. Hydrogen atoms and toluene solvent molecules removed for clarity.

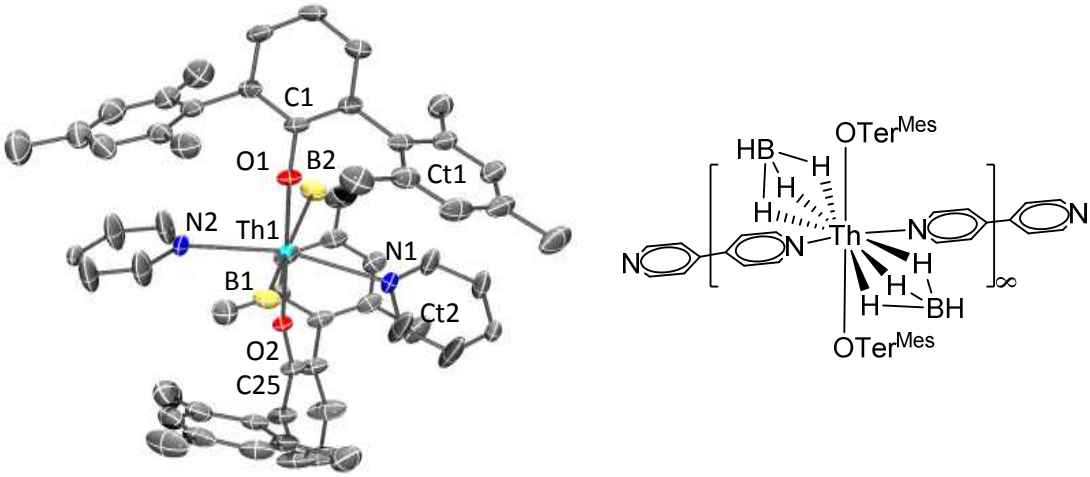

Figure 4.11: Displacement ellipsoid drawing of the solid-state molecular structure of $[Th(OTer^{Mes})_2((\mu\text{-}H)_3BH)_2(4,4'\text{-}NC_5H_4C_5H_4N)]_\infty$, **4.3** (50 % probability ellipsoids). Hydrogen atoms and co-crystallised solvent molecules are omitted for clarity.

Table 4.4: Selected distances and angles for **4.3**

Atom	Distance (Å) / angle (°)
Th1-O1, Th1-O2	2.1682(15), 2.2096(15)
Th1-B1, Th1-B2	2.667(3), 2.673(3)
Th1-N1, Th1-N2	2.6263(19), 2.6442(19)
C1-O1, C25-O2	1.342(3), 1.354(3)
C1-O1-Th1, C25-O2-Th1	161.09(15), 166.01(15)
O1-Th1-O2	179.00(6)
O1-Th1-B1, O1-Th1-B2, O2-Th1-B1, O2-Th1-B2	84.25(8), 83.96(8), 94.88(7), 96.95(8)
B1-Th1-B2	167.33(10)
B1-Th1-N1, B1-Th1-N2, B2-Th1-N1, B2-Th1-N2	89.19(9), 92.02(9), 88.61(9), 93.68(9)
O1-Th1-N1, O1-Th1-N2, O2-Th1-N1, O1-Th1-N2	101.54(6), 95.27(6), 78.93(6), 84.26(6)
N1-Th1-N2	163.19(7)
Th1-Th1'-Th1''	152.40(5)

4.3.3 Reaction of $Th(OTer^{Mes})_2((\mu\text{-}H)_3BH)_2DME$ with (Me allyl)Mg Cl

In addition to attempts to transform or remove the chelating DME molecule from **4.1**, experiments were performed with the goal of replacing the borohydrido-ligands into ligands that may enable small molecule activations to occur, *i.e.* hydrides or carbon-ligating moieties.

The reaction of 2 equivalents of a THF solution of 2-methyl allyl magnesium chloride with **4.1**, with the aim of examining if a monomeric allyl species or a dimeric cage in analogy to **3.11**, was undertaken as shown in **Scheme 4.2**. After workup of this reaction, colourless crystals were isolated in a 60 % yield from a saturated hexane solution stored at -30°C and characterised as $Mg(OTer^{Mes})((\mu\text{-}H)_3BH)THF)_2$, **4.4.** The solid state structure of **4.4** is displayed in **Figure 4.12** and selected bond angles and distances calculated from the solid state structure of **4.4** are shown in **Table 4.5.**

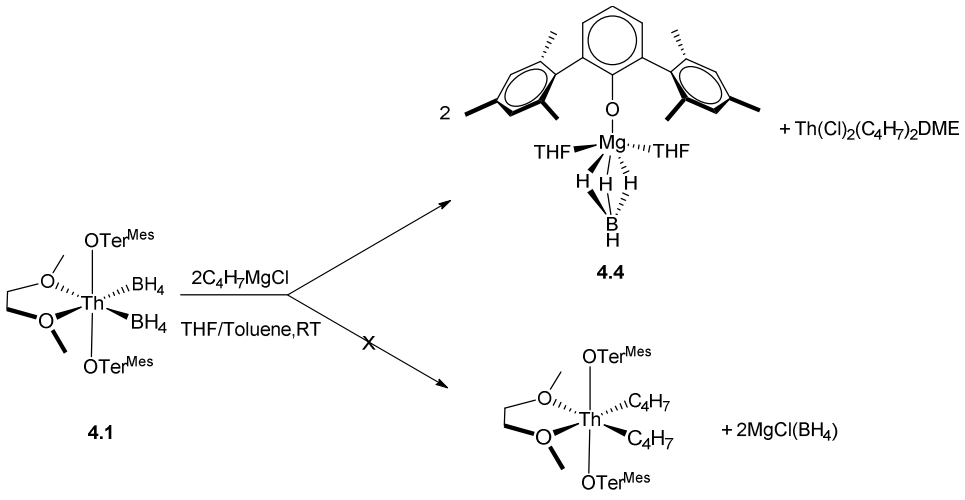

Scheme 4.2: Synthetic route towards the formation of **4.4**

The borohydride hydrogen atoms were located crystallographically and found to bind to the magnesium centre in a tridentate manner. However, due to the size of the borohydride ellipsoid it is likely that there is significant thermal motion at this position. As a result the location of the borohydride hydrogen atoms is less well defined than for the other hydrogen atoms within the structure. This is reflected by the thermal parameter for these atoms which lies in the range 0.11-0.19, whilst ideally this should be around 0.05, as is the case for the majority of other atoms in this structure solution. The solid state structure of **4.4** depicts the magnesium cation adopting a *pseudo*-tetrahedral geometry, in which the steric effects of the terphenolate ligand cause the largest deviation from the idealised tetrahedral angle of 107.5°, in the O1-Mg1-B1 angle of 128.2(2)°. The second largest deviation from the idealised tetrahedral angle is observed in the narrowing of the angle of the THF molecules (O2-Mg1-O3 = 96.57(11)°), which is likely to be a function of the larger sterics involved in a terphenolate and borohydrido- ligand when compared to a THF ligand. Comparison to the bromido- and chlorido-analogues of this complex, 3.8 and 3.7, respectively, discussed in Section *3.4* finds that the O1-Mg1-X angle is the largest observed for this class of compound, whilst the O_{THF}-Mg1-O_{THF} angle is the shallowest. These observations are not unexpected in the case of the chlorido-analogue as the size of a borohydrido-ligand is large compared to a chlorido ligand. Specifically, the thermochemical radius of BH_4^- is 1.93 Å whilst the ionic radii of Cl^- and Br^- are 1.81 and 1.96 Å, respectively.[20-22] These observations are also not unexpected in the case of the bromido-analogue, as a tridentate borohydride ligand is more sterically demanding than a bromide ligand.

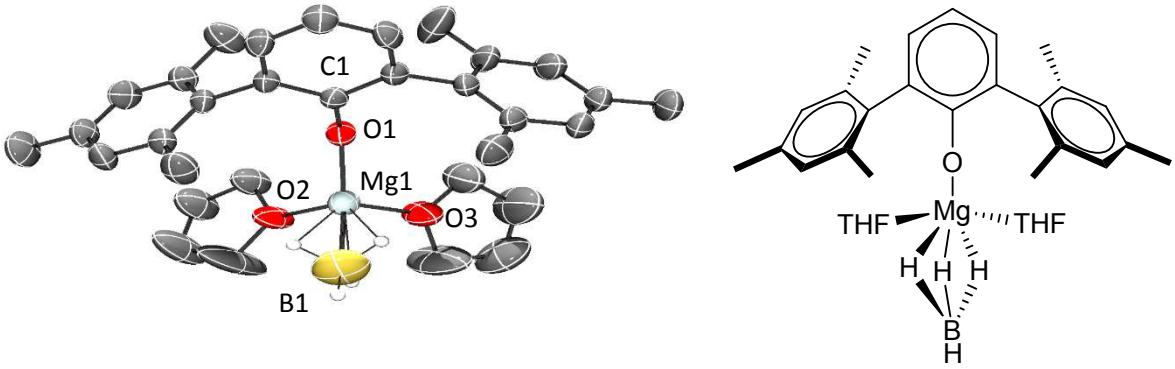

Figure 4.12: Displacement ellipsoid drawing of the solid-state molecular structure of $Mg(OTer^{Mes})((\mu\text{-}H)_3BH)THF)_2$, **4.4** (50 % probability ellipsoids). Non B-H hydrogen atoms are omitted for clarity.

In **4.4,** the Mg1-$O_{terphenolate}$ bond distance of 1.862(2) Å is short in comparison to all magnesium aryloxide complexes, which range from 1.784 to 2.517 Å .[10] Comparison of this bond distance to the analogous bond distances in **3.7** and **3.8** found that they are identical within s.u.s. Similarly, the Mg-O_{THF} bond distances in **4.4** of 1.987(2) and 1.992(2) Å, are identical within s.u.s to those seen in **3.7** and **3.8**. The C-O bond distance of 1.322(3) Å is also identical to those seen in **3.7** and **3.8** within s.u.s. The Mg-B distance in **4.4** is 2.300(6) Å, which is substantially shorter than the Mg-X, where X is Cl or Br, distance observed in **3.7** (2.450(9) Å) and **3.8** (2.4381(8) Å). This is due to the reduced size of the respective constituent parts of a borohydride ligand, as well as the increased polarisation that exists upon tridentate ligation. The Mg1-O1-C1 bond angle of 140.78(17)° in **4.4** is wider than the analogous angle observed for **3.8** (137.68(13)°), which again is likely due to the increased steric demands of the tridentate borohydride ligand. Surprisingly, this angle is significantly more acute than the corresponding angle in **3.7** (162.0(14)°). This may be a result of packing effects, due to these structures being isolated in different lattice systems.

Tridentate ligated borohydride complexes of magnesium are not common within the literature, with the only 11 fully characterised examples; these are shown in **Figure 4.13.**[23-29]

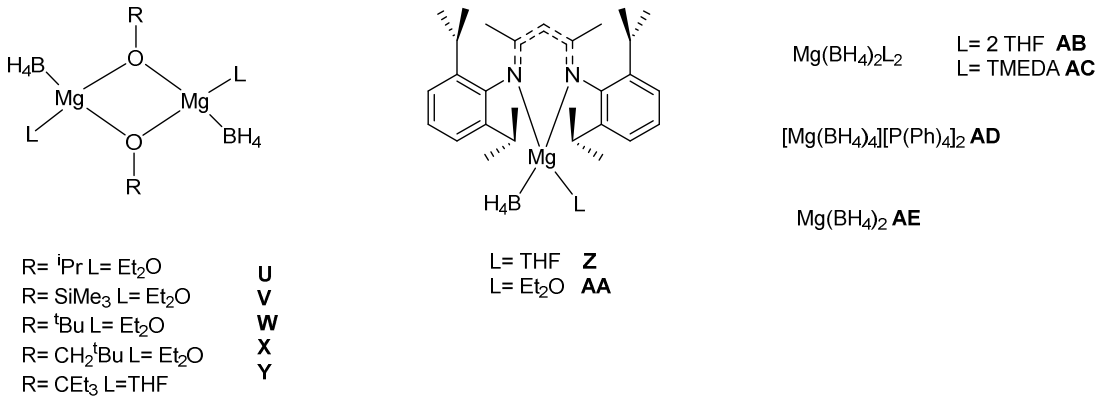

Figure 4.13: Fully characterised examples of tridentate ligated borohydride complexes of magnesium as reported by Sadikov, Zhao, Roesky, Lobkovsky, Wagner, Mountford and Yvon *et al*.[23-29]

These previously fully characterised tridentate ligated magnesium borohydride complexes can be placed into three main categories; systems containing bridging alkoxides, **U-Y**, systems based upon an amidinate ligand, **Z-AA**, and simple salts, **AB-AE**. This brief survey of the literature demonstrates that **4.4** represents the first example of an aryloxide ligand stabilising this moiety sufficiently to obtain a solid state structure. In addition, **4.4** is the first heteroleptic example characterised that does not include chelating or bridging ligands.

The formation of **4.4** is further evidence supporting the propensity of these systems to undergo transmetallation reactions as was identified in *Chapter Three*. It is interesting to note that whilst the chlorido-analogue, **3.2**, formed the trimetallic thorium-magnesium cluster **3.11** when reacted with 2-methyl allyl magnesium chloride, in the case of the borohydrido-analogue, **4.1**, reaction with 2-methyl allyl magnesium chloride led to transmetallation. This provides a clear example of the difference of reactivities between chlorido- and borohydrido-ligands.

Table 4.5: Selected distances and angles for **4.4**

Atom	Distance (Å) / angle (°)
Mg1-O1	1.862(2)
Mg1-O2, Mg1-O3	1.987(2), 1.992(2)
Mg1-B1	2.300(6)
Mg1-H1B, Mg1-H2B, Mg1-H3B	2.16(5), 1.94(4), 1.98(5)
C1-O1	1.322(3)
B1-H1B, B1-H2B, B1-H3B, B1-H4B	1.13(6), 1.11(5), 1.01(6), 1.01(7)
O1-Mg-O2, O1-Mg-O3, O2-Mg-O3	104.83(9), 105.99(9),96.57(11)
B1-Mg1-O1, B1-Mg1-O2, B1-Mg1-O3	128.2(2), 109.1(2), 107.5(2)
C1-O1-Mg1	140.78(17)

4.4 Reactivity of $Th(OTer^{Mes})_2((\mu\text{-}H)_3BH)_2$

As was covered briefly in *4.3.1*, complex **4.2** was thought to be a good candidate for small molecule activations reactivity. In the following, attempts to activate a variety of substrates using **4.2** are described.

Prerequisites for small molecule activation are the availability, both sterically and kinetically, and the ability, thermodynamically, of a substrate to bind to a metal centre. Once bound to a metal centre the resulting metal-substrate complex must then have at least one pathway available whereby a re-arrangement can occur in order to activate the small molecule.

Complex **4.2** satisfies these prerequisites. Firstly, the loss of the chelating DME molecule and adoption of labile aryl interactions with the *ortho* phenyl groups of the terphenolate ligands means that the co-ordination sphere around **4.2** is more open, and thus amenable to the binding of potential substrates. Secondly, the presence of borohydride ligands provides a potential reduction pathway to transform the bound substrate, in addition to the Lewis acid based catalysis that is well precedented for thorium, as discussed in *Chapter Two*.

4.4.1 Reaction with CS_2

4.4.1.1 Reaction with excess CS_2

Addition of excess CS_2 to a toluene solution of **4.2** at room temperature results in no reaction. Application of heat to this reaction mixture results in reaction occurring and the slow formation of a yellowish precipitate (Equation 4.4). Workup results in the isolation of $HB(OTer^{Mes})_2$, **4.5**, as colourless crystals from a saturated hexane solution stored at -30 °C in a 55% yield. The solid state structure of **4.5** is displayed in **Figure 4.15**. Selected bond angles and distances calculated from the solid state structure of **4.5**, are shown in **Table 4.6.**

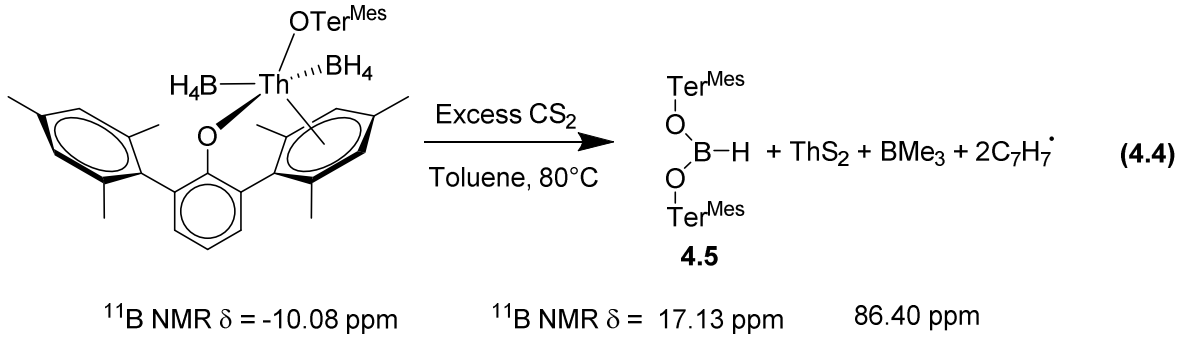

The ^{11}B NMR spectrum of this reaction, recorded in a C_6D_6, shows two resonances indicating the formation of two boron containing products. One resonance, a singlet at 17.13 ppm was assigned to **4.5**, whilst the other resonance, a singlet at 86.40 ppm, was assigned to the formation of BMe_3. This agrees well with previous literature studies on the ^{11}B NMR of BMe_3.[30, 31] These boron resonances show a clear shift from the resonance of the starting material **4.2**, at -10.08 ppm. The ^{1}H NMR spectra of this reaction also supports the formation of BMe_3 as it contains singlet at 0.73 ppm, which also agrees with previous studies within the literature.[32]

To exclude the possibility that CS_2 could be converted to BMe_3 by any metal borohydride complex, i.e. solely the BH_4^- anion, a perdeuterated benzene solution of CS_2 was refluxed with an equivalent of $NaBH_4$ over a fortnight, but no reaction occurred. It has previously been found that in co-ordinating solvents (THF, Acetonitrile) $NaBH_4$ will react with CS_2 to form $NaB(SCH_2S)_4$, so this lack of reactivity suggests that a donating solvent which partially solubilises the BH4 anion is key in promoting this transformation.[33]

In Equation 4.4, it can be seen that the carbon atom of CS_2 is activated to form BMe_3 and it is proposed that the hydrides that reduce the carbon atoms in this process originate from the borohydride ligands. However, due to the presence of one borohydride hydrogen atom in **4.5**, two hydrogen atoms required to form BMe_3 remain unaccounted for. It was postulated that these additional hydrogens may be abstracted from the perdeuterated benzene solvent. To ascertain where the hydrogen atoms in the products of this reaction came from, deuteration studies were undertaken.

$$CaI_2 + 2Na(BD_4) \xrightarrow{THF} Ca(BD_4)_2THF_2 + 2NaI \qquad \textbf{(4.5)}$$

In order to carry out deuteration studies, $Ca(BD_4)_2(THF)_2$ needed to be synthesised. This proved facile by means of reaction between sodium borodeuteride and calcium iodide in a THF solution, yielding $Ca(BD_4)_2(THF)_2$ as a colourless powder in a 82% yield (Equation 4.5). Following this, reaction between $Ca(BD_4)_2THF_2$ and **3.2** resulted in the BD_4 analogue of **4.1** (**4.1**-d^8). Treatment of **4.1**-d^8 with one equivalent of $AlMe_3$ resulted in the BD_4 analogue of **4.2**, **4.2**-d^8, making deuteration studies possible (Equation 4.6).

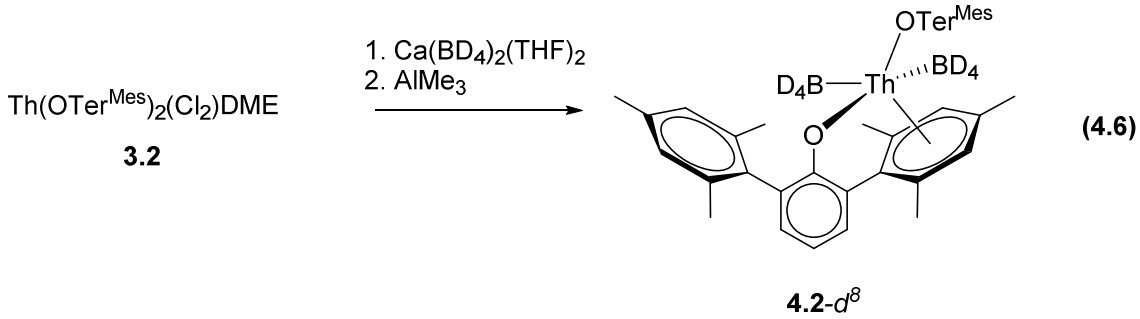

(4.6)

4.2-d^8

The reaction of an excess of CS_2 with a perdeuterated solution of **4.2**-d^8 at room temperature resulted, in direct analogy to the perproteo analogue, in no reaction being observed. Upon refluxing the mixture overnight it appeared that a reaction had occurred as indicated by the observation of a colour change to yellow (Equation 4.7). This was confirmed by ^1H and ^{11}B NMR spectroscopy. The ^{11}B NMR spectrum confirmed the formation of BMe_3 and the mono-deuterated version of **4.5**, **4.5**-d^1. The ^1H NMR spectrum of this reaction provided strong evidence for the BMe_3 produced containing no protium, as the resonance attributed to BMe_3 in the non-deuterated reaction was not observed. The ^2H NMR spectrum also confirmed this. Given the high levels of deuteration observed in the BMe_3 produced in this reaction it is proposed that the additional hydrogen atoms are a result of activation of the perdeuterated benzene solvent. This proposal is supported by the ability of **4.2** to undergo aryl interactions

with the *ortho* mesityl rings of the terphenolate ligands. The co-ordination of a benzene molecule to a thorium centre has precedent from the earlier mentioned example, **L**, by Emslie *et al*.[13]

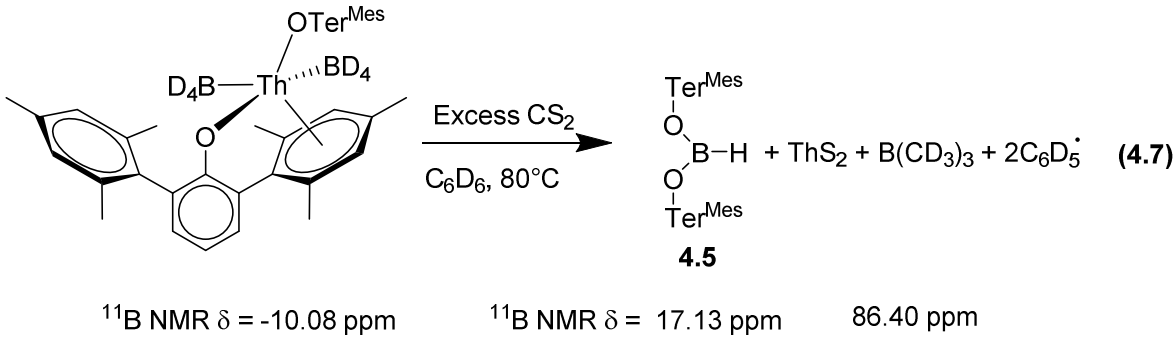

In the solid state structure of **4.5** the B**H** atom was located crystallographically. A mirror plane passing through the BH bond renders the OTer^{Mes} ligands equivalent by symmetry. The three-co-ordinate boron atom adopts a *pseudo*-trigonal planar geometry as evidenced by the angles of O1-B1-O1' (114.3(4)°), H1B-B1-O1 (122.9(2)°) and H1B-B1-O1' (122.9(2)°) tending towards 120 °. The torsion angle calculated from H1B-B1-O1-C1 of 1.2° supports the planarity of this moiety within the structure. The torsion angle of H1B-B1-O1-O1' is 0°, but this is partially symmetry generated.

The O1-B1-O1' angle is clearly more acute than the other angles around the boron centre and this is likely a result of a combination of π–donation from the oxygen atoms into the vacant p-orbital of boron and the sterics of the terphenolate ligands. In the structure of **4.5** the C-O$_{terphenolate}$ bond length is 1.390(3) Å, with only **4.1**-**2** having equivalent bond lengths within s.u.s. The lengthening of this bond is likely due to the oxygen atoms participating in π-donation into the vacant B *p* orbital, thereby reducing the electron density on the oxygen atoms. This would result in reduced electrostatic attraction between the carbon and oxygen atoms, leading to the lengthening of the bond. The B-O bond distance of 1.348(4) Å in **4.5** is short for all B-O interactions reported to date.[10] When restricting the comparison to three-co-ordinate boron centres the B-O bond distance is typical.[10] When considering only bis aryloxide complexes of thorium, the B-O distance in **4.5** is again found to be short.[10]

Fully characterised *bis* alkoxide boranes, such as **4.5**, are rare, with the only three previously reported examples, **AF**-**H**, shown in **Figure 4.14**. [34-36]

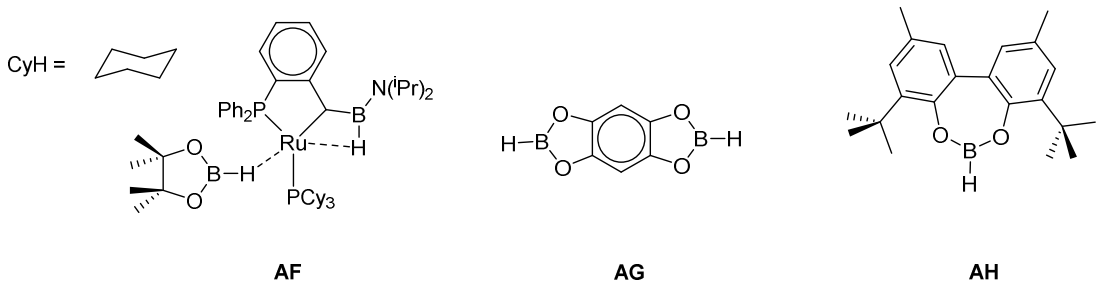

Figure 4.14: The structures of crystallographically characterised *bis* aryloxide borane complexes, **AF**-**H**, as reported by Sabo-Etienne, Aldridge and Noth *et al*. [34-36]

Complex **4.5** therefore represents the first crystallographically characterised example of a *bis* aryloxide borane complex in which the aryloxide components are not chelating. This is further evidence supporting the idea that the large steric bulk of the terphenolate ligand aids in stabilising complexes that would not be otherwise expected to be kinetically stable.

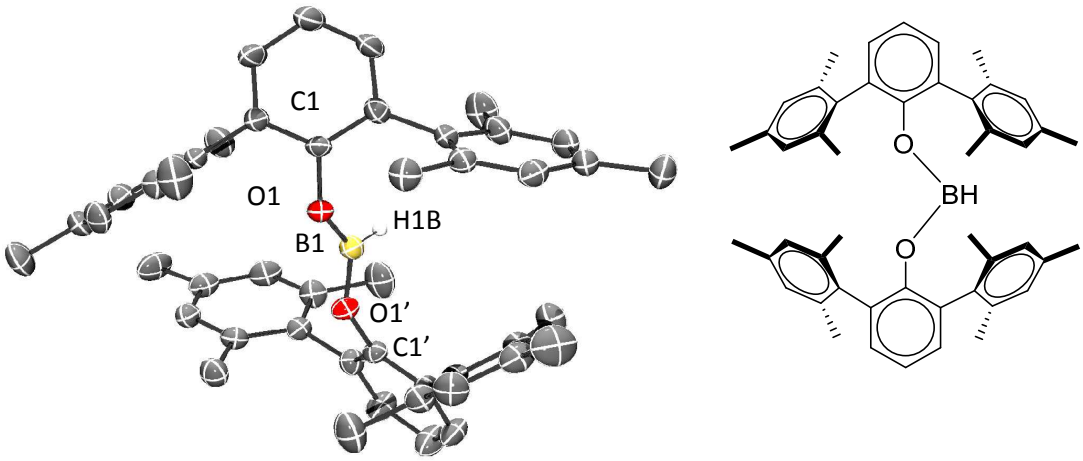

Figure 4.15: Displacement ellipsoid drawing of the solid-state molecular structure of $HB(OTer^{Mes})_2$, **4.5** (50 % probability ellipsoids). Non B-H hydrogen atoms are omitted for clarity.

Table 4.6: Selected distances and angles for **4.5**

Atom	Distance (Å) / angle (°)
B1-O1	1.348(4)
B1-H1B	1.12(4)
C1-O1	1.390(3)
O1-B1-O1'	114.3(4)
C1-O1-B1	123.6(3)
H1B-B1-O1, H1B-B1-O1'	122.9(2), 122.9(2)

4.4.1.2 Reaction with stoichiometric CS_2

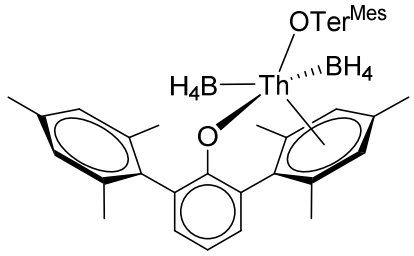

1 Eq. CS_2

C_6D_6, 80°C

unidenitified $Th(OTerMes)_n(BH_4)_x$ + $B(Me_3)_3$ **(4.8)**

^{11}B NMR δ = -10.08 ppm

^{11}B NMR δ = 11.32 ppm

86.40 ppm

Addition of one equivalent of CS_2 to a perdeuterated benzene solution of complex **4.2** resulted in no initial reaction being observed. After heating the solution overnight to reflux the pale yellow solution was found to contain a fine colourless precipitate and a reaction was confirmed to have occurred by ^{1}H and ^{11}B NMR spectroscopy (Equation 4.8). The ^{11}B NMR spectrum contains two resonances of roughly equal relative integration. This does not necessarily indicate equimolarity due to the presence of borosilicates in the glass that the NMR tube within which the reaction was carried out affecting the validity of relative integrations. The two resonances were observed as a singlet at 86.41 ppm and a poorly resolved pentet at -11.32 ppm (J= 82.6Hz). Combined with a resonance at 0.73 ppm in the ^{1}H NMR spectrum, the resonance at 86.41 ppm can be attributed to BMe_3 and this agrees well with literature precedent. [30-32] The resonance at -11.32 ppm has a similar chemical shift to that of the starting material, **4.2**. Combined with the similar coupling constant and shape of the resonance, it is proposed that this resonance is due to a thorium borohydride complex that has retained a terphenolate ligand. This is supported by the similarity of the resonance, in terms of chemical shift, coupling constant and shape of the resonance, and full width at

high maximum (fwhm of 197 Hz for this resonance and 232, 343 and 315 Hz for **4.1**-**3** respectively) to those seen for the fully characterised thorium borohydride complexes **4.1**-**3**.

4.4.2 Reaction with CO_2

The difference in the physical and chemical properties of CS_2 and CO_2 are quite marked. Whilst CS_2 is a volatile liquid (boiling point 46.3 °C), whilst CO_2 is a gas at standard temperature and pressure. An important chemical difference between these substrates is the difference in electron affinity between CS_2 and CO_2 (1.0 vs -0.6 eV respectively).[37] In view of these differences, it is expected that the reaction of CO_2 and CS_2 with complex **4.2** may result in divergent reactivities.

Exposure of a perdeuterated benzene solution of complex **4.2** to a pressure of one bar of CO_2 resulted in a reaction proceeding at room temperature, accompanied by the almost instantaneous formation of a white precipitate (Equation 4.9). This is in direct contrast to the reaction with CS_2, which required the application of heat to occur.

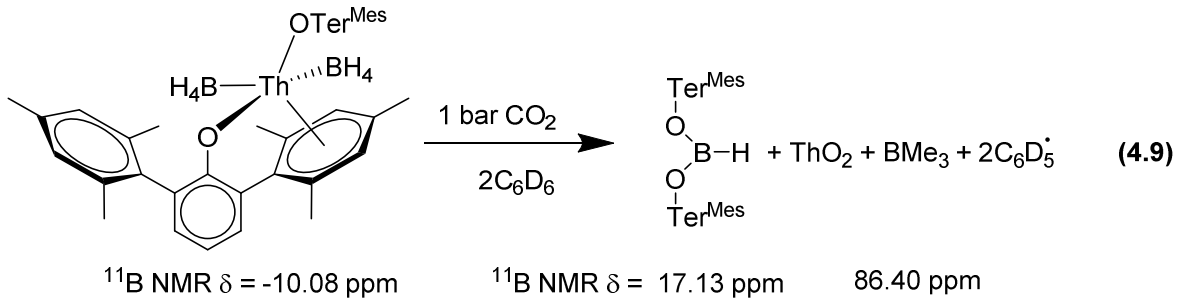

(4.9)

The ^{11}B and ^{1}H NMR spectra of the solubilised products in this reaction mixture suggest that the same boron containing products were formed that were identified in the reaction with CS_2. The thorium containing side product in this case is postulated to be ThO_2, and combined with the increased reactivity of CO_2 compared to CS_2, this may be key in explaining why this reaction is thermodynamically or kinetically favoured over the analogous CS_2 reaction. Comparison of the corresponding $\Delta_f G^o$ for ThO_2 (-1169.20 kJ mol^{-1}) and ThS_2 (-620.1 kJ mol^{-1}) is very illuminating when considering the deeper thermodynamic sink that exists upon the formation of ThO_2 over ThS_2.[22] A further kinetic consideration to explain this observed difference in reactivity is that the significant difference in size of an oxygen and sulfur atom (covalent radii = 0.66 and

1.05 Å respectively)[38] may result in a more hindered co-ordination site in the case of CS_2, thus reducing the reactivity.

4.4.3 Reaction with CO

The exposure of a perdeuterated benzene solution of **4.2** to a pressure of 1 bar of CO showed limited initial reactivity, but application of heat proved to accelerate reactivity. The 1H and ^{11}B NMR spectra of this reaction, both before and (more certainly) after heating, suggest the formation of BMe_3 analogous to the results observed in *4.4.1-2.* However, in contrast with the results observed in *4.4.1-2* there was no evidence for the formation of $HB(OTer^{Mes})_2$ in the reaction with CO. Instead a second boron resonance was observed as a doublet of doublets at -11.62 ppm. The coupling constants for this resonance were 174.2 and 85.3 Hz, which compares to a coupling constant of *circa* 80.6 Hz observed for complex **4.2** which, due to the poor resolution of the pentet in **4.2** the coupling constants are not as well-resolved as those observed for this reaction. The combination of similar coupling constants and chemical shifts of this ^{11}B resonance leads to the postulation that this resonance originates from a thorium borohydride complex, which also contains the terphenolate ligand, as the ^{1}H NMR spectrum supports a terphenolate ligand being bound to a metal centre. (See Equation 4.10)

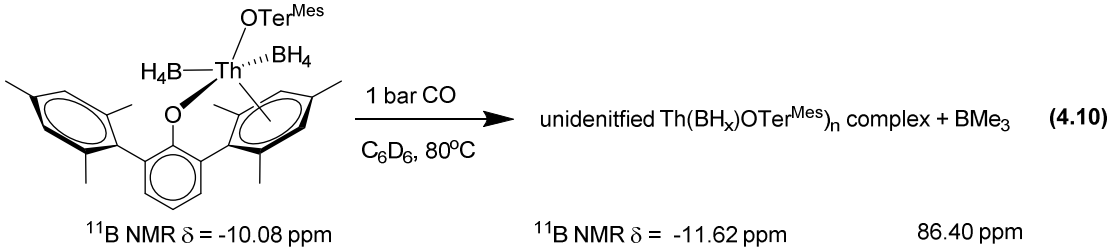

The difference in reactivity between CO and CO_2 is not unexpected as CO contains a substantial dipole of 0.122 D.[39] In addition, the C≡O bond in CO is the strongest bond known to exist in nature (ΔHf_{298} = 1076.5(4) kJ mol^{-1} for CO whilst for CO_2 ΔHf_{298} = 532.2(4) kJ mol^{-1}),[22] which has a significant effect upon the ability to cleave this bond, which would be required for CO to follow the reactivity observed for CO_2. A further consideration in the differences in reactivity is the binding that each moiety would favour towards a metal centre. Whilst CO_2 will favour side-on binding to the metal centre, CO favours head-on binding through the carbon atom, although is also capable of side on binding as shown in **Figure 4.16**.

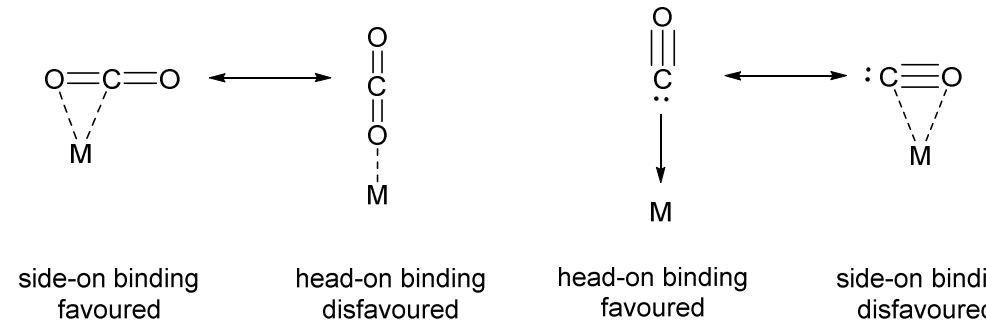

Figure 4.16: The difference in preferred binding modes between CO_2 and CO

4.4.4 Reaction with DCC

To diversify the substrates probed in the investigation of potential small molecule activations by **4.2** the reaction of a pnictogen analogue (dicyclohexylcarbodiimide, DCC) of the successfully activated chalcogen-based CO_2 and CS_2 substrates was investigated. The initial assumption was that the large steric bulk of the cyclohexyl groups may prevent the reaction proceeding in a fashion similar to that seen in *4.4.1-2*, potentially leading to the isolation of a thorium-containing species.

The reaction of one equivalent of DCC with a perdeuterated benzene solution of complex **4.2** resulted in no reactivity being observed at room temperature. Upon heating for 48 hours a reaction was observed to have taken place by an intensification of the yellow colour of the solution and the formation of a small amount of colourless precipitate. (Equation 4.11)

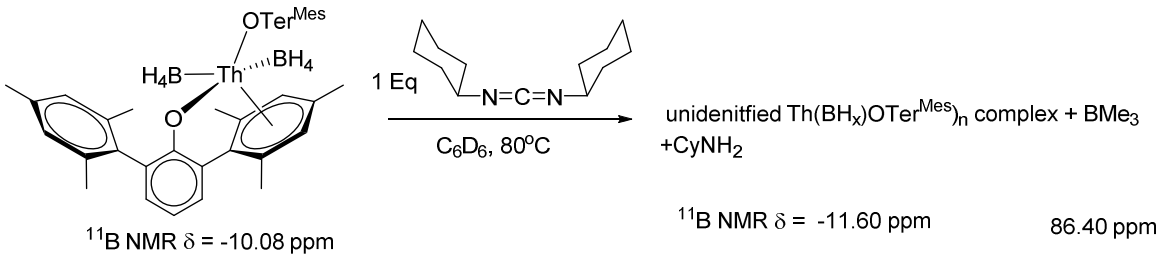

(4.11)

The ^{11}B NMR spectrum contained two resonances. One of these was a singlet at 86.44 ppm attributed to BMe_3, with the corresponding peak in the ^{1}H NMR spectrum confirming its identity. The second resonance, in remarkable similarity to the results observed in reaction with CO, appeared as a doublet of doublets (J = 173.4, 85.9 Hz) at -11.60 ppm.

4.4.5 Reaction with H_2/CO

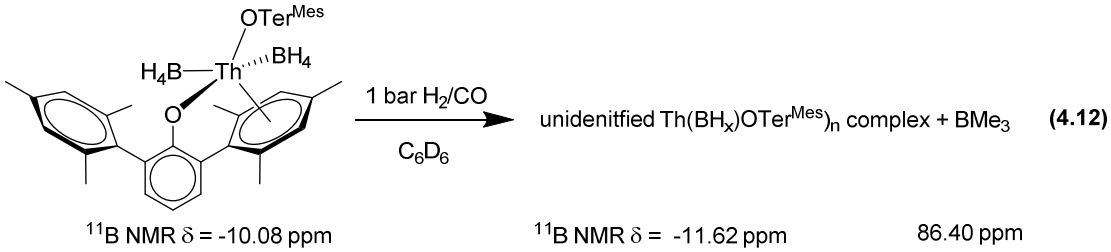

The reaction with a 33% mixture of CO in H_2 gas was carried out. One bar of pressure of this mixture was applied to a perdeuterated benzene solution of **4.2**. At room temperature, similar to the reaction with CO gas in *4.4.3,* there was limited initial reactivity by NMR spectroscopy, although a small amount of fine colourless precipitate was observed (Equation 4.12). Upon heating at reflux overnight the reaction was observed to accelerate by ^{1}H and ^{11}B NMR spectroscopy. The ^{1}H and ^{11}B NMR spectra showed formation of BMe_3, which is highly suggestive of complex 4.2 favouring reactivity with CO over H_2. This is not an unexpected result, as CO would be expected to have preferential binding over a H_2 molecule to a thorium centre.

4.4.6 Reaction with S_8

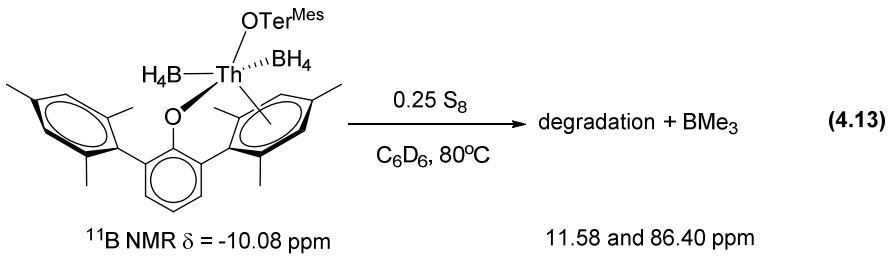

In an attempt to probe the reactivity with substrates not containing carbon, small molecule activation of elemental sulphur, in the form of its most stable allotrope, S_8, was investigated. Reaction of a quarter of an equivalent of S_8 with a perdeuterated benzene solution of complex **4.2** produced no reaction at room temperature (Equation 4.13). Upon heating at reflux for four hours, a fine colourless precipitate was formed. The ^{11}B NMR spectrum of this reaction contained two major resonances. One of these resonances was a poorly resolved pentet (J = 82.6 Hz) at -11.58 ppm. The ^{1}H NMR spectrum of this reaction suggested that this reaction produced multiple products. There was evidence of multiple terphenolate environments with some of these

environments indicating a loss of symmetry within the terphenolate ligand. Surprisingly, the other major resonance in the ^{11}B NMR spectrum was a singlet at -86.46 ppm, *i.e.* in a region that would be attributed to BMe_3. The formation of BMe_3 from this reaction is also supported by the ^{1}H NMR spectrum. The results of this reaction are suggestive of multiple reaction products as it appears that degradation of the ligand has occurred, whilst the ^{11}B resonance at -11.58 ppm could be attributed to a thorium complex containing borohydride and (modified or otherwise) terphenolate moieties.

4.4.7 Reaction with P_4

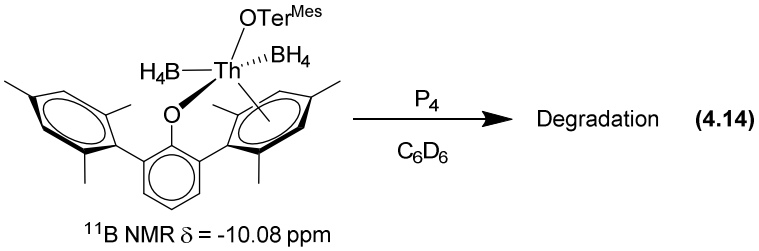

To continue the probing of the activation of elemental ring systems, small molecule activation of the white phosphorus allotrope, P_4, was investigated (Equation 4.14). In similarity to the reaction with S_8 no reaction was observed at room temperature. Upon heating at reflux overnight a reaction was observed to have formed evidenced by the formation of a brown solution with a dark coloured precipitate, which NMR spectroscopy suggested was the result of degradation of the complex by P_4.

4.4.8 Reaction with sodium acetylide

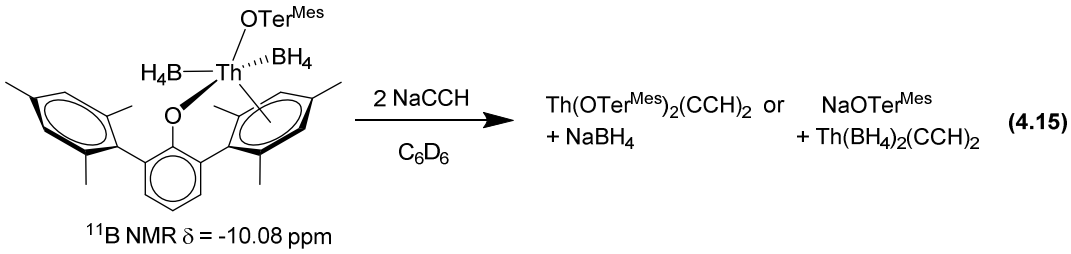

An acetylide derivative of **4.2**, was targeted by reaction with sodium acetylide (Equation 4.15). Given the previous experiences detailed in this chapter and *Chapter Three* transmetallation was initially expected to occur. However, the ^{1}H NMR spectrum of this reaction was inconclusive as to whether transmetallation of the terphenolate

ligands or ligand substitution had occurred and further attempts at characterisation were unsuccessful. This led to the outcome of this reaction being unknown.

4.5 Catalysis

The results described in sections *4.4.1-7* demonstrate that complex **4.2** is adept in facilitating small molecule activations for selected substrates. The next logical step in the investigation of the reactivity of **4.2** was to probe whether **4.2** was a suitable precatalyst for oligomerisation reactions. In *Chapter Two*, the oligomerisation of terminal acetylenes was discussed as a suitable test reaction.

4.5.1 Acetylenes

To probe the potential catalytic activity of **4.2** for the reaction of terminal acetylenes, three substrates were investigated; 1-hexyne (nBuC≡CH), phenyl acetylene (PhC≡CH) and trimethylsilyl acetylene ($SiMe_3C$≡CH). The variety of sterics and electronics of the selected substrates provides a thorough exploration into the robustness and scope of this reaction if catalysed by complex **4.2**.

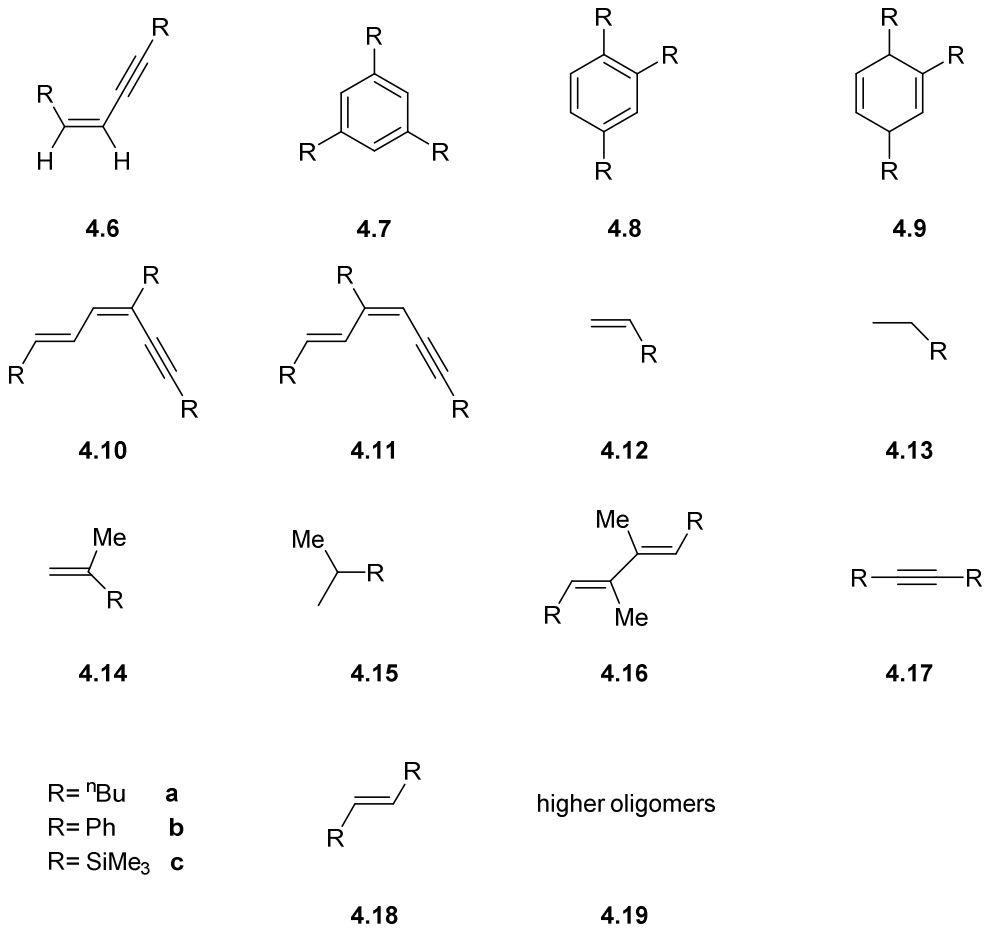

Figure 4.17: Products of catalysis from reaction of terminal acetylenes with **4.2**

As can be seen from **Figure 4.17**, a variety of products are yielded from the reaction of sub-stoichiometric quantities of terminal alkynes with complex **4.2**. The formation of **4.6**, the *cis* dimer, cannot occur via the mechanisms proposed in *Chapter Two* and hints at either migratory hydride/functional group reactions or redox chemistry occurring at this substrate. It may also be the result of a different mechanism altogether which predominates this reaction. The formation of **4.7**-**4.11** could follow the mechanism and reactivity observed in *Chapter Two*. The formation of the remaining products, **4.12**-**4.19,** is a result of reduction and/or methylation. The observation of reduced species, given the formation of BMe_3 *via* reduction in *4.4.1-4.4.4*, is unsurprising. The diversity of these products illustrates that multiple reaction pathways are possible and followed within this reaction.

A striking aspect of the results of the catalytic reactivity of **4.2** with terminal acetylenes is that the conversions observed for this catalyst are far poorer than those seen under identical conditions for the catalysts described in *Chapter Two* in respect to both poorer activity as well as selectivity. This is to be expected given that these are preliminary

results. Clear differences in the favoured products, however, are seen upon changing substrates which indicates that this system is very sensitive to changes in electronics and sterics of the substrate, and worthy of optimisation.

*4.5.1.1 Oligomerisation, cyclotrimerisation and reduction of 1-hexyne by **4.2***

The most notable aspect of the catalytic reaction of **4.2** with 1-hexyne is its abysmal performance as a catalyst. With only 12% conversion of the terminal acetylene and 10% catalyst loading, this reaction only barely surpasses a stoichiometric reaction. The small amount of product yielded form this reaction, indicates that the formation of two major products is favoured, the *cis* dimer, **4.6a** (37%), and the hydrogenation product **4.12a** (56%). The remaining minor products were the cyclotrimers **4.7a** (4%) and **4.8a** (2%). The favouring of the hydrogenation product, **4.12a**, illustrates the key role that the borohydride ligands play in the catalytic activity of **4.2**. The favouring of the reduction product, **4.12**, may also explain the very poor conversion observed. Once alkyne has formed, it may to provide a pathway towards catalyst poisoning or irreversible binding to the metal centre (competitive inhibition), which would prevent further reactivity. It is possible that the alkene product is only released from the metal centre upon workup with methanol.

Statistically, it is expected that cyclotrimer **4.8a** would be favoured over cyclotrimer **4.7a** due to the latter requiring two consecutive head-to-tail insertions, whilst the formation of the former only requires either (or both) of the insertion steps to be tail-to-tail. This indicates preferential head-to-tail insertion, although the very low activity observed makes this observation something of a moot point.

*4.5.1.2 Reduction and methylation of phenyl acetylene by **4.2***

The catalytic reaction of a more electron-poor alkyne (compared to 1-hexyne) in the form of phenyl acetylene was probed. Due to the relative electron deficiency of this alkyne it was expected that reduction would be favoured.

An obvious and striking initial observation upon change of substrate to phenyl acetylene was the vast improvement in conversion of the substrate. The observed conversion rate of 56%, however, remains fairly mediocre. Again, this may be a result of the reaction not being optimised. The reaction does show a high level of selectivity for the major product, which is again the hydrogenation product, **4.12b** (87%). In contrast to the results seen for 1-hexyne, the minor products were found to be **4.13b**

(6%), **4.14b** (1%) and **4.15b** (7%). These products are the result of a mixture of reduction and methylation. Complex **4.13b** is more likely to be a product of reduction of **4.12b** rather than two consecutive reductions upon the metal centre. That the formation of **4.13b** in such low proportions relative to **4.12b**, despite the seemingly high concentration of **4.12b** in solution, suggests that **4.12b** does not bind to the metal centre in an efficient way that enables continued reactivity. This may also support the low conversion observed for 1-hexyne. Perhaps surprisingly, the reduced methylated product **4.15b** was observed in significantly greater amount than the merely methylated product **4.14b**. This suggests that the reduction step after methylation of phenyl acetylene is comparatively fast.

A notable observation of the methylation products of this reaction is that methylation only occurs at the *β*-position of the terminal acetylene. Given the electronic properties of an alkyne moiety bound to a metal centre, it is expected that methylation would occur at the *β*-position if the methylating agent provided a δ^- methyl substituent as illustrated in **Figure 4.18**. This is exacerbated by the relatively electron-deficient effect of a phenyl substituent upon the alkyne bond. Given the propensity for the formation of BMe_3 by complex **4.2,** and indeed the ^{11}B NMR spectrum taken whilst monitoring this reaction suggested the formation of a small amount of BMe_3, it may be proposed that this side product is responsible for the methylation results seen in this reaction.

Table 4.7: Preliminary **r**esults for the catalytic oligomerisation/cyclotrimerisation/reduction/methylation of terminal alkynes by complex **4.2**[a]

			Yield (%)													
Entry (R[b])	Loading (%)	Conversion (%)	**4.6**	**4.7**	**4.8**	**4.9**	**4.10**	**4.11**	**4.12**	**4.13**	**4.14**	**4.15**	**4.16**	**4.17**	**4.18**	**4.19**
1 (^{n}Bu)	10	12	37	4	2				56							
2 (Ph)	10	56							87	6	1	7				
3 (TMS)	10	61		9		10	3	6					9	15	24	13

[a]Product percentages are ratios of converted substrate. Reactions were run for 72 h at 75 °C in C6D6. [b]R = substituent of the corresponding RC≡CH.

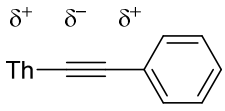

favours methylation by a δ^-
methyl group at the β position

Figure 4.18: An illustration of the relative electron affinities resulting in favoured site for methylation for phenyl acetylene

*4.5.1.3 Oligomerisation, cyclotrimerisation, reduction and methylation of trimethylsilyl acetylene by **4.2***

Following the observation of improved reactivity of complex **4.2** with phenyl acetylene, a relatively electron-poor substrate compared to 1-hexyne, trimethylsilyl acetylene, a relatively electron rich substrate was investigated as a substrate. The trimethyl silyl moiety has been experimentally and computationally established to be a steric equivalent to a methyl group at the *α*-position.[40-43] This allows for the comparison with the results of 1-hexyne to be considered mainly with respect to the differing electronic properties of the substrates. Due to the inductive effects of a Si-C bond, the trimethyl silyl moiety is well known for its ability to stabilise of α-carbanions and β-carbocations.[44-46] If oligomerisation was to occur in this reaction, it would be expected that tail-to-head insertion would be favoured, with the increased electron density in the acetylene bond also expected to increase the favourability of cyclotrimerisation. (see section *2.5*).

In the reaction of complex **4.2** with trimethylsilyl acetylene the conversion was the best observed in this study (61%). While remaining mediocre overall, the selectivity of this reaction was poor, with the most diverse range of products produced in this study. The major product of this reaction was complex **4.18c** (24%), which is the result of the migration of a $SiMe_3$ moiety from one alkyne molecule to another, followed by a subsequent reduction (hydrogenation) to form the alkene product. The migration of $SiMe_3$ groups is well precedented.[47-50] However, it is also known that mass spectrometry may be the cause of the migration of silyl groups.[51, 52] As a product of hydrogenation, complex **4.18c** was deemed a product of catalysis in addition to a rearrangement product of the mass spectrometry characterisation. The lack of evidence of formation of **4.12c**, even though this was the major product in the case of the other substrates supports the supposition that the second $SiMe_3$ group is a formed in the process of mass spectral characterisation.[51]

The relatively minor products of this reaction were **4.17c** (15%, $SiMe_3$ migration of non-hydrogenated acetylene product), **4.19c**, (13%, higher linear oligomers), the reduced form of the 1,2,4 cyclotrimer **4.9c** (10%), the 1,3,5 cyclotrimer **4.7c**, (9%) and a reduced bimethylated dimer **4.16c** (9%). There was also evidence of formation of two linear trimers; **4.10c** (3%) and **4.11c** (6%). The formation of **4.17c** is likely to be a result of a rearrangement during the mass spectral characterisation. The products of this reaction were observed to be prone to oxidation, which would support the formation of **4.9c**. The tendency towards the formation of linear trimer **4.11c** over **4.10c** by this reaction indicates a slight preference for head-to-tail insertion.

It is interesting to note that whilst the electronically 'neutral' substrate, 1-hexyne, was observed to have extremely low conversion, exchanging substituents of the alkyne bond to create relatively electronically 'poor' or 'rich' bonds resulted in increased conversion (**Figure 4.19** provides a summarising cartoon). This suggests that activation of the bond may be essential to induce catalytic activity of acetylenes with complex **4.2**. This requirement, along with the mediocre yields observed, somewhat limits the scope of this catalysis. A potential solution would be to probe the reactivity of a π-rich system with an inherent activation to the multiple bond. For this reason the catalysis of isonitrile substrates was probed.

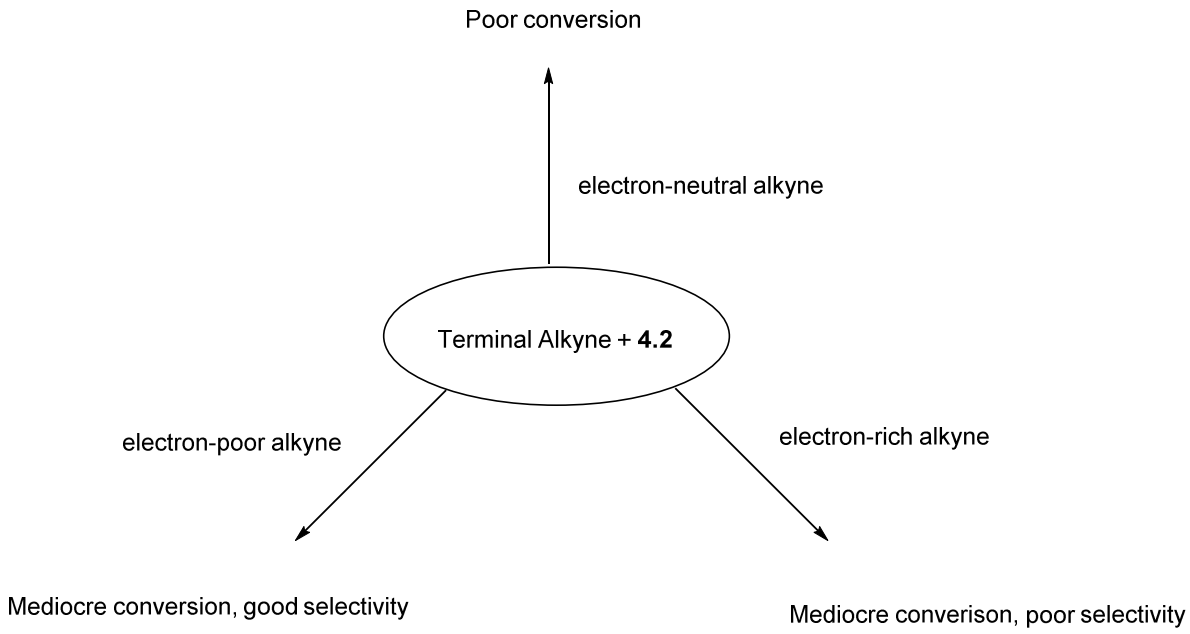

Figure 4.19: A summary of the catalysis of terminal alkynes by complex **4.2**

4.5.2 Isonitriles

The C=N bond in an isonitrile moiety is polarised towards the nitrogen atom due to the differences in electronegativity (3.04 and 2.55 for nitrogen and carbon, respectively).[22] The C=N bond is capable of two main resonance forms, shown in **Figure 4.20**, and as a strong *σ*-donor (comparable to CO) the carbon atom retains a significant amount of electron density. As such, isonitrile should be able to easily displace the labile aryl interactions present within complex **4.2**.

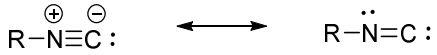

Figure 4.20 Canonical forms of an isonitrile moiety

The inherent polarisation of the C=N bond in an isonitrile moiety may overcome the problem of low conversion encountered in the reaction with 1-hexyne. This assumes, however, that the reaction pathway remains the same. Before describing the catalytic reaction, the stoichiometric reaction of isonitriles was investigated.

4.5.2.1 Stoichiometric reaction

The two isonitrile compounds used in this study, cyclohexyl isonitrile (CyNC) and *tert*-butyl isonitrile (^{t}BuNC) have broadly similar electronic properties, meaning that the differences in their reactivities are primarily based on their differing sterics. Comparison of the steric parameter between a *tert*-butyl and cyclohexyl substituent (ν_{tBu} = 1.24, ν_{Cy} = 0.87) finds that the former is substantially more sterically demanding.[53] As such, the cyclohexyl substituted substrate may be expected to demonstrate improved conversion due to the reduced steric hindrance.

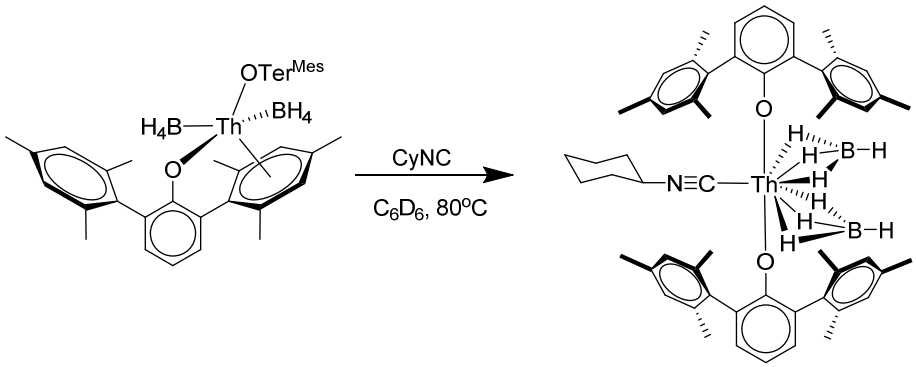

(4.16)

Reaction of one equivalent of cyclohexyl isonitrile with a colourless perdeuterated benzene solution of **4.2** yielded an orange solution (Equation 4.16). The results of ^{1}H and ^{11}B NMR experiments, conducted within thirty minutes of the addition, suggest that a substantial amount of divergent reactivity had occurred. For the most part this was

distinctly illustrated by the presence of three major boron environments the ^{11}B spectra, with none of them attributed to the starting complex **4.2**. These three resonances were observed as a poorly resolved triplet (possibly a pentet) at -11.01 ppm (J = 76.3 Hz), a triplet at -25.28 ppm (J = 84.6 Hz) and a quartet at -44.07 ppm (J = 96.1 Hz). The resonance at -11.01 ppm is similar in chemical shift to that of the starting material, so it is proposed that this peak is due to ligation of the strong σ-donating isonitrile group to the thorium centre. The ^{1}H NMR spectroscopy also indicated small shifts in the resonances of the CyNC starting material, perhaps resulting from the ligation of the isonitrile moiety.

The resonances at -25.28 (relative integration = 0.03) and -44.07 ppm (relative integration = 0.01) were minor compared to the resonance observed at -11.01 ppm (relative integration = 1.00) and as resonances in these regions are moistly associated with complexes with 'free' borohydride moieties (such as KBH_4 for example) they were attributed to degradation products. Following the seemingly successful ligation of the isonitrile moiety, as characterised by NMR spectroscopy, it was investigated whether the application of heat could induce activation of the ligated molecule.

After refluxing the orange perdeuterated benzene solution overnight, the formation of a red suspension containing some colourless, white precipitate was observed. The ^{1}H and ^{11}B NMR spectra of this reaction mixture indicated that significant degradation of the product had occurred. This was most clearly illustrated by the presence of ten resonances in the ^{11}B NMR spectrum. These resonances were observed at 45.0 ppm as a singlet, at 28.29 ppm as a doublet (J = 741.7 Hz), at 19.87 ppm as a doublet (J = 148.4 Hz), at -7.27 ppm as a doublet (J = 208.6 Hz), at -11.25 as a doublet (J = 82.0 Hz), at -13.59 ppm as a doublet (J = 189.3 Hz), at -15.69 ppm as a doublet (J = 88.6 Hz), as a doublet -17.25 ppm (J = 100.5 Hz), at -20.69 ppm as a doublet (J = 94.5 Hz) and at -25.65 ppm as a doublet of doublets (J = 208.4, 85.4 Hz) (see **Figure 4.21**). This is fairly convincing evidence of the degradation of the boron containing species in this reaction, which implies a similar degradation of the proposed isonitrile species. To ascertain the organic products of this reaction a GCMS was run on the product mixture after quenching with methanol. This suggested that the major product of the reaction was $CyNH_2$.

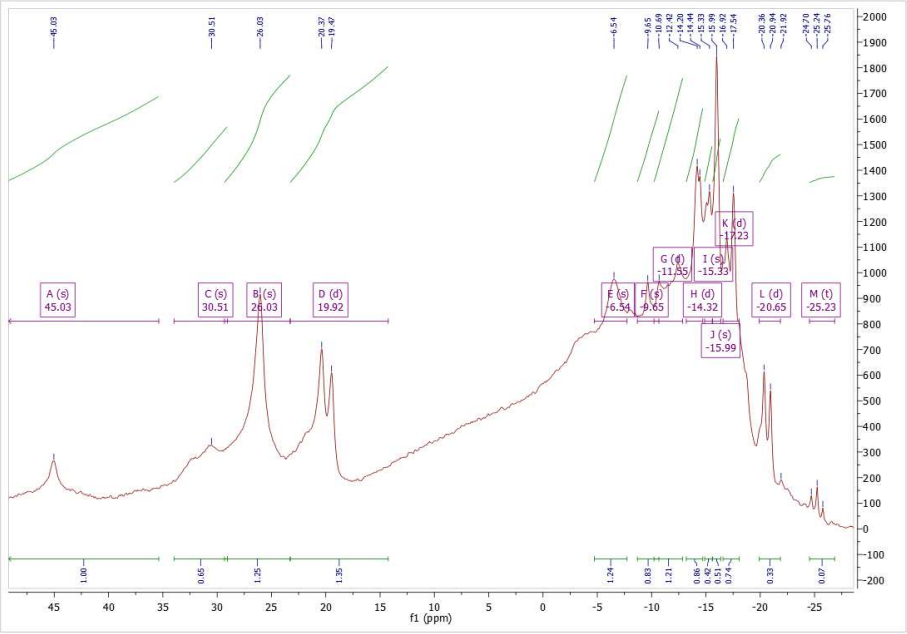

Figure 4.21: The ^{11}B NMR spectrum of the product mixture of the reaction of sub-stoichiometric amounts of complex **4.2** with CyNC. Large broad peak from 10- -20 ppm is due to borosilicate peak from the borosilicate glass NMR tube.

This was a surprising result as for the formation of $CyNH_2$ from CyNC two reduction steps accompanied by the abstraction of the isonitrile carbon must occur. The abstraction of the isonitrile carbon requires the cleavage of a C-N bond with a bond order lying between 2 and 3, which would be expected to be an energetically demanding reaction pathway as ΔHf_{298} = 887 kJ mol^{-1} for C≡N and 619 kJ mol^{-1} for C=N.[22, 54]

The conversion of an isonitrile moiety to a primary amine is a fairly well researched organic transformation that is conventionally achieved by addition of a mineral acid.[55-58] Indeed the conversion of CyNC to $CyNH_2$ has precedence by this method.[59, 60] It has not, however, been observed to occur catalytically.

Conversion of an isonitrile moiety to a primary amine in acid-free conditions by a metal centre is unprecedented. This is likely due to the ease of conversion *via* organic transformations, however, as this reaction is unable to accommodate acid-labile functional groups, there is a possibility for this reaction, once optimised, to potentially fill a niche in isonitrile chemistry. Further investigations into this reaction detailing the effect of the application of different temperatures on the stability and degradation products of isonitrile ligated-**4.2** and the catalytic potential of this reaction are

described in Section *4.5.1.2*. First, however, the results of the stoichiometric reaction of ^{t}BuNC with complex **4.2** will be presented.

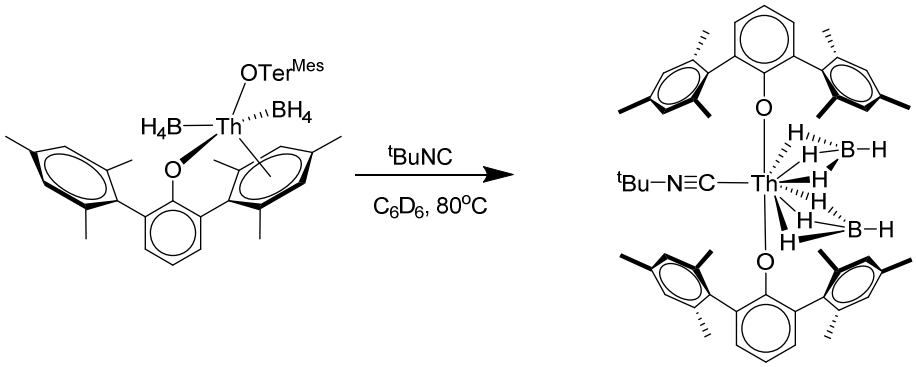

(4.17)

Reaction of one equivalent of ^{t}BuNC with a colourless perdeuterated benzene solution of **4.2** yielded a pale yellow solution (Equation 4.17). The results of ^{1}H and ^{11}B NMR experiments, conducted within thirty minutes of the addition, suggest that a small amount of degradation had occurred in addition to ligation of the isonitrile ligand. This is distinctly apparent from the observation of two resonances in the ^{11}B NMR spectrum. These consisted of a very poorly resolved pentet at -10.37 ppm (J = 77.8 Hz) and a quartet at -43.86 ppm (J = 97.2 Hz). The resonance at -10.37 ppm is attributed to the *tert*-butyl analogue of the isonitrile ligated species postulated in Equation 4.12 (see Equation 4.13). The resonance at -43.86 ppm is reminiscent of a similar degradation product seen in the stoichiometric reaction with CyNC, especially as it was similarly minor in comparison to the peak attributed to isonitrile ligation (relative integration of 0.02 observed for the peak at -43.86 ppm compared to a relative integration of 1.00 observed for the peak at -10.37 ppm).

To probe the effect of varying the temperature the pale yellow perdeuterated benzene solution was refluxed overnight resulting in a colour change, observed as the formation of a red suspension containing some colourless, white precipitate. The ^{1}H and ^{11}B NMR spectra of this reaction mixture indicate significant degradation of the proposed isonitrile complex, in analogy to the results observed for the CyNC substrate. This is most discernible by analysing the ^{11}B NMR spectrum. Following reflux, the ^{11}B NMR spectrum contained nine separate resonances. These resonances were observed as a singlet at 45.32 ppm, a singlet at 26.48 ppm, a singlet at 23.82 ppm, a triplet at 19.62 ppm (J = 144.9 Hz), a doublet at -0.86 ppm (, J = 257.4 Hz), a singlet at -4.17 ppm, a multiplet centred at -10.89 ppm, a multiplet centred at – 18.09 ppm and a singlet at -26.18 ppm. This constitutes convincing evidence of the degradation of the boron

containing species in this reaction, and hence a great likelihood of degradation of the proposed isonitrile species as well. To ascertain the organic products of this reaction a GCMS was run upon the reaction after quenching with methanol. The results of this attempted characterisation were inconclusive, but there was no evidence for the analogous hydrogenation and carbon extraction product, $^{t}BuNH_2$, that was found in the stoichiometric reaction with CyNC.

*4.5.1.2 Catalytic reactions of complex **4.2** with isonitriles*

Having examined the stoichiometric reactivity with two isonitrile substrates, the catalytic activity, at 10% loading of complex **4.2**, was investigated. **Figure 4.22** illustrates the diverse range of products that were observed from the catalytic reaction of isonitrile substrates with complex **4.2**.

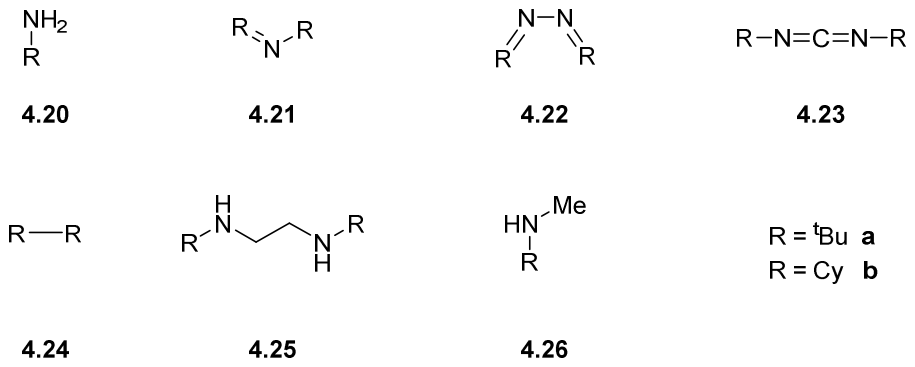

Figure 4.22 Products of catalysis from reaction of isonitriles with **4.2**

Table 4.8: Preliminary results of the catalytic coupling/ reduction of terminal isonitriles by complex **4.2**

Entry (R)	Loading (%)	Conversion (%)	Yields (%) **4.20**	**4.21**	**4.22**	**4.23**	**4.24**	**4.25**	**4.26**
1 (tBu)	10	49					73	27	
2 (Cy)	10	36	91	2	1	1			5

The catalytic results presented in **Table 4.8** indicate that the conversion of isonitriles by complex **4.2** is mediocre. However, the catalytic conversions observed for these isonitrile substrates are far greater than those observed for 1-hexyne in the study of the catalytic activity of terminal acetylenes as detailed in Section *4.5.1.1*. This supports the

earlier supposition that the inherent activation of the CN triple bond in an isonitrile would lead to increased activity being observed with these substrates. A further notable observation is that the selectivity observed for the catalytic reaction of isonitriles is good, with the major produced yielded in 73% or higher.

The results for ^{t}BuNC show a mediocre conversion of 49%. This must, however, be considered at least in part to be a result of the preliminary nature of these results. As a result of the selectivity observed for ^{t}BuNC the coupled 'R' group product, **4.24a**, ^{t}Bu-^{t}Bu, was the major product (73%). The only minor product found by GCMS, **4.25a,** was a result of coupling and reduction. Complex **4.25a** requires two reduction steps in addition to the coupling step in order to be formed. This illustrates the variety of the reaction pathways that are available within this reaction. A mystery arising from this reaction is the fate of the NC moieties, which must be abstracted from the isonitrile in the formation of **4.24a**. This may be explained by the observation of a greater amount of precipitate in this reaction than for the corresponding CyNC reaction. Unfortunately, this residue proved to be intractable, making characterisation of its constituents, and the identification of the possible fate of the NC moiety, impossible.

The results for CyNC indicate a poorer conversion (36%) than that seen for ^{t}BuNC. However, with an excellent 91% towards the formation of **4.20b** the results for this catalytic reaction display the highest selectivity achieved with complex **4.2** to date,. This is the same product that was seen in the stoichiometric reaction with CyNC. The minor products in this reaction were a mixture of reduction, α-carbon abstraction and coupling products. These were found to be **4.21b** (2%), **4.22b** (1%), **4.23b** (1%) and **4.26b** (5%). Complex **4.26b** is a product solely of reduction and appears to be on a divergent reaction pathway to the formation of the other products, which may explain its relative abundance compared to the other minor products. Complexes **4.21-3b** represent coupled dimers with varying levels of α-carbon abstraction from the starting isonitrile moiety. It can be argued that these are products formed upon quenching intermediates found during the formation of **4.20b**. This supposition is illustrated in **Scheme 4.3**.

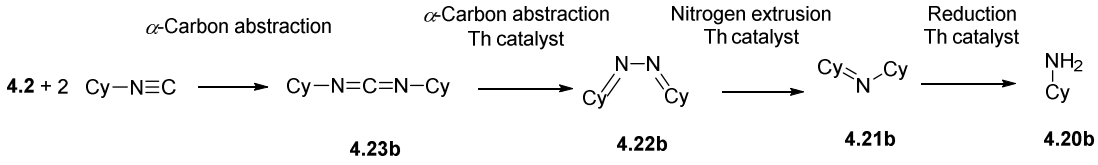

Scheme 4.3: Postulated reaction pathway towards the formation of **4.20b** *via* possible intermediate species.

As **Scheme 4.3** is speculation based upon the minor products characterised from the catalytic reaction it is not a definitive postulated mechanism. Reduction is the common major reaction when catalysing the reaction of both isonitriles and terminal acetylenes as substrates with complex **4.2**, suggesting that as a catalyst complex **4.2** favours reduction. This is unsurprising considering that the activation of small molecules investigated in *4.4.1-4* almost exclusively caused the formation of BMe_3, which could only result from reduction.

4.6 Conclusions and Summary

In summary, we have seen the successful transformation of a heteroleptic thorium terphenolate chlorido-complex to a heteroleptic thorium borohydrido-complex, **4.1**, *via* a precedented reaction route.[6] The use of ancillary borohydrido-ligands has resulted in more robust complexes including examples showing more versatile reactivity compared to their chlorido- analogues. Despite the increased robustness of the borohydrido-analogues, transmetallation of the terphenolate ligands was still observed when using Group I or II transfer reagents. Complex **4.1** was found to undergo more controlled reactions than its chlorido- analogue **3.2**. Reaction with a Lewis acid was found to desolvate the chelating DME molecule from complex **4.1**, resulting in the formation of two rare, labile neutral η^{6-} aryl interactions with the thorium cation in complex **4.2**. This compound was also found to facilitate small molecule activation of energetically demanding bonds, especially in the case of CO and CO_2. These examples of small molecule activation fulfil one of the primary aims of this research. It is unfortunate that the major product of small molecule activation by complex **4.2** is BMe_3, which is unlikely to be a commercially or industrially viable activation product. Some investigative forays into the catalytic reactions of complex **4.2** with terminal acetylenes and isonitriles were made. Poor to mediocre conversions were observed for all substrates. In some examples good to excellent selectivity was observed, but in the case of other substrates the selectivity was almost non-existent. In general complex **4.2** favours reduction of any electron rich substrate it interacts with. This tendency to

favour reductive pathways leads to the conclusion that **4.2** may prove to be a good catalyst for reduction of electron-rich substrates, however this would require further work to both examine the scope and optimise the conditions required for this reactive pathway. This would also require the reaction to turnover to regenerate the active catalyst, which would also need to be investigated.

4.7 References

1. J. McKinven, G. S. Nichol and P. L. Arnold, *Dalton Trans.*, 2014, 43, 17416-17421.
2. R. Hoffmann, *Angew. Chem., Int. Ed. Engl.*, 1982, 21, 711-724.
3. D. Hohl and N. Roesch, *Inorg. Chem.*, 1986, 25, 2711-2718.
4. T. J. Marks and J. R. Kolb, *Chem. Rev.*, 1977, 77, 263-293.
5. H. W. Turner, R. A. Andersen, A. Zalkin and D. H. Templeton, *Inorg. Chem.*, 1979, 18, 1221-1224.
6. T. M. Trnka, J. B. Bonanno, B. M. Bridgewater and G. Parkin, *Organometallics*, 2001, 20, 3255-3264.
7. S. R. Daly, P. M. B. Piccoli, A. J. Schultz, T. K. Todorova, L. Gagliardi and G. S. Girolami, *Angew. Chem., Int. Ed. Engl.*, 2010, 49, 3379-3381.
8. R. Shinomoto, J. G. Brennan, N. M. Edelstein and A. Zalkin, *Inorg. Chem.*, 1985, 24, 2896-2900.
9. R. Shinomoto, E. Gamp, N. M. Edelstein, D. H. Templeton and A. Zalkin, *Inorg. Chem.*, 1983, 22, 2351-2355.
10. F. Allen, *Acta Crystallogr., Sect. B: Struct. Sci*, 2002, 58, 380-388.
11. C. A. Cruz, D. J. H. Emslie, L. E. Harrington and J. F. Britten, *Organometallics*, 2007, 27, 15-17.
12. I. Korobkov, B. Vidjayacoumar, S. I. Gorelsky, P. Billone and S. Gambarotta, *Organometallics*, 2010, 29, 692-702.
13. C. A. Cruz, D. J. H. Emslie, C. M. Robertson, L. E. Harrington, H. A. Jenkins and J. F. Britten, *Organometallics*, 2009, 28, 1891-1899.
14. K. Biradha, M. Sarkar and L. Rajput, *Chem. Commun.*, 2006, 4169-4179.
15. T. Kawasaki, T. Nishimura and T. Kitazawa, *Bull. Chem. Soc. Jpn.*, 2010, 83, 1528-1530.
16. L. A. Borkowski and C. L. Cahill, *Cryst. Growth Des.*, 2006, 6, 2248-2259.
17. T. Mehdoui, J.-C. Berthet, P.Thuery and M.Ephritikhine, *Private Communication*, 2013.
18. J.-C. Berthet, P. Thuéry, N. Garin, J.-P. Dognon, T. Cantat and M. Ephritikhine, *J. Am. Chem. Soc.*, 2013, 135, 10003-10006.
19. Y.-C. He, J. Guo, H.-M. Zhang, J.-F. Ma and Y.-Y. Liu, *CrystEngComm*, 2014, 16, 5450-5457.
20. H. K. Roobottom, H. D. B. Jenkins, J. Passmore and L. Glasser, *J. Chem. Educ.*, 1999, 76, 1570.
21. H. D. B. Jenkins and K. P. Thakur, *J. Chem. Educ.*, 1979, 56, 576.
22. J. A. Dean and N. A. Lange, *Lange's handbook of chemistry*, McGraw-Hill, 1992.
23. V. D. Makhaev, A. P. Borisov, A.S. Antsyshkina and G. G. Sadikov, *Zh. Neorg. Khim.*, 2004, 49, 371-379.
24. G. Soloveichik, J.-H. Her, P. W. Stephens, Y. Gao, J. Rijssenbeek, M. Andrus and J. C. Zhao, *Inorg. Chem.*, 2008, 47, 4290-4298.

25. J. Prust, K. Most, I. Müller, E. Alexopoulos, A. Stasch, I. Usón and H. W. Roesky, *Z. Anorg. Allg. Chem.*, 2001, 627, 2032-2037.
26. G. L. Soloveichik, M. Andrus and E. B. Lobkovsky, *Inorg. Chem.*, 2007, 46, 3790-3791.
27. M. Bremer, G. Linti, H. Nöth, M. Thomann-Albach and G. E. W. J. Wagner, *Z. Anorg. Allg. Chem.*, 2005, 631, 683-697.
28. R. A. Collins, J. Unruangsri and P. Mountford, *Dalton Trans.*, 2013, 42, 759-769.
29. R. Černý, Y. Filinchuk, H. Hagemann and K. Yvon, *Angew. Chem., Int. Ed. Engl.*, 2007, 46, 5765-5767.
30. B. Wrackmeyer and O. L. Tok, *Z. Naturforsch.*, 2005, 60b, 259-264.
31. J. R. Medina, G. Cruz, C. R. Cabrera and J. A. Soderquist, *J. Org. Chem*, 2003, 68, 4631-4642.
32. D. Mathis, E. P. A. Couzijn and P. Chen, *Organometallics*, 2011, 30, 3834-3843.
33. H. Binder and W. Diamantikos, *Z. Naturforsch., B: Anorg. Chem., Org. Chem.*, 1983, 38B, 203-207.
34. A. Lang, H. Nöth and M. Thomann-Albach, *Chem. Ber.*, 1997, 130, 363-370.
35. S. Aldridge, R. J. Calder, A. Rossin, A. A. Dickinson, D. J. Willock, C. Jones, D. J. Evans, J. W. Steed, M. E. Light, S. J. Coles and M. B. Hursthouse, *Journal of the Chemical Society, Dalton Transactions*, 2002, 2020-2026.
36. A. Cassen, Y. Gloaguen, L. Vendier, C. Duhayon, A. Poblador-Bahamonde, C. Raynaud, E. Clot, G. Alcaraz and S. Sabo-Etienne, *Angew. Chem., Int. Ed. Engl.*, 2014, 53, 7569-7573.
37. G. L. Gutsev, R. J. Bartlett and R. N. Compton, *The Journal of Chemical Physics*, 1998, 108, 6756-6762.
38. B. Cordero, V. Gomez, A. E. Platero-Prats, M. Reves, J. Echeverria, E. Cremades, F. Barragan and S. Alvarez, *Dalton Trans.*, 2008, 2832-2838.
39. G. E. Scuseria, M. D. Miller, F. Jensen and J. Geertsen, *The Journal of Chemical Physics*, 1991, 94, 6660-6663.
40. Y. Apeloig and A. Stanger, *J. Am. Chem. Soc.*, 1985, 107, 2806-2807.
41. Y. Apeloig, R. Biton and A. Abu-Freih, *J. Am. Chem. Soc.*, 1993, 115, 2522-2523.
42. J. Frey, E. Schottland, Z. Rappoport, D. Bravo-Zhivotovskii, M. Nakash, M. Botoshansky, M. Kaftory and Y. Apeloig, *J. Chem. Soc., Perkin Trans. 2*, 1994, 2555-2562.
43. A. D. Allen, R. Krishnamurti, G. K. S. Prakash and T. T. Tidwell, *J. Am. Chem. Soc.*, 1990, 112, 1291-1292.
44. J. B. Lambert, Y. Zhao, R. W. Emblidge, L. A. Salvador, X. Liu, J.-H. So and E. C. Chelius, *Acc. Chem. Res.*, 1999, 32, 183-190.
45. J. B. Lambert, *Tetrahedron*, 1990, 46, 2677-2689.
46. J. B. Lambert, G. T. Wang, R. B. Finzel and D. H. Teramura, *J. Am. Chem. Soc.*, 1987, 109, 7838-7845.
47. A. J. Ashe, *Tetrahedron Lett.*, 1970, 11, 2105-2108.
48. P. K. G. Hodgson, R. Katz and G. Zon, *J. Organomet. Chem.*, 1976, 117, C63-C67.
49. A. V. Lis, I. P. Tsyrendorzhieva, A. I. Albanov, V. I. Rakhlin and M. G. Voronkov, *Russ. J. Org. Chem.*, 2013, 49, 1451-1453.
50. P. K. Sharma, M. Dawid, J. Warkentin, R. M. Vestal and F. Wudl, *J. Org. Chem*, 2001, 66, 7496-7499.
51. P. W. Meg Annan, LeQuesne and V. Paul, *J. Am. Soc. Mass Spectrom.*, 1993, 4, 327-335.
52. A. G. Smith, S. J. Gaskell and C. J. W. Brooks, *Biomed. Mass Spectrom.*, 1976, 3, 161-165.
53. M. Charton, *J. Am. Chem. Soc.*, 1975, 97, 1552-1556.

54. R. S. Macomber, *Organic Chemistry*, University Science Books, 1996.
55. S. Kotha and E. Brahmachary, *J. Org. Chem*, 2000, 65, 1359-1365.
56. S. Kotha and E. Brahmachary, *J. Organomet. Chem.*, 2004, 689, 158-163.
57. P. G. Gassman and T. L. Guggenheim, *J. Am. Chem. Soc.*, 1982, 104, 5849-5850.
58. E. G. J. Hartley, *Journal of the Chemical Society, Transactions*, 1911, 99, 1549-1553.
59. J. Azuaje, A. Coelho, A. E. Maatougui, J. M. Blanco and E. Sotelo, *ACS Combinatorial Science*, 2011, 13, 89-95.
60. H. Yamada, Y. Wada, S. Tanimoto and M. Okano, *Bull. Chem. Soc. Jpn.*, 1982, 55, 2480-2483.

Chapter 5: Phosphorus as the ligating atom in terphenyl ligands

5.1 Introduction

An isolated intermediate in the synthesis of $Ter^{Mes}OH$, $Ter^{Mes}I$, was thought to be an ideal starting material for examining the effects of changing the donor atom from the oxygen atom seen in *Chapters Three and Four*. The potential of the formation and isolation of a Th=P bond from a phosphorus ligating complex was a major aim of this research pathway. Given the ease of transformation it was decided that the easier ligand to synthesise would be a phosphine based ligand; $Ter^{Mes}PH_2$. This had the added benefit of increasing the number of NMR active nuclei that are present within the reaction. This allows for a convenient means for monitoring the progress of the reaction. This is especially true in the case of a phosphine moiety as the P-H coupling in the ^{31}P NMR means that assignment of the number of protons bound to a phosphorus atom within the products of the reaction becomes facile.

Bonding interactions between actinide and phosphorus atoms are fairly common, but are mostly constrained to compound based upon chelating ligands where the phosphorus atom acts as a donor, with the 1,2- *bis*(dimethylphosphino)ethane (DMPE) ligand particularly prevalent.[1-5] Selected examples of phosphorus atom donors towards actinide centres are shown in **Figure 5.1**.

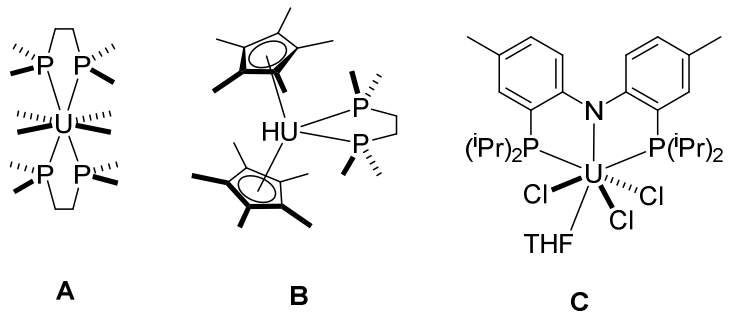

Figure 5.1: Selected examples of dative An-P interactions as reported by Shores, Marks and Kiplinger *et al*.[1, 3, 5]

It should be noted that the examples in **Figure 5.1**, **A**-**C**, contain An-P interactions that can be described as a dative bond as a result of the Lewis basic phosphorus atom

donating electron density into vacant orbitals of the Lewis acidic actinide metal centre. Examples of An-P complexes containing bonds that are not a result of these dative interactions are rare[1, 6-10] especially examples containing thorium.[7-9] Some of these non-dative An-P complexes are a result of activation of P_4 and as a result are unlikely to be ideal candidates for probing the isolation of a An=P bond.[11, 12] (see **Figure 5.2**)

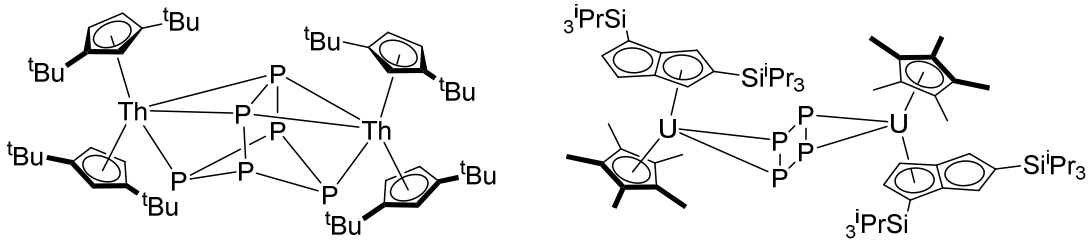

Figure 5.2 Selected examples of non-dative An-P bonds as described by Wolmerhauser and Cloke *et al*.[11, 12]

Selected examples of non-dative An-P complexes that are not a result of activation of P_4 are depicted in **Figure 5.3.**

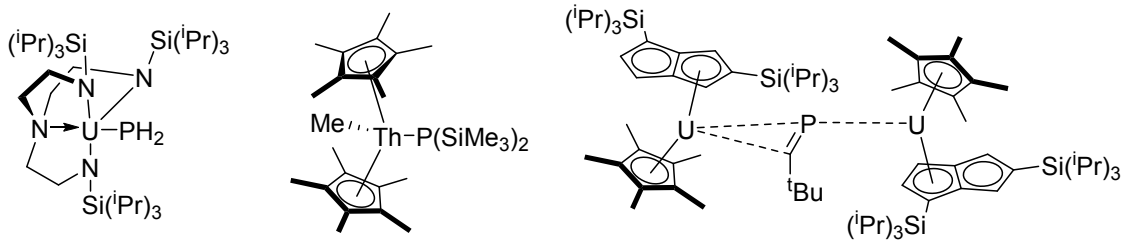

Figure 5.3 Selected examples of non-dative An-P bonds as described by Liddle, Sattelberger and Cloke *et al*.[6, 8, 10]

Compound **F**, depicted in **Figure 5.3** shows the only example of a phosphido actinide complex with no organic substituents on the phosphorus atom.[6] The metal-PH_2 moiety is rare and the nine known well characterised examples are mostly restricted to main group examples, particularly of group XIV with five well characterised examples of germanium and tin known. (**Figure 5.4**)[13-16]

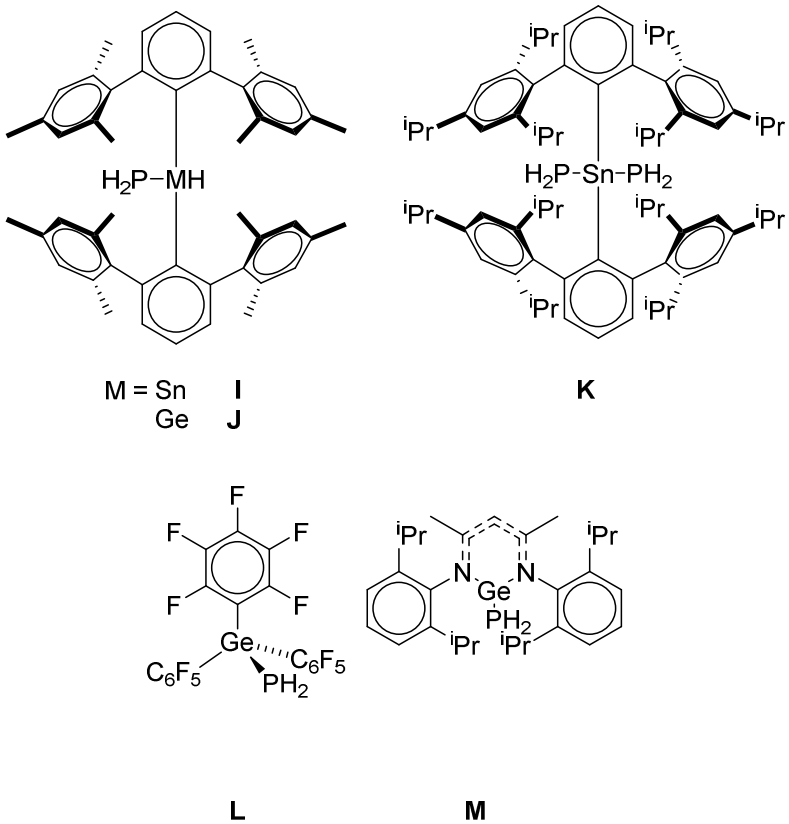

Figure 5.4: Group XIV M-PH_2 complexes as described by Ragogna, Monse, Driess and Merz *et al*.[13-16]

There is one well characterised example of M-PH_2 amongst both the d-block and s-block metals.[17, 18] The d-block example is an iridium complex, **N**,[18] (see **Figure 5.5**) which, combined with the prevalence of group XIV examples (**Figure 5.4**), suggests that this motif favours electron-rich metal centres to stabilise the relatively high electronegativity of a phosphorus atom (2.19 V[19]).

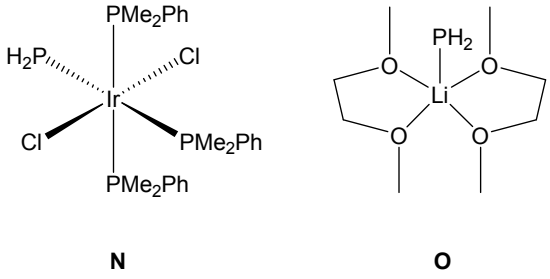

Figure 5.4 s- and d-block examples of M-PH_2 complexes as reported by Schmidt and Senior *et al*.[17, 18]

Compound **G**, depicted in **Figure 5.3** shows an example of the ubiquitous metallocene structure stabilising an phosphido- complex, which has been found to form a metallacycle, $(Cp^*)_2Th(\kappa^2\text{-}[P\{SiMe_3\}SiMe_2CH_2]$, upon heating.[8] Compound **H** is formed

by reduction of a phospha-alkyne moiety mediated by the uranium (III) centres. The paucity of well characterised examples of An-PR_2 is surprising when considering the potentially high reactivity and likelihood of small molecule activation by an An-P bond (a Th-P bond has a bond dissociation energy of 377 KJ mol^{-1} whilst a Th-O bond has a bond dissociation energy of 854(13) KJ mol^{-1}).[19] Another attractive target is the An=P double bond, which could be synthesised from a Th-bound phosphide ligand, for example by HX elimination. (**Equation 5.1**)

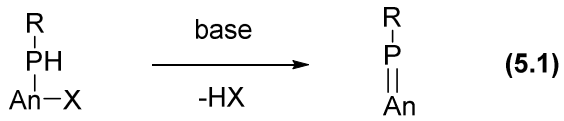

(5.1)

5.2 Synthesis of $Ter^{Mes}PH_2$ and its Group I salts

5.2.1 Synthesis of $Ter^{Mes}PH_2$

The synthesis of the phosphorus analogue of the terphenolate ligand proceeded from a common intermediate in the formation of the terphenolate ligand; terphenyl dimesityl iodide, $Ter^{Mes}I$. Lithiation of $Ter^{Mes}I$ with $^{n}BuLi$, followed by reaction with phosphorus trichloride resulted in the formation of the PCl_2 analogue, $Ter^{Mes}PCl_2$ (see **Scheme 5.1**). Conversion of the $Ter^{Mes}PCl_2$ to the PH_2 species, $Ter^{Mes}PH_2$, **5.1,** then proved facile via reduction with $LiAlH_4$ (see **Scheme 5.1**). Attempts to deprotonate this ligand and ligate it to actinides are detailed below.

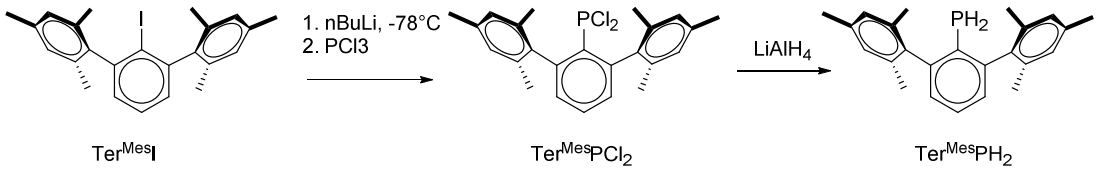

Scheme 5.1: Formation of terphenyl phosphine ligands

The phosphorus resonance in the ^{31}P NMR spectrum of a perdeuterated benzene solution of $Ter^{Mes}PH_2$ is observed as a triplet at -147.30 ppm, with a $^{1}J_{PH}$ coupling of 209.7 Hz (500 MHz spectrometer). The ^{1}H NMR spectrum shows a doublet at 3.26 ppm, with a $^{1}J_{PH}$ coupling of 209.7 Hz (500 MHz spectrometer) assigned as the PH_2 protons. The methyl protons of the mesityl groups show small couplings (due to long range through-bond coupling to the phosphorus) of 2.4 Hz for the *ortho* groups and 2.8 Hz for the *para* groups. The *meta* aromatic protons of the central aryl ring are also observed

as a doublet of doublets due to a small coupling of 2.3 Hz on top of the coupling observed due to the *para* aromatic proton.

5.2.2 Deprotonation of $Ter^{Mes}PH_2$

The deprotonation of a solution of $Ter^{Mes}PH_2$ in perdeuterated benzene was studied with a range of bases.

5.2.2.1 Reaction of $Ter^{Mes}PH_2$ with KH

(5.2)

Reaction of one equivalent of a perdeuterated benzene solution of $Ter^{Mes}PH_2$ with a slight excess of potassium hydride resulted in no reaction occurring initially visually and by NMR spectroscopy. Heating this suspension at 80°C for 16 hours resulted in a reaction occurring. The NMR spectra of this reaction showed that this attempt at deprotonation did not proceed smoothly. The ^{1}H NMR spectrum showed evidence of hydrogen evolution at 4.47 ppm in addition to multiple products in the aromatic and benzyl regions. The ^{31}P NMR spectrum showed multiple products, the major one of which was a doublet at -129.8 Hz, assigned to be $KHPTer^{Mes}$. Deprotonation by KH was therefore found to be unsuitable in investigating further reactivity with this ligand so a different base was investigated in the deprotonation of $Ter^{Mes}PH_2$. An explanation for this reaction not proceeding smoothly to give the desired product, despite the high pKa (relative to a phosphine moiety) of KH of >35[20] (Equation 5.2) is that the insolubility of KH in benzene resulting in a slow reaction.

5.2.2.2 Reaction of $Ter^{Mes}PH_2$ with KN"

Potassium hexamethyldisilazane (Pk_a of -30 in DMSO)[21] was chosen as a non-nucleophillic base, as an alternative to KH. KN" has the benefit over KH of being soluble in a wider range of organic solvents.

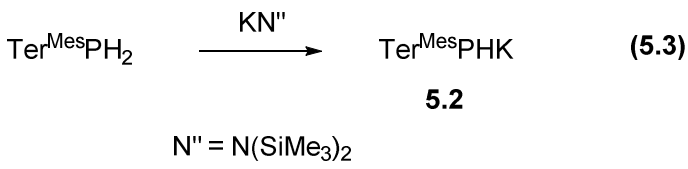

(5.3)

Treatment of one equivalent of a perdeuterated benzene solution of $Ter^{Mes}PH_2$ with one equivalent of potassium hexamethyldisilazane (KN") resulted in a reaction being

observed to have taken place visually by the formation of a green suspension. The ^{1}H and ^{31}P NMR spectra of this product solution showed a clean deprotonation to form $Ter^{Mes}PHK$, **5.2** as evidenced by the shift of the P**H** proton resonance from a doublet at 3.26 ppm with integration of 2H in the ^{1}H NMR spectrum of starting material to a doublet at 1.47 ppm with integration of 1H in the ^{1}H NMR spectrum of this reaction. There is also a reduction in the $^{1}J_{PH}$ coupling constant upon deprotonation from 209.7 Hz in the spectrum of $Ter^{Mes}PH_2$ to 174.2 Hz in that of $Ter^{Mes}PHK$. This clean deprotonation is also seen clearly in the ^{31}P NMR spectra (see **Figure 5.5**) as the starting material $Ter^{Mes}PH_2$ has a chemical shift of -147.3 ppm, a triplet with a $^{1}J_{PH}$ coupling constant of 209.6 Hz, whereas after deprotonation the phosphorus resonance in $Ter^{Mes}PHK$ shifts to – 129.8 ppm and appears as a doublet with a $^{1}J_{PH}$ coupling constant of 171.4Hz.

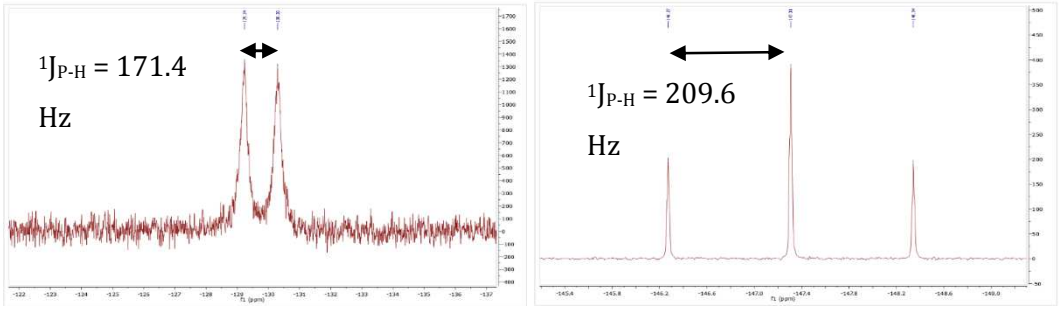

Figure 5.5: Left; ^{31}P NMR spectrum of $KPHTer^{Mes}$, Right; ^{31}P NMR spectrum of $Ter^{Mes}PH_2$

5.3 Reactions of $Ter^{Mes}PHK$ with thorium (IV) halides

5.3.1 Reaction of $Ter^{Mes}PH_2$ with $ThCl_4(DME)_2$

$$2Ter^{Mes}PH_2 \xrightarrow[-2HN''\ \ 2KN'']{} 2Ter^{Mes}PHK \xrightarrow[-2KCl\ \ ThCl_4(DME)_2]{} ThCl_2(Ter^{Mes}PH)_2(DME)_2$$

$N'' = N(SiMe_3)_2$

Scheme 5.2: Attempted Synthesis of $ThCl_2(Ter^{Mes}PH)_2(DME)_2$

The reaction of two equivalents of *in situ* generated $Ter^{Mes}PHK$, from reaction of two equivalents of KN" and $TerMesPH_2$, with one equivalent of $ThCl_4(DME)_2$ in toluene and THF solution resulted in a green-yellow suspension with a light coloured precipitate being formed (**Scheme 5.2**). The ^{1}H NMR spectrum of a perdeuterated benzene solution of the products of this reaction indicated that a reaction had occurred, with

clear shifts in the terphenolate resonances. It appeared that the DME molecules of the thorium starting material remained ligated to the metal centre as implied by a shift in their resonances, which did not align with that of 'free' DME. However, a resonance relating to the P**H** proton could not be assigned. The ^{31}P NMR spectrum of this reaction showed two doublets, both of which displayed a considerable alteration form the chemical shift of Ter^{Mes}PHK as seen in *5.2.2.2*. The doublets appeared at -88.0 and -137.1 ppm with $^{1}J_{PH}$ coupling constants of 22.18 and 188.1 Hz respectively and had relative integrations of 1:10. Attempts to isolate and characterise the major product did not prove successful.

5.3 Reactions of Ter^{Mes}PHK with uranium (III) and uranium (IV) halides and borohydrides

5.3.1 Reactions with Uranium (IV) halides

5.3.1.1 Reaction of Ter^{Mes}PHK with UCl_4

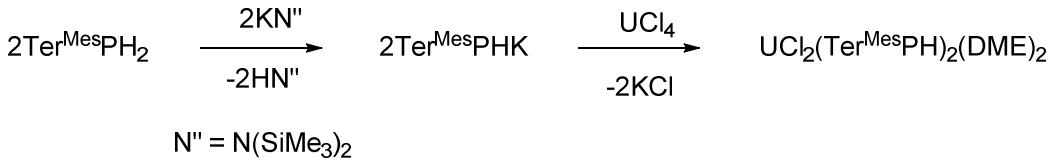

Scheme 5.3: Attempted Synthesis of $ThCl_2(Ter^{Mes}PH)_2(DME)_2$

Reaction of two equivalents of *in situ* generated Ter^{Mes}PHK, from reaction of two equivalents of KN" and TerMesPH$_2$, with one equivalent of UCl_4 in toluene and THF solution resulted in a brown suspension with a light coloured precipitate being formed (**Scheme 5.3**). The ^{1}H NMR spectrum of the products of this reaction shows that one major paramagnetic terphenyl set of resonances could be observed. The ^{31}P NMR spectrum shows two diamagnetic resonances, both of which are doublets in a 1:5 ratio. The minor phosphorus containing product has a resonance at -101.5 ppm and has a coupling constant of 155.0 Hz, so this is likely to be due to one bond phosphorus hydrogen coupling. The major non-paramagnetic phosphorus containing product has a resonance at -135.7 ppm and has a coupling constant of 166.8 Hz, so this is also likely to be due to one bond phosphorus hydrogen coupling. These products are likely due to ligand degradation. Attempts to isolate one of the products of this reaction were not successful so further reactivity was investigated with other uranium starting materials.

5.3.1.2 Reaction of $Ter^{Mes}PHK$ with $UI_4(dioxane)_2$

Reaction of two equivalents of *in situ* generated $Ter^{Mes}PHK$, from reaction of two equivalents of KN" and $TerMesPH_2$, with one equivalent of $UI_4(dioxane)_2$ in THF solution resulted in a purple suspension being formed. Extraction of this solution by hexane resulted in a brown solution, from which colourless crystals were grown determined to be $(Ter^{Mes}PH)_z$ **5.1**. The solid state structure of **5.3** is displayed in **Figure 5.9**. Selected bond angles and distances calculated from the solid state structure of **5.3** are shown in **Table 5.1**.

The purple colour formed upon addition of the phosphido- ligand to the uranium metal salt may be an indication of the formation of a uranium (III) species, suggesting that the formation of **5.3** may be due to a reductive elimination pathway, (**Scheme 5.4**) whereby the uranium (IV) complexes ligate the phosphine- ligands and then reductively eliminate the phosphorus-bond containing coupled product $(Ter^{Mes}PH)_z$, which presumably forms by radical coupling of the phosphoryl radicals.

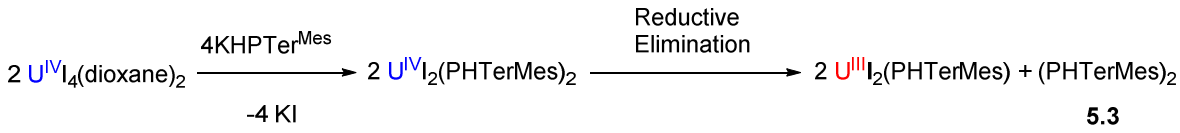

Scheme 5.4: Proposed route for the formation of **5.3**

This reductive elimination pathway would suggest that the uranium (IV) species is thermally unstable and perhaps could be isolated by lowering the reaction temperatures. Isolation of this uranium (IV) species may also be aided by increasing the bulk of the terphenolate ligands as seen in *5.3.1.7*.

The solid state structure of **5.3** contains a phosphorus-phosphorus bond, which due to stereochemically active lone pairs contains stereochemistry. The phosphine hydrogen atoms (H1p and H1p') adopt *trans* conformations to each other, whilst similar trans conformations are observed for the terphenolate ligands. The bond angles around the phosphorus atom are almost orthogonal with angles of 98.50(10), 98.5(15) and 96.0(14), this deviation from tetrahedral to angles more reminiscent of octahedral complexes is likely due to the stereochemically active lone pairs of phosphorus and the steric bulk of the terphenolate ligands. The P1-P1' bond of 2.2453(15) Å is typical for complexes of this type[22-26].

Previous examples of terphenyl phosphorus compounds containing phosphorus-phosphorus bonds have resulted in insertion of the phosphorus atom into the ortho-protecting groups, or in the formation of a phosphorus to phosphorus double bond.[27-32] (see **Figure 5.6**)

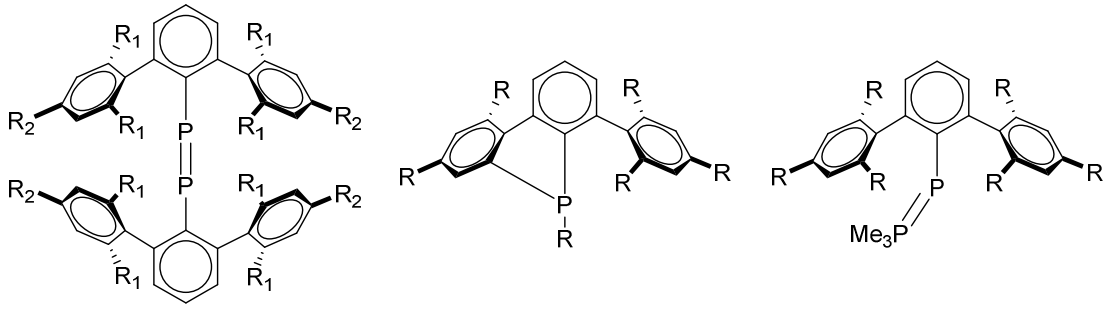

R_1=R_2= Me **P**
R_1=R_2= ^{i}Pr **Q**
R_1= Me R_2=H **R**

R=Me **S**
R= ^{i}Pr **T**

R=Me **U**
R= ^{i}Pr **V**

Figure 5.6: Selected examples of terphenyl phosphorus compounds as described by Protasiewicz and Power *et al*.[27-32]

Compound **P**, $Ter^{Mes}P{=}PTer^{Mes}$, allows for a comparison to be made with **5.3** concentrating on the effect of multiple bond character between the phosphorus atoms on the P-P distance. Whilst bond length is a good indicator for bond order in bonding interactions between first row main group elements, the shortening of the bond upon increasing bond order becomes less pronounced for heavier main group analogues, which is indicative of the reduced π overlap present within these systems. In compound **P** the P-P bond distance was initially reported, in 1996, as being 1.985 (2) Å[32] but was revised, in 2010, upon further and more thorough X-ray crystallography experiments at lower temperatures (100 K) to be 2.029(1) Å.[31] Both of these bond lengths represent a considerable contraction of 9.7 % when compared to the P-P bond length of 2.2453(15) Å in **5.3**, which is typical for other contractions of this kind seen within the literature.[31]

The ^{1}H and ^{31}P NMR spectra of **5.3** exhibits some interesting coupling and multiplets. In the ^{1}H NMR the PH proton resonance is observed as a multiplet at around 3 ppm, shown in **Figure 5.7**, which is a very well behaved example of an AA'XX' splitting pattern. An almost identical splitting pattern is observed in the ^{31}P NMR spectrum at around -100.3 ppm, which is to be expected of an AA'XX' system (**Figure 5.8**). The AA'XX' system arises due to the phosphorus and hydrogen atoms of the $(PH)_2$ motif

being chemically equivalent, but magnetically inequivalent. In an AA'XX' system there are two half spectrums consisting of a 1:1 doublet and two ab quartets with 'normal' intensity ratios and apparent couplings. However, these couplings cannot be distinguished or identified to an ab pair and this ambiguity extends to the relative sign of the couplings and the identity of each number that can be obtained from these apparent couplings.

These observations can be summarised in four relationships:-[33]

$|K| = |J_{AA'} + J_{XX'}|$ "J" of one ab quartet

$|L| = |J_{AX} - J_{AX'}|$ "δ" of both ab quartets

$|M| = |J_{AA'} - J_{XX'}|$ "J" of other ab quartet

$|N| = |J_{AX} + J_{AX'}|$ "doublet"

Due to through-space coupling to the phosphorus atoms the methyl groups on the mesityl rings are inequivalent by NMR spectroscopy and appear as doublets in the ^{1}H NMR spectrum.

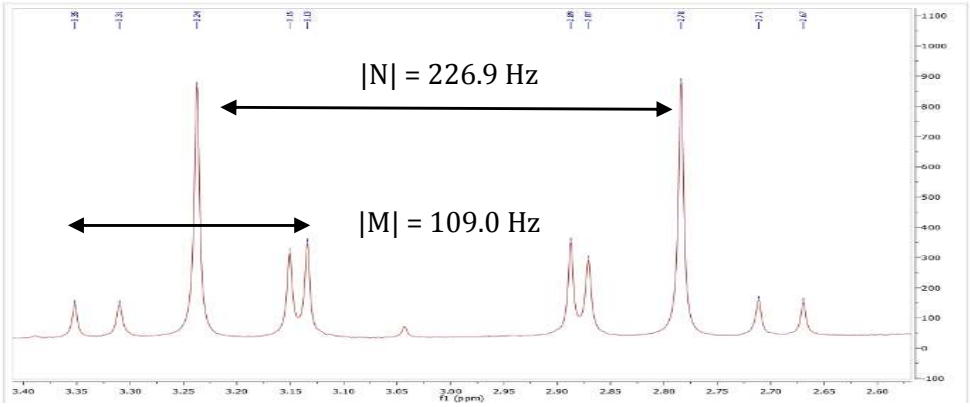

Figure 5.7: The AA'XX' system in the ^{1}H NMR spectrum of the PH proton of **5.3**, $(PHTer^{Mes})_2$

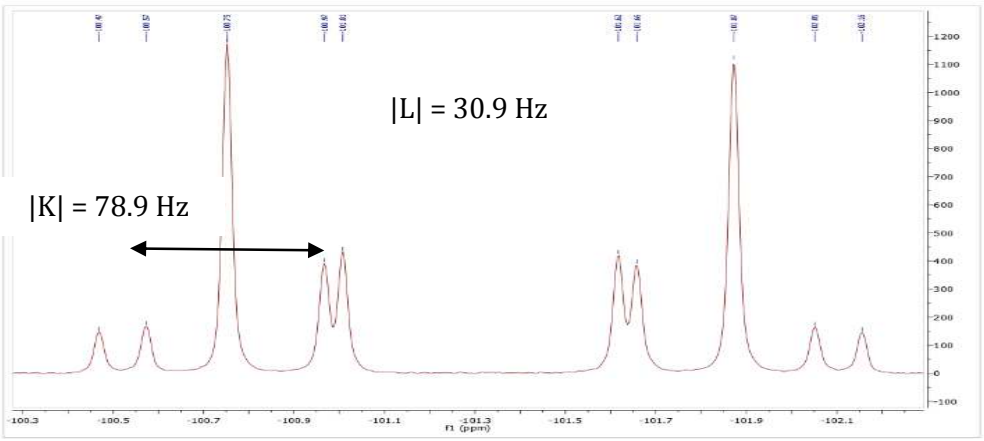

Figure 5.8: The AA'XX' system in the ^{31}P NMR spectrum of **5.3**, $(PHTer^{Mes})_2$

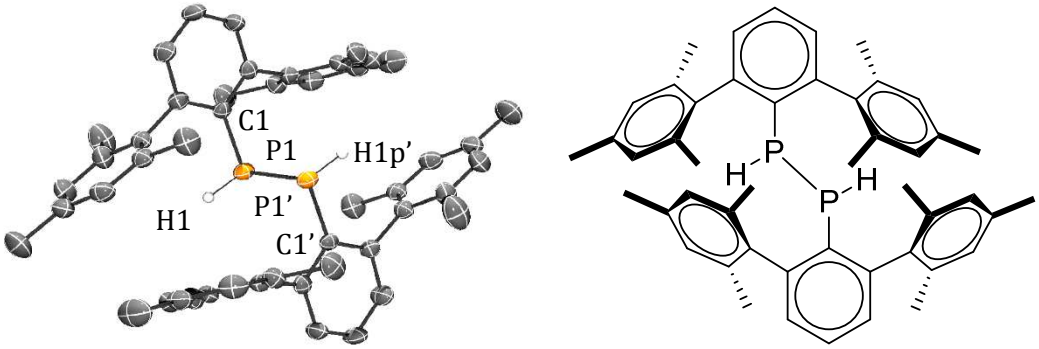

Figure 5.9: Displacement ellipsoid drawing of the solid state molecular structure of **5.3, (**$Ter^{Mes}PH)_2$. Non- phosphine hydrogen atoms are omitted for clarity.

Table **5.1** : Selected X-ray crystallographic data for **5.3**

Bond	Bond distance (Å) / angle (°)
P1-P1'	2.2453(15)
P1-C1	1.839(3)
C1-P1-P1'	98.50(10)
C1-P1-H1p	98.5(15)
H1p-P1-P1'	96.0(14)

5.3.2 Synthesis of $Ter^{Trip}PH_2$ and its Group I salts

5.3.2.1 Synthesis of $Ter^{Trip}PH_2$

One avenue for increasing the steric bulk of the terphenolate ligands is to place isopropyl groups in the place of the methyl groups on the terphenolate ligand. This ligand can be prepared in an analogous way to the preparation of $Ter^{Mes}PH_2$, by forming the terphenyl iodide via a Grignard reaction, then subjecting this product to lithiation, treatment with PCl_3 and then reduction via $LiAlH_4$ to form the phosphine ligand. This process is detailed in **Scheme 5.5**.

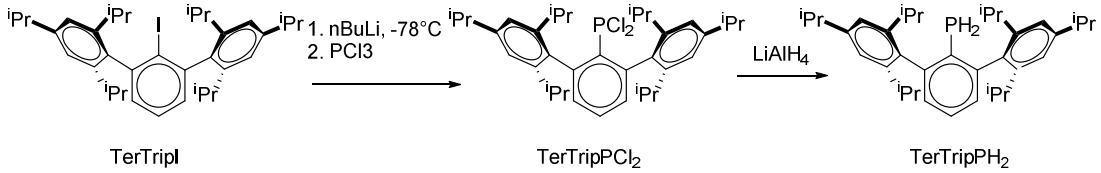

Scheme 5.5: Synthetic route to $Ter^{Trip}PH_2$

The ^{31}P NMR spectrum of $Ter^{Trip}PH_2$ is observed to contain only one resonance, a triplet with a $^1J_{PH}$ coupling of 210.7 Hz (500 MHz spectrometer) at -140.4 ppm. In the ^1H NMR spectrum the P**H** protons appear as a doublet ($^1J_{PH}$ coupling of 210.7 Hz) at 3.34 ppm. The C**H**Me_2 protons of the isopropyl groups have resonances that overlap with one another in a perdeuterated benzene solution so appear as a multiplet at 2.85 ppm. The methyl groups appear as doublets between 1.4 and 1.1 ppm.

5.3.3 Reactions with thorium salts

5.3.3.1 Reaction of $Ter^{Trip}PHK$ with $ThCl_4(DME)_2$

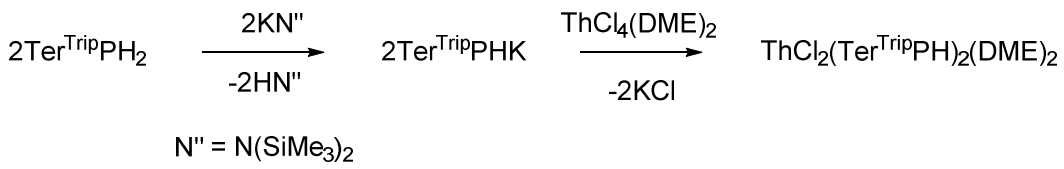

Scheme 5.6: Attempted synthesis of $ThCl_2(Ter^{Trip}PH)_2(DME)_2$

The reaction of a yellow–green perdeuterated benzene solution of two equivalents of *in situ* generated $Ter^{Trip}PHK$, from reaction of KN" with $Ter^{Trip}PH_2$, with a $ThCl_4(DME)_2$ resulted in a colour change to yellow being observed (**Scheme 5.6**). The ^1H NMR spectrum of the products of this reaction showed a clear shift of the PH proton resonances, which appeared as doublet, from 3.34 ppm with $^1J_{PH}$ coupling of 210.7 Hz in the $Ter^{Trip}PH_2$ starting material to 1.87 ppm with $^1J_{PH}$ coupling of 182.3 Hz in the products. There was also a clear shift observed in the resonances assigned to the isopropyl protons, suggesting that a reaction has occurred. This is supported by the ^{31}P NMR spectrum (see **Figure 5.10**) which shows four resonances; two doublets, a small triplet assigned to unreacted starting material and a doublet of triplets. The doublet of triplets, located at -144.8 ppm and with coupling constants of 74.4 and 37.4 Hz is assigned as a product of degradation. This leaves assignation of the remaining two doublets, located at -86.4 and 116.5 ppm with $^1J_{PH}$ coupling constants of 225.5 and 194.2 Hz respectively with relative integration of 1 to 5. These values lead to the conclusion that the doublet at -116.5 ppm is attributed to the PH-Th resonance, whilst the doublet at – 86.4 ppm is likely to be a degradation product. Attempts to isolate and further characterise this product did not prove successful.

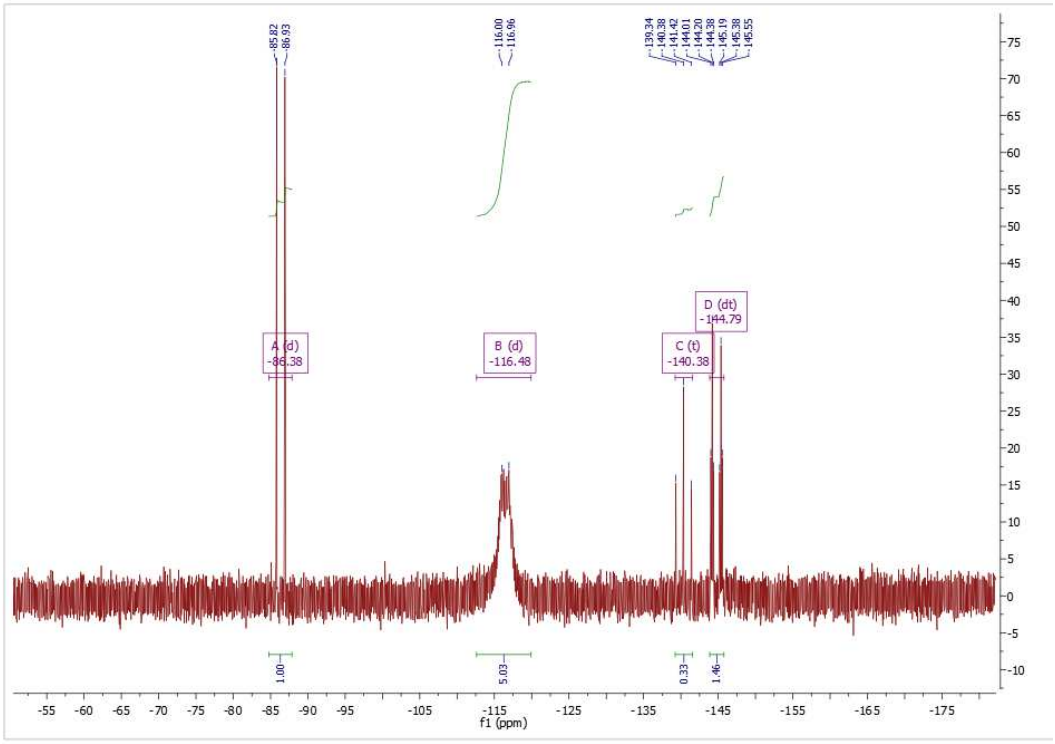

Figure 5.10: The ^{31}P NMR spectrum of the reaction of Ter^{Trip}PHK with $ThCl_4(DME)_2$

5.3.4 Reaction with Uranium (IV) halides

5.3.4.1 Reaction of Ter^{Trip}PHK with UCl_4

N" = $N(SiMe_3)_2$

Scheme 5.7: Attempted synthesis of UCl_2(Ter^{Trip}PH)$_2$

The reaction of a yellow-green perdeuterated benzene solution of two equivalents of *in situ* generated Ter^{Trip}PHK, from reaction of KN" with Ter$^{Trip}PH_2$, with a green THF solution of UCl_4 resulted in a colour change to brown being observed (**Scheme 5.7**). The ^{1}H NMR spectrum of this reaction showed four broad resonances in the diamagnetic region. Two of these resonances were assigned to fluxional THF ligation to a uranium centre, whilst another resonance was assigned to the benzene resonance. There was no sign of resonances which could be attributed to a complex containing the Ter$^{Trip}PH_2$ moiety and the uranium centre. The ^{31}P NMR spectrum of the reaction products showed four resonances, a singlet, two doublets and one triplet, which matched the resonance of the Ter$^{Trip}PH_2$ starting material. The doublets were found at -95.1 and -

152.7 ppm with $^{1}J_{PH}$ coupling constants of 165.5 and 209.3 Hz respectively and are most likely to be degradation products. The singlet was located at -100.6 ppm and is also likely to be due to a degradation product. Attempts to isolate the paramagnetic products from this reaction did not prove successful.

5.3.4.2 Reaction of $Ter^{Trip}PHK$ with $UI_4(dioxane)_2$

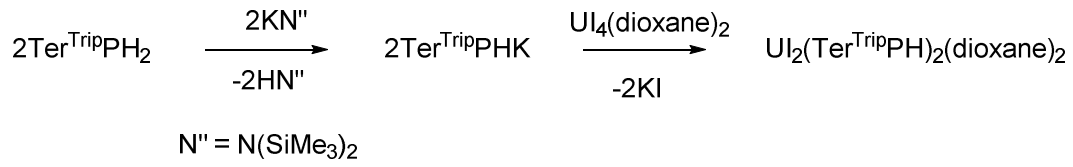

Scheme 5.8: Attempted synthesis of $UI_2(Ter^{Trip}PH)_2(dioxane)_2$

The reaction of a yellow-green perdeuterated benzene solution of two equivalents of *in situ* generated $Ter^{Trip}PHK$, from reaction of KN" with $Ter^{Trip}PH_2$, with a dark red THF solution of $UI_4(dioxane)_2$ resulted in a colour change to dark purple being observed (**Scheme 5.8**). The ^{1}H NMR spectrum of the products of this reaction indicate that a reaction has occurred as one set of paramagnetic resonances that can be assigned to the desired product are observed. The ^{31}P NMR spectrum shows three resonances; two doublet of doublets and a doublet. The doublet of doublets are observed at -95.1 and -100.8 ppm with coupling constants of 166.3, 50.9 and 142.8, 73.0 Hz respectively and are likely to be due to degradation products. The doublet is observed at -106.5 ppm with coupling constant of 186.0 Hz and has relative integration of 12 compared to the doublets of doublets 2 and 1 respectively. These resonances are all in a similar region of around -100 ppm, suggesting that they are not the resonances of a phosphorus bond to a uranium atom due to there being a lack of paramagnetic shift, which would be expected. Attempts to isolate and further characterise the paramagnetic products from this reaction did not prove successful.

5.4 Attempted Synthesis of $(SiMe_3)PHTer^{Mes}$

An alternate route in attempting to prevent the coupling of the phosphine ligands is to increase the steric bulk directly on the phosphorus atom. This was attempted by synthesising a phosphorus ligand where one of the phosphine hydrogen atoms was transformed into a $SiMe_3$ group via a lithiation and then salt elimination reaction detailed in Equation 5.4**.**

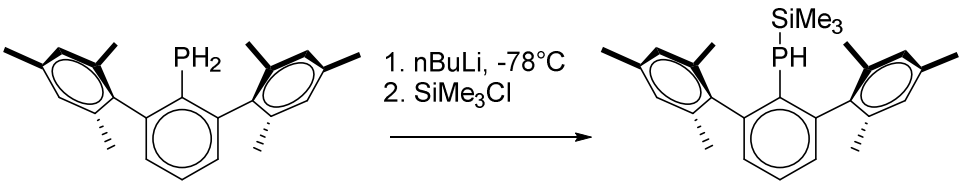

(5.4)

$TerMesPH_2$ $TerMesP(H)SiMe_3$

The NMR spectra of the products of this reaction indicated that this reaction was not successful as in addition to the resonances of the $Ter^{Mes}PH_2$ starting material, degradation products were also observed. In an attempt to synthesise $Ter^{Mes}P(H)SiMe_3$ by a different route KN" was used as a deprotonation agent whilst still using $SiMe_3Cl$ as the silylation agent. However this also led to decomposition products and not the desired $Ter^{Mes}P(H)SiMe_3$ ligand. This led to investigation into other routes towards the synthesis of $Ter^{Mes}P(H)SiMe_3$.

This alternative route involved using the $Ter^{Mes}PCl_2$ intermediate in the formation of $Ter^{Mes}PH_2$ and reacting it with one equivalent of trimethyl silyl Grignard reagent before reduction to form the phosphine (**Scheme 5.9**)

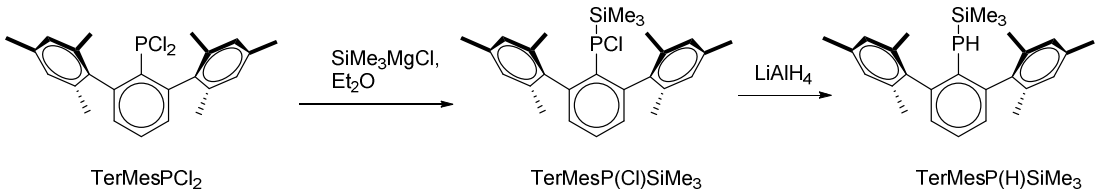

$TerMesPCl_2$ $TerMesP(Cl)SiMe_3$ $TerMesP(H)SiMe_3$

Scheme 5.9: Alternate synthetic route to $Ter^{Mes}P(H)SiMe_3$

Unfortunately this route did not prove successful, as shown by the regeneration of the $Ter^{Mes}PH_2$ starting material after workup.

5.5 Reactions with uranium (III) salts

Given the results presented in *5.3.1*, in particular the reductive elimination pathway towards the formation of **5.1** it seemed prudent to remove this pathway from the reaction mixture by reducing the propensity of the uranium centre to undergo reductive pathways by changing to uranium (III) salts from uranium (IV) salts. The reduction in reductive pathways propensity is due to the U(III)/U(II) redox couple being a prohibitive -2.9 V[34] especially when compared to the U(IV)/U(III) redox couple of a more reasonable, in terms of allowing redox reactions to occur, -0.6 V. [34]

5.5.1 Reaction of $Ter^{Mes}PHK$ with UI_3

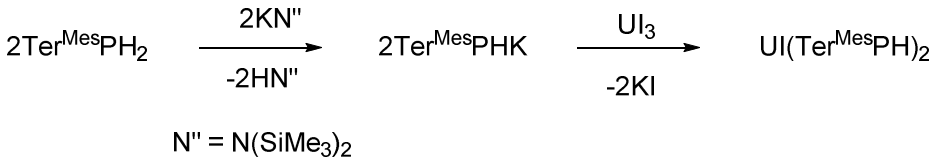

Scheme 5.10: Attempted synthesis of $UI(Ter^{Mes}PH)_2$

Reaction of two equivalents of *in situ* generated $KPHTer^{Mes}$ with a THF solution of UI_3 in perdeteuterated benzene in a J-Youngs' valve equipped NMR tube results in the formation of multiple products by NMR spectroscopy (**Scheme 5.10**). The ^{1}H NMR spectrum of this reaction shows twenty paramagnetic resonances. The ^{31}P NMR spectrum shows two diamagnetic resonances; a triplet at -147.3 ppm, assigned to the starting phosphine, $Ter^{Mes}PH_2$ and a doublet at -64.2 ppm with coupling of 221.6 Hz, which are likely to be due to degradation products of the aryl phosphine. The phosphorus resonances due to the paramagnetism of the uranium centre did not appear in the usual phosphorus NMR window as is to be expected. Attempts to isolate products of this reaction did not prove successful, so use of the bulkier $Ter^{Trip}PH_2$ ligand were made in an effort to examine the reactivity.

5.5.2 Reaction of $Ter^{Trip}PHK$ with UI_3

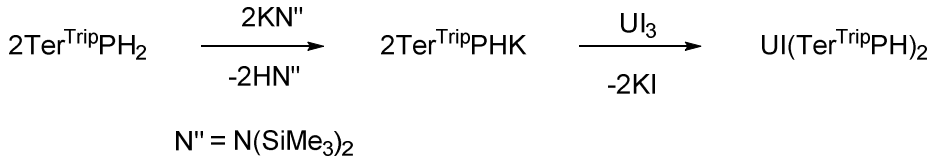

Scheme 5.11: Attempted synthesis of $UI(Ter^{Trip}PH)_2$

Reaction of two equivalents of *in situ* generated $KPHTer^{Trip}$ with a THF solution of UI_3 in perdeteuterated benzene in a J-Youngs' valve equipped NMR tube results in the formation of multiple products by NMR spectroscopy (**Scheme 5.11**). The ^{1}H NMR spectrum of this reaction shows eighteen paramagnetic resonances. The ^{31}P NMR spectrum shows no diamagnetic resonances, suggesting that the degradation products that were observed in *5.3.2.1* were not formed in this reaction. The phosphorus resonances due to the paramagnetism of the uranium centre did not appear in the usual phosphorus NMR window as is to be expected. Attempts to isolate products of this reaction did not prove successful, so use of a different uranium (III) salt in the form of $U(BH_4)_3(THF)_2$ was investigated.

5.5.3 Reaction of $Ter^{Trip}PHK$ with $U(BH_4)_3(THF)_2$

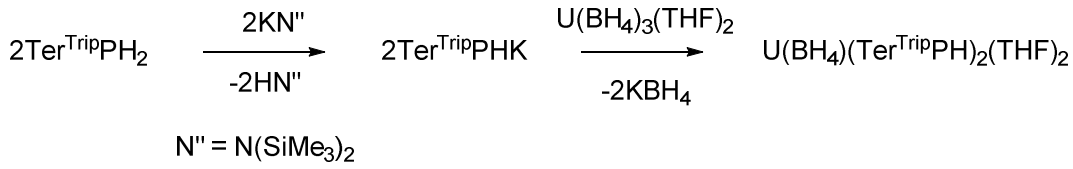

Scheme 5.12: Attempted synthesis of $U(BH_4)(Ter^{Trip}PH)_2(THF)_2$

Reaction of two equivalents of *in situ* generated $KPHTer^{Trip}$ with a THF solution of $U(BH_4)_3(THF)_2$ in perdeteuterated benzene in a J-Youngs' valve equipped NMR tube results in the formation of multiple products by NMR spectroscopy (**Scheme 5.12**). The ^{1}H NMR spectrum of this reaction shows twenty-eight paramagnetic resonances. The ^{31}P NMR spectrum shows one small resonance at -152.8 appearing as a doublet of doublets with coupling constants 219.8 and 22.6 Hz, in addition to a much larger triplet resonance for starting material (relative integration 1:9). Attempts to isolate and characterise the paramagnetic products of this reaction did not prove successful.

5.6 Reaction of thorium salts with terphenyl ligands

5.6.1 Rationale

A common precursor in the synthesis of $Ter^{Mes}OH$ (*Chapters 3 and 4*) and $Ter^{Mes}PH_2$ (*Chapter 5*) was the iodide analogue, $Ter^{Mes}I$. Given that this complex was being synthesised on a regular basis and the relative dearth of Th-aryl complexes within the literature, with only six crystallographic examples being reported (see **Figure 5.11**).[35-38]

As can be seen from **Figure 5.11**, all of the previously crystallographically characterised thorium aryl complexes are a result of metalation of the aryl position after ligation via another atom to the thorium centre, thus suggesting that the chelate effect is important in stabilising these interactions. This is suggestive that arylations by simple aryl groups are kinetically or thermodynamically unstable, but it may be the case that with substituted terphenyl ligands such as $Ter^{Mes}I$ stabilisation of non-cyclo-metalated thorium aryl complexes may be possible.

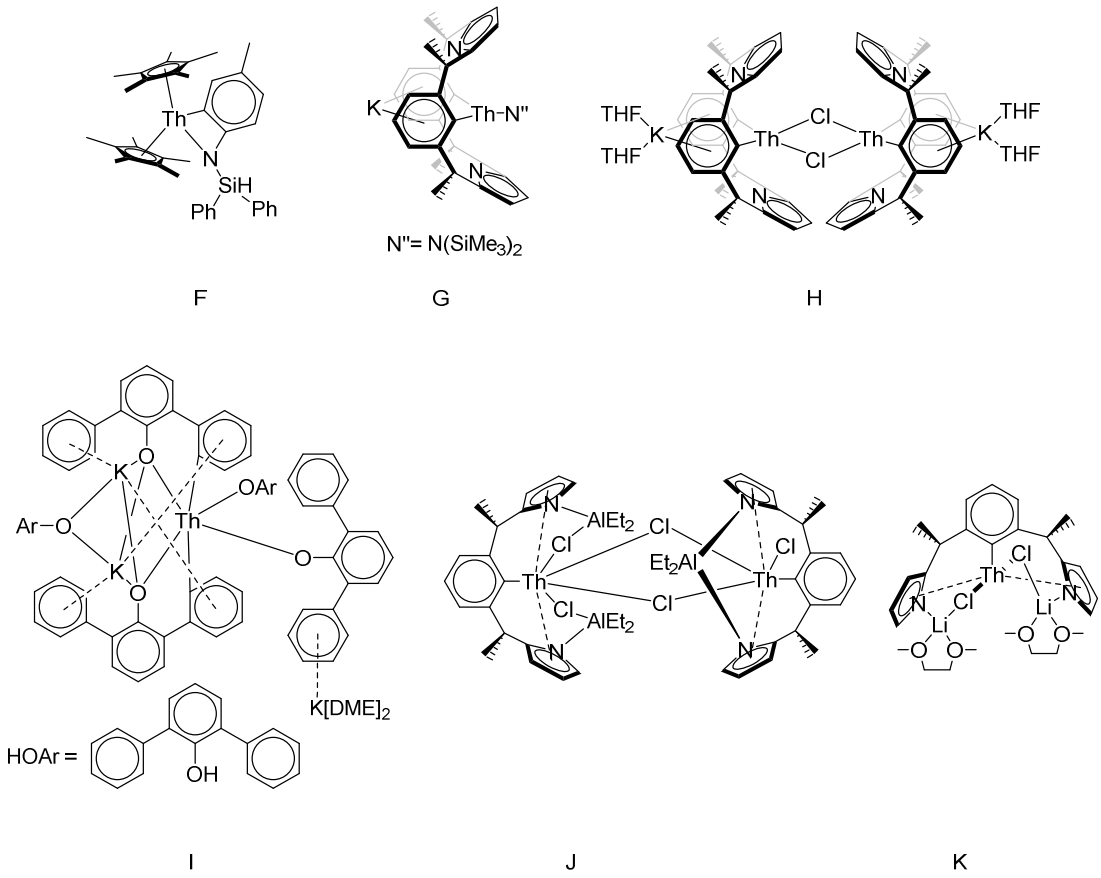

Figure 5.11: Literature examples of thorium aryl complexes[35-38]

5.6.2 Ligand synthesis

Ter^{Mes}I was synthesised according to literature preparations reported by Power *et al* causing the formation of an analytically pure white powder on a gram scale.[39]

5.6.3 Reaction of $ThCl_4(DME)_2$ with Ter^{Mes}Li

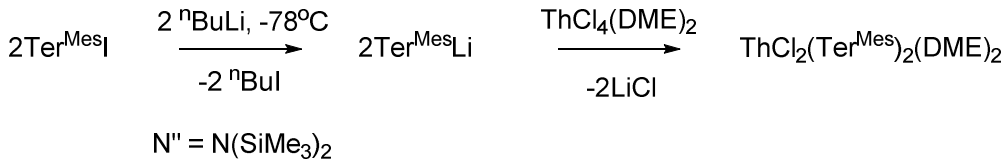

Scheme 5.13: Attempted synthesis of $ThCl_2(Ter^{Mes})_2(DME)_2$

Reaction of an orange-brown THF solution of *in situ* generated Ter^{Mes}Li, from reaction of Ter^{Mes}I and ^{n}BuLi, with $ThCl_4(DME)_2$ resulted in formation of a yellow solution (**Scheme 5.13**). After work up a micro-crystalline yellow powder was isolated. The ^{1}H NMR spectrum of the products of this reaction suggested the formation of multiple

products, and attempts to isolate these multiple products and further characterise them did not prove successful.

The decision was made to proceed with these attempted arylation reactions using the bulkier $Ter^{Trip}I$ precursor, which shall be detailed in *5.6.4.*

5.6.4 Reaction of $ThCl_4(DME)_2$ with $Ter^{Trip}Li$

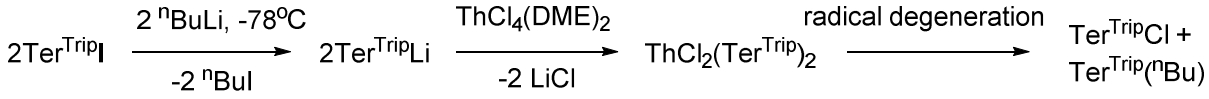

Scheme 5.14: Synthetic route to the formation of $Ter^{Trip}(^{n}Bu)$, **5.3** and $Ter^{Trip}Cl$, **5.4**

Reaction of a yellow THF solution of *in situ* generated $Ter^{Trip}Li$, from reaction of $Ter^{Trip}I$ and $^{n}BuLi$, with $ThCl_4(DME)_2$ resulted in formation of a yellow suspension(**Scheme 5.14**). After work up two separate crystalline products were isolated from a toluene extraction and X-ray quality crystals were grown and were determined to be $^{n}BuTer^{Trip}$, **5.3,** and $ClTer^{Trip}$, **5.4**. The solid state structures of **5.4** and **5.5** are displayed in **Figure 5.12** and **5.13** respectively. Selected bond angles and distances calculated from the solid state structure of **5.3** and **5.4** are shown in **Tables 5.2** and **5.3** respectively.

The products of this reaction are likely a result of radical degeneration of the aryl thorium complex upon allowing the reaction mixture to thaw to room temperature, suggesting thermal instability of this type of complex. Another explanation for the formation of **5.3** would be a reaction of excess $^{n}BuLi$ with the $Ter^{Mes}I$ starting material, in a dehalogenation side reaction. (See Equation 5.5)

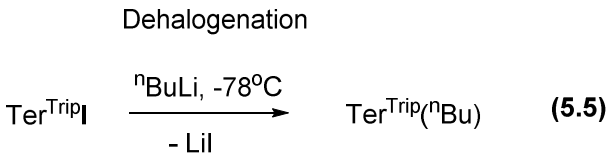

(5.5)

A common feature of the solid state structures of **5.3** and **5.4** is the position of the *ortho* isopropyl groups which are arranged in such a way that the smallest substituent, H, adopts the position of most steric interaction with the central phenyl ring, in order to reduce steric clashes. The formation of these radical degradation products led to the halting of this avenue of research.

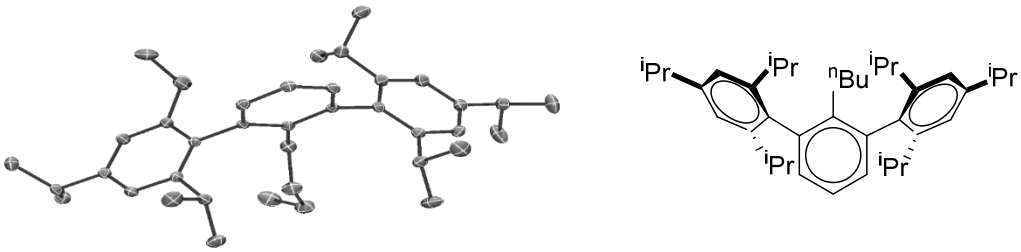

Figure 5.12: Displacement ellipsoid drawing of the solid state molecular structure of **5.3,** ^{n}BuTer^{Trip}, with hydrogen atoms omitted for clarity.

Table **5.2**: Selected X-ray crystallographic data for **5.3**

Bond	Bond distance (Å) / angle (°)
C1-C2, C2-C3, C3-C4, C4-C5	1.515(3), 1.519(2), 1.535(2), 1.522(2)
C1-C2-C3, C2-C3-C4, C3-C4-C5, C4-C5-C6	114.17(15), 113.47(13), 113.22(12), 120.01(12)

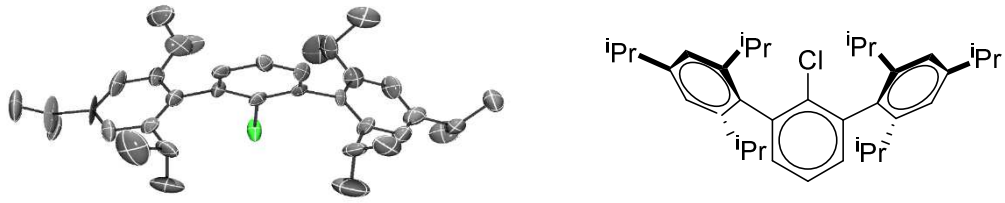

Figure 5.13: Displacement ellipsoid drawing of the solid state molecular structure of **5.4,** ClTer^{Trip}, with hydrogen atoms omitted for clarity.

Table **5.3**: Selected X-ray crystallographic data for **5.4**

Bond	Bond distance (Å) / angle (°)
Cl1-C1	1.84(3)
Cl1-C1-C2	121.13(6)

5.6 Conclusions and Summary

This chapter has seen investigations into the chemistry of the phosphorus ligating analogue of the ligand that was investigated in *Chapters three* and *four*. A common observation is that the attempted synthesis of phosphorus-ligated analogues has proven to be less facile than that observed for the oxygen ligated analogues. Characterisation of complexes in this chapter was aided by the NMR active and 100% naturally abundant ^{31}P nuclei, however despite this complete characterisation of the complexes that were attempted to be synthesised in this chapter has proved troublesome. Some success was seen in the formation of **5.1**, which is proposed to form after ligation to the uranium centre is followed by a reductive elimination pathway. The formation of **5.3** and **5.4** from an attempted arylation reaction suggests that the formation of thorium aryl complexes is hindered by thermal instability of these complexes.

5.7 References

1. M. R. Duttera, V. W. Day and T. J. Marks, *J. Am. Chem. Soc.*, 1984, 106, 2907-2912.
2. A. Zalkin, J. G. Brennan and R. A. Andersen, *Acta Crystallogr., Sect. C: Cryst. Struct. Commun.*, 1987, C43, 421-423.
3. B. S. Newell, T. C. Schwaab and M. P. Shores, *Inorg. Chem.*, 2011, 50, 12108-12115.
4. J. Brennan, R. Shinomoto, A. Zalkin and N. Edelstein, *Inorg. Chem.*, 1984, 23, 4143-4146.
5. T. Cantat, B. L. Scott, D. E. Morris and J. L. Kiplinger, *Inorg. Chem.*, 2009, 48, 2114-2127.
6. B. M. Gardner, G. Balázs, M. Scheer, F. Tuna, E. J. L. McInnes, J. McMaster, W. Lewis, A. J. Blake and S. T. Liddle, *Angew. Chem., Int. Ed. Engl.*, 2014, 53, 4484-4488.
7. P. J. Hay, R. R. Ryan, K. V. Salazar, D. A. Wrobleski and A. P. Sattelberger, *J. Am. Chem. Soc.*, 1986, 108, 313-315.
8. S. W. Hall, J. C. Huffman, M. M. Miller, L. R. Avens, C. J. Burns, A. P. Sattelberger, D. S. J. Arney and A. F. England, *Organometallics*, 1993, 12, 752-758.
9. D. A. Wrobleski, R. R. Ryan, H. J. Wasserman, K. V. Salazar, R. T. Paine and D. C. Moody, *Organometallics*, 1986, 5, 90-94.
10. N. Tsoureas, A. F. R. Kilpatrick, O. T. Summerscales, J. F. Nixon, F. G. N. Cloke and P. B. Hitchcock, *Eur. J. Inorg. Chem.*, 2013, 2013, 4085-4089.
11. A. S. P. Frey, F. G. N. Cloke, P. B. Hitchcock and J. C. Green, *New J. Chem.*, 2011, 35, 2022-2026.
12. O. J. Scherer, B. Werner, G. Heckmann and G. Wolmershäuser, *Angew. Chem., Int. Ed. Engl.*, 1991, 30, 553-555.
13. J. W. Dube, Z. D. Brown, C. A. Caputo, P. P. Power and P. J. Ragogna, *Chem. Commun.*, 2014, 50, 1944-1946.
14. M. Driess, K. Merz and C. Monse, *Chem. Commun.*, 2003, 2608-2609.
15. S. Yao, M. Brym, K. Merz and M. Driess, *Organometallics*, 2008, 27, 3601-3607.
16. M. Driess, C. Monsé and K. Merz, *Z. Anorg. Allg. Chem.*, 2001, 627, 1225-1230.

17. G. Becker, B. Eschbach, O. Mundt, M. Reti, E. Niecke, K. Issberner, M. Nieger, V. Thelen, H. Nöth, R. Waldhör and M. Schmidt, *Z. Anorg. Allg. Chem.*, 1998, 624, 469-482.
18. A. J. Deeming, S. Doherty, J. E. Marshall, J. L. Powell and A. M. Senior, *Journal of the Chemical Society, Dalton Transactions*, 1993, 1093-1100.
19. J. A. Dean and N. A. Lange, *Lange's handbook of chemistry*, McGraw-Hill, 1992.
20. C. A. Brown, *J. Org. Chem*, 1974, 39, 3913-3918.
21. F. G. Bordwell, *Acc. Chem. Res.*, 1988, 21, 456-463.
22. R. A. Barlett, H. V. R. Dias, K. M. Flynn, H. Hope, B. D. Murray, M. M. Olmstead and P. P. Power, *J. Am. Chem. Soc.*, 1987, 109, 5693-5698.
23. M. P. Duffy, L. Y. Ting, L. Nicholls, Y. Li, R. Ganguly and F. Mathey, *Organometallics*, 2012, 31, 2936-2939.
24. P. G. Jones, H. W. Roesky, H. Grutzmacher and G. M. Sheldrick, *Z. Naturforsch.* , 1985, 40b, 590-593.
25. G. Huttner, H. D. Muller, V. Benjenke and O. Orama, *Z. Naturforsch.*, 1976, 31b, 1166-1169.
26. S. Kurz, H. Oesen, J. Sieler and E. Hey-hawkins, *Phosphorus, Sulfur, and Silicon and the Related Elements*, 1996, 117, 189-196.
27. R. C. Smith, S. Shah and J. D. Protasiewicz, *J. Organomet. Chem.*, 2002, 646, 255-261.
28. S. Shah, M. C. Simpson, R. C. Smith and J. D. Protasiewicz, *J. Am. Chem. Soc.*, 2001, 123, 6925-6926.
29. B. Twamley, C. D. Sofield, M. M. Olmstead and P. P. Power, *J. Am. Chem. Soc.*, 1999, 121, 3357-3367.
30. Rhett C. Smith, T. Ren and John D. Protasiewicz, *Eur. J. Inorg. Chem.*, 2002, 2002, 2779-2783.
31. J. D. Protasiewicz, M. P. Washington, V. B. Gudimetla, J. L. Payton and M. Cather Simpson, *Inorg. Chim. Acta*, 2010, 364, 39-45.
32. E. Urnezius and J. D. Protasiewicz, *Main Group Chem.*, 1996, 1, 369-372.
33. H. Gunther, *Angew. Chem., Int. Ed.*, 1972, 11, 861-874.
34. S. G. Bratsch and J. J. Lagowski, *J. Phys. Chem.*, 1986, 90, 307-312.
35. I. Korobkov, B. Vidjayacoumar, S. I. Gorelsky, P. Billone and S. Gambarotta, *Organometallics*, 2010, 29, 692-702.
36. I. Korobkov, A. Arunachalampillai and S. Gambarotta, *Organometallics*, 2004, 23, 6248-6252.
37. P. L. Arnold, J. H. Farnaby, R. C. White, N. Kaltsoyannis, M. G. Gardiner and J. B. Love, *Chem. Sci.*, 2014, 5, 756-765.
38. W. Ren, E. Zhou, B. Fang, G. Zi, D.-C. Fang and M. D. Walter, *Chem. Sci.*, 2014, 5, 3165-3172.
39. B. Schiemenz and P. P. Power, *Organometallics*, 1996, 15, 958-964.

Chapter 6: Experimental

6.1 General Experimental

All manipulations were carried out using standard Schlenk line or glovebox techniques under an atmosphere of dinitrogen unless otherwise stated. DME was distilled from sodium under dinitrogen prior to use. Hexane, THF, diethyl ether and toluene were degassed by sparging with dinitrogen and dried by passing through a column of activated sieves in Vacuum Atmospheres solvent towers. Solvents were stored over activated 4 Å molecular sieves. Deuterated solvents (d_8-toluene, d_5-pyridine and C_6D_6) were boiled over potassium, vacuum-transferred and freeze-pump-thaw degassed three times prior to use.

^{1}H NMR, and ^{13}C{^{1}H} NMR spectra were recorded on a Bruker PRO500 spectrometer operating at 499.90 and 125.76 MHz respectively and were referenced to external $SiMe_4$. ^{11}B and ^{11}B{^{1}H} NMR spectra were recorded at 298 K on a Bruker PRO500 at 160.49 MHz and were referenced to external $BF_3.OEt_2$. ^{31}P and ^{31}P{^{1}H} NMR spectra were recorded at 298K on a Bruker PRO500 at 202 MHz and were referenced to external 85% phosphoric acid solution in D_2O. ^{29}Si INEPT NMR spectra were recorded at 298K on a PRO500 at 99.325 MHz and were referenced to a dilute solution of tetramethylsilane in $CDCl_3$. Chemical shifts are reported in parts per million and referenced to residual proton resonances calibrated against external TMS (δ = 0 ppm). All spectra were recorded at 298 K unless otherwise stated.

X-ray crystallographic data were collected at 170 K on an Oxford Diffraction Excalibur diffractometer using graphite monochromated Mo-Kα radiation equipped with an Eos CCD detector or at 100 K on an Oxford Diffraction Supernova diffractometer using mirror monochromated Cu-Kα radiation (λ = 1.5418 Å) and an Atlas CCD detector. Structures were solved using either SHEL-XS-97 direct methods,[1] SHEL-XS-97 Patterson methods,[1] or the SUPERFLIP charge-flipping program[2] and refined using a full-matrix least square refinement on $|F|^2$ using SHELXL-97.[1] All programs were used within the WinGx suite.[3] All non-hydrogen atoms refined with anisotropic displacement parameters and H-parameters were constrained to parent atoms and refined using a riding model unless otherwise stated.

Elemental analyses were carried out by Mr. Stephen Boyer, London Metropolitan University, Analytische Laboratorien Germany and Medac Ltd UK. Infrared spectra were recorded on a Jasco 410 spectrophotometer, w = weak, m = medium, s = strong intensity on in a Nujol mull on BaF_2 or NaCl plates. BaF_2 plates do not allow transmission below 1000 cm^{-1}.

$HOTer^{Mes}$ was synthesised according to literature procedures. [4-7] $Ca(BH_4)_2THF_2$ was purchased from Sigma Aldrich and used as received. $UI_4(dioxane)_2$,[8] $U(BH_4)_3(THF)_2$[9] and UCl_4[10] were prepared according to literature procedures. Potassium hydride was purchased from Sigma Aldrich in mineral oil and was washed with hexane and vacuum dried with use of a filter stick and Schlenk techniques prior to use. $KN(SiMe_3)_2$,[11] was synthesised according to literature procedures. KC_8 was prepared by addition of potassium to eight molar equivalents of ground graphite at 100 °C.[12] All other reagents were purchased and used without further purification.

6.1.1 Synthesis of 6.1.1 $Ter^{Mes}OH$:

6.1.1.1 Conversion of 2,6 dibromoaniline to 2,6 dibromoiodobenzene

2,6 dibromoaniline (70g, 0.279 mol) was stirred vigorously with hydrochloric acid (200mL) to form a white suspension. The suspension was cooled to 0-5°C and kept at this temperature whilst adding a solution of sodium nitrite (24.0g, 0.348 mol) in water (200 mL) dropwise, when a brown gas was observed to be evolved the rate of addition was reduced. The resultant orange yellow suspension was stirred for 30 minutes, after which time aqueous KI (200g, 1.2 mol, 200 mL) was added and stirred vigorously for 1 hour, with substantial effervescence observed and production of a black-brown material. CH_2Cl_2 (200mL) and 1M sodium sulphite aqueous (100mL) were added successively, and more effervescence observed. The aqueous layer was separated and washed with CH_2Cl_2 (3 X 200 mL), the organic layers combined and washed with 10% aq NaOH solution (100mL) and water (100mL) and the solvent was removed on rotary evaporator to give an orange powder (96.215g, 0.266 mol) in a 95.3 % yield.

^{1}H NMR (400 MHz, C_6D_6) δ (ppm) 6.94 (d, *J* = 8.0 Hz, 2H, *meta* Ar), 6.14 (t, *J* = 8.0 Hz, 1H, *para* Ar).

6.1.1.2 2,6 diisopropylaniline to 2,6 diisopropylbenzene

Following a literature preparation[13] gave a mixture of starting material and 2,6 diisopropylbenzene.

^{1}H NMR (400 MHz, C_6D_6) δ (ppm) 7.29 (s, 5H, Ar), 7.25 (d, *J* = 5.7 Hz, 6H, Ar), 7.05 (dd, *J* = 8.3, 6.8 Hz, 4H, Ar), 6.96 (d, *J* = 7.9 Hz, 9H, Ar), 3.94 (dt, *J* = 13.3, 6.7 Hz, 5H, Isopropyl H), 3.59 (dt, *J* = 13.7, 6.8 Hz, 8H, Isopropyl H), 3.44 – 3.33 (m, 3H), 3.23 (q, *J* = 7.0 Hz, 7H), 2.79 – 2.65 (m, 4H), 1.31 (d, *J* = 6.6 Hz, 3H, Isopropyl methyl groups), 1.16 (s, 13H, Isopropyl methyl groups), 1.14 (d, *J* = 6.8 Hz, 64H, Isopropyl methyl groups), 1.09 (d, *J* = 7.0 Hz, 10H, Isopropyl methyl groups), 1.07 (s, 4H), 0.96 (d, *J* = 6.9 Hz, 39H, Isopropyl methyl groups), 0.30 (s, 3H).4.3

6.1.1.3 2,6 dimesityl terphenyl iodide

Following a literature preparation[6] 2, 6 dimesityl terphenyl iodide was synthesised as a colourless powder (8.283g, 0.019 mol, 36.4 % yield). There was one small modification to the literature preparation, gentle heating (50°C) of a THF suspension of magnesium turnings with the addition of a couple of drops of iodoethane occurred until a milky suspension had formed.

^{1}H NMR (400 MHz, C_6D_6) δ (ppm) 7.09 (t, *J* = 7.5 Hz, 1H, *para* Ar, central phenyl ring), 6.89 (s, 4H, *meta* Ar, mesityl rings), 6.86 (d, *J* = 7.5 Hz, 2H, *meta* Ar, central phenyl ring), 2.21 (s, 6H, *para* mesityl methyl), 2.08 (s, 12H, *ortho* mesityl methyl).

6.1.1.4 2,6 ((tri 2,4,6 isopropyl)phenyl) terphenyl iodide

With the same small modification to a literature preparation[6] as for *6.1.1.3* 2,6 ((tri 2,4,6 isopropyl)phenyl) terphenyl iodide was synthesised as a white powder (9.067 g, 0.0149 mol, 42.0 %).

^{1}H NMR (400 MHz, $CDCl_3$) δ (ppm) 7.39 (t, *J* = 7.5 Hz, 1H, *para* Ar, central phenyl ring), 7.14 (d, *J* = 7.5 Hz, 2H, *meta* Ar, central phenyl ring), 7.05 (s, 4H, *meta* Ar, tri-isopropyl phenyl rings), 2.95 (dt, *J* = 13.8, 6.9 Hz, 2H, Isopropyl H, *para*), 2.52 (hept, *J* = 6.8 Hz, 4H, Isopropyl H, *ortho*), 1.31 (d, *J* = 6.9 Hz, 12H, Isopropyl methyl groups), 1.21 (d, *J* = 6.9 Hz, 12H, Isopropyl methyl groups), 1.08 (d, *J* = 6.8 Hz, 12H, Isopropyl methyl groups).

6.1.1.5 Synthesis of 2,6 ((di 2,6 isopropyl)phenyl) terphenyl iodide

With the same small modification to a literature preparation[6] as for *6.1.1.3* and *6.1.1.4* 2,6 ((di 2,6 isopropyl)phenyl) terphenyl iodide was synthesised as an off-white powder (3.87 g, 0.0073 mmol, 70%).

^{1}H NMR (400 MHz, $CDCl_3$) δ (ppm) 7.44 – 7.41 (m, broad, 1H, Ar), 7.40 (d, *J* = 7.7 Hz, 1H, Ar), 7.23 (d, *J* = 7.7 Hz, 3H, Ar), 7.15 (d, *J* = 7.5 Hz, 2H, Ar), 2.53 (dt, *J* = 13.7, 6.9 Hz, 3H, Isopropyl H), 1.23 (d, *J* = 6.9 Hz, 9H, Isopropyl methyl groups), 1.09 (d, *J* = 6.8 Hz, 8H, Isopropyl methyl groups).

6.1.1.6 Conversion of dimesityl terphenyl iodide to mesityl terphenol

Following a minor modification of a literature preparation[7] in which the product was recrystallized from a diethyl ether solution via slow evaporation of solvent to give yellowish plates of 2,6 dimesityl terphenol (0.971 g, 2.94 mmol, 45%).

^{1}H NMR (500 MHz, C_6D_6) δ (ppm) 6.95 (d, *J* = 7.5 Hz, 2H, *meta,* Ar, central phenyl ring), 6.84 (s, 4H, *meta* C-H, mesityl rings, Ar), 6.66 (t, *J* = 7.5 Hz, 1H, *para,* Ar, central phenyl ring), 4.54 (s, 1H, ArO**H**), 2.16 (s, 6H, *para* mesityl methyl), 2.12 (s, 12H, *ortho* mesityl methyl).

^{13}C NMR (126 MHz, C_6D_6) δ (ppm) 137.28 (s), 137.16 (s), 133.90 (s), 133.79 (s), 129.95 (s), 129.10 (s), 128.96 (s), 128.87 (s), 128.68 (s), 128.51 (s), 128.36 (s), 128.03 (s), 127.73 (s), 123.38 (s), 121.06 (s), 21.16 (s), 20.50 (s).

6.1.1.7 Conversion of triisopropyl terphenyl iodide to triisopropyl terphenol

Following a literature preparation[4, 5] with a slight modification allowing a longer time for stirring to allow complete lithiation to occur in the first step, the triisopropyl derivative was synthesised giving an overall yield of 1.271 g, 2.55 mmol, 58.8%, of di [2,6 (2,4,6 triisopropylphenyl)] terphenol as off white needles.

^{1}H NMR (400 MHz, C_6D_6) δ (ppm) 7.23 (s, 4H, *meta* Ar, tri-isopropyl phenyl rings), 7.07 (d, *J* = 7.5 Hz, 2H, *meta* Ar, central phenyl ring), 6.92 – 6.87 (m, 1H, *meta* Ar, central phenyl ring), 4.58 (s, 1H, ArO**H**), 3.08 – 2.95 (m, 5H, Isopropyl H, *ortho*), 2.85 (dt, *J* = 13.7, 7.0 Hz, 2H, Isopropyl H, *para*), 1.28 (d, *J* = 6.9 Hz, 12H, Isopropyl methyl groups), 1.25 (d, *J* = 6.9 Hz, 11H, Isopropyl methyl groups), 1.22 (d, *J* = 6.9 Hz, 12H, Isopropyl methyl groups).

6.1.1.8 Conversion of Diiisopropyl terphenyl iodide to Diisopropyl terphenol

Following a literature preparation[4, 5] with a slight modification allowing a longer time for stirring to allow the lithiation to occur in the first step, the diisopropyl derivative was synthesised giving an overall yield of 0.474 g, 1.14 mmol, 46.3 %, of di [2,6 (2,6. diisopropylphenyl)] terphenol as greenish plates

^{1}H NMR (400 MHz, $CDCl_3$) δ (ppm) 7.45 (t, *J* = 7.6 Hz, 18H, Ar), 7.37 – 7.31 (m, 32H, Ar), 7.21 (s, 33H, Ar), 7.19 (s, 23H, Ar), 7.18 (d, *J* = 1.6 Hz, 15H, Ar), 7.16 (d, *J* = 1.6 Hz, 13H, Ar), 7.08 (d, *J* = 7.6 Hz, 22H, Ar), 4.48 (s, 1H, ArO**H**), 2.80 – 2.67 (m, 64H, Isopropyl H), 1.31 – 1.27 (m, 114H, Isopropyl methyl groups), 1.14 (d, *J* = 6.9 Hz, 183H, Isopropyl methyl groups), 1.06 (d, *J* = 6.9 Hz, 159H, Isopropyl methyl groups).

6.1.2. $ThCl_4(DME)_2$

Following a literature preparation[14] $ThCl_4(DME)_2$ was synthesised as a colourless powder (6.7034 g, 0.0121 mol, 68.4 %).

^{1}H NMR (500 MHz, C_6D_6) δ 3.76 (s, 3H, **Me**OCH_2CH_2O**Me**), 3.34 (s, 2H, MeO**CH_2CH_2**OMe).

6.2 Synthetic procedure, reactivity and catalysis for reactions from Chapter Two

Syntheses:

6.2.1 N"$_2$Th(IV){κ²-N(SiMe$_3$)SiMe$_2$CH$_2$)

Following a literature preparation[15] $(N(SiMe_3))_2Th(IV)\{\kappa^2\text{-}N(SiMe_3)SiMe_2CH_2\}$ was synthesised as a white solid (0.588 g, 0.826 mmol, 59% yield).

^{1}H NMR (500 MHz, C_6D_6) δ (ppm) 0.93 (s, 2H, $(N(SiMe_3))_2Th(IV)\{\kappa^2\text{-}N(SiMe_3)SiMe_2$**$CH_2$**$\}$), 0.54 (s, 6H, $(N(SiMe_3))_2Th(IV)\{\kappa^2\text{-}N(SiMe_3)Si$**$Me_2$**$CH_2\}$) , 0.36 (s, 35H, $(N($**$SiMe_3$**$))_2Th(IV)\{\kappa^2\text{-}N(SiMe_3)SiMe_2CH_2\}$), 0.34 (s, 11H, $(N(SiMe_3))_2Th(IV)\{\kappa^2\text{-}N($**$SiMe_3$**$)SiMe_2CH_2\}$).

Catalyses:

6.2.2 General Procedure for Actinide-Mediated Alkyne Oligomerisation/ Cyclotrimerisation.

In a typical experiment, 0.5 mL of a ~30 mM solution of catalyst in benzene-d_6 was transferred to a J. Young Teflon-sealed NMR tube. Either 10 or 100 equivalents of

terminal alkyne was transferred to the same tube, which was then sealed, shaken briefly to ensure complete mixing, and heated to 75 °C for 72 h. The reaction mixtures were monitored by ^{1}H, ^{13}C, and two-dimensional NMR spectroscopy, and the data were compared to literature values for the organic products. Following this, samples were quenched by the addition of a few drops of methanol, filtered through a short Celite plug, and analysed by GC/MS or LC/MS methods, depending on the nature of the product mixtures. Product ratios were determined by either ^{1}H NMR spectroscopy or UV−vis spectroscopy interfaced to the LC/MS system.

*6.2.2.1 Oligomerisation of 1-hexyne by complex **2.1** (1% precatalyst loading)*

172 µL of 1-hexyne; 86% conversion; **2.4a** (92%); **2.8a** (7%) ^{1}H NMR (400 MHz,C_6D_6) δ 6.39 (s, 1H), 5.00 (d, J = 1.0 Hz, 1H), 4.93 (d, J = 1.0 Hz, 1H), 2.54 (t, J = 6.0 Hz, 2H), 2.46 (t, J = 9.0 Hz, 4H), 1.41 (m, 2H), 1.34 (m, 6H), 1.22 (m, 4H), 0.90 (t, J = 7.2 Hz, 9H).

*6.2.2.2 Oligomerisation of 1-hexyne by complex **2.1** (10% precatalyst loading)*

17 µL of 1-hexyne; 99% conversion; **2.4a** (93%); **2.8a** (7%) ^{1}H NMR (400 MHz,C_6D_6) δ 6.39 (s, 1H), 5.00 (d, J = 1.0 Hz, 1H), 4.93 (d, J = 1.0 Hz, 1H), 2.54 (t, J = 6.0 Hz, 2H), 2.46 (t, J = 9.0 Hz, 4H), 1.41 (m, 2H), 1.34 (m, 6H), 1.22 (m, 4H), 0.90 (t, J = 7.2 Hz, 9H).

*6.2.2.3 Oligomerisation of 1-hexyne by complex **2.2** (1% precatalyst loading)*

172 µL of 1-hexyne; 88% conversion; **2.4a** (96%); **2.8a** (2%) ^{1}H NMR (400 MHz,C_6D_6) δ 6.39 (s, 1H), 5.00 (d, J = 1.0 Hz, 1H), 4.93 (d, J = 1.0 Hz, 1H), 2.54 (t, J = 6.0 Hz, 2H), 2.46 (t, J = 9.0 Hz, 4H), 1.41 (m, 2H), 1.34 (m, 6H), 1.22 (m, 4H), 0.90 (t, J = 7.2 Hz, 9H); **2.10a** (1%); **2.11a** (1%).

*6.2.2.4 Oligomerisation of 1-hexyne by complex **2.2** (10% precatalyst loading)*

17 µL of 1-hexyne; 100% conversion; **2.10a** (41%); **2.11a** (37%); **2.12a** (22%) ^{1}H NMR (300 MHz, C_6D_6) δ 5.77 (ddt, 1H), 5.11−4.95 (m, 2H), 1.96 (q, J = 6.0 Hz, 2H), 1.41−1.27 (m, 4H), 0.88 (t, J = 6.0 Hz).

*6.2.2.5 Oligomerisation of 1-hexyne by complex **2.3** (1% precatalyst loading)*

172 µL of 1-hexyne; 88% conversion; **2.4a** (91%); **2.8a** (5%); ^{1}H NMR (300 MHz,C_6D_6) δ 6.39 (s, 1H), 5.00 (d, J = 1.0 Hz, 1H), 4.93 (d, J = 1.0 Hz, 1H), 2.54 (t, J = 6.0 Hz, 2H), 2.46 (t, J = 9.0 Hz, 4H), 1.41 (m, 2H), 1.34 (m, 6H), 1.22 (m, 4H), 0.90 (t, J = 7.2 Hz, 9H); **2.10a** (2%); **2.11a** (1%).

*6.2.2.6 Oligomerisation of 1-hexyne by complex **2.3** (10% precatalyst loading)*

17 μL of 1- hexyne; 100% conversion; **2.4a** (13%); **2.10a** (29%); **2.11a** (42%); **2.12a** (15%); ^{1}H NMR (300 MHz, C_6D_6) δ 5.77 (ddt, 1H), 5.11−4.95 (m, 2H), 1.96 (q, J = 6.0 Hz, 2H), 1.41−1.27 (m, 4H), 0.88 (t, J = 6.0 Hz).

*6.2.2.7 Oligomerisation of tert-butylacetylene by complex **2.1** (1% precatalyst loading)*

185 μL of tert-butylacetylene; 70% conversion; **2.4b** (41%); **2.5b** (43%); **2.9b** (16%), ^{1}H NMR (400 MHz, C_6D_6) δ 6.06 (d, J = 15 Hz, 1H), 5.63 (d, J = 15 Hz, 1H), 5.46 (s, 1H), 1.47 (s, 9H), 1.44 (s, 9H), 1.25 (s, 9H).

*6.2.2.8 Oligomerisation of tert-butylacetylene by complex **2.1** (10% precatalyst loading)*

19 μL of tert-butylacetylene; 97% conversion; **2.4b** (14%); **2.5b** (46%); **2.9b** (39%), ^{1}H NMR (400 MHz, C_6D_6) δ 6.06 (d, J = 15 Hz, 1H), 5.63 (d, J = 15 Hz, 1H), 5.46 (s, 1H), 1.47 (s, 9H), 1.44 (s, 9H), 1.25 (s, 9H).

*6.2.2.9 Oligomerisation of tert-butylacetylene by complex **2.2** (1% precatalyst loading)*

185 μL of tert-butylacetylene; 77% conversion; **2.4b** (60%); **2.5b** (22%); **2.8b** (9%); ^{1}H NMR (400 MHz, C_6D_6) δ 5.90 (d, J = 1.8 Hz, 1H), 5.86 (d, J = 1.8 Hz, 1H), 5.80 (s, 1H), 1.23 (s, 18H), 1.18 (s, 9H); **2.10b** (3%); **2.11b** (1%); **2.12b** (5%).

*6.2.2.10 Oligomerisation of tert-butylacetylene by complex **2.2** (10% precatalyst loading)*

19 μL of tert-butylacetylene; 100% conversion; **2.5b** (54%); **2.8b** (23%), ^{1}H NMR (400 MHz, C_6D_6) δ 5.90 (d, J = 1.8 Hz, 1H), 5.86 (d, J = 1.8 Hz, 1H), 5.80 (s, 1H), 1.23 (s, 18H), 1.18 (s, 9H); **2.10b** (6%); **2.11b** (2%); **2.12b** (16%).

*6.2.2.11 Oligomerisation of tert-butylacetylene by complex **2.3** (1% precatalyst loading)*

185 μL of tert-butylacetylene ; 87% conversion; **2.4b** (22%); **2.5b** (40%); **2.9b** (21%); ^{1}H NMR (400 MHz, C_6D_6) δ 6.06 (d, J = 15 Hz, 1H), 5.63 (d, J = 15 Hz, 1H), 5.46 (s, 1H), 1.47 (s, 9H), 1.44 (s, 9H), 1.25 (s, 9H); **2.10b** (8%); **2.11b** (1%); **2.12b** (7%).

*6.2.2.12 Oligomerisation of tert-butylacetylene by complex **2.3** (10% precatalyst loading)*

19 μL of tert-butylacetylene; 100% conversion; **2.5b** (55%); **2.11b** (22%); **2.12b** (23%).

*6.2.2.13 Oligomerisation of ethynyltrimethylsilane by complex **2.1** (1% precatalyst loading)*

214 μL of ethynyltrimethylsilane; 64% conversion; **2.4c** (22%); **2.5c** (43%); **2.7c** (35%).

*6.2.2.14 Oligomerisation of ethynyltrimethylsilane by complex **2.1** (10% precatalyst loading)*

21 μL of ethynyltrimethylsilane; 87% conversion; **2.4c** (27%); **2.5c** (32%); **2.7c** (41%),

*6.2.2.15 Oligomerisation of ethynyltrimethylsilane by complex **2.2** (1% precatalyst loading)*

214 μL of ethynyltrimethylsilane; 97% conversion; **2.4c** (32%); **2.5c** (8%); **2.6c** (38%); **2.7c** (19%); ^{1}H NMR (300 MHz, C_6D_6) δ 7.03(m, 1H), 6.90 (m, 1H), 6.84 (s, 1H), 0.10 (s, 27H); **2.10c** (2%); **2.11c** (2%).

*6.2.2.16 Oligomerisation of ethynyltrimethylsilane by complex **2.2** (10% precatalyst loading)*

21 μL of ethynyltrimethylsilane; 100% conversion; **2.4c** (34%); **2.5c** (25%); **2.10c** (23%); **2.11c** (19%).

*6.2.2.17 Oligomerisation of ethynyltrimethylsilane by complex **2.3** (1% precatalyst loading)*

214 μL of ethynyltrimethylsilane; 42% conversion; **2.4c** (50%); **2.5c** (11%); **2.10c** (22%); **2.11c** (17%).

*6.2.2.18 Oligomerisation of ethynyltrimethylsilane by complex **2.3** (10% precatalyst loading)*

21 μL of ethynyltrimethylsilane; 100% conversion; **2.10c** (58%); **2.11c** (42%).

*6.2.2.19 Oligomerisation of phenylacetylene by complex **2.1** (1% precatalyst loading)*

165 μL of phenyacetylene; 99% conversion; **2.4d** (91%); **2.5d** (9%).

*6.2.2.20 Oligomerisation of phenylacetylene by complex **2.1** (10% precatalyst loading)*

17 μL of phenyacetylene; 100% conversion; **2.4d** (77%); **2.5d** (15%); **2.12d** (8%).

*6.2.2.21 Oligomerisation of phenylacetylene by complex **2.2** (1% precatalyst loading)*

165 μL of phenyacetylene; 96% conversion; dimers (19%), MS (ESI$^+$): m/z 204.16 (M^+), 127.01 ($H_2CC(Ph)(C{\equiv}C)^+$); trimers (5%), MS (ESI$^+$): m/z 306.34 (M_+), 204.16 (H2CC(Ph)(CHCPh)$^+$); **2.10d** (35%), MS (ESI$^+$): m/z 306.30 (M^+), 229.23 ($Ph_2C_6H_3^+$); **2.11d** (40%), MS (ESI$^+$): m/z 306.31 (M^+), 229.20 ($Ph_2C_6H_3^+$).

*6.2.2.22 Oligomerisation of phenylacetylene by complex **2.2** (10% precatalyst loading)*

17 μL of phenyacetylene; 100% conversion; dimers (2%), MS (ESI$^+$) m/z 205.25 ([M + H]$^+$), 126.91 ($H_2CC(Ph)(C{\equiv}C)^+$); **2.10d** (48%), MS (ESI$^+$) m/z 306.30 (M^+), 229.25 ($Ph_2C_6H_3^+$); **2.11d** (49%), MS (ESI+)m/z 306.37 (M_+), 229.36 ($Ph_2C_6H_3^+$).

*6.2.2.23 Oligomerisation of phenylacetylene by complex **2.3** (1% precatalyst loading)*

165 μL of phenyacetylene; 92% conversion; dimers (5%), MS (ESI$^+$) m/z 205.16 ([M + H]$^+$), 126.94 ($H_2CC(Ph)(C{\equiv}C)^+$); trimers (7%), MS (ESI$^+$) m/z 306.37 (M^+), 205.10

($H_2CC(Ph)(CHCPh)^+$); **2.10d** (25%), MS (ESI+) m/z 306.34 (M^+), 229.18 ($Ph_2C_6H_3^+$); **2.11d** (63%), MS (ESI^+) m/z 306.33 (M^+), 229.12 ($Ph_2C_6H_3^+$).

*6.2.2.24 Oligomerisation of phenylacetylene by complex **2.3** (10% precatalyst loading)*

17 μL of phenyacetylene; 100% conversion; dimers (2%), MS (ESI^+) m/z 205.17 ([M + H]$^+$), 126.30 ($H_2CC(Ph)(C{\equiv}C)^+$); **2.10d** (48%), MS (ESI^+) m/z 306.11 (M^+), 229.23 ($Ph_2C_6H_3^+$); **2.11d** (49%), MS (ESI+)m/z 306.39 (M^+), 229.26 ($Ph_2C_6H_3^+$).

6.3 Synthetic procedure for reactions from Chapter 3

6.3.1 $ThCl_2(OTer^{Mes})_2(H_2O)_3$

To a Schlenk charged with a stirrer bar and $HOTer^{Mes}$ (0.966 g, 2.92 mmol), was added *circa* 40 mL of THF, forming a brown solution. To this solution was added a colourless THF solution of KN" (0.583 g, 2.92 mmol, 30 mL) causing the formation of a brown orange solution. After three hours, this solution was cannulated onto a rapidly stirred colourless THF solution of $ThCl_4(DME)_2$ (0.810 g, 1.46 mmol, 30 mL) causing the formation of a green-brown suspension in the brown solution. After 16 hours the brown solid was isolated by cannula filtration and dried under reduced pressure, causing the formation of a brown powder, which was washed twice with 30 mL portions of hexane and then further dried under reduced pressure giving a light brown powder characterised as $ThCl_2(OTer^{Mes})_2(H_2O)_3$, **3.1**, (0.404 g, 0.399 mmol, 27 % yield). Single crystals suitable for X-ray crystallography can be grown by storage of a concentrated toluene solution at -30°C for 3 days. Elemental analysis calculated: 56.75% C 5.56 % H found: 56.93% C 6.02% H

^{1}H NMR (500 MHz, C_6D_6) δ 7.25 (t, *J* = 3.1 Hz, 1H, *para* Ar, central phenyl ring), 6.87 (d, *J* = 3.1 Hz, 2H, *meta* Ar, central phenyl ring), 6.73 (s, 4H, *meta* Ar, mesityl rings), 2.21 (s, 6H, *para* mesityl methyl), 2.07 (s, 12H, *ortho* mesityl methyl), -0.41 (s, 3H, bound $\mathbf{H}_2O$).

6.3.2 Synthesis of $ThCl_2(OTer^{Mes})_2DME$

To a Schlenk charged with a stirrer bar and $HOTer^{Mes}$ (1.3955g, 4.22 mmol), was added *circa* 40 mL of dry DME, forming a brown solution. This solution was cannulated onto powdered KH in a Schlenk charged with a stirrer bar (169.3 mg, 4.22 mmol), causing vigorous effervescence and the formation of a pale brown suspension which was allowed to stir for 2 hours. This suspension was then cannulated onto a DME suspension of $ThCl_4(DME)_2$ causing the formation of a dark brown suspension which

was allowed to stir for 16 h. The red-brown solution was isolated by cannula filtration from a grey powder and volatiles were removed from the filtrate under reduced pressure. The resultant brown residue was extracted with 2 x 30 mL portions of toluene, and the combined extracts concentrated and cooled to -30°C, yielding colourless crystals of $ThCl_2(OTer^{Mes})_2DME$, **3.2**, (1.4683g, 1.39 mmol, 66% yield). Single crystals suitable for X-ray crystallography were grown from a saturated solution of toluene stored at -30°C.

Elemental analysis; calculated: C 61.23%, H 5.93%; found: C 61.38%, H 6.04%.

^{1}H NMR (500 MHz) δ 6.97 (t, *J* = 1.7 Hz, 1H, *para* Ar, central phenyl ring), 6.93 (d, *J* = 1.7 Hz, 2H, *meta* Ar, central phenyl ring), 6.87 (s, 4H, *meta* Ar, mesityl rings), 3.15 (s, 3H, $\boldsymbol{CH_3}OCH_2CH_2O\boldsymbol{CH_3}$), 2.27 (s, 12H, *ortho* mesityl methyl), 2.26 (s, 6H, *ortho* mesityl methyl), 2.02 (s, 2H, $CH_3O\boldsymbol{CH_2CH_2}OCH_3$).

^{13}C{^{1}H} NMR (500 MHz) δ (ppm) 161.42 (qt, C1), 137.36 (qt, C2, C6), 135.84 (qt, C7, C16), 131.60 (qt, C8, C12, C17, C21), 129.96 (s, C4), 129.33 (qt, C10, C19), 128.71 (s, C9, C11, C18, C20), 120.49 (s, C3, C5), 72.22 (s, $CH_3O\boldsymbol{CH_2CH_2}OCH_3$ [C26,C27]), 63.49 (s, $\boldsymbol{CH_3}OCH_2CH_2O\boldsymbol{CH_3}$ [C25,C29]), 21.54 (s, C13, C15, C22, C24), 21.30 (s, C14, C23).

6.3.3 Synthesis of $[(THF)K(OTer^{Mes})]_2$

To a Schlenk charged with a stirrer bar and **3.2** (65.0 mg, 0.06 mmol) was added THF (*circa* 20 mL) to form a brown solution. To this solution was added potassium graphite (10.0 mg, 0.07 mmol) whereupon immediate effervescence was observed and allowed to stir for 3 hours. A yellow solution formed immediately and a black precipitate was observed. A colour change to orange-yellow was observed after 5 minutes. The solution was filtered to give a yellow solution and a black precipitate and the THF was removed under reduced pressure to yield a green-yellow powder which was recrystallized from hexane as colourless needles of **3.3**, $[(THF)K(OTer^{Mes})]_2$ (12.3 mg, 0.01 mmol 22.6 %).

^{1}H NMR (500 MHz, C_6D_6) δ (ppm) 7.03 – 6.99 (m, 9H, Ar), 6.88 (d, *J* = 6.9 Hz, 3H, Ar), 6.73 (s, 14H, Ar), 3.65 – 3.47 (m, 10H, bound THF), 2.16 (s, 21H, *para* mesityl methyl), 2.12 (d, *J* = 10.1 Hz, 44H, *ortho* mesityl methyl), 1.51 – 1.32 (m, 13H, bound THF).

6.3.4 Synthesis of $[(THF)Li(OTer^{Mes})]_2$

To a Schlenk charged with a stirrer bar and **3.2** (54.9 mg, 0.05 mmol) was added a THF solution of $LiCH_2SiMe_3$ (15.0 mg, 0.16 mmol, *ca.* 20 mL) upon which the mixture changed

colour to yellow, and was allowed to stir for 16 h. The product mixture afforded was cannula filtered to give a yellow solution and a colourless precipitate. Removal of volatiles from the filtrate under reduced pressure afforded a yellow powder which was recrystallized from toluene to give $[(THF)Li(OTer^{Mes})]_2$, **3.4** as colourless blocks (10mg, 0.1 mmol, 23.4%).

^{1}H NMR (400 MHz, C_6D_6) δ (ppm) 7.03 (d, *J* = 7.4 Hz, 2H, Ar), 6.97 (d, *J* = 7.1 Hz, 4H, Ar), 6.88 (s, 4H, Ar), 6.83 (s, 6H, Ar), 6.76 (t, *J* = 7.2 Hz, 2H, Ar), 3.44 (s, 16H, bound THF), 2.22 (s, 11H, Alk), 2.20 (s, 14H, Alk), 2.07 (s, 6H, Alk), 2.05 (s, 18H, Alk), 1.41 (s, 18H, bound THF), 0.29 (s, 11H), 0.00 (s, 2H), -0.42 (s, 5H).

6.3.5 Synthesis of μ^3-(Ter^{Mes}O)μ^3-(CH_2SiMe_3)$_3$Li$_4$

To a Schlenk charged with a stirrer bar and **3.1**, (100 mg, 0.10 mmol) was added dry toluene (*circa* 20 mL). To this brown solution was added $LiCH_2SiMe_3$ (46.3 mg, 0.49 mmol) resulting in the formation of a pale yellow solution which was allowed to stir overnight during which time a fine white precipitate was observed. The suspension was filtered to give a yellow solution and concentrated, whereupon the solution became orange. Standing of this solution at -30°C ruled in the formation of crystals as colourless blocks which were suitable for single-crystal X-ray crystallography, and were determined to be μ^3-(Ter^{Mes}O)μ^3-(CH_2SiMe_3)$_3$Li$_4$, **3.5**, (22.0 mg, 0.04 mmol, 44% yield).

Elemental analysis; calculated 69.83% C, 9.45% H, found 69.84% C, 9.29% H

^{1}H NMR (400 MHz, C_6D_6) δ 7.25 (t, *J* = 7.6 Hz, 2H, Ar), 7.04 – 6.97 (m, 5H, Ar), 6.88 (d, *J* = 5.0 Hz, 8H, Ar), 6.76 (d, *J* = 8.8 Hz, 3H, Ar), 2.22 (s, 17H, *para* mesityl methyl), 2.08 (s, 25H, *ortho* mesityl methyl), 2.00 (s, 4H), 0.00 (s, 2H), -0.41 (s, 1H).

^{7}Li NMR (156 MHz, C_6D_6) δ 0.42 (s), -0.59 (s), -0.86 (s), -1.68 (s).

^{29}Si NMR (79 MHz, C_6D_6) δ -110.88 (s).

6.3.6 Synthesis of $LiAlH_2(OTer^{Mes})_2$

An ampoule was charged with **3.2** (150 mg, 0.14 mmol) and toluene (*circa* 20 mL). The resultant brown solution was treated with lithium aluminium hydride (16.8 mg, 0.439 mmol) in dry THF (*circa* 20 mL) and heated to reflux with stirring for 16 h. A yellowish suspension formed immediately and following stirring overnight a clear solution was observed with a metallic mirror around the inner surface of the ampoule. The solution

was isolated by cannula filtration and volatiles removed *in vacuo* to give a yellow orange powder which was extracted with 2 x 20 mL portions of hexane to give a colourless solution and a yellow residue. The volume of hexane was reduced by half and upon storage at a temperature of -30°C gave colourless X-ray quality single crystals of $LiAlH_2(OMes)_2$, **3.6**, (65.7 mg, 0.07 mmol 52.2%).

^{1}H NMR (400 MHz, C_6D_6) δ (ppm) 7.03 (d, *J* = 7.5 Hz, 4H, Ar), 6.94 (t, *J* = 9.1 Hz, 5H, Ar), 6.86 (d, *J* = 12.7 Hz, 16H, Ar), 6.82 (s, 10H, Ar), 3.61 (t, *J* = 5.2 Hz, 83H), 2.34 (s, 9H), 2.28 (s, 2H), 2.21 (d, *J* = 3.9 Hz, 34H), 2.16 (s, 16H *para* mesityl methyl), 2.06 (s, 11H), 2.03 (s, 30H *ortho* mesityl methyl), 1.41 (s, 69H), 0.28 (s, 49H), -0.42 (s, 12H, Al**H$_2$**).

6.3.7 Synthesis of MgCl(OTer^{Mes})(THF)$_2$

To a pale brown solution of **3.2** (20 mg, 0.019 mmol) in d_6-benzene (0.6 mL) in a Teflon-valved valve NMR tube was added EtMgBr (0.1 mL of a 1.0 M solution in THF , 0.1 mmol, 5 equiv) resulting in a yellow solution. Transfer of the solution to a vial, and allowing this solution to stand resulted in the formation of colourless crystals of $MgCl(OTer^{Mes})(THF)_2$, **3.7**, (8.0 mg, 0.015 mmol, 39% yield) suitable for single crystal X-ray crystallography.

^{1}H NMR (400 MHz, C_6D_6) δ 7.25 (t, *J* = 7.6 Hz, 1H, *para* Ar, central phenyl ring), 7.02 (d, *J* = 7.6 Hz, 2H, *meta* Ar, central phenyl ring), 6.85 (s, 4H, *meta* Ar, mesityl rings), 3.64 (s, 8H, bound THF), 2.33 (s, 12H, *ortho* mesityl methyl), 2.11 (s, 6H, *para* mesityl methyl), 1.48 (s, 8H, bound THF).

6.3.8 Synthesis of MgBr(OTer^{Mes})(THF)$_2$

To a Schlenk charged with a stirrer bar and **3.2** (0.075g, 0.07 mmol) was added *circa* 20 mL of dry toluene causing the formation of a brown solution. To this rapidly stirring solution was added bromo-magnesium acetylide (0.3 mL of a 0.5M solution in THF, 0.15 mmol) resulting in the initial formation of a yellow solution. After five minutes this solution had passed thorugh orange and was observed to be brown, and after 2 hours a fine light coloured suspension was observed. The suspension was stirred for 16 hours, after which time it was filtered and the solvent removed in *vacuo*. Extraction with hexane and subsequent crystallisation from a concentrated solution left to stand at a temperature of -30°C gave colourless crystals of X-ray quality of $MgBr(OTer^{Mes})(THF)_2$, **3.8**, (0.053g, 0.09 mmol, 63% yield).

^{1}H NMR (500 MHz, C_6D_6) δ 6.96 (d, *J* = 2.6 Hz, 2H, *meta* Ar, central phenyl ring), 6.94 (t, *J* = 2.6 Hz, 1H, *para* Ar, central phenyl ring), 6.85 (s, 4H, *meta* Ar, mesityl rings), 3.27 (s, 8H, bound THF), 2.38 (s, 12H, *ortho* mesityl methyl), 2.20 (s, 6H, *para* mesityl methyl), 1.19 (s, 8H, bound THF).

6.3.9 Synthesis of $Fe(OTer^{Mes})_2(py)_2$

To a Schlenk charged with a stirrer bar and $FeCl_2(py)_4$ (84 mg, 0.19 mmol) was added circa 30 mL of dry hexane, to form a yellow suspension. This suspension was cooled to -40°C, and $LiCH_2SiMe_3$ solution in hexanes (1.0 M, 0.40 mL, 0.40 mmol) was added with rapid stirring. This suspension was stirred for 2 hours, and it was observed that the suspension changed colour to a dark purple. This suspension was filtered through a diatomaceous earth column to give a red solution. This solution was cannulated onto a suspension of $Th(OTer^{Mes})_2Cl_2DME$ (200 mg, 0.19 mmol) in dry hexane with stirring to give a yellow suspension. The reaction mixture was stirred overnight, at which point was filter cannulated to give a yellow solution. The resultant yellow solution had its solvent removed *in vacuo*, and the yellow powder that resulted was vacuum dried to give **3**, as a yellow powder (32.8 mg, 0.04 mmol, 20 % yield) characterised by elemental analysis. Crystals suitable for x-ray diffraction can be grown from a saturated hexane solution at -30°C.

6.3.10 Synthesis of $Li_2(OTer^{Mes})_2THF$

To a Schlenk charged with a stirrer bar and $ThCl_4(DME)_2$ (400 mg, 0.72 mmol) was added *circa* 40 mL of toluene, causing the formation of a white suspension. To this suspension was added a 1.0M of $LiCH_2SiMe_3$ in pentane at -50 °C (3.6 mL, 3.6 mmol, 5 equivalents) causing the formation of a brown suspension. After stirring for four hours, whilst keeping the temperature steady at -50 °C, a solution of $Ter^{Mes}OH$ (716mg, 2.16 mmol, 3 equivalents) in THF was cannulated onto this suspension, causing the instantaneous formation of an orange suspension. Upon stirring overnight with thawing, it was observed that a yellow suspension had formed. This suspension was allowed to settle, filtered and the resultant yellow solution had its solvent removed *in vacuo*. The resultant yellow residue was extracted with toluene, giving a white powder and an orange solution. The orange solution was reduced in volume and after standing a saturated solution at -30 °C, single crystals of $Li_2(OTer^{Mes})_2THF$ (425 mg, 0.57 mmol, 79 % yield) suitable for X-ray crystallography were grown, further characterised by ^{1}H NMR spectroscopy.

^{1}H NMR (500 MHz, C_6D_6) δ 6.98 (d, *J* = 7.3 Hz, 3H, Ar), 6.79 (s, 4H, Ar), 3.18 (s, 8H, bound THF), 2.20 (s, 6H, *para* mesityl methyl), 2.02 (s, 12H, *ortho* mesityl methyl), 1.90 (s, 4H), 1.34 (s, 4H, bound THF).

6.3.11 Synthesis of [$MgTh_2\mu^2$-$Cl_2\mu^3$-$Cl(OTer^{Mes})_2(C_4H_7)_2\mu$-$\eta^3$:$\eta^3(C_4H_7)H$]

To a Schlenk charged with a stirrer bar and $Th(OTer^{Mes})_2Cl_2DME$ (500 mg, 0.475 mmol) was added *circa* 30 mL of dry toluene, to form an orange-brown solution. To this solution was added ClMg(Me-allyl) (1.9mL of a 0.5M solution, 0.951 mmol) with rapid stirring to form a yellow suspension with copious precipitate after 2 hours. The reaction mixture was allowed to stir overnight, at which point the solvent was removed *in vacuo*, resulting in a yellow residue. This residue was extracted with hexane to give a yellow solution and a white precipitate. The resultant yellow solution had its solvent removed *in vacuo*, and the yellow powder that resulted was vacuum dried to give **3.11**, [$MgTh_2\mu^2$-$Cl_2\mu^3$-$Cl(OTer^{Mes})_2(C_4H_7)_2\mu$-$\eta^3$:$\eta^3(C_4H_7)H$], as a yellow powder (192 mg, 0.122 mmol, 52% yield) characterised by NMR spectroscopy and elemental analysis. Crystals suitable for x-ray diffraction were grown from a saturated hexane solution at -30°C.

Elemental analysis; calculated: C 52.32%, H 5.49%, found: C 52.16%, H 5.38%

^{1}H NMR (500 MHz, C_6D_6) δ 7.10 (d, *J* = 6.0 Hz, 1H, Ar), 6.98 (d, *J* = 6.6 Hz, 2H, Ar), 6.87 (s, 3H, Ar), 6.80 (d, *J* = 8.2 Hz, 4H, Ar), 6.52 (s, 1H, Ar), 4.72 (s, 2H), 3.45 (s, 4H)(Bound THF), 2.22 (s, 4H, alk), 2.20 (s, 3H, alk), 2.17 (s, 4H, alk), 2.12 (s, 13H, *ortho* mesityl methyl), 2.07 (s, 5H, alk), 1.65 (s, 2H)(Th-hydrides) , 1.60 (s, 1H), 1.40 (s, 1H), 1.37 (s, 3H) (Bound THF) , 1.25 (s, 2H), 0.88 (t, *J* = 6.3 Hz, 1H), 0.59 (s, 1H), 0.27 (s, 2H).

IR spectroscopy (NaCl Plates) 2958, 2924, 2873, 2856, 2732, 2673, 1613, 1582, 1456, 1418, 1378, 1295, 1245, 1080, 1032, 870, 850, 801, 756, 663 cm^{-1}

6.3.12 Synthesis of ClMg(Meallyl)[16]

In an ampoule equipped with a stirrer bar was added magnesium chloride (1.052 g, 0.011 mol) and potassium metal (0.43 g, 0.011 mol). THF (*circa* 20 mL) was then added to the solids, forming a white suspension. This suspension was refluxed for 2 hours until a black suspension had formed. This suspension was cooled to –95 °C whereupon the colourless oil 1-chloro-2 methylprop-2-ene was syringed onto the reaction mixture (1g, 0.917 mL, 0.11 mol). This caused the formation of a colourless suspension which was stirred for 16 hours. This colourless suspension was filtered to give a colourless

solution. The solvent was removed in vacuo to give a white powder, ClMg(Me-allyl) (1.11 g, 0.0096 mol 88 % yield).

^{1}H NMR (500 MHz, C_6D_6) δ 3.61 (s, 8H, bound THF), 2.98 (s, 4H,**CH_2**CMe**CH_2**), 2.23(s, 3H, CH_2C**Me**CH_2), 1.41 (s, 8H, bound THF).[17]

6.3.13 Synthesis of $Mg(OTer^{Mes})_2(THF)_2$

To a Schlenk charged with a stirrer bar and $Th(OTer^{Mes})_2Cl_2DME$ (200 mg, 0.190 mmol) was added *circa* 30 mL of dry toluene, to form an orange-brown solution. To this solution was added a colourless solution of pure ClMg(Me-allyl) in THF with rapid stirring, causing the formation of a yellow suspension. This suspension was filtered overnight and then filtered to give a pale yellow solution. The solvent was removed *in vacuo* and the resultant yellow residue was extracted with hexane. Fractional crystallisation enabled the separation of $[MgTh_2\mu^2\text{-}Cl_2\mu^3\text{-}Cl(OTer^{Mes})_2(C_4H_7)_2\mu\text{-}\eta^3\text{:}\eta^3(C_4H_7)H]$, (145 mg, 0.093 mmol 49% yield) which crystallised first by standing the concentrated hexane solution at -30°C, followed by isolation of $Mg(OTer^{Mes})_2(THF)_2$ (28 mg, 0.038 mmol, 20 % yield) as colourless crystals after attempting to grow a second crop whilst standing the hexane solution at -30 °C.

Elemental analysis: calculated 81.49% C 8.25% H, found 82.22% C, 7.82% H

^{1}H NMR (500 MHz, C_6D_6) δ 7.04 (t, J = 6.0 Hz 1H, *para* Ar, central phenyl ring), 6.94, (d, J= 6.0 Hz, 2H, *meta* Ar, central phenyl ring), 6.82 (s, 4H *meta* Ar, mesityl rings), 3.39 (s, 4H) (bound THF), 2.19 (s, 6H, *para* mesityl methyl), 2.01 (s, 12H, *ortho* mesityl methyl), 1.45 (s, 4H) (bound THF).

6.3.14 Reaction of $[MgTh_2\mu^2\text{-}Cl_2\mu^3\text{-}Cl(OTer^{Mes})_2(C_4H_7)_2\mu\text{-}\eta^3\text{:}\eta^3(C_4H_7)H]$ with CO_2

A yellow solution of **3.11,** (9 mg, 0.006 mmol) in d_6-benzene (0.6 mL) in a Teflon-valved valve NMR tube was freeze-pump-thaw degassed 3 times prior to being placed under a 1 atm CO_2 atmosphere by use of a CO_2 cylinder connected to a Schlenk line with a t-piece. The introduction of the CO_2 atmosphere, after thawing of the solution, was observed to result in complete decolourisation of the solution. NMR experiments were run at room temperature and 323K.

^{1}H NMR (500 MHz, C_6D_6) δ 7.00 (dd, *J* = 7.5, 1.7 Hz, 3H, Ar), 6.96 (dd, *J* = 13.4, 7.0 Hz, 3H, Ar), 6.90 (dd, *J* = 11.2, 5.1 Hz, 3H, Ar), 6.87 (s, 2H, Ar), 6.83 (d, *J* = 13.7 Hz, 4H, Ar), 3.52

(s, 6H, bound THF), 2.26 (d, *J* = 5.3 Hz, 7H, alk), 2.23 – 2.19 (m, 6H, alk), 2.17 (d, *J* = 6.2 Hz, 6H, alk), 2.12 (s, 9H, alk), 2.07 (d, *J* = 3.4 Hz, 6H), 1.41 (d, *J* = 9.2 Hz, 9H, bound THF).

^{1}H NMR (323K) (500 MHz, C_6D_6) δ 7.02 – 6.99 (m, 11H, Ar), 6.97 (d, *J* = 2.0 Hz, 5H, Ar), 6.95 (s, 6H, Ar), 6.94 – 6.91 (m, 12H, Ar), 6.88 (d, *J* = 8.0 Hz, 17H, Ar), 6.85 (s, 16H, Ar), 4.78 (d, *J* = 55.5 Hz, 37H), 4.50 (s, 15H, H_2), 3.52 (s, 58H, bound THF), 2.35 (ddd, *J* = 31.4, 28.2, 17.3 Hz, 100H, alk), 2.22 (s, 40H, alk), 2.17 (s, 35H, alk), 2.11 (s, 52H, alk), 2.07 (s, 17H, alk), 2.06 (s, 16H, alk), 2.00 (d, *J* = 14.1 Hz, 25H, alk), 1.60 (s, 10H), 1.42 (d, *J* = 22.2 Hz, 56H, bound THF), 1.24 (s, 21H), 0.88 (t, *J* = 6.9 Hz, 19H).

6.3.15 Reaction of [MgTh$_2$$\mu^2$-Cl$_2$$\mu^3$-Cl(OTer^{Mes})$_2$(C$_4H_7$)$_2$$\mu$-η^3:η^3(C$_4H_7$)H] with CO

A yellow solution of **3.11,** (29 mg, 0.019 mmol) in d_6-benzene (0.6 mL) in a Teflon-valved valve NMR tube was freeze-pump-thaw degassed 3 times prior to being placed under a 1 atm CO atmosphere by use of a CO cylinder connected to a Schlenk line with a t-piece. The introduction of the CO atmosphere, after thawing of the solution, was observed to result in a darkening of the solution to orange.

^{1}H NMR (500 MHz, C_6D_6) δ 7.01 (dd, *J* = 8.2, 3.9 Hz, 14H, Ar), 6.97 – 6.94 (m, 4H, Ar), 6.92 (dd, *J* = 8.5, 5.9 Hz, 5H, Ar), 6.88 (d, *J* = 6.5 Hz, 9H, Ar), 6.85 – 6.82 (m, 7H, Ar), 6.82 (s, 6H, Ar), 6.80 (s, 20H, Ar), 2.66 (ddd, *J* = 42.5, 35.7, 30.8 Hz, 31H, alk), 2.24 (s, 36H, alk), 2.21 (d, *J* = 3.3 Hz, 13H, alk), 2.18 (d, *J* = 6.0 Hz, 61H, alk), 2.15 (s, 8H, alk), 2.13 (d, *J* = 5.6 Hz, 11H, alk), 2.07 (d, *J* = 2.9 Hz, 17H, alk), 1.90 (s, 5H, alk), 1.57 (d, *J* = 25.6 Hz, 7H), 1.40 (s, 2H), 1.11 (s, 28H), 0.88 (dt, *J* = 11.0, 5.5 Hz, 6H), 0.28 (d, *J* = 15.5 Hz, 12H).

6.3.16 Reaction of [MgTh$_2$$\mu^2$-Cl$_2$$\mu^3$-Cl(OTer^{Mes})$_2$(C$_4H_7$)$_2$$\mu$-η^3:η^3(C$_4H_7$)H] with H$_2$

A yellow solution of **3.11,** (19 mg, 0.013 mmol) in d_8-toluene (0.6 mL) in a Teflon-valved valve NMR tube was freeze-pump-thaw degassed 3 times prior to being placed under a 1 atm H_2 atmosphere by use of a H_2 cylinder connected to a Schlenk line with a t-piece. The introduction of the H_2 atmosphere, after thawing of the solution, was observed to result in a decolourisation of the solution with some fine light coloured precipitate formed. NMR experiments were run at room temperature and 338 K.

^{1}H NMR (500 MHz, Tol) δ 7.24 (dd, *J* = 9.6, 5.6 Hz, 5H, Ar), 6.91 (dd, *J* = 9.3, 4.8 Hz, 21H, Ar), 6.82 (d, *J* = 9.3 Hz, 27H, Ar), 6.74 (ddd, *J* = 16.2, 10.5, 4.3 Hz, 40H, Ar), 6.60 (s, 14H, Ar), 4.82 (s, 4H), 4.71 (dt, *J* = 2.1, 1.0 Hz, 6H), 4.50 (s, 5H, H_2), 4.43 (s, 3H), 3.51 (s, 50H), 2.31 (d, *J* = 2.7 Hz, 8H, alk, bound THF), 2.27 (s, 12H, alk), 2.25 (s, 8H, alk), 2.22 (t, *J* = 5.1 Hz, 58H, alk), 2.17 (t, *J* = 6.3 Hz, 44H, alk), 2.12 (dd, *J* = 13.1, 8.8 Hz, 50H, alk), 2.10 –

2.06 (m, 73H, alk), 2.04 (t, *J* = 4.1 Hz, 18H, alk), 2.02 (s, 9H, alk), 2.01 (s, 24H, alk), 1.97 (d, *J* = 7.1 Hz, 22H, alk), 1.90 (s, 9H, alk), 1.70 (d, *J* = 13.7 Hz, 10H, alk), 1.59 (t, *J* = 1.1 Hz, 16H, bound THF), 1.55 (s, 4H), 1.44 (s, 5H), 0.31 (s, 3H), 0.26 (s, 19H).

^{1}H NMR (338K) (500 MHz, Tol) δ 6.90 (dd, *J* = 12.2, 4.4 Hz, 56H, Ar), 6.83 (dt, *J* = 14.4, 7.3 Hz, 71H, Ar), 6.78 – 6.70 (m, 87H, Ar), 4.82 (s, 7H, Ar), 4.71 (d, *J* = 8.3 Hz, 14H), 4.50 (s, 10H), 4.40 (s, 3H, H_2), 3.45 (s, 63H), 2.28 (t, *J* = 14.0 Hz, 84H, alk), 2.21 (d, *J* = 2.5 Hz, 121H, alk), 2.18 (d, *J* = 5.2 Hz, 51H, alk), 2.16 (d, *J* = 2.1 Hz, 40H, alk), 2.14 (d, *J* = 7.0 Hz, 35H, alk), 2.10 (dt, *J* = 4.5, 2.4 Hz, 311H, alk), 2.04 (d, *J* = 5.2 Hz, 48H, alk), 2.00 (t, *J* = 4.0 Hz, 72H, alk), 1.98 (s, 51H, alk), 1.91 (d, *J* = 10.5 Hz, 22H, alk), 1.60 (s, 38H), 1.46 (t, *J* = 10.4 Hz, 54H), 0.99 – 0.81 (m, 19H), 0.33 (s, 5H), 0.25 (d, *J* = 10.4 Hz, 47H).

6.3.17 Reaction of [MgTh$_2$$\mu^2$-Cl$_2$$\mu^3$-Cl(OTer^{Mes})$_2$(C$_4H_7$)$_2$$\mu$-η^3:η^3(C$_4H_7$)H] with D$_2$

A yellow solution of **3.11,** (9 mg, 0.06 mmol) in d_8-toluene (0.6 mL) in a Teflon-valved valve NMR tube was freeze-pump-thaw degassed 3 times prior to being placed under a 1 atm D_2 atmosphere by use of a D_2 cylinder connected to a schlenk line with a t-piece. The introduction of the D_2 atmosphere, after thawing of the solution, was observed to result in a decolourisation of the solution with some fine light coloured precipitate formed.

^{1}H NMR (500 MHz, C_6D_6) δ 7.24 (t, *J* = 7.6 Hz, 11H, Ar), 7.00 (dd, *J* = 11.9, 4.3 Hz, 36H, Ar), 6.98 – 6.93 (m, 17H, Ar), 6.91 (dd, *J* = 8.5, 6.1 Hz, 18H, Ar), 6.87 (s, 26H, Ar), 6.85 – 6.80 (m, 26H, Ar), 6.77 (s, 31H, Ar), 4.74 (s, 29H), 4.53 (s, 22H, H_2), 3.54 (s, 118H, bound THF), 2.34 (dd, *J* = 26.9, 13.4 Hz, 46H, alk), 2.23 (s, 52H, alk), 2.21 (s, 42H, alk), 2.16 (d, *J* = 9.0 Hz, 88H, alk), 2.12 (s, 41H, alk), 2.07 (s, 85H, alk), 1.59 (s, 35H, bound THF), 1.38 – 1.12 (m, 79H), 0.87 (dd, *J* = 16.7, 9.5 Hz, 33H), 0.29 (s, 34H).

^{2}H NMR (77 MHz, C_6D_6) δ 4.46 (s, 1H, D_2).

6.3.18 Reaction of [MgTh$_2$$\mu^2$-Cl$_2$$\mu^3$-Cl(OTer^{Mes})$_2$(C$_4H_7$)$_2$$\mu$-η^3:η^3(C$_4H_7$)H] with C$_6D_6$

A yellow solution of **3.11,** (9 mg, 0.06 mmol) in d_6-benzene (0.6 mL) in a Teflon-valved valve NMR tube was heated overnight at 80°C. This resulted in no reaction being observed by NMR spectroscopy.

6.3.19 Reaction of [MgTh$_2$$\mu^2$-Cl$_2$$\mu^3$-Cl(OTer^{Mes})$_2$(C$_4H_7$)$_2$$\mu$-η^3:η^3(C$_4H_7$)H] with C$_7D_8$

A yellow solution of **3.11,** (9 mg, 0.06 mmol) in d_8-toluene (0.6 mL) in a Teflon-valved valve NMR tube was heated overnight at 110 °C. This resulted in no reaction being observed by NMR spectroscopy.

6.3.20 Reaction of [MgTh$_2$$\mu^2$-Cl$_2$$\mu^3$-Cl(OTer^{Mes})$_2$(C$_4H_7$)$_2$$\mu$-η^3:η^3(C$_4H_7$)H] with Et$_3$SiH

To a yellow solution of **3.11,** (10 mg, 0.006 mmol) in C_6D_6 (0.6 mL) in a Teflon-valved valve NMR tube was added Et_3SiH as a colourless oil (0.1 mL, 0.06 mmol, 10 equiv) resulting in no observable colour change.

^{1}H NMR (500 MHz, C_6D_6) δ 7.00 – 6.64 (m, 115H, Ar), 4.72 (dd, *J* = 2.2, 1.1 Hz, 3H), 4.02 (dt, *J* = 6.3, 3.2 Hz, 8H), 3.87 – 3.82 (m, 362H), 3.67 (dt, *J* = 6.3, 3.2 Hz, 11H, bound THF), 2.34 – 1.96 (m, 331H, alk), 1.61 (t, *J* = 1.1 Hz, 18H, Bound THF), 1.12 – 1.04 (m, 131H, Et_3Si analogues), 1.04 – 0.90 (m, 5990H), 0.89 – 0.77 (m, 80H), 0.72 – 0.62 (m, 47H), 0.63 – 0.47 (m, 3548H), 0.48 – 0.37 (m, 64H), 0.24 (s, 19H).

6.3.21 Reaction of [MgTh$_2$$\mu^2$-Cl$_2$$\mu^3$-Cl(OTer^{Mes})$_2$(C$_4H_7$)$_2$$\mu$-η^3:η^3(C$_4H_7$)H] with PhSiH$_3$

To a yellow solution of **3.11,** (8 mg, 0.005 mmol) in C_6D_6 (0.6 mL) in a Teflon-valved valve NMR tube was added Et_3SiH as a colourless oil (0.1 mL, 0.06 mmol, 10 equiv) resulting in no observable colour change.

^{1}H NMR (500 MHz, C_6D_6) δ 7.54 (dd, *J* = 6.7, 1.0 Hz, 34H, Ar), 7.45 – 7.42 (m, 66H, Ar), 7.41 – 7.36 (m, 3009H, Ar, $PhSiH_3$), 7.28 (s, 8H, Ar), 7.24 – 7.19 (m, 50H, Ar), 7.14 (t, *J* = 1.3 Hz, 203H, Ar), 7.13 – 7.11 (m, 620H, Ar, $PhSiH_3$), 7.11 (t, *J* = 1.5 Hz, 594H, Ar, $PhSiH_3$), 7.09 (s, 1059H, Ar, $PhSiH_3$), 7.07 (d, *J* = 1.4 Hz, 1422H, Ar, $PhSiH_3$), 7.06 (t, *J* = 1.4 Hz, 545H, Ar, $PhSiH_3$), 7.03 – 6.99 (m, 36H, Ar), 6.98 – 6.94 (m, 27H, Ar), 6.91 (dd, *J* = 10.8, 4.4 Hz, 45H, Ar), 6.87 (s, 14H, Ar), 6.85 – 6.80 (m, 25H, Ar), 6.78 (s, 24H, Ar), 5.07 (s, 1H), 4.49 (s, 21H), 4.43 (s, 84H, H_2), 4.23 (s, 6636H, PhSi**H$_3$**), 4.03 (s, 116H), 3.57 (d, *J* = 3.1 Hz, 25H, Bound THF), 3.04 (s, 12H), 2.30 (d, *J* = 8.5 Hz, 61H, alk), 2.25 (d, *J* = 6.0 Hz, 115H, alk), 2.23 – 2.20 (m, 89H, alk), 2.18 (s, 21H, alk), 2.19 – 2.11 (m, 268H, alk), 2.07 (s, 70H, alk), 2.03 (d, *J* = 7.2 Hz, 45H, alk), 2.01 – 1.93 (m, 47H, alk), 1.78 (d, *J* = 12.9 Hz, 13H, alk), 1.60 (t, *J* = 1.1 Hz, 30H, bound THF), 1.40 (s, 16H), 1.12 (d, *J* = 7.2 Hz, 51H), 0.88 (d, *J* = 7.1 Hz, 19H), 0.29 (s, 77H), 0.19 (t, *J* = 4.2 Hz, 17H).

6.3.22 Reaction of ThCl$_2$(OTer^{Mes})$_2$DME with pyridine

To a yellow solution of **3.2,** (8 mg, 0.005 mmol) in C_6D_6 (0.6 mL) in a Teflon-valved valve NMR tube was added 3 drops of pyridine resulting in no observable colour change.

^{1}H NMR (500 MHz, C_6D_6) δ 7.02 (s, 3H, Ar), 6.94 (d, *J* = 7.1 Hz, 14H, Ar), 6.62 (s, 16H, Ar), 3.54 (t, *J* = 6.1 Hz, 8H, bound THF), 3.32 (s, 5H), 3.11 (s, 4H), 2.44 (s, 9H, *para* mesityl methyl), 2.18 (s, 9H, *para* mesityl methyl), 2.17 (s, 15H, , *ortho* mesityl methyl), 2.02 (s, 13H, *ortho* mesityl methyl), 1.47 – 1.33 (m, 10H, bound THF).

6.3.23 Reaction of $ThCl_2(OTer^{Mes})_2DME$ with 4,4 bipyridine

To a brown solution of **3.2,** (10 mg, 0.010 mmol) in C_6D_6 (0.6 mL) in a Teflon-valved valve NMR tube was added as a white crystalline solid 4,4' bipyridine (3 mg, 0.020 mmol, 2 equiv) resulting in a brown-orange solution. Allowing this solution to stand at room temperature resulted in the formation of colourless needles of $[Th(OTer^{Mes})_2(Cl)_2(4,4'\text{-bipyridyl})_{1.5}]_\infty$, **3.12**, (5.0 mg, 0.005 mmol, 47% yield) suitable for single crystal X-ray crystallography.

^{1}H NMR (500 MHz, C_6D_6) δ 7.01 (d, *J* = 1.6 Hz, 1H, Ar), 7.00 (s, 4H, Ar), 6.84 (s, 4H, Ar), 6.78 (s, 4H, Ar), 6.51 (s, 4H, Ar), 6.28 (d, *J* = 0.8 Hz, 2H, Ar), 2.19 (s, 12H, *ortho* mesityl methyl), 2.15 (s, 6H, *para* mesityl methyl), 2.11 (s, 12H, *ortho* mesityl methyl), 2.07 (s, 6H, *para* mesityl methyl).

6.3.24 Reaction of $ThCl_2(OTer^{Mes})_2DME$ with $AlMe_3$

To a brown solution of **3.2,** (20 mg, 0.019 mmol) in C_6D_6 (0.6 mL) in a Teflon-valved valve NMR tube was added a 1.0 M solution of $AlMe_3$ in hexanes (0.02 mL, 0.04 mmol) resulting in no observable colour change.

^{1}H NMR (400 MHz, C_6D_6) δ 6.86 (s, 8H, Ar), 6.85 – 6.79 (m, 21H, Ar), 6.75 (s, 14H, Ar), 3.16 (s, 13H), 2.87 (s, 13H), 2.29 (s, 28H, *ortho* mesityl methyl), 2.20 (d, *J* = 4.4 Hz, 6H), 2.16 (d, *J* = 4.9 Hz, 5H, *para* mesityl methyl), 2.13 (s, 4H), 2.10 (s, 2H), 2.05 (d, *J* = 4.6 Hz, 5H), 1.93 (d, *J* = 45.0 Hz, 19H).

6.3.25 Reaction of $ThCl_2(OTer^{Mes})_2DME$ with Al^iPr_3

To a brown solution of **3.2,** (10 mg, 0.01 mmol) in C_6D_6 (0.6 mL) in a Teflon-valved valve NMR tube was added a 1.0 M solution of Al^iPr_3 in hexanes (0.01 mL, 0.02 mmol) resulting in no observable colour change.

^{1}H NMR (400 MHz, C_6D_6) δ 7.12 (d, *J* = 7.5 Hz, 6H, Ar), 7.01 (d, *J* = 7.4 Hz, 8H, Ar), 6.88 – 6.78 (m, 45H, Ar), 6.58 (d, *J* = 7.5 Hz, 2H, Ar), 4.75 – 4.72 (m, 5H), 4.03 (s, 7H), 3.33 (s, 30H), 2.93 (s, 43H), 2.32 (s, 67H, *ortho* mesityl methyl), 2.13 (s, 28H, *para* mesityl methyl), 1.41 (s, 59H), 0.97 (d, *J* = 6.6 Hz, 170H).

6.4 Synthetic procedure for reactions from Chapter 4

6.4.1 Synthetic Procedure for $Th(BH_4)_2(OTer^{Mes})_2DME$

To a Schlenk charged with a stirrer bar and **3.2** (150 mg, 0.142 mmol), was added *circa* 20 mL of dry toluene, forming an orange- brown solution. To this solution was added a colourless solution of $Ca(BH_4)_2(THF)_2$ (30.5 mg, 0.142 mmol) in toluene forming a pale yellow suspension upon addition. After 2 days of stirring, this suspension had progressed to colourless. The suspension was filtered to give a colourless solution, and this solution was concentrated and cooled to -30°C, to give colourless crystals of $Th(BH_4)_2(OTer^{Mes})_2DME$**,** (87.3 mg, 0.089 mmol, 63% yield. Single crystals suitable for X-ray crystallography were grown from a saturated solution of toluene held at a temperature of -30°C. Elemental analysis; calculated: C 61.79%, H 6.78%, found: C 61.64%, H 6.82%.

^{1}H NMR (500 MHz, C_6D_6) δ 6.87 (m, 3H, Ar overlapping *para* and *ortho* central phenyl ring), 6.81 (s, 4H, *meta* Ar, mesityl rings), 3.03 (s, 7H, overlapping $B\boldsymbol{H_4}$ and $\boldsymbol{CH_3}OCH_2CH_2O\boldsymbol{CH_3}$), 2.25 (s, 6H, *para* mesityl methyl), 2.18 (s, 12H) (*ortho* mesityl methyl), 2.12 (s, 2H) ($CH_3O\boldsymbol{CH_2CH_2}OCH_3$) ^{11}B NMR (160 MHz, C_6D_6) δ -12.46 (p, *J*= 82.6 Hz). ^{11}B{^{1}H} NMR (160 MHz, C_6D_6) δ -12.42 (s). ^{13}C NMR (126 MHz, C_6D_6) δ 161.76 (s), 138.27 (s), 137.19 (s), 135.95 (s), 131.52 (s), 130.44 (s), 129.95 (s), 129.34 (s), 128.88 (s), 128.69 (s), 128.57 (s), 128.35 (s), 125.70 (s), 120.08 (s), 72.64 (s), 64.38 (s), 21.67 (s), 21.22 (s). FTIR Spectroscopy (Nujol mull on BaF_2 Plates) 2726 (m), 2474 (m), 2456 (m), 2226 (m), 2164 (m), 1460 (s), 1377 (s) cm^{-1}.

6.4.2 Synthetic Procedure for $Th(BH_4)_2(OTer^{Mes})_2$

To a Schlenk charged with a stirrer bar and **4.1** (208.1 mg, 0.206 mmol), was added *circa* 20 mL of dry toluene, forming a yellow-orange solution. To this solution was added *via* syringe a solution of $AlMe_3$ in hexanes (2.0M, 0.21mL, 0.41 mmol), causing a lightening of the solution to yellow, and subsequent formation of a fine suspension. After stirring overnight, the suspension was filtered to give a pale yellow solution. This solution was concentrated and cooled to -30°C, to give colourless needles of

$Th(BH_4)_2(OTer^{Mes})_2$, (95.3 mg, 0.104 mmol, 50% yield). Single crystals suitable for X-ray crystallography were grown from a saturated solution of toluene stored at -30°C. Elemental analysis; calculated: C 62.62%, H 6.36%, found: C 62.48%, H 6.44%.

^{1}H NMR (500 MHz, C_6D_6) δ 6.88 (d, *J* = 2.9 Hz, 1H, Ar), 6.87 (s, 2H, Ar), 6.79 (s, 4H, Ar), 3.12 (s, 11H), 2.83 (s, 14H), 2.24 (s, 6H, *para* mesityl methyl), 2.08 (s, 12H, *ortho* mesityl methyl), -0.39 (s, 4H) (B**H$_4$**). ^{11}B NMR (160 MHz, C_6D_6) δ -10.08 (p, *J* = 83.7 Hz). ^{11}B{^{1}H} NMR (160 MHz, C_6D_6) δ -10.08 (s).^{13}C NMR (126 MHz, C_6D_6) δ 161.38 (s), 148.00 (s), 141.99 (s), 139.50 (s), 139.26 (s), 138.61 (s), 138.46 (s), 137.47 (s), 137.21 (s), 136.46 (s), 135.79 (s), 135.39 (s), 130.77 (s), 130.46 (s), 130.24 (s), 130.16 (s), 130.06 (s), 129.37 (s), 128.99 (s), 128.87 (s), 128.68 (s), 128.51 (s), 128.35 (s), 128.16 (s), 127.97 (s), 127.74 (s), 120.72 (s), 120.05 (s), 21.66 (s), 21.48 (s), 21.28 (s), 21.25 (s), 21.16 (s), 20.98 (s), 20.84 (s), 20.50 (s). FTIR Spectroscopy (Nujol mull on NaCl plates) 2957 (s), 2922 (s), 2853 (s), 2474 (m), 2217 (m), 2149(m), 1611 (m), 1455 (m) cm^{-1}.

6.4.3 Synthetic Procedure for $Th(BH_4)_2(OTer^{Mes})_2$(4,4' bipyridine)$_\infty$

To a pale yellow solution of **4.1** (10 mg, 0.010 mmol) in d_8-toluene (0.6 mL) in a Teflon-valved valve NMR tube was added as a white crystalline solid 4,4' bipyridine (3 mg, 0.020 mmol, 2 equiv) resulting in a yellow solution. Transfer of the solution to a vial, and allowing this solution to stand resulted in the formation of yellow crystals of $Th(BH_4)_2(OTer^{Mes})_2$(4,4' bipyridine)$_\infty$, (7.0 mg, 0.006 mmol, 66% yield) suitable for single crystal X-ray crystallography. Elemental analysis; calculated: C 64.69%, H 6.18%,N 2.60% found: C 64.44%, H 5.85%, N 2.72%

^{1}H NMR (500 MHz, C_7D_8) δ 7.01 (s, 2H, Ar), 6.97 (s, 4H, Ar), 6.81 (s, 1H, Ar), 6.74 (s, 4H, Ar), 6.55 (s, 4H, Ar), 3.28 (s, 4H, B**H$_4$**), 2.08 (s, 6H, *para* mesityl methyl), 2.00 (s, 12H, *ortho* mesityl methyl). ^{11}B NMR (160 MHz, C_7D_8) δ -6.42 (s). ^{13}C NMR (126 MHz, C_6D_6) δ 161.69 (s), 150.69 (s), 145.30 (s), 137.18 (s), 135.79 (s), 129.33 (s) 120.94 (s), 119.97 (s), 21.72 (s), 20.54 (s). FTIR Spectroscopy (Nujol mull on NaCl Plates) 2938 (s), 2901 (s), 2831 (s), 2454 (m), 2237 (m), 2171(m), 1618 (m), 1458 (m) cm^{-1}.

6.4.4 Synthesis of $Mg(OTer^{Mes})((\mu\text{-}H)_3BH)THF)_2$

To a Schlenk charged with a stirrer bar and **4.1** (175 mg, 0.173 mmol) was added *circa* 20 mL of dry toluene forming a pale yellow solution. To this solution was added a colourless solution of methylallyl magnesium chloride in THF solution (0.5M, 1.7 mL,

0.34 mmol) causing an immediate darkening of the solution and the observation of the formation of a fine white precipitate. Upon stirring overnight a yellow suspension was observed to have formed. Filtration and extraction with hexane caused the formation of a yellow solution, which allowed for the isolation of a colourless crystalline material, $Mg(OTer^{Mes})((\mu\text{-}H)_3BH)THF)_2$ (121 mg, 0.236 mmol, 60% yield). Single crystals suitable for X-ray crystallography were grown from a saturated hexane solution stored at -30°C. This complex was characterised by ^1H and ^{11}B NMR spectroscopy.

^1H NMR (500 MHz, C_6D_6) δ 7.12 (d, *J* = 7.3 Hz, 2H, Ar), 6.92 (dd, *J* = 12.2, 4.9 Hz, 1H, Ar), 6.87 (s, 4H, Ar), 3.13 (s, 8H, bound THF), 2.36 (s, 12H, *ortho* mesityl methyl), 2.21 (s, 6H, *para* mesityl methyl), 1.14 (s, 8H, Bound THF), -0.11 (q, *J* = 82.3 Hz, 2H, BH_4). ^{11}B NMR (160 MHz, C_6D_6) δ -44.36 (p, *J* = 82.2 Hz).

6.4.5 Reaction of $Th(BH_4)_2(OTer^{Mes})_2$ with excess CS_2

To a Schlenk charged with a stirrer bar and **4.2** (100 mg, 0.108 mmol) was added *circa* 20 mL of dry toluene forming a pale yellow solution. Upon addition of CS_2 (0.3 mL, 0.380 mg, 4.988 mmol), with vigorous stirring, no colour change was observed. Upon refluxing this solution overnight it was observed that a bright yellow suspension had formed. Following filtration and extraction with hexane a colourless powder was isolated as $HB(OTer^{Mes})_2$ (40 mg, 0.06 mmol, 55 % yield). Single crystals suitable for X-ray diffraction were grown from a saturated hexane solution stored at -30°C. This complex was characterised by ^1H and ^{11}B NMR spectroscopy.

^1H NMR (500 MHz, C_6D_6) δ 7.01 (d, *J* = 7.6 Hz, 4H, *meta* Ar, central phenyl ring), 6.96 (t, *J* = 7.6 Hz 2H, *para* Ar, central phenyl ring), 6.87 (s, 8H, *meta* Ar, mesityl rings), 2.28 (s, 12H, *para* mesityl methyl), 1.93 (s, 1H, B**H**), 1.89 (s, 24H, *ortho* mesityl methyl), 0.73 (s, 9H, $\mathbf{BMe_3}$). ^{11}B NMR (160 MHz, C_6D_6) δ 86.41 (s, $\mathbf{BMe_3}$), 17.13 (s).

6.4.7 Synthesis of $Th(BD_4)_2(OTer^{Mes})_2$

To a Schlenk charged with a stirrer bar was placed calcium iodide (1.053g, 3.58 mmol) and sodium borodeuteride (0.300 g, 7.16 mmol). To these two powders was added, with vigorous stirring, *circa* 50 mL of dry THF forming a white suspension. This suspension was stirred for 18 hours, then allowed to settle before filtration. The solvent was then removed in vacuo to give a white powder characterised by ^1H, ^2H and ^{11}B NMR spectrospcopy to be $Ca(BD_4)_2THF_2$ (0.650 g, 2.92 mmol, 82% yield).

^{1}H NMR (500 MHz, THF) δ 3.54 (s, 4H, bound THF), 1.69 (s, 4H, bound THF), -0.24 (q, *J* = 81.9 Hz, 4H, B**H$_4$**). ^{2}H NMR (77 MHz, THF) δ -0.27 (q, *J* = 12.2 Hz, 4H, B**H$_4$**). ^{11}B NMR (160 MHz, THF) δ -36.62 (p, *J* = 81.9 Hz).

To a Schlenk charged with a stirrer bar and **3.2** (500 mg, 0.475 mmol) was added the $Ca(BD_4)_2THF_2$ (105.5 mg, 0.475 mmol). To these two powders was added *circa* 50 mL of dry toluene, forming a brown suspension. This suspension was stirred for 18 hours and then filtered. To the resultant brown solution was added $AlMe_3$ in hexane solution (2.0M, 0.24 mL, 0.475 mmol) causing the formation of a fine precipitate. This suspension was stirred for 18 hours, at which point it was filtered and the resultant brown solution had its solvent removed *in vacuo*. This resulted in the isolation of a pale brown powder, $Th(BD_4)_2(OTer^{Mes})_2$ (368 mg, 0.397 mmol, 84 % yield) characterised by ^{1}H, ^{2}H and ^{11}B NMR spectroscopy.

^{1}H NMR (500 MHz, C_6D_6) δ 6.88 (d, *J* = 2.9 Hz, 1H, Ar), 6.87 (s, 2H, Ar), 6.79 (s, 4H, Ar), 3.12 (s, 11H), 2.83 (s, 14H), 2.24 (s, 6H, *para* mesityl methyl), 2.08 (s, 12H, *ortho* mesityl methyl), -0.39 (s, 4H) (B**H$_4$**). ^{2}H NMR (77 MHz, C_6D_6) δ -0.39 (s, 8H). ^{11}B NMR (160 MHz, C_6D_6) δ -10.08 (s).

6.4.8 Reaction of $Th(BD_4)_2(OTer^{Mes})_2$ with excess CS_2

To a yellow solution of **4.2***d*^{8}**,** (17 mg, 0.018 mmol) in d_6-benzene (0.6 mL) in a Teflon-valved valve NMR tube was added CS_2 (excess) causing the formation of a pale yellow solution. Refluxing this solution overnight caused the formation of a yellow suspension. Characterisation of the products of this reaction came *via* ^{1}H, ^{2}H and ^{11}B NMR spectroscopy.

^{1}H NMR (500 MHz, C_6D_6) δ 7.27 – 7.22 (m, 4H, Ar), 6.87 (s, 1H, Ar), 6.86 (s, 2H, Ar), 6.84 (s, 1H, Ar), 6.83 (s, 2H, Ar), 6.81 (s, 4H, Ar), 2.27 (s, 6H, *para* mesityl methyl), 2.02 (d, *J* = 2.0 Hz, 12H, *ortho* mesityl methyl), 0.74 (s, 1H, **BMe$_3$**). ^{2}H NMR (77 MHz, C_6D_6) δ 2.11 (t, *J* = 2.1 Hz, 4H), 1.31 (s, 1H). 11B NMR (160 MHz, C6D6) δ 86.41 (s, **BMe$_3$**), 17.13 (s).

6.4.9 Stoichiometric reaction of $Th(BH_4)_2(OTer^{Mes})_2$ with CS_2

To a Schlenk charged with a stirred bar was added **4.2** (100mg, 0.109 mmol) and *circa* 20 mL of dry toluene. To this pale brown solution was added a prepared stock solution of CS_2 in toluene (0.166 M, 0.65 mL, 0.109 mmol). After refluxing overnight the solution was observed to be very pale yellow to colourless. ^{1}H and ^{11}B NMR spectroscopy were performed.

^{1}H NMR (500 MHz, C_6D_6) δ 7.24 (t, *J* = 7.6 Hz, 8H, Ar), 7.13 – 7.10 (m, 6H, Ar), 7.02 – 6.98 (m, 18H, Ar), 6.86 (d, *J* = 2.5 Hz, 16H, Ar), 2.21 (s, 30H, alk), 2.16 (s, 17H, alk), 2.10 (s, 20H, alk), 2.07 (s, 29H, alk), 2.06 (s, 15H, alk), 2.01 (s, 14H, alk). ^{11}B NMR (160 MHz, C_6D_6) δ -11.52 (t, *J* = 81.3 Hz).

6.4.10 Reaction of $Th(BH_4)_2(OTer^{Mes})_2$ with CO_2

To a yellow solution of **4.2,** (20 mg, 0.022 mmol) in d_6-benzene (0.6 mL) in a Teflon-valved valve NMR tube was freeze-pump-thaw degassed 3 times prior to being placed under a 1 atm CO_2 atmosphere by use of a CO_2 cylinder connected to a Schlenk line with a t-piece. The formation of a small amount of white precipitate was observed. Characterisation of the products of this reaction came *via* ^{1}H and ^{11}B NMR spectroscopy.

^{1}H NMR (500 MHz, C_6D_6) δ 8.61 (s, 9H, Ar), 7.25 (t, *J* = 7.6 Hz, 48H, Ar), 7.07 (d, *J* = 1.5 Hz, 10H, Ar), 7.05 (s, 17H, Ar), 7.00 (dd, *J* = 7.6, 1.7 Hz, 71H, Ar), 6.87 (s, 86H, Ar), 6.84 (d, *J* = 4.4 Hz, 36H, Ar), 6.82 (s, 19H, Ar), 6.79 – 6.76 (m, 27H, Ar), 6.73 (s, 10H, Ar), 6.67 (d, *J* = 8.7 Hz, 9H, Ar), 3.59 (s, 47H), 3.31 (d, *J* = 23.7 Hz, 145H), 3.16 (s, 170H), 2.39 (s, 50H, alk), 2.31 (s, 52H, alk), 2.26 (s, 35H, alk), 2.25 (s, 49H, alk), 2.22 (s, 70H, alk), 2.22 (s, 115H, alk), 2.20 (s, 103H, alk), 2.18 (s, 130H, alk), 2.14 (s, 51H, alk), 2.12 (s, 31H, alk), 2.11 (s, 27H, alk), 2.10 (s, 11H, alk), 2.09 (s, 15H, alk), 2.07 (s, 206H, alk), 2.02 (s, 20H, alk), 1.44 (s, 28H), 1.38 – 1.26 (m, 77H), 0.91 (d, *J* = 6.7 Hz, 57H), 0.73 (s, 298H, **BMe_3**), 0.28 (s, 53H), 0.15 (s, 13H), 0.03 (s, 25H). ^{11}B NMR (160 MHz, C_6D_6) δ 86.42 (s, **BMe_3**).

6.4.11 Reaction of $Th(BH_4)_2(OTer^{Mes})_2$ with CO

To a yellow solution of **4.2,** (20 mg, 0.022 mmol) in d_6-benzene (0.6 mL) in a Teflon-valved valve NMR tube was freeze-pump-thaw degassed 3 times prior to being placed under a 1 atm CO atmosphere by use of a CO cylinder connected to a Schlenk line with a t-piece. The colour of the solution was observed to intensify, but the initial reactivity at room temperature was observed to be limited by NMR spectroscopy. After refluxing the solution overnight, characterisation of the products of this reaction came *via* ^{1}H and ^{11}B NMR spectroscopy.

^{1}H NMR (500 MHz, C_6D_6) δ 6.94 – 6.91 (m, 1H, Ar), 6.87 (d, *J* = 5.8 Hz, 2H, Ar), 6.80 (s, 3H, Ar), 3.03 (s, 2H), 2.37 (d, *J* = 2.7 Hz, 1H), 2.24 (s, 4H, alk), 2.18 (s, 9H, alk), 2.07 (s,

2H, alk), 0.72 (s, 1H, **BMe$_3$**). ^{11}B NMR (160 MHz, C_6D_6) δ 86.45 (s, **BMe$_3$**), -2.07 (d, *J* = 350.5 Hz), -11.62 (dd, *J* = 174.2, 85.3 Hz).

6.4.12 Reaction of Th(BH$_4$)$_2$(OTer^{Mes})$_2$ with DCC

To a yellow solution of **4.2,** (20 mg, 0.022 mmol) in d_6-benzene (0.6 mL) in a Teflon-valved valve NMR tube was added DCC (dicyclohexylcarbodimide, 4.5 mg, 0.022 mmol) causing the formation of a pale yellow solution. No initial reactivity was observed by NMR spectroscopy. After refluxing overnight, the yellow colour of the solution had intensified and a small amount of colourless precipitate was observed.

^{1}H NMR (500 MHz, C_6D_6) δ 7.02 – 6.98 (m, 39H, Ar), 6.95 – 6.92 (m, 65H, Ar), 6.90 – 6.86 (m, 104H, Ar), 6.82 (d, *J* = 6.8 Hz, 118H, Ar), 3.04 (s, 126H), 2.65 (s, 57H), 2.53 (s, 77H), 2.35 (d, *J* = 23.9 Hz, 154H, alk), 2.23 – 2.14 (m, 535H, alk), 2.06 (d, *J* = 14.6 Hz, 151H, alk), 1.37 (s, 117H), 0.75 (s, 3H, **BMe$_3$**). ^{11}B NMR (160 MHz, C_6D_6) δ 86.44 (s, **BMe$_3$**), -11.60 (dd, *J* = 173.4, 85.9 Hz).

6.4.13 Reaction of Th(BH$_4$)$_2$(OTer^{Mes})$_2$ with H$_2$/CO

To a yellow solution of **4.2,** (20 mg, 0.022 mmol) in d_6-benzene (0.6 mL) in a Teflon-valved valve NMR tube was freeze-pump-thaw degassed 3 times prior to being placed under a 1 atm 33% CO in H_2 atmosphere by use of a 33% CO in H_2 cylinder connected to a Schlenk line with a t-piece. A small amount of small white precipitate was observed to form, but the initial reactivity at room temperature was observed to be limited by NMR spectroscopy. After refluxing the solution overnight, characterisation of the products of this reaction came *via* ^{1}H and ^{11}B NMR spectroscopy.

^{1}H NMR (500 MHz, C_6D_6) δ 7.01 (dd, *J* = 7.5, 1.8 Hz, 8H, Ar), 6.94 (s, 8H, Ar), 6.87 (q, *J* = 3.0 Hz, 38H, Ar), 6.87 – 6.85 (m, 23H, Ar), 6.81 (s, 14H, Ar), 6.79 (s, 32H, Ar), 4.47 (s, 10H, H_2), 3.11 (s, 26H), 3.04 (s, 16H), 2.38 (s, 19H, alk), 2.24 (d, *J* = 4.8 Hz, 60H, alk), 2.22 (s, 33H, alk), 2.19 (s, 37H, alk), 2.09 (d, *J* = 7.9 Hz, 127H, alk), 0.73 (s, 1H, **BMe$_3$**), -0.55 (s, 49H). ^{11}B NMR (160 MHz, C_6D_6) δ 86.47 (s, **BMe$_3$**), -9.79 (t, *J* = 80.1 Hz).

6.4.14 Reaction of Th(BH$_4$)$_2$(OTer^{Mes})$_2$ with S$_8$

To a yellow solution of **4.2,** (20 mg, 0.022 mmol) in d_6-benzene (0.6 mL) in a Teflon-valved valve NMR tube was added S_8 (1.4 mg, 0.005 mmol) causing the formation of a pale yellow solution. No initial reactivity was observed by NMR spectroscopy. After

refluxing overnight, the yellow colour of the solution had intensified and a small amount of colourless precipitate had formed.

^{1}H NMR (500 MHz, C_6D_6) δ 7.05 – 6.74 (m, 155H, Ar), 2.65 (s, 11H, alk), 2.38 (s, 24H, alk), 2.25 (dd, *J* = 10.3, 4.2 Hz, 67H, alk), 2.22 (d, *J* = 6.4 Hz, 57H, alk), 2.20 – 2.16 (m, 89H, alk), 2.08 (s, 32H, alk), 0.73 (s, 32H, **BMe$_3$**), 0.29 (d, *J* = 6.5 Hz, 13H), 0.15 (s, 5H). ^{11}B NMR (160 MHz, C_6D_6) δ 86.46 (s, **BMe$_3$**), 47.33 (d, *J* = 202.3 Hz), -0.95 (s), -11.58 (d, *J* = 82.6 Hz), -39.69 (s).

6.4.15 Reaction of Th(BH$_4$)$_2$(OTer^{Mes})$_2$ with P$_4$

To a yellow solution of **4.2,** (20 mg, 0.022 mmol) in d_6-benzene (0.6 mL) in a Teflon-valved valve NMR tube was added P_4 (22.8 mg, 0.017 mmol) causing the formation of a pale yellow solution. No initial reactivity was observed according to ^{1}H, ^{11}B or ^{31}P NMR spectroscopy. After heating to reflux overnight, solution was observed to be brown in colour with a dark brown precipitate.

^{1}H NMR (500 MHz, C_6D_6) δ 7.25 (s, 2H, Ar), 7.08 (d, *J* = 7.4 Hz, 3H, Ar), 7.03 – 6.98 (m, 7H, Ar), 6.95 (s, 2H, Ar), 6.93 (d, *J* = 2.2 Hz, 8H, Ar), 6.91 (s, 5H, Ar), 6.88 – 6.85 (m, 18H, Ar), 6.80 (s, 3H, Ar), 6.78 (s, 10H, Ar), 3.31 (t, *J* = 5.5 Hz, 4H), 3.03 (s, 6H), 2.64 (s, 10H, alk), 2.37 (s, 14H, alk), 2.34 (s, 9H, alk), 2.29 (s, 2H, alk), 2.26 (s, 8H, alk), 2.23 (s, 15H, alk), 2.22 (s, 10H, alk), 2.21 (s, 23H, alk), 2.17 (s, 12H, alk), 2.07 (s, 40H, alk), 0.72 (s, 3H, **BMe$_3$**), 0.28 (s, 8H), 0.15 (s, 2H), -0.41 (s, 6H), -0.56 (s, 16H), -0.80 (s, 10H), -1.08 (s, 10H). ^{11}B NMR (160 MHz, C_6D_6) δ 86.33 (s, **BMe$_3$**), -10.68 (p, *J* = 88.1 Hz). ^{31}P NMR (202 MHz, C_6D_6) δ -520.54 (s) (P_4).

6.4.16 Reaction of Th(BH$_4$)$_2$(OTer^{Mes})$_2$ with NaC≡CH

To a yellow solution of **4.2,** (20 mg, 0.022 mmol) in d_6-benzene (0.6 mL) in a Teflon-valved valve NMR tube was added NaC≡CH (2.1 mg, 0.044 mmol) causing the formation of a brown solution.

^{1}H NMR (500 MHz, C_6D_6) δ 7.00 (dd, *J* = 7.6, 1.7 Hz, 8H, Ar), 6.88 (t, *J* = 2.0 Hz, 11H, Ar), 6.87 (d, *J* = 4.1 Hz, 21H, Ar), 6.80 (s, 33H, Ar), 3.03 (s, 32H), 2.24 (s, 56H, alk),), 2.23 (s, 17H, alk),), 2.21 (s, 30H, alk),), 2.18 (s, 108H, alk),), 2.07 (s, 24H, alk),), 0.28 (s, 12H), 0.15 (s, 6H), -0.29 (s, 9H), -0.42 (s, 10H), -0.51 (s, 5H), -1.01 (s, 6H). ^{11}B NMR (160 MHz, C_6D_6) δ -2.89 (s), -12.20 (d, *J* = 73.8 Hz), -15.43 (s), -18.14 (s).

6.4.17 General Procedure for Complex 4.2-Mediated Alkyne Reduction/Oligomerisation/ Cyclotrimerisation/Methylation.

In a typical experiment, 0.5 mL of a ~10 mM solution of catalyst in benzene-d^6 was transferred to a J. Young Teflon-sealed NMR tube. 10 equivalents of terminal alkyne was transferred to the same tube, which was then sealed, shaken, and heated to 75 °C for 72 h to ensure completion of the reaction. The samples were analysed as crude reaction mixtures by ^{1}H NMR spectroscopy, and the data were compared to literature values for the organic products. Following this, samples were quenched by the addition of a few drops of methanol, filtered through a short Celite plug, and analysed by GC/MS methods on the reaction mixtures. Product ratios were determined by either ^{1}H NMR spectroscopy or UV−vis spectroscopy interfaced to the GC/MS system.

*6.4.17.1 Catalytic reaction of complex **4.2** with 1-hexyne*

272 µL of 1-hexyne; 12% conversion; **4.6a** (37%), **4.7a** (4%), **4.8a** (2%), **4.12a** (56%), ^{1}H NMR (500 MHz, C_6D_6) δ 7.26 (t, *J* = 7.6 Hz, 23H), 7.16 – 7.04 (m, 41H), 7.02 – 6.96 (m, 30H), 7.00 – 6.88 (m, 73H), 6.93 – 6.77 (m, 69H), 6.80 – 6.66 (m, 19H), 5.75 (ddt, *J* = 16.9, 10.2, 6.7 Hz, 9H), 5.22 (dd, *J* = 142.6, 1.9 Hz, 25H), 5.02 – 4.98 (m, 8H), 4.97 – 4.93 (m, 7H), 3.16 – 2.97 (m, 66H), 2.97 – 2.80 (m, 61H), 2.45 – 2.22 (m, 296H), 2.29 – 2.16 (m, 207H), 2.05 – 1.90 (m, 1381H), 1.85 – 1.69 (m, 415H), 1.69 – 1.50 (m, 209H), 1.54 – 1.18 (m, 3324H), 1.00 – 0.77 (m, 499H), 0.71 – 0.57 (m, 109H), 0.26 (s, 18H), 0.15 (s, 33H), -1.14 (s, 23H). ^{11}B NMR (160 MHz, C_6D_6) δ 86.44 (s), -7.74 (s), -11.08 (dd, *J* = 170.1, 85.5 Hz).

*6.4.17.2 Catalytic reaction of complex **4.2** with phenyl acetylene*

292 µL of phenyl acetylene; 56% conversion; **4.12b** (87%), **4.13b** (6%), **4.14b** (1%), **4.15b** (7%), 1H NMR (500 MHz, C6D6) δ 7.39 (dd, J = 7.8, 1.7 Hz, 1229H), 7.14 – 6.80 (m, 3576H), 6.59 (d, J = 10.9 Hz, 63H), 6.55 (d, J = 10.9 Hz, 51H), 6.41 (d, J = 11.9 Hz, 48H), 5.79 (d, J = 11.9 Hz, 17H), 5.72 (d, J = 29.1 Hz, 26H), 5.59 (dd, J = 17.6, 0.8 Hz, 26H), 5.06 (d, J = 10.9 Hz, 23H), 2.72 (s, 263H), 2.45 – 2.22 (m, 532H), 2.28 – 2.16 (m, 304H), 2.19 – 2.01 (m, 433H), 1.46 – 1.20 (m, 117H), 1.12 (d, J = 6.9 Hz, 9H), 0.88 (dd, J = 34.9, 28.1 Hz, 107H), 0.14 (s, 128H). 11B NMR (160 MHz, C6D6) δ 86.44 (s), -7.96 (s), -11.03 (dd, J = 170.1, 85.2 Hz).

*6.4.17.3 Catalytic reaction of complex **4.2** with trimethylsilyl acetylene*

281 µL of trimethylsilyl acetylene; 61% conversion; **4.7c** (9%), **4.9c** (10%), **4.10c** (3%), **4.11c** (6%), **4.16c** (9%), **4.17c** (15%), **4.18c** (24%), **4.19c** (13%),1H NMR (500 MHz,

C6D6) δ 7.11 (d, J = 7.6 Hz, 16H), 7.07 (s, 6H), 7.04 (d, J = 6.7 Hz, 15H), 7.01 (s, 10H), 6.85 (d, J = 10.8 Hz, 18H), 6.78 (s, 10H), 6.52 (d, J = 19.3 Hz, 37H), 6.36 (dd, J = 14.0, 6.9 Hz, 23H), 6.25 (d, J = 15.1 Hz, 15H), 6.22 (s, 4H), 6.19 (s, 7H), 6.15 (d, J = 5.7 Hz, 12H), 6.14 (d, J = 3.4 Hz, 11H), 6.12 (s, 5H), 6.08 (d, J = 9.4 Hz, 12H), 6.06 (d, J = 3.3 Hz, 5H), 6.00 (ddd, J = 10.4, 6.6, 3.1 Hz, 34H), 5.93 (d, J = 6.9 Hz, 11H), 5.91 (d, J = 3.8 Hz, 11H), 5.88 (d, J = 3.8 Hz, 12H), 5.77 (d, J = 2.6 Hz, 8H), 5.71 – 5.69 (m, 7H), 5.65 (dd, J = 20.3, 3.8 Hz, 38H), 5.59 (dd, J = 14.0, 1.5 Hz, 19H), 5.55 (d, J = 3.4 Hz, 17H), 5.47 (d, J = 3.1 Hz, 9H), 2.30 (s, 18H), 2.11 (s, 26H), 2.06 (s, 745H), 1.92 (d, J = 6.5 Hz, 13H), 1.82 (s, 17H), 1.71 (d, J = 6.8 Hz, 17H), 1.67 (ddd, J = 17.3, 6.5, 1.6 Hz, 47H), 1.56 (s, 155H), 0.21 (s, 82H), 0.20 (s, 37H), 0.20 (s, 45H), 0.19 (s, 51H), 0.14 (d, J = 1.3 Hz, 57H), 0.14 (d, J = 0.8 Hz, 109H), 0.12 – 0.07 (m, 16761H), 0.04 (s, 142H), -0.03 (s, 86H), -0.09 (s, 72H). ^{11}B NMR (160 MHz, C_6D_6) δ 86.46 (s), 81.85 (s), -9.94 (d, *J* = 74.3 Hz). ^{29}Si NMR (99 MHz, C_6D_6) δ 2.45 (s), -17.71 (s), -21.92 (s).

6.4.18 Stoichiometric reaction of 4.2 with CyNC

To a yellow solution of **4.2,** (20 mg, 0.022 mmol) in d_6-benzene (0.6 mL) in a Teflon-valved valve NMR tube was added CyNC (2.4 mg, 0.022 mmol) causing the formation of an orange solution. The solution was refluxed over a period of 48 hours, at which point a red solution with a small amount of colourless precipitate was observed.

^{1}H NMR (500 MHz, C_6D_6) δ 7.12 (d, *J* = 7.6 Hz, 1H), 7.05 (d, *J* = 7.5 Hz, 5H), 7.01 (d, *J* = 10.5 Hz, 24H), 4.30 (ddd, *J* = 23.9, 11.3, 6.2 Hz, 28H), 3.31 (s, 7H), 3.14 (s, 8H), 2.91 (s, 49H), 2.31 – 2.14 (m, 27H), 2.07 (d, *J* = 22.5 Hz, 13H), 1.82 (dd, *J* = 27.7, 18.7 Hz, 18H), 1.58 – 1.44 (m, 27H), 1.39 – 1.29 (m, 210H), 1.29 – 1.18 (m, 119H), 1.10 – 0.92 (m, 122H), 0.92 – 0.78 (m, 118H), 0.15 (s, 2H), -0.16 (s, 4H), -0.45 (s, 3H), -0.49 (s, 2H), -0.52 (s, 3H). ^{11}B NMR (160 MHz, C_6D_6) δ -11.01 (d, *J* = 76.3 Hz), -25.28 (t, *J* = 84.6 Hz), -29.76 (d, *J* = 87.2 Hz), -34.73 (s), -44.07 (d, *J* = 96.1 Hz).

6.4.19 Stoichiometric reaction of 4.2 with ^{t}BuNC

To a yellow solution of **4.2,** (20 mg, 0.022 mmol) in d_6-benzene (0.6 mL) in a Teflon-valved valve NMR tube was added ^{t}BuNC (2.4 mg, 0.022 mmol) causing the formation of a pale yellow solution. The solution was refluxed over a period of 48 hours, at which point an orange solution with a small amount of colourless precipitate was observed. ^{1}H NMR (500 MHz, C_6D_6) δ 7.35 – 7.24 (m, 181H), 7.06 – 6.93 (m, 488H), 6.93 – 6.82 (m, 326H), 6.46 – 6.28 (m, 40H), 6.19 (s, 23H), 5.84 (s, 15H), 4.80 – 4.71 (m, 30H), 4.62 (s,

17H), 4.39 (s, 20H), 4.14 (s, 18H), 3.52 (s, 38H), 3.26 (s, 166H), 3.11 (s, 234H), 2.33 (t, *J* = 10.4 Hz, 402H), 2.30 – 2.23 (m, 367H), 2.25 – 2.21 (m, 329H), 2.21 – 2.18 (m, 131H), 2.13 (d, *J* = 13.0 Hz, 93H), 2.09 – 2.02 (m, 309H), 1.92 (s, 54H), 1.73 – 1.67 (m, 48H), 1.60 (dd, *J* = 3.9, 2.8 Hz, 109H), 1.53 – 1.47 (m, 133H), 1.44 – 1.39 (m, 135H), 1.38 – 1.32 (m, 364H), 1.36 – 1.31 (m, 324H), 1.28 (dddd, *J* = 17.3, 9.0, 4.6, 1.7 Hz, 531H), 1.24 – 1.19 (m, 294H), 1.18 – 1.14 (m, 267H), 1.16 – 1.11 (m, 300H), 1.10 – 1.06 (m, 220H), 1.04 – 0.99 (m, 192H), 1.01 – 0.92 (m, 333H), 0.91 – 0.82 (m, 1941H), 0.78 (t, *J* = 7.8 Hz, 105H), 0.64 (d, *J* = 16.8 Hz, 108H), 0.55 (t, *J* = 3.3 Hz, 98H), 0.44 (s, 53H), 0.29 (s, 86H), 0.16 (s, 61H), -0.04 (dd, *J* = 7.5, 3.4 Hz, 56H), -0.21 (ddd, *J* = 11.6, 10.0, 5.7 Hz, 142H), -0.24 – -0.32 (m, 130H), -0.40 (ddd, *J* = 8.5, 6.4, 4.6 Hz, 116H), -0.74 (s, 70H), -0.91 (d, *J* = 4.3 Hz, 118H), -1.02 (d, *J* = 32.1 Hz, 83H). ^{11}B NMR (160 MHz, C_6D_6) δ 45.32 (s), 26.48 (s), 23.82 (s), 23.27 – 16.96 (m), 19.19 (d, *J* = 144.9 Hz), -0.86 (d, *J* = 257.4 Hz), -4.17 (s), -5.74 – -14.25 (m), -14.25 – -21.96 (m), -26.18 (s).

6.4.20 General Procedure for the catalytic reaction of complex 4.2 with isonitrile substrates

In a typical experiment, 0.5 mL of a ~10 mM solution of catalyst in benzene-d^6 was transferred to a J. Young Teflon-sealed NMR tube. 10 equivalents of isonitrile was transferred to the same tube, which was then sealed, shaken, and heated to 75 °C for 72 h to ensure completion of the reaction. The samples were analysed as crude reaction mixtures by ^{1}H NMR spectroscopy, and the data were compared to literature values for the organic products. Following this, samples were quenched by the addition of a few drops of methanol, filtered through a short Celite plug, and analysed by GC/MS methods on the reaction mixtures. Product ratios were determined by either ^{1}H NMR spectroscopy or UV–vis spectroscopy interfaced to the GC/MS system.

*6.4.20.1 Catalytic reaction of complex **4.2** with ^{t}BuNC*

303 µL of ^{t}BuNC; 49% conversion; **4.24a** (73%), **4.25b** (27%), ^{1}H NMR (500 MHz, C_6D_6) δ 8.10 (s, 5H), 8.05 (s, 4H), 8.01 (d, *J* = 2.3 Hz, 6H), 7.99 (s, 14H), 7.83 (d, *J* = 10.0 Hz, 12H), 7.77 (d, *J* = 10.5 Hz, 13H), 7.61 (s, 24H), 7.49 (d, *J* = 4.0 Hz, 21H), 7.34 – 7.29 (m, 265H), 7.28 – 7.23 (m, 239H), 7.07 (d, *J* = 7.4 Hz, 237H), 7.03 – 6.99 (m, 443H), 6.98 – 6.94 (m, 221H), 6.90 (s, 396H), 6.87 (d, *J* = 6.9 Hz, 428H), 6.84 (s, 91H), 6.81 (s, 92H), 6.78 (t, *J* = 1.5 Hz, 100H), 6.72 (dt, *J* = 11.5, 4.9 Hz, 92H), 6.39 (d, *J* = 13.8 Hz, 15H), 6.34 (s, 10H), 6.20 (d, *J* = 4.6 Hz, 7H), 6.15 – 6.08 (m, 13H), 5.84 (s, 7H), 5.76 (s, 8H), 5.52 (d, *J* = 1.3 Hz, 19H), 5.46 (d, *J* = 4.1 Hz, 4H), 5.24 (d, *J* = 4.3 Hz, 8H), 5.15 (d, *J* = 4.6 Hz, 7H),

5.10 (s, 9H), 5.00 (s, 8H), 4.80 – 4.71 (m, 47H), 4.62 (s, 23H), 4.39 (s, 39H), 4.13 (s, 19H), 3.60 – 3.53 (m, 97H), 3.52 (d, *J* = 5.5 Hz, 66H), 3.45 (dd, *J* = 17.8, 8.5 Hz, 91H), 3.39 (s, 69H), 3.37 – 3.30 (m, 123H), 3.23 (s, 305H), 3.18 – 3.06 (m, 592H), 3.04 (s, 117H), 3.00 (s, 109H), 2.98 – 2.90 (m, 244H), 2.81 (d, *J* = 14.7 Hz, 58H), 2.68 (s, 31H), 2.61 (d, *J* = 4.5 Hz, 79H), 2.49 – 2.38 (m, 517H), 2.33 – 2.27 (m, 1743H), 2.25 – 2.19 (m, 1243H), 2.14 – 2.11 (m, 180H), 2.08 (s, 825H), 2.05 – 2.00 (m, 204H), 1.74 (t, *J* = 2.0 Hz, 90H), 1.62 – 1.58 (m, 196H), 1.52 – 1.47 (m, 334H), 1.41 (d, *J* = 1.9 Hz, 151H), 1.37 (dt, *J* = 3.7, 3.0 Hz, 383H), 1.32 (dd, *J* = 4.1, 3.5 Hz, 367H), 1.30 (dd, *J* = 5.9, 2.6 Hz, 502H), 1.28 (d, *J* = 2.7 Hz, 288H), 1.27 – 1.25 (m, 475H), 1.24 – 1.21 (m, 486H), 1.20 – 1.18 (m, 551H), 1.16 (q, *J* = 3.0 Hz, 641H), 1.13 – 1.10 (m, 595H), 1.08 (s, 329H), 1.05 (dd, *J* = 6.0, 2.3 Hz, 303H), 1.02 (dd, *J* = 8.1, 3.1 Hz, 513H), 0.96 (ddd, *J* = 11.7, 5.5, 2.1 Hz, 485H), 0.92 (d, *J* = 3.7 Hz, 208H), 0.89 (dd, *J* = 8.5, 4.1 Hz, 274H), 0.62 (s, 82H), 0.29 (s, 102H), 0.17 – 0.15 (m, 72H), -0.05 (d, *J* = 4.1 Hz, 142H), -0.17 – -0.20 (m, 215H), -0.28 (d, *J* = 6.6 Hz, 144H), -0.38 – -0.40 (m, 95H), -0.49 (s, 143H), -0.97 (d, *J* = 8.4 Hz, 340H). ^{11}B NMR (160 MHz, C_6D_6) δ 45.26 (s), 39.53 (s), 32.29 (s), 26.48 (s), 24.56 (s), 21.61 – 16.44 (m), 0.18 (s), -1.70 (s), -4.18 (s), -11.01 (dd, *J* = 207.2, 68.7 Hz), -15.36 (d, *J* = 45.6 Hz), -16.50 (d, *J* = 41.5 Hz), -17.37 (s), -19.89 (d, *J* = 58.8 Hz), -26.48 (s).

*6.4.20.2 Catalytic reaction of complex **4.2** with CyNC*

313 µL of CyNC; 36% conversion **4.20b** (91%), **4.21b** (2%), **4.22b** (1%), **4.23b** (1%), **4.26b** (5%), ^{1}H NMR (500 MHz, C_6D_6) δ 7.26 (d, *J* = 7.6 Hz, 49H), 7.11 – 6.97 (m, 239H), 7.05 – 6.74 (m, 638H), 6.43 (s, 11H), 6.35 (d, *J* = 11.3 Hz, 9H), 6.28 (d, *J* = 8.3 Hz, 14H), 6.09 (d, *J* = 8.6 Hz, 7H), 5.98 (s, 7H), 5.09 (d, *J* = 169.1 Hz, 99H), 3.35 (d, *J* = 32.1 Hz, 266H), 3.14 (s, 302H), 2.87 (s, 401H), 2.40 – 2.13 (m, 1431H), 2.13 – 1.96 (m, 746H), 1.78 (d, *J* = 27.2 Hz, 687H), 1.72 – 1.56 (m, 1191H), 1.63 – 1.40 (m, 1531H), 1.40 – 1.27 (m, 1676H), 1.20 (dt, *J* = 35.5, 15.5 Hz, 1272H), 1.08 – 0.90 (m, 1259H), 0.88 – 0.69 (m, 946H), 0.29 (d, *J* = 22.1 Hz, 103H), 0.15 (s, 69H), -0.01 – -0.24 (m, 354H), -0.22 – -0.66 (m, 607H), -0.97 (d, *J* = 11.5 Hz, 111H). ^{11}B NMR (160 MHz, C_6D_6) δ 45.03 (s), 30.51 (s), 26.03 (s), 19.92 (d, *J* = 145.6 Hz), -6.54 (s), -9.65 (s), -11.55 (d, *J* = 277.9 Hz), -14.32 (d, *J* = 38.0 Hz), -15.33 (s), -15.99 (s), -17.23 (d, *J* = 98.3 Hz), -20.65 (d, *J* = 93.8 Hz), -25.23 (t, *J* = 84.7 Hz).

6.5 Synthetic procedure for reactions from Chapter 5

6.5.1 Synthesis of $Ter^{Mes}PH_2$

To a Schlenk charged with a stirrer bar and $Ter^{Mes}I$ (1.00g, 2.27 mmol, white powder) was added dry diethyl ether (*circa* 30 mL), whereupon a white suspension was formed with stirring. After cooling to -95 °C (via acetone/N_2 slush bath) 1.42 mL (2.27 mmol) of a 1.6 M ^{n}BuLi in hexanes solution was added via syringe causing the formation of a yellow solution. After allowing the solution to stir, with thawing for two hours, the reaction mixture was re-cooled to -95 °C, whereupon 0.2 mL (2.27 mmol) of PCl_3 was added *via* syringe causing the immediate formation of an orange suspension. This suspension was then stirred with thawing overnight and then filtered resulting in an orange solution. The solvent was removed *in vacuo* to leave an orange powder, which was then redissolved in dry diethyl ether (*circa* 30 mL), forming an orange solution and then cannulated onto the grey powder, $LiAlH_4$ (0.20 g, 5.26 mmol) causing immediate effervescence and forming a grey suspension. This suspension was allowed to stir overnight, then allowed to settle before filtering to give a colourless solution. The solvent was removed *in vacuo* to give a white powder, $Ter^{Mes}PH_2$, (0.76g, 2.19 mmol, 96.4% yield) which was analytically pure by ^{1}H and ^{31}P NMR spectroscopy. ^{1}H NMR (500 MHz, C_6D_6) δ 7.10 (t, J = 7.5 Hz, 1H, *para* Ar, central phenyl ring), 6.94 (dd, J = 7.6, 2.3 Hz, 2H, *meta* Ar, central phenyl ring), 6.89 (s, 4H, *meta* Ar, mesityl rings), 3.26 (d, J = 209.7 Hz, 2H, P**H$_2$**), 2.21 (d, J = 2.8 Hz, 6H, *para* mesityl methyl), 2.08 (d, J = 2.4 Hz, 12H, *ortho* mesityl methyl). ^{31}P NMR (202 MHz, C_6D_6) δ -147.30 (t, J = 209.7 Hz).

6.5.2 Deprotonation of $Ter^{Mes}PH_2$

6.5.2.1 KH

To a colourless solution of $Ter^{Mes}PH_2$**,** (20 mg, 0.058 mmol) in d_6-benzene (0.6 mL) in a Teflon-valved valve NMR tube was added KH (2.3 mg, 0.058 mmol) causing the formation of a grey suspension. At room temperature the ^{1}H NMR spectrum showed no reaction. The suspension was refluxed overnight, at which point an orange solution with a grey precipitate was observed.

^{1}H NMR (500 MHz, C_6D_6) δ 7.25 (t, *J* = 7.6 Hz, Ar), 7.02 – 6.99 (m, 7H, Ar), 6.87 (s, 18H, Ar), 4.47 (s, 3H, H_2), 2.42 – 2.38 (m, 4H, alk), 2.36 (d, *J* = 12.2 Hz, 8H, alk), 2.30 (t, *J* = 5.6 Hz, 12H, alk), 2.25 (s, 17H, alk), 2.22 (s, 75H, alk), 2.16 – 2.11 (m, 11H, alk), 2.08 (s, 34H, alk), 2.05 (s, 6H, alk), 1.97 (s, 5H, alk), 1.91 (d, *J* = 5.7 Hz, 5H, alk).

^{31}P NMR (202 MHz, C_6D_6) δ -100.53 (d, *J* = 21.7 Hz), -100.99 (d, *J* = 8.0 Hz), -100.69 – -101.92 (m), -100.43 – -102.20 (m), -101.64 (d, *J* = 8.2 Hz), -102.11 (d, *J* = 22.1 Hz), -

109.84 (dd, *J* = 137.8, 75.2 Hz), -129.83 (d, *J* = 173.9 Hz), -165.23 (s), -184.80 (s), -198.04 (s), -204.12 (d, *J* = 157.4 Hz), -211.03 (d, *J* = 154.6 Hz).

6.5.2.2 KN"

To a colourless solution of $Ter^{Mes}PH_2$**,** (20 mg, 0.058 mmol) in d_6-benzene (0.6 mL) in a Teflon-valved valve NMR tube was added KN" (11.5 mg, 0.058 mmol) causing the formation of a yellow green suspension.

^{1}H NMR (400 MHz, C_6D_6) δ 6.96 (t, *J* = 7.3 Hz, 1H, *para* Ar, central phenyl ring), 6.87 (s, 4H, *meta* Ar mesityl rings), 6.79 (d, *J* = 7.3 Hz, 2H *meta* Ar, central phenyl ring), 2.22 (d, *J* = 5.2 Hz, 12H, *ortho* mesityl methyl), 2.06 (s, 6H, *para* mesityl methyl), 1.47 (d, *J* = 174.2 Hz, 1H) (P**H**K). ^{31}P NMR (162 MHz, C_6D_6) δ -129.77 (d, *J* = 171.4 Hz) (P**H**K).

6.5.3 Reaction of $Ter^{Mes}PH_2$ with $ThCl_4(DME)_2$

To a colourless solution of $Ter^{Mes}PH_2$**,** (20 mg, 0.058 mmol) in d_6-benzene (0.6 mL) in a Teflon-valved valve NMR tube was added KN" (11.5 mg, 0.058 mmol) causing the formation of a yellow green suspension. To this green suspension was added $ThCl_4(DME)_2$ (16.0 mg, 0.029 mmol) causing the formation of an orange solution, with some effervescence observed.

^{1}H NMR (400 MHz, C_6D_6) δ 7.04 – 6.71 (m, 252H, Ar), 4.48 (s, 7H, H_2), 3.29 (d, *J* = 5.7 Hz, 36H), 2.94 (s, 242H), 2.84 (s, 167H, alk), 2.24 (d, *J* = 15.0 Hz, 389H, alk), 2.07 (s, 281H, alk), 1.08 (s, 44H), 0.50 (d, *J* = 22.0 Hz, 861H), 0.40 (s, 600H), 0.34 (s, 687H), 0.10 (s, 393H), -0.29 (s, 40H). ^{31}P NMR (162 MHz, C_6D_6) δ -88.02 (d, J = 221.8 Hz), -137.07 (d, J = 188.1 Hz).

6.5.4 Reaction of $Ter^{Mes}PH_2$ with UCl_4

To a colourless solution of $Ter^{Mes}PH_2$**,** (20 mg, 0.058 mmol) in d_6-benzene (0.6 mL) in a Teflon-valved valve NMR tube was added KN" (11.5 mg, 0.058 mmol) causing the formation of a yellow green suspension. To this green suspension was added a green solution of UCl_4 in THF (11.0 mg, 0.029 mmol) causing the formation of a black suspension, with copious effervescence observed.

^{1}H NMR (500 MHz, C_6D_6) δ 38.76 (s, 90H), 31.31 (s, 42H), -3.79 (s, 15H), -5.13 (s, 537H), -2.96 – -8.04 (m, 710H), -5.84 (s, 119H), -6.97 (d, *J* = 330.1 Hz, 30H), -15.20 (s, 3H), -21.96 (s, 39H), -35.98 (s, 96H). ^{31}P NMR (202 MHz, C_6D_6) δ -101.48 (d, *J* = 155.0 Hz), -135.68 (d, *J* = 166.8 Hz).

6.5.5 Reaction of $Ter^{Mes}PH_2$ with $UI_4(dioxane)_2$

In a Schlenk charged with a stirrer bar and $Ter^{Mes}PH_2$ (300mg, 0.865 mmol) was added KN" (173 mg, 0.865 mmol). To these powders were added *circa* 50 mL of dry toluene with vigorous stirring, forming a green suspension. A red THF solution of $UI_4(dioxane)_2$ (399 mg, 0.432 mmol) was cannulated onto this suspension causing the instantaneous formation of a deep purple suspension. This suspension was stirred overnight, at which point it was allowed to settle, whereupon copious amounts of a lilac coloured precipitate was observed. This suspension was filtered and the solvent was removed *in vacuo*. Extraction of the dark purple residue with hexane allowed for the isolation from the yellow brown solution of a colourless crystalline material, $(Ter^{Mes}PH)_2$ (168 mg, 0.246 mmol, 57 % yield). Crystals suitable for X-ray crystallography were grown from a saturated hexane solution stored at a temperature of -30 °C.

^1H NMR (500 MHz, C_6D_6) δ 6.99 (t, *J* = 7.5 Hz, 1H, *para* Ar, central phenyl ring), 6.83 (d, *J* = 12.5 Hz, 4H, *meta* Ar, mesityl rings), 6.76 (d, *J* = 7.5 Hz, 2H, *meta* Ar, central phenyl ring), 3.02 (dtd, *J* = 226.9, 21.1, 8.2 Hz, 2H, P**H**), 2.30 (d, *J* = 7.7 Hz, 6H, mesityl methyl), 2.07 (d, *J* = 8.4 Hz, 6H, mesityl methyl), 1.92 (d, *J* = 5.6 Hz, 6H, mesityl methyl).

^{31}P NMR (202 MHz, C_6D_6) δ -101.31 (dtd, *J* = 226.9, 21.1, 8.2 Hz).

6.5.6 Synthesis of $Ter^{Trip}PH_2$

To a Schlenk charged with a stirrer bar and $Ter^{Trip}I$ (1.03g, 1.64 mmol, white powder) was added dry diethyl ether (*circa* 30 mL), whereupon a white suspension was formed with stirring. After cooling to -95 °C (via acetone/N_2 slush bath) 1.0 mL (1.64 mmol) of a 1.6 M ^nBuLi in hexanes solution was added via syringe causing the formation of a yellow solution. After allowing the solution to stir, with thawing for two hours, the reaction mixture was recooled to -95 °C, whereupon 0.14 mL (1.64 mmol) of PCl_3 was added *via* syringe causing the immediate formation of an orange suspension. This suspension was then stirred with thawing overnight and then filtered resulting in an orange solution. The solvent was removed *in vacuo* to leave an orange powder, which was then redissolved in dry diethyl ether (*circa* 30 mL), forming an orange solution and then cannulated onto the grey powder, $LiAlH_4$ (0.11 g, 2.89 mmol) causing immediate effervescence and forming a grey suspension. This suspension was allowed to stir overnight, then allowed to settle before filtering to give a colourless solution. The

solvent was removed *in vacuo* to give a white powder, $Ter^{Trip}PH_2$, (0.807g, 1.56 mmol, 95.1% yield) which was analytically pure by ^1H and ^{31}P NMR spectroscopy.

^1H NMR (500 MHz, C_6D_6) δ 7.23 (d, J = 3.3 Hz, 4H *meta* Ar, mesityl rings), 7.20 (s, 1H *para* Ar, central phenyl ring), 7.06 – 7.03 (m, 2H *meta* Ar, central phenyl ring), 3.33 (d, J = 210.8 Hz, 2H, P**H**$_2$), 2.92 – 2.69 (m, 8H, Isopropyl H), 1.43 (d, J = 6.9 Hz, 6H, *para* isopropyl Me), 1.37 (d, J = 6.9 Hz, 6H, *para* isopropyl Me), 1.26 (dd, J = 6.9, 1.1 Hz, 12H, *ortho* isopropyl Me), 1.16 (dd, J = 6.8, 1.4 Hz, 12H, *ortho* isopropyl Me). ^{31}P NMR (202 MHz, C_6D_6) δ -140.36 (t, J = 210.7 Hz).

6.5.7 Reaction of $Ter^{Trip}PHK$ with UCl_4

To a colourless solution of $Ter^{Trip}PH_2$**,** (20 mg, 0.039 mmol) in d_6-benzene (0.6 mL) in a Teflon-valved valve NMR tube was added KN" (7.8 mg, 0.039 mmol) causing the formation of a green suspension. To this green suspension was added a green solution of UCl_4 in THF (7.4 mg, 0.019 mmol) causing the formation of a black suspension, with copious effervescence observed.

^1H NMR (500 MHz, C_6D_6) δ 7.06 (s, 4H, Ar), 3.05 (ddd, *J* = 138.1, 68.4, 39.2 Hz, 142H), 1.33 (s, 19H, alk), 1.25 (d, *J* = 25.8 Hz, 37H, alk), 1.08 (s, 56H, alk), 0.27 (t, *J* = 29.0 Hz, 50H).

6.5.8 Reaction of $Ter^{Trip}PHK$ with $UI_4(dioxane)_2$

To a Schlenk charged with a stirrer bar and $Ter^{Trip}PH_2$ (200 mg, 0.388 mmol) was added KN" (78 mg, 0.388mmol). To these white powders was added *circa* 30 mL of dry toluene, with vigorous stirring, causing the formation of a green suspension. After stirring overnight a red solution of $UI_4(dioxane)_2$ in THF was cannulated onto this suspension causing the formation of a dark brown suspension. After stirring overnight, this suspension was allowed to settle and filtered. The solvent was removed *in vacuo* to leave a brown-black residue (150 mg).

^1H NMR (500 MHz, C_6D_6) δ 32.26 (s, 4H), 19.03 (s, 9H), 13.15 (s, 12H), -1.68 (s, 51H), -3.18 (d, *J* = 145.0 Hz, 26H), -3.33 (s, 16H), -5.50 (s, 29H), -9.21 (s, 46H), -13.50 (s, 7H), -15.95 (s, 14H), -20.53 (s, 4H), -26.24 (s, 5H). ^{31}P NMR (202 MHz, C_6D_6) δ -101.62 (ddd, *J* = 227.0, 44.1, 8.2 Hz), -148.29 (s).

6.5.9 Reaction of $Ter^{Trip}PHK$ with $ThCl_4(DME)_2$

To a Schlenk charged with a stirrer bar and $Ter^{Trip}PH_2$ (844 mg, 1.61 mmol) was added KH (66 mg, 1.61mmol). To these white powders was added *circa* 30 mL of dry toluene, with vigorous stirring, causing the formation of a green suspension. To this suspension was added $ThCl_4(DME)_2$ (454mg, 0.82mmol) which caused the suspension to progress to grey after stirring for one hour. After stirring overnight, this suspension was allowed to settle and filtered. The solvent has removed *in vacuo* and the resultant yellow residue was extracted with hexane, which allowed for the isolation of a yellow powder (427 mg).

^{1}H NMR (500 MHz, C_6D_6) δ 7.25 (s, 6H, Ar), 7.24 (d, *J* = 1.6 Hz, 3H, Ar), 7.22 (s, 3H, Ar), 7.21 (s, 11H, Ar), 7.11 (d, *J* = 1.6 Hz, 4H, Ar), 7.09 (d, *J* = 1.5 Hz, 4H, Ar), 3.76 (s, 7H), 3.56 (s, 3H), 3.34 (s, 16H), 3.13 (d, *J* = 2.5 Hz, 17H), 2.98 (td, *J* = 13.8, 6.9 Hz, 21H, Isopropyl H), 2.92 – 2.81 (m, 24H, Isopropyl H), 1.47 (s, 4H, alk), 1.43 (d, *J* = 6.9 Hz, 5H, Isopropyl Me), 1.38 (d, *J* = 6.9 Hz, 17H, Isopropyl Me), 1.35 (d, *J* = 6.9 Hz, 5H, Isopropyl Me), 1.29 (d, *J* = 6.9 Hz, 40H, Isopropyl Me), 1.27 (d, *J* = 6.9 Hz, 17H, Isopropyl Me), 1.20 (t, *J* = 7.1 Hz, 71H, alk), 1.17 (d, *J* = 6.8 Hz, 17H, alk), 0.30 (d, *J* = 3.4 Hz, 25H).

^{31}P NMR (202 MHz, C_6D_6) δ -86.36 (d, *J* = 227.9 Hz), -140.35 (t, *J* = 210.6 Hz).

6.5.10 Attempted Syntheses of $(SiMe_3)PHTer^{Mes}$

6.5.10.1 Lithiation of $Ter^{Mes}PH_2$ and attempted quenching with $SiMe_3Cl$

In a Schlenk charged with a stirrer bar and $Ter^{Mes}PH_2$ (200 mg, 0.58 mmol) was added circa 30 mL of toluene, forming a pale yellow solution. This solution was cooled to -95°C by means of an acetone/liquid N_2 slush bath, whereupon a 1.6M hexane solution of ^{n}BuLi (0.36 mL, 0.58 mmol) was added causing the formation of a pale green solution initially. Upon thawing and stirring overnight a green suspension was observed. To this solution was added $SiMe_3Cl$ (0.07 mL, 0.58 mmol) causing the formation of a grey suspension instantaneously. This suspension, was filtered to give a grey residue and a pale yellow solution, and the solvent was removed *in vacuo* to give an off-white powder (189 mg), characterised by ^{1}H, ^{29}Si and ^{31}P NMR spectroscopy.

^{1}H NMR (500 MHz, C_6D_6) δ 7.25 (t, *J* = 7.6 Hz, 12H, Ar), 7.01 (dd, *J* = 7.6, 1.7 Hz, 20H, Ar), 6.95 (d, *J* = 2.1 Hz, 9H, Ar), 6.97 – 6.92 (m, 31H, Ar), 6.93 (d, *J* = 2.3 Hz, 7H, Ar), 6.90 (s, 32H, Ar), 6.88 (d, *J* = 4.6 Hz, 56H, Ar), 6.77 (t, *J* = 1.5 Hz, 8H, Ar), 4.81 (d, *J* = 195.9 Hz, 21H), 3.78 (s, 72H), 3.34 – 3.26 (m, 5H), 3.27 (d, *J* = 210.2 Hz, 44H), 2.22 (s, 52H, alk), 2.21 (d, *J* = 5.0 Hz, 146H, alk), 2.21 (s, 91H, alk), 2.17 (s, 96H, alk), 2.08 (s, 185H, alk),

1.35 (dd, *J* = 7.9, 4.9 Hz, 74H), 1.06 – 0.96 (m, 41H), 0.60 (t, *J* = 7.0 Hz, 28H), 0.29 (s, 8H), 0.12 (s, 2H, $SiMe_3$ groups), -0.18 (s, 5H, $SiMe_3$ groups).

^{29}Si NMR (99 MHz, C_6D_6) δ -21.86 (s).

^{31}P NMR (202 MHz, C_6D_6) δ -61.15 (d, *J* = 195.9 Hz), -69.13 (s), -147.32 (t, *J* = 196.9 Hz, $Ter^{Mes}PH_2$).

6.5.10.2 Potassiation of $Ter^{Mes}PH_2$ and attempted quenching with $SiMe_3Cl$

In a Schlenk charged with a stirrer bar and $Ter^{Mes}PH_2$ (300 mg, 0.86 mmol) was added circa 30 mL of toluene, forming a pale yellow solution. This solution was cooled to -95°C by means of an acetone/liquid N_2 slush bath, whereupon a toluene solution of KN" (173 mg, 0.86 mmol) was added causing the formation of a yellow suspension. The suspension was allowed to thaw and stir overnight. The suspension was recooled to -95°C before the addition of $SiMe_3Cl$ (0.011 mL, 0.86 mmol) causing no immediate observed change to the yellow solution. Upon stirring overnight with thawing a colourless suspension was observed. This suspension, was filtered to give a colourless residue and a colourless solution, and the solvent was removed *in vacuo* to give an off-white powder (295 mg), characterised by ^{1}H, ^{29}Si and ^{31}P NMR spectroscopy.

^{1}H NMR (500 MHz, C_6D_6) δ 7.10 (d, *J* = 7.6 Hz, 9H, Ar), 7.08 – 7.04 (m, 16H, Ar), 6.97 (dd, *J* = 7.6, 1.6 Hz, 15H, Ar), 6.92 – 6.87 (m, 51H, Ar), 6.87 – 6.83 (m, 109H, Ar), 4.19 – 4.07 (m, 68H), 3.71 (d, *J* = 6.5 Hz, 33H), 2.35 (s, 47H, alk), 2.29 (s, 43H, alk), 2.23 (s, 97H, alk), 2.22 (s, 122H, alk), 2.20 (t, *J* = 3.8 Hz, 98H, alk), 2.11 (s, 23H, alk), 2.04 (s, 45H, alk), 2.03 (d, *J* = 5.9 Hz, 124H, alk), 0.51 (d, *J* = 5.0 Hz, 486H), 0.46 (s, 56H), 0.34 (s, 141H), 0.30 (d, *J* = 3.4 Hz, 134H), 0.19 (s, 7481H, $SiMe_3$ groups), 0.09 – 0.07 (m, 291H, $SiMe_3$ groups), -0.01 (t, *J* = 11.0 Hz, 1066H, $SiMe_3$ groups).

^{29}Si NMR (99 MHz, C_6D_6) δ 30.05 (s), 1.94 (s), 1.18 (s), 0.34 (s), -0.28 (s), -2.19 (s), -16.55 (s).

^{31}P NMR (202 MHz, C_6D_6) δ -137.01 (d, *J* = 217.6 Hz), -143.56 (d, *J* = 230.7 Hz), -145.97 – -149.02 (m), -160.11 (d, *J* = 217.8 Hz).

6.5.10.3 $Ter^{Mes}PCl_2$ and $SiMe_3MgCl$

To a Schlenk charged with a stirrer bar and $Ter^{Mes}PCl_2$ (600 mg, 1.45 mmol) was added *circa* 40 mL of dry diethyl ether with vigorous stirring, causing the formation of a colourless solution. After cooling to -30°C, to this solution was added a 1.0M diethyl ether solution of $SiMe_3MgCl$ (), causing the immediate formation of an orange solution

which progressed to a yellow suspension upon thawing. This suspension was filtered and the resultant yellow solution had its solvent removed *in vacuo* to give a yellow powder (656 mg) thought $SiMe_3PClTer^{Mes}$ to be characterised by ^1H, ^{29}Si and ^{31}P NMR spectroscopy.

^1H NMR (500 MHz, C_6D_6) δ 7.09 (s, 13H, Ar), 7.00 (dd, *J* = 7.6, 1.5 Hz, 8H, Ar), 6.89 – 6.85 (m, 35H, Ar), 6.82 (s, 25H, Ar), 6.79 (s, 22H, Ar), 3.40 (q, *J* = 7.0 Hz, 77H, Et_2O), 2.36 (s, 12H, alk), 2.26 (d, *J* = 33.8 Hz, 14H, alk), 2.21 (s, 19H, alk), 2.20 (s, 25H, alk), 2.17 (s, 32H, alk), 2.08 (s, 63H, alk), 2.06 (d, *J* = 3.1 Hz, 94H, alk), 2.00 (s, 22H, alk), 1.87 (d, *J* = 3.1 Hz, 14H), 0.88 (t, *J* = 7.1 Hz, 121H, Et_2O), 0.39 (s, 220H), 0.28 (s, 51H), -1.09 (s, 50H, $SiMe_3$).

^{29}Si NMR (99 MHz, C_6D_6) δ 0.55 (s), -21.55 (s).

^{31}P NMR (202 MHz, C_6D_6) δ 160.79 (s), 136.27 (s), 70.61 (s), 68.72 (s).

The crude product of the above reaction was placed in a Schlenk with $LiAlH_4$ () and a stirrer bar. To these powders was added *circa* 50 mL of diethyl ether with vigorous stirring, resulting in a green-yellow suspension, which progressed to yellow-grey upon stirring overnight. This suspension was filtered, resulting in a white grey residue and a yellow solution. The solvent was removed *in vacuo* resulting in an off-white powder (547 mg) characterised by ^1H, ^{29}Si and ^{31}P NMR spectroscopy.

^1H NMR (500 MHz, C_6D_6) δ 7.24 (d, *J* = 7.6 Hz, 4H, Ar), 7.09 (t, *J* = 7.5 Hz, 6H, Ar), 7.00 (dd, *J* = 7.6, 1.7 Hz, 8H, Ar), 6.93 (dd, *J* = 7.6, 2.3 Hz, 8H, Ar), 6.88 (s, 19H, Ar), 6.85 (dd, *J* = 9.5, 2.0 Hz, 19H, Ar), 6.83 – 6.78 (m, 12H, Ar), 6.78 – 6.75 (m, 10H, Ar), 3.25 (d, *J* = 209.6 Hz, 155H, $Ter^{Mes}P\mathbf{H_2}$), 2.30 (d, *J* = 5.7 Hz, 9H, alk), 2.28 (s, 6H, alk), 2.23 (s, 11H, alk), 2.21 (s, 17H, alk), 2.20 (d, *J* = 2.8 Hz, 32H, alk), 2.18 (s, 6H, alk), 2.16 (s, 4H, alk), 2.14 (s, 7H, alk), 2.10 (s, 3H, alk), 2.07 (s, 61H, alk), 2.06 (s, 51H, alk), 2.05 (s, 8H, alk), 1.96 (s, 6H, alk), 1.93 (s, 4H, alk), 1.90 (s, 4H, alk), 1.89 (s, 4H, alk), 1.88 (s, 13H, alk), 1.83 (s, 6H, alk), 1.61 (s, 3H), 1.08 (s, 112H, $SiMe_3$ groups), 0.35 (d, *J* = 3.5 Hz, 75H, $SiMe_3$ groups), 0.31 – 0.23 (m, 349H, $SiMe_3$ groups).

^{29}Si NMR (99 MHz, C_6D_6) δ -21.86 (s).

^{31}P NMR (202 MHz, C_6D_6) δ -23.30 (s), -49.38 – -52.22 (m), -101.32 (d, *J* = 227.8 Hz), -147.31 (t, *J* = 209.7 Hz, $Ter^{Mes}PH_2$).

6.5.11 Reaction of $Ter^{Mes}PHK$ with UI_3

To a Schlenk charged with a stirrer bar and $Ter^{Mes}PH_2$ (200mg, 0.58 mmol) was added KN" (115 mg, 0.58 mmol). To these powders was added, with vigorous stirring, circa 30 mL of dry toluene, causing the formation of a green suspension. This suspension was stirred for two hours, whereupon a purple suspension of UI_3 (179 mg, 0.29 mmol) in DME was cannulated onto the green suspension, causing the formation of a grey suspension. This suspension was stirred overnight, then allow to settle and filtered. The resultant brown solution had its solvent removed in vacuo to leave a brown residue (218 mg).

^{1}H NMR (500 MHz, C_6D_6) δ 7.25 (t, *J* = 7.6 Hz, 8H, Ar), 7.04 (d, *J* = 7.3 Hz, 5H, Ar), 7.00 (dd, *J* = 4.5, 2.8 Hz, 13H, Ar), 6.99 (d, *J* = 1.7 Hz, 7H, Ar), 6.97 (d, *J* = 1.9 Hz, 4H, Ar), 6.95 (d, *J* = 1.9 Hz, 5H, Ar), 6.92 (s, 9H, Ar), 6.89 (s, 3H, Ar), 6.86 (s, 24H, Ar), 6.85 (s, 4H, Ar), 6.84 (s, 9H, Ar), 6.81 (d, *J* = 1.2 Hz, 2H, Ar), 6.80 (s, 2H, Ar), 6.78 (s, 2H, Ar), 6.76 (dd, *J* = 3.6, 1.8 Hz, 9H, Ar), 6.74 (s, 4H, Ar), 4.17 – 4.08 (m, 5H), 3.69 – 3.63 (m, 5H), 2.87 (s, 3H), 2.76 (s, 3H), 2.43 (s, 6H, alk), 2.25 (s, 6H, alk), 2.23 (s, 24H, alk), 2.20 (d, *J* = 4.3 Hz, 63H, alk), 2.18 (s, 10H, alk), 2.11 (d, *J* = 4.4 Hz, 15H, alk), 2.07 (s, 73H, alk), 2.04 (s, 29H, alk), 0.54 (q, *J* = 2.5 Hz, 119H), 0.50 (s, 7H), 0.47 (d, *J* = 1.2 Hz, 14H), 0.47 (s, 6H), 0.39 (s, 16H), 0.37 (s, 4H), 0.35 (s, 4H), 0.34 (s, 2H), 0.32 – 0.30 (m, 10H), 0.28 (s, 4H), 0.27 (s, 2H), 0.16 (s, 2H), 0.09 (s, 5H).

^{31}P NMR (202 MHz, C_6D_6) δ -64.13 (d, *J* = 220.8 Hz), -87.97 (d, *J* = 221.7 Hz), -101.32 (d, *J* = 226.6 Hz), -147.32 (t, *J* = 209.7 Hz), -149.68 – -151.46 (m).

6.5.12 Reaction of $Ter^{Trip}PHK$ with UI_3

To a Schlenk charged with a stirrer bar and $Ter^{Trip}PH_2$ (200mg, 0.39 mmol) was added KN" (78 mg, 0.39 mmol). To these powders was added, with vigorous stirring, circa 30 mL of dry toluene, causing the formation of a green-yellow suspension. This suspension was stirred for two hours, whereupon a purple suspension of UI_3 (120 mg, 0.19 mmol) in DME was cannulated onto the green suspension, causing the formation of a brown suspension. This suspension was stirred overnight, then allow to settle and filtered. The resultant brown solution had its solvent removed in vacuo to leave a brown residue (187 mg).

^{1}H NMR (500 MHz, C_6D_6) δ 7.25 (s, 23H), 7.24 (d, *J* = 1.4 Hz, 10H, Ar), 7.22 (s, 8H, Ar), 7.21 (s, 56H, Ar), 7.14 (s, 20H, Ar), 7.13 (s, 17H, Ar), 7.11 (s, 9H, Ar), 7.09 (s, 18H, Ar), 2.99 (dq, *J* = 20.7, 7.0 Hz, 94H, Isopropyl H), 2.86 (ddt, *J* = 25.6, 13.7, 6.9 Hz, 109H,

Isopropyl H), 1.45 (d, *J* = 6.9 Hz, 36H, alk), 1.38 (d, *J* = 6.9 Hz, 80H, alk), 1.29 (d, *J* = 7.0 Hz, 164H, alk), 1.28 (s, 17H, alk), 1.27 (d, *J* = 1.2 Hz, 29H, alk), 1.26 (s, 29H, alk), 1.20 (t, *J* = 7.1 Hz, 325H, alk), 1.17 (d, *J* = 6.8 Hz, 116H, alk), 1.14 (d, *J* = 6.8 Hz, 85H, alk), 0.47 (s, 40H), 0.46 (d, *J* = 1.9 Hz, 71H), 0.44 (s, 96H), 0.43 (s, 188H), 0.39 (s, 99H), 0.30 (s, 57H), 0.10 – 0.08 (m, 70H).

^{31}P NMR (202 MHz, C_6D_6) δ -71.38 (d, *J* = 221.5 Hz), -140.35 (t, *J* = 210.7 Hz).

6.5.13 Reaction of $Ter^{Trip}PHK$ with $U(BH_4)_3(THF)_2$

To a colourless solution of $Ter^{Trip}PH_2$**,** (20 mg, 0.039 mmol) in d_6-benzene (0.6 mL) in a Teflon-valved valve NMR tube was added KN" (7.8 mg, 0.039 mmol) causing the formation of a green suspension. To this green suspension was added $U(BH_4)_3(THF)_2$ (11.1 mg, 0.019 mmol) causing the formation of a black suspension.

^{1}H NMR (500 MHz, C_6D_6) δ 14.86 (s, 232H), 11.70 (s, 147H), 9.30 (s, 86H), 8.89 (s, 87H), 8.12 (s, 263H), 5.45 (s, 185H), 4.97 (s, 250H), 3.20 (d, *J* = 68.4 Hz, 1123H), 2.86 (s, 599H), 2.31 (s, 249H), 1.63 – 0.87 (m, 4082H), 0.46 (d, *J* = 67.6 Hz, 2932H), -0.58 (s, 85H), -0.76 (s, 46H), -1.09 (s, 81H), -2.69 (s, 74H), -3.22 (d, *J* = 78.2 Hz, 152H), -4.66 (s, 78H), -5.34 (s, 93H), -6.76 (s, 119H), -8.61 (s, 84H), -9.16 (s, 65H), -11.56 (s, 61H), -12.72 (s, 69H), -16.87 (s, 225H), -22.10 (s, 32H), -31.26 (s, 13H), -43.16 (s, 2H).

^{31}P NMR (202 MHz, C_6D_6) δ -140.38 (t, *J* = 211.2 Hz), -152.81 (dd, *J* = 219.8, 22.6 Hz).

6.5.14 Reaction of UCl_4 with $Ter^{Mes}OK$

To a Schlenk charged with a stirrer bar and $Ter^{Mes}OH$ (248 mg, 0.75 mmol) was added KN" (150 mg, 0.75 mmol). To these powders was added circa 40 mL of dry toluene, with vigorous stirring, causing the formation of a brown-green solution. After stirring for 6 hours, a pale green THF solution of UCl_4 (142 mg, 0.38 mmol) was added, causing the formation of a brown-orange suspension. This solution was stirred overnight, whereupon it was observed that a red-orange suspension had formed. This suspension was allowed to settle, then filtered to give a red solution. After the solvent was removed *in vacuo*, extraction with hexane allowed, upon standing a saturated solution at -30C, for the formation of dark black crystals suitable for X-ray crystallography, characterised as $U_4K_2Cl_8(\mu^3\text{-})O_2(Ter^{Mes}O)_6$, **5.3** (30 mg, 0.009 mmol, 10% yield). **5.3** was also characterised by ^{1}H NMR spectroscopy.

^{1}H NMR (400 MHz, C_6D_6) δ 39.86 (s, 1H), 39.66 (s, 19H), 34.85 (s, 237H), 33.00 (s, 1H), 25.74 (s, 105H), 19.00 (s, 294H), 14.52 (s, 2021H), 13.99 (s, 391H), 6.86 (s, 235H), -2.55 (s, 289H), -3.38 (s, 534H), -6.54 (s, 172H), -7.11 (s, 768H), -7.50 (s, 181H).

6.5.15 Reaction of $UI_4(dioxane)_2$ with $Ter^{Mes}OK$

To a Schlenk charged with a stirrer bar and $Ter^{Mes}OH$ (611 mg, 1.85 mmol) was added KH (74 mg, 1.85 mmol). To these powders was added circa 40 mL of dry toluene, with vigorous stirring, causing the formation of a brown-green suspension. After stirring for 4 hours, a red THF solution of $UI_4(dioxane)_2$ (852 mg, 0.92 mmol) was added causing the formation of a red suspension initially. After stirring for 48 hours a dark brown suspension, with copious amounts of a light coloured precipitate, was observed. This suspension was allowed to settle and then filtered to give a dark brown solution. The solvent was removed *in vacuo* to give a dark brown powder (684 mg) characterised by ^{1}H NMR spectroscopy.

^{1}H NMR (500 MHz, C_6D_6) δ 12.49 (s, 18H), 12.17 (s, 10H), 11.06 (d, *J* = 7.2 Hz, 10H), 10.55 (s, 6H), 9.28 (d, *J* = 8.0 Hz, 2H), 8.89 (s, 3H), 8.61 (d, *J* = 18.4 Hz, 2H), 7.26 (t, *J* = 7.6 Hz, 3H), 7.01 (dd, *J* = 7.6, 1.6 Hz, 4H), 6.87 (s, 7H), 6.77 (t, *J* = 1.5 Hz, 2H), 4.74 (s, 7H), 4.47 (s, 4H), 3.11 – 2.24 (m, 31H), 2.21 (d, *J* = 6.6 Hz, 11H), 2.08 (s, 23H), 0.88 (s, 51H), -1.83 (s, 9H), -5.81 (s, 10H), -7.13 (s, 43H).

6.5.16 Reaction of UI_3 with $Ter^{Mes}OK$

In a Schlenk charged with a stirrer bar and $Ter^{Mes}OH$ (300 mg, 0.91 mmol) was added KH (37 mg, 0.91 mmol). To these powders was added circa 40 mL of dry toluene, with vigorous stirring, causing the formation of a brown-green suspension. After 4 hours stirring, a purple THF solution of UI_3 (281 mg, 0.45 mmol) was cannulated onto this suspension, causing the instantaneous formation of a dark green suspension, which progressed to a yellow brown suspension upon stirring overnight. This suspension was filtered to give a brown solution and the solvent was removed *in vacuo* to leave a brown powder (281 mg) characterised by ^{1}H NMR spectroscopy.

^{1}H NMR (500 MHz, C_6D_6) δ 38.12 (s, 4H), 29.84 (s, 23H), 23.09 (s, 26H), 19.32 (s, 44H), 14.52 (s, 108H), 14.18 (s, 62H), 12.06 (d, *J* = 116.7 Hz, 173H), 11.95 (s, 58H), 11.05 (d, *J* = 7.2 Hz, 194H), 10.55 (s, 109H), 10.30 (s, 113H), 8.62 (s, 120H), 4.52 (s, 181H), 1.04 (d, *J* = 28.2 Hz, 115H), 0.86 (s, 277H), -1.04 (s, 102H), -1.85 (s, 114H), -2.43 (d, *J* = 31.3 Hz, 167H), -3.35 (s, 112H), -5.82 (s, 156H), -6.41 (s, 73H), -10.82 (s, 54H), -14.12 (s, 16H).

6.5.17 Reaction of $U(BH_4)_3(THF)_2$ with $Ter^{Mes}OK$

In a Schlenk charged with a stirrer bar and $Ter^{Mes}OH$ (270 mg, 0.82 mmol) was added KN" (163 mg, 0.82 mmol). To these powders was added circa 40 mL of dry toluene, with vigorous stirring, causing the formation of a brown-green suspension. After 4 hours stirring, this suspension was cannulated onto $U(BH_4)_3(THF)_2$ (233 mg, 0.4085), causing the formation of a brown suspension, which progressed to a yellow brown suspension upon stirring overnight. This suspension was filtered to give a brown solution and the solvent was removed *in vacuo* to leave a brown powder (378 mg) characterised by ^{1}H and ^{11}B NMR spectroscopy.

^{1}H NMR (500 MHz, C_6D_6) δ 20.15 (s, 7H), 15.89 (s, 43H), 15.45 (s, 3H), 11.37 (s, 6H), 11.07 (s, 6H), 9.42 (s, 10H), 8.96 (s, 17H), 8.05 (s, 12H), 7.64 (s, 45H), 7.01 (s, 15H), 6.88 (s, 10H), 6.70 (s, 31H), 2.85 (s, 113H), 2.17 (d, *J* = 29.0 Hz, 163H), 0.99 (d, *J* = 53.7 Hz, 194H), 0.20 (d, *J* = 95.6 Hz, 452H), -1.81 (s, 19H), -2.02 (s, 17H), -3.68 (s, 6H), -5.78 (s, 14H), -7.10 (s, 10H), -7.55 (s, 39H), -9.08 (s, 7H), -10.89 (s, 20H), -15.46 (s, 96H).

^{11}B NMR (160 MHz, C_6D_6) δ 172.14 (s), 142.92 (s), 109.85 (s), 82.40 (s), -9.01 (s), -26.47 (s), -34.85 (s), -57.21 (s).

6.5.18 Reaction of *in situ* generated $Ter^{Mes}Li$ with $ThCl_4(DME)_2$

In a Schlenk charged with a stirrer bar and $Ter^{Mes}I$ (400 mg, 0.91 mmol) was added *circa* 30 mL of THF forming a pale yellow solution. Added to this solution was a 1.6 M solution of $^{n}BuLi$ in hexanes (0.60mL, 0.96 mmol) at -95°C causing the observation of a darkening of the solution. Upon addition of this solution to a colourless THF solution of $ThCl_4(DME)_2$ (252 mg, 0.45 mmol) a yellow suspension was formed. The solution was filtered giving a yellow solution, which was dried under reduced pressure giving a colourless microcrystalline material (110 mg).

^{1}H NMR (400 MHz, C_6D_6) δ 7.26 (t, *J* = 7.5 Hz, 218H, Ar), 7.19 (d, *J* = 7.6 Hz, 55H, Ar), 7.12 (d, *J* = 7.5 Hz, 114H, Ar), 7.00 (d, *J* = 1.7 Hz, 196H, Ar), 6.98 (d, *J* = 1.7 Hz, 173H, Ar), 6.96 (d, *J* = 7.5 Hz, 133H, Ar), 6.88 (s, 226H, Ar), 6.88 – 6.87 (m, 465H, Ar), 6.87 (s, 177H, Ar), 6.87 – 6.85 (m, 708H, Ar), 6.85 (s, 170H, Ar), 6.75 (t, *J* = 1.5 Hz, 180H, Ar), 3.75 (ddd, *J* = 6.6, 4.2, 2.6 Hz, 1563H), 2.21 (d, *J* = 2.2 Hz, 2013H, alk), 2.20 (s, 370H, alk), 2.11 (d, *J* = 4.4 Hz, 760H, alk), 2.05 (d, *J* = 2.8 Hz, 3999H, alk), 1.59 – 1.38 (m, 1446H), 1.28 – 1.15 (m, 164H), 0.93 – 0.75 (m, 181H), 0.44 (t, *J* = 7.3 Hz, 177H), 0.29 (s, 252H), -0.43 (s, 12H).

6.5.19 Reaction of *in situ* generated $Ter^{Trip}Li$ with $ThCl_4(DME)_2$

In a Schlenk charged with a stirrer bar and $Ter^{Trip}I$ (237 mg, 0.39 mmol) was added *circa* 30 mL of THF forming a pale yellow solution. Added to this solution was a 1.6 M solution of $^{n}BuLi$ in hexanes (0.25mL, 0.39 mmol) at -95°C causing the observation of a darkening of the solution. Upon addition of this solution to a colourless THF solution of $ThCl_4(DME)_2$ (72 mg, 0.13 mmol) a yellow suspension was formed. The solution was filtered giving a yellow solution, which had its solvent removed *in vacuo*. Extraction with toluene allowed the isolation of crystalline material of X-ray quality, determined by X-ray crystallography to be $^{n}BuTer^{Trip}$**5.3**, and $ClTer^{Trip}$, **5.4.** (combined 60 mg, 0.12 mmol, ~30 % yield)

^{1}H NMR (400 MHz, C_6D_6) δ 7.22 – 7.20 (m, 1H, Ar), 7.19 (d, *J* = 0.9 Hz, 15H, Ar), 7.18 – 7.17 (m, 2H, Ar), 7.15 (s, 1H, Ar), 7.13 (s, 3H, Ar), 7.12 (dd, *J* = 1.4, 0.9 Hz, 9H, Ar), 7.10 (t, *J* = 1.5 Hz, 4H, Ar), 7.04 (q, *J* = 1.3 Hz, 4H, Ar), 7.02 – 7.00 (m, 5H, Ar), 3.82 – 3.69 (m, 17H, Isopropyl H), 2.97 – 2.71 (m, 46H, Isopropyl H), 1.40 (d, *J* = 6.9 Hz, 21H, alk), 1.34 – 1.30 (m, 26H, alk), 1.25 (d, *J* = 6.9 Hz, 45H, alk), 1.23 (d, *J* = 3.6 Hz, 29H, alk), 1.21 (d, *J* = 3.6 Hz, 23H, alk), 1.18 – 1.14 (m, 90H, alk), 1.12 (t, *J* = 6.6 Hz, 43H, alk), 0.85 – 0.65 (m, 6H), 0.44 (t, *J* = 7.3 Hz, 6H), 0.29 – 0.19 (m, 6H).

6.6 References

1. G. Sheldrick, *Acta Crystallogr., Sect. A*, 2008, 64, 112-122.
2. L. Palatinus and G. Chapuis, *J. Appl. Crystallogr.*, 2007, 40, 786-790.
3. L. Farrugia, *J. Appl. Crystallogr.*, 1999, 32, 837-838.
4. K. Ruhlandt-Senge, J. J. Ellison, R. J. Wehmschulte, F. Pauer and P. P. Power, *J. Am. Chem. Soc.*, 1993, 115, 11353-11357.
5. C. Stanciu, Marilyn M. Olmstead, Andrew D. Phillips, M. Stender and Philip P. Power, *Eur. J. Inorg. Chem.*, 2003, 2003, 3495-3500.
6. B. Schiemenz and P. P. Power, *Organometallics*, 1996, 15, 958-964.
7. D. A. Dickie, I. S. MacIntosh, D. D. Ino, Q. He, O. A. Labeodan, M. C. Jennings, G. Schatte, C. J. Walsby and J. A. C. Clyburne, *Can. J. Chem.*, 2008, 86, 20-31.
8. M. J. Monreal, R. K. Thomson, T. Cantat, N. E. Travia, B. L. Scott and J. L. Kiplinger, *Organometallics*, 2011, 30, 2031-2038.
9. P. L. Arnold, C. J. Stevens, J. H. Farnaby, M. G. Gardiner, G. S. Nichol and J. B. Love, *J. Am. Chem. Soc.*, 2014, 136, 10218-10221.
10. J. L. Kiplinger, D. E. Morris, B. L. Scott and C. J. Burns, *Organometallics*, 2002, 21, 5978-5982.
11. S. M. Mansell, B. F. Perandones and P. L. Arnold, *J. Organomet. Chem.*, 2010, 695, 2814-2821.
12. J. M. Lalancette, G. Rollin and P. Dumas, *Can. J. Chem.*, 1972, 50, 3058-3062.

13. M. W. Wallasch, D. Weismann, C. Riehn, S. Ambrus, G. Wolmershauser, A. Lagutschenkov, G. Niedner-Schatteburg and H. Sitzmann, *Organometallics*, 2010, 29, 806-813.
14. T. Cantat, B. L. Scott and J. L. Kiplinger, *Chem. Commun. (Cambridge, U. K.)*, 2010, 46, 919-921.
15. A. Dormond, B. A. A. El and C. Moise, *J. Chem. Soc., Chem. Commun.*, 1985, 914-916.
16. K. V. Baker, J. M. Brown, N. Hughes, A. J. Skarnulis and A. Sexton, *J. Org. Chem*, 1991, 56, 698-703.
17. M. Galajov, C. Garcia and M. Gomez, *Dalton Trans.*, 2011, 40, 413-420.

7. Appendix

7.1 Crystallography tables

7.1.1 $Th(OTer^{Mes})_2Cl_2(H_2O)_3$, **3.1**

Table 7.1 Experimental details

	p13142e : $Th(OTer^{Mes})_2Cl_2(H_2O)_3$
Crystal data	
Chemical formula	$C_{48}H_{56}Cl_2O_5Th$
M_r	1018.94
Crystal system, space group	Triclinic, *P*1
Temperature (K)	150
a, *b*, *c* (Å)	13.4867 (4), 13.5411 (5), 14.7266 (4)
α, β, γ (°)	75.834 (3), 82.172 (2), 73.219 (3)
V (Å^3)	2490.38 (14)
Z	2
Radiation type	Mo *K*α
μ (mm^{-1})	3.13
Crystal size (mm)	0.41 × 0.14 × 0.06
Data collection	
Diffractometer	Bruker *SMART APEX* CCD area detector diffractometer
Absorption correction	Multi-scan *CrysAlis PRO*, Agilent Technologies, Version 1.171.36.24 (release 03-12-2012 CrysAlis171 .NET) (compiled Dec 3 2012,18:21:49) Empirical absorption correction using spherical harmonics, implemented in SCALE3 ABSPACK scaling algorithm.
T_{min}, T_{max}	0.687, 1.000
No. of measured, independent and observed [$I > 2\sigma(I)$] reflections	34798, 10167, 8974
R_{int}	0.047
$(\sin\theta/\lambda)_{max}$ (Å^{-1})	0.625
Refinement	
$R[F^2 > 2\sigma(F^2)]$, $wR(F^2)$, *S*	0.051, 0.159, 1.08

No. of reflections	10167
No. of parameters	515
H-atom treatment	H atoms treated by a mixture of independent and constrained refinement $w = 1/[\sigma^2(F_o^2) + (0.0878P)^2 + 17.0208P]$ where $P = (F_o^2 + 2F_c^2)/3$
$\Delta\rho_{max}$, $\Delta\rho_{min}$ (e Å^{-3})	4.14, −1.25

Computer programs: *CrysAlis PRO*, Agilent Technologies, Version 1.171.35.19 (release 27-10-2011 CrysAlis171 .NET) (compiled Oct 27 2011,15:02:11), *SIR92* (Giacovazzo, 1994), *SHELXL2014* (Sheldrick, 2014), *ORTEP* (Farrrugia, 1997), *Mercury*.

In the crystal structure refinement of **3.1**, using SHELX's software package, the DFIX restraint was required in order to place the hydrogen atoms bonded to the water molecules ligated to the thorium centre. They were placed geometrically from residual electron density surrounding the oxygen atoms and then fixed to a bond distance consistent with O-H distances for water molecules. **REF**

7.1.2 $Th(OTer^{Mes})_2Cl_2DME$, **3.2**

Table 7.2 . Experimental details

	P13181: $Th(OTer^{Mes})_2Cl_2DME$
Crystal data	
Chemical formula	$C_{52}H_{60}Cl_2O_4Th{\cdot}4(C_7H_8)$
M_r	1420.47
Crystal system, space group	Monoclinic, *C*2/*c*
Temperature (K)	170
a, *b*, *c* (Å)	18.6655 (8), 21.3909 (9), 19.2081 (10)
β (°)	109.480 (5)
V (Å^3)	7230.2 (6)
Z	4
Radiation type	Mo *K*α
μ (mm^{-1})	2.18
Crystal size (mm)	1.05 × 0.73 × 0.54
Data collection	
Diffractometer	Xcalibur, Eos diffractometer
Absorption correction	Analytical *CrysAlis PRO*, Agilent Technologies, Version 1.171.35.19 (release 27-10-2011 CrysAlis171 .NET) (compiled Oct 27 2011,15:02:11) Analytical numeric absorption correction using a multifaceted crystal model based on expressions derived by R.C. Clark & J.S. Reid. (Clark, R. C. & Reid, J. S. (1995). Acta Cryst. A51, 887-897)
T_{min}, T_{max}	0.663, 0.778

No. of measured, independent and observed [$I > 2\sigma(I)$] reflections	34187, 8282, 6690
R_{int}	0.059
$(\sin\theta/\lambda)_{max}$ (Å^{-1})	0.649

Refinement	
$R[F^2 > 2\sigma(F^2)]$, $wR(F^2)$, S	0.048, 0.122, 1.10
No. of reflections	8282
No. of parameters	378
No. of restraints	59
H-atom treatment	H-atom parameters constrained
$\Delta\rho_{max}$, $\Delta\rho_{min}$ (e Å^{-3})	1.70, −0.88

Computer programs: *CrysAlis PRO*, Agilent Technologies, Version 1.171.35.19 (release 27-10-2011 CrysAlis171 .NET) (compiled Oct 27 2011,15:02:11), *SIR92* (Giacovazzo, 1994), *SHELXL2014* (Sheldrick, 2014), *ORTEP* (Farrrugia, 1997), *Mercury*.

Crystallisation of **3.2**, from a saturated toluene solution gave crystals in the monoclinic lattice system of space group C2/c. In the crystal structure refinement of **3.2**, using SHELX's software package, restraints were required in order to model successfully the diffraction data. The co-crystallised toluene molecules, not shown in **Figure 3.2**, required the SIMU and DELU restraints to improve the shape and directionality of the thermal ellipsoids. The toluene molecules also required the AFIX 66 command to model the disorder of the phenyl ring. . The toluene methyl groups of C28 and C35 were restrained by the DFIX command in order to prevent the bond length to the aromatic ring being modelled as too long for a bond to be reasonably seen as a bonding interaction within the model.

7.1.3 $[(THF)K(\mu^2\text{- }OTer^{Mes})]_2$, **3.3**

Table 7.3 Experimental details

	p13046: $[(THF)K(\mu^2\text{- }OTer^{Mes})]_2$
Crystal data	
Chemical formula	$C_{112}H_{132}K_4O_8$
M_r	1762.58
Crystal system, space group	Monoclinic, $P2_1/n$
Temperature (K)	150
a, b, c (Å)	12.4809 (4), 24.3846 (7), 17.1033 (7)
β (°)	105.060 (4)
V (Å^3)	5026.5 (3)
Z	2

Radiation type	Mo *K*α
μ (mm^{-1})	0.23
Crystal size (mm)	0.85 × 0.21 × 0.11

Data collection	
Diffractometer	BRUKER *SMART APEX* CCD area detector diffractometer
Absorption correction	Multi-scan
T_{min}, T_{max}	0.821, 1.000
No. of measured, independent and observed [$I > 2\sigma(I)$] reflections	36383, 8261, 6026
R_{int}	0.038
$(\sin\theta/\lambda)_{max}$ ($Å^{-1}$)	0.581

Refinement	
$R[F^2 > 2\sigma(F^2)]$, $wR(F^2)$, S	0.066, 0.182, 1.03
No. of reflections	8261
No. of parameters	559
H-atom treatment	H atoms treated by a mixture of independent and constrained refinement
$\Delta\rho_{max}$, $\Delta\rho_{min}$ (e $Å^{-3}$)	0.66, −0.44

Computer programs: *CrysAlis PRO*, Agilent Technologies, Version 1.171.35.19 (release 27-10-2011 CrysAlis171 .NET) (compiled Oct 27 2011,15:02:11), *SIR92* (Giacovazzo, 1994), *SHELXL2014* (Sheldrick, 2014), *ORTEP* (Farrrugia, 1997), *Mercury*.

Crystallisation of **3.3**, from a saturated hexane solution gave crystals in the monoclinic lattice system of space group P2(1)/n. No special restraints were required in the crystal structure refinement of **3.3**.

7.1.4 $[(THF)Li(\mu^2\text{-}OTer^{Mes})]_2$, **3.4**

Table 7.4 Experimental details

	p13068 : $[(THF)Li(\mu^2\text{-}OTer^{Mes})]_2$,
Crystal data	
Chemical formula	$C_{56}H_{66}Li_2O_4$
M_r	816.84
Crystal system, space group	Monoclinic, $P2_1/n$
Temperature (K)	150
a, b, c (Å)	11.4195 (7), 29.5610 (17), 14.6652 (10)
β (°)	102.789 (6)

V (Å^3)	4827.7 (5)
Z	32
Radiation type	Mo $K\alpha$
μ (mm^{-1})	0.07
Crystal size (mm)	1.03 × 0.11 × 0.05

Data collection	
Diffractometer	BRUKER *SMART APEX* CCD area detector diffractometer
Absorption correction	Multi-scan
T_{min}, T_{max}	0.854, 1.000
No. of measured, independent and observed [$I > 2\sigma(I)$] reflections	35942, 12413, 5050
R_{int}	0.089
$(\sin\theta/\lambda)_{max}$ (Å^{-1})	0.704

Refinement	
$R[F^2 > 2\sigma(F^2)]$, $wR(F^2)$, S	0.106, 0.267, 1.02
No. of reflections	12413
No. of parameters	559
H-atom treatment	H atoms treated by a mixture of independent and constrained refinement
$\Delta\rho_{max}$, $\Delta\rho_{min}$ (e Å^{-3})	0.37, −0.32

Computer programs: *CrysAlis PRO*, Agilent Technologies, Version 1.171.35.19 (release 27-10-2011 CrysAlis171 .NET) (compiled Oct 27 2011,15:02:11), *SIR92* (Giacovazzo, 1994), *SHELXL2014* (Sheldrick, 2014), *ORTEP* (Farrrugia, 1997), *Mercury*.

Crystallisation of **3.4**, from a saturated hexane solution produced crystals of the monoclinic lattice system of space group P2(1)/n. No special restraints were required in the crystal structure refinement of **3.4**.

7.1.5 μ^3-(Ter^{Mes}O)μ^3-$(CH_2SiMe_3)_3Li_4$, **3.5**

Table 7.5 Experimental details

	po4002_refinalized: μ^3-(Ter^{Mes}O)μ^3-$(CH_2SiMe_3)_3Li_4$
Crystal data	
Chemical formula	$C_{56}H_{58}Li_4O_2Si_3$
M_r	618.85
Crystal system, space group	Triclinic, $P\bar{1}$
Temperature (K)	150

a, *b*, *c* (Å)	10.4560 (2), 11.3391 (3), 19.2701 (5)
α, β, γ (°)	73.008 (2), 86.871 (2), 65.844 (2)
V (Å^3)	1988.09 (8)
Z	2
Radiation type	Mo *K*α
μ (mm^{-1})	0.14
Crystal size (mm)	0.40 × 0.25 × 0.19

Data collection	
Diffractometer	SuperNova (Mo) X-ray Source diffractometer
Absorption correction	Gaussian
T_{min}, T_{max}	0.603, 0.739
No. of measured, independent and observed [$I > 2\sigma(I)$] reflections	84464, 12131, 10063
R_{int}	0.042
$(\sin\theta/\lambda)_{max}$ (Å^{-1})	0.729

Refinement	
$R[F^2 > 2\sigma(F^2)]$, $wR(F^2)$, S	0.064, 0.165, 1.05
No. of reflections	12131
No. of parameters	434
H-atom treatment	H atoms treated by a mixture of independent and constrained refinement
$\Delta\rho_{max}$, $\Delta\rho_{min}$ (e Å^{-3})	1.12, −0.70

Computer programs: *CrysAlis PRO*, Agilent Technologies, Version 1.171.35.19 (release 27-10-2011 CrysAlis171 .NET) (compiled Oct 27 2011,15:02:11), *SIR92* (Giacovazzo, 1994), *SHELXL2014* (Sheldrick, 2014), *ORTEP* (Farrrugia, 1997), *Mercury*.

Crystallisation of **3.5**, from a saturated hexane solution produced crystals of the triclinic lattice system of space group P-1. Restraints were required, using SHELX's software package, to prevent the model indicating that there were bonds between Li3 and C32 and Li4 and C36 by use of the FREE command. The solid state structure of **3.5** consists of a central Li_4 tetrahedral, with the three neosilyl and one terphenolate ligand capping each face of the tetrahedral, thus binding to 3 separate lithium atoms in the cluster. Two of the neosilyl ligands participate in agnostic interactions between one of the C-H bonds of the TMS groups and a neighbouring lithium cation.

7.1.6 $LiAlH_2(\mu^2\text{-}OTer^{Mes})_2$, **3.6**

Table 7.6 Experimental details

p13074a: $LiAlH_2(\mu^2\text{-}OTer^{Mes})_2$

Crystal data	
Chemical formula	$C_{48}H_{52}AlLiO_2$
M_r	694.82
Crystal system, space group	Monoclinic, $P2_1/c$
Temperature (K)	150
a, b, c (Å)	10.7789 (3), 15.3337 (5), 24.7207 (7)
β (°)	95.320 (2)
V (Å^3)	4068.2 (2)
Z	4
Radiation type	Mo $K\alpha$
μ (mm^{-1})	0.09
Crystal size (mm)	0.90 × 0.15 × 0.11

Data collection	
Diffractometer	BRUKER *SMART APEX* CCD area detector diffractometer
Absorption correction	Multi-scan
T_{min}, T_{max}	0.866, 1.000
No. of measured, independent and observed [$I > 2\sigma(I)$] reflections	45684, 10829, 7391
R_{int}	0.040
$(\sin\theta/\lambda)_{max}$ (Å^{-1})	0.706

Refinement	
$R[F^2 > 2\sigma(F^2)]$, $wR(F^2)$, S	0.057, 0.143, 1.02
No. of reflections	10829
No. of parameters	489
H-atom treatment	H atoms treated by a mixture of independent and constrained refinement
$\Delta\rho_{max}$, $\Delta\rho_{min}$ (e Å^{-3})	0.38, −0.26

Computer programs: *CrysAlis PRO*, Agilent Technologies, Version 1.171.35.19 (release 27-10-2011 CrysAlis171 .NET) (compiled Oct 27 2011,15:02:11), *SIR92* (Giacovazzo, 1994), *SHELXL2014* (Sheldrick, 2014), *ORTEP* (Farrrugia, 1997), *Mercury*.

Crystallisation of **3.6**, from a saturated hexane solution resulted in crystals in the monoclinic lattice system of space group P2(1)/c. No special restraints were required in the crystal structure refinement of **3.6**.

7.1.7 $MgCl(OTer^{Mes})(THF)_2$, **3.7**

Table 7.7 Experimental details

P13175a : $MgCl(OTer^{Mes})(THF)_2$

Crystal data	
Chemical formula	$C_{32}H_{41}ClMgO_3$
M_r	533.41
Crystal system, space group	Orthorhombic, $Cmc2_1$
Temperature (K)	170
a, b, c (Å)	17.382 (3), 15.6925 (16), 11.9522 (19)
V (Å^3)	3260.2 (8)
Z	4
Radiation type	Mo $K\alpha$
μ (mm^{-1})	0.16
Crystal size (mm)	0.99 × 0.65 × 0.43

Data collection	
Diffractometer	Xcalibur, Eos diffractometer
Absorption correction	Multi-scan
T_{min}, T_{max}	0.300, 1.000
No. of measured, independent and observed [$I > 2\sigma(I)$] reflections	9723, 2244, 1654
R_{int}	0.081
θ_{max} (°)	22.7
$(\sin\theta/\lambda)_{max}$ (Å^{-1})	0.543

Refinement	
$R[F^2 > 2\sigma(F^2)]$, $wR(F^2)$, S	0.124, 0.338, 1.30
No. of reflections	2244
No. of parameters	179
No. of restraints	37
H-atom treatment	H-atom parameters constrained
$\Delta\rho_{max}$, $\Delta\rho_{min}$ (e Å^{-3})	0.68, −0.51
Absolute structure	Flack x determined using 623 quotients [(I+)-(I-)]/[(I+)+(I-)] (Parsons, Flack and Wagner, Acta Cryst. B69 (2013) 249-259).
Absolute structure parameter	0.44 (7)

Computer programs: *CrysAlis PRO*, Agilent Technologies, Version 1.171.35.19 (release 27-10-2011 CrysAlis171 .NET) (compiled Oct 27 2011,15:02:11), *SIR92* (Giacovazzo, 1994), *SHELXL2014* (Sheldrick, 2014), *ORTEP* (Farrrugia, 1997), *Mercury*.

Crystallisation of **3.7**, from a saturated deuterated benzene solution resulted in crystals of lattice system orthorhombic of space group Cmc21. In the crystal structure refinement of **3.7**, modelling the disorder in the ligating THF molecules required use of the DANG, SIMU and RIGU restraints, using SHELX's software package.

7.1.8 $MgBr(OTer^{Mes})(THF)_2$, **3.8**

Table 7.8 Experimental details

	PO4024: $MgBr(OTer^{Mes})(THF)_2$
Crystal data	
Chemical formula	$C_{32}H_{41}BrMgO_3$
M_r	577.87
Crystal system, space group	Monoclinic, $P2_1/c$
Temperature (K)	120
a, b, c (Å)	14.8944 (1), 8.5838 (1), 23.6604 (2)
β (°)	97.949 (1)
V (Å^3)	2995.93 (5)
Z	4
Radiation type	Mo $K\alpha$
μ (mm^{-1})	1.42
Crystal size (mm)	0.16 × 0.08 × 0.08
Data collection	
Diffractometer	SuperNova (Cu) X-ray Source diffractometer
Absorption correction	Gaussian *CrysAlis PRO*, Agilent Technologies, Version 1.171.37.31 (release 14-01-2014 CrysAlis171 .NET) (compiled Jan 14 2014,18:38:05) Numerical absorption correction based on gaussian integration over a multifaceted crystal model Empirical absorption correction using spherical harmonics, implemented in SCALE3 ABSPACK scaling algorithm.
T_{min}, T_{max}	0.921, 0.959
No. of measured, independent and observed [$I > 2\sigma(I)$] reflections	47916, 6256, 5704
R_{int}	0.036
$(\sin\theta/\lambda)_{max}$ (Å^{-1})	0.630
Refinement	

$R[F^2 > 2\sigma(F^2)]$, $wR(F^2)$, S	0.043, 0.120, 1.02
No. of reflections	6256
No. of parameters	340
H-atom treatment	H-atom parameters constrained
$\Delta\rho_{max}$, $\Delta\rho_{min}$ (e Å^{-3})	1.19, −0.82

Computer programs: *CrysAlis PRO*, Agilent Technologies, Version 1.171.37.31 (release 14-01-2014 CrysAlis171 .NET) (compiled Jan 14 2014,18:38:05), *SIR92* (Giacovazzo, 1994), *SHELXL2014* (Sheldrick, 2014), *ORTEP* (Farrrugia, 1997), *Mercury*.

Crystallisation of **3.8**, from a saturated toluene solution resulted in crystals of the monoclinic lattice system, within the space group P121/C1. No special restraints were required in the crystal structure refinement of **3.8**.

7.1.9 $Fe(OTer^{Mes})_2(py)_2$, **3.9**

Table 7.9 Experimental details

	P15001a: $Fe(OTer^{Mes})_2(py)_2$
Crystal data	
Chemical formula	$C_{58}H_{60}FeN_2O_2$
M_r	872.93
Crystal system, space group	Orthorhombic, *Pbca*
Temperature (K)	170
a, b, c (Å)	22.4008 (12), 16.2106 (7), 25.8660 (14)
V (Å^3)	9392.7 (8)
Z	8
Radiation type	Mo $K\alpha$
μ (mm^{-1})	0.37
Crystal size (mm)	0.52 × 0.17 × 0.13
Data collection	
Diffractometer	Xcalibur, Eos diffractometer
Absorption correction	Analytical *CrysAlis PRO*, Agilent Technologies, Version 1.171.37.34 (release 22-05-2014 CrysAlis171 .NET) (compiled May 22 2014,16:03:01) Analytical numeric absorption correction using a multifaceted crystal model based on expressions derived by R.C. Clark & J.S. Reid. (Clark, R. C. & Reid, J. S. (1995). Acta Cryst. A51, 887-897) Empirical absorption correction using spherical harmonics, implemented in SCALE3 ABSPACK scaling algorithm.
T_{min}, T_{max}	0.939, 0.980

No. of measured, independent and observed [$I > 2\sigma(I)$] reflections	112113, 4921, 3611
R_{int}	0.238
θ_{max} (°)	20.9
$(\sin\theta/\lambda)_{max}$ (Å^{-1})	0.501

Refinement	
$R[F^2 > 2\sigma(F^2)]$, $wR(F^2)$, S	0.070, 0.124, 1.06
No. of reflections	4921
No. of parameters	580
H-atom treatment	H-atom parameters constrained
	$w = 1/[\sigma^2(F_o^2) + (0.0318P)^2 + 18.188P]$ where $P = (F_o^2 + 2F_c^2)/3$
$\Delta\rho_{max}$, $\Delta\rho_{min}$ (e Å^{-3})	0.29, −0.31

Computer programs: *CrysAlis PRO*, Agilent Technologies, Version 1.171.37.34 (release 22-05-2014 CrysAlis171 .NET) (compiled May 22 2014,16:03:01), *SIR92* (Giacovazzo, 1994), *SHELXL2014* (Sheldrick, 2014), *ORTEP* (Farrrugia, 1997), *Mercury*.

Crystallisation of **3.9**, from a saturated hexane solution resulted in crystals of the orthorhombic lattice system in space group Pbca. No special restraints were required in the crystal structure refinement of **3.9**.

7.1.10 $Li_2(OTer^{Mes})_2(THF)$, **3.10**

Table 7.10 Experimental details

	P15101b: $Li_2(OTer^{Mes})_2(THF)$
Crystal data	
Chemical formula	$C_{52}H_{58}Li_2O_3$
M_r	744.86
Crystal system, space group	Orthorhombic, $P2_12_12_1$
Temperature (K)	170
a, b, c (Å)	13.0681 (3), 16.7992 (4), 20.2557 (4)
V (Å^3)	4446.81 (17)
Z	4
Radiation type	Mo $K\alpha$
μ (mm^{-1})	0.07
Crystal size (mm)	0.36 × 0.24 × 0.13

Data collection	
Diffractometer	Xcalibur, Eos diffractometer
Absorption correction	Multi-scan
T_{min}, T_{max}	0.824, 1.000
No. of measured, independent and observed [$I > 2\sigma(I)$] reflections	85052, 7843, 5819
R_{int}	0.079
$(\sin\theta/\lambda)_{max}$ (Å^{-1})	0.595

Refinement	
$R[F^2 > 2\sigma(F^2)]$, $wR(F^2)$, S	0.053, 0.119, 1.03
No. of reflections	7843
No. of parameters	526
No. of restraints	33
H-atom treatment	H-atom parameters constrained
$\Delta\rho_{max}$, $\Delta\rho_{min}$ (e Å^{-3})	0.20, −0.20
Absolute structure	Flack x determined using 2058 quotients [(I+)-(I-)]/[(I+)+(I-)] (Parsons, Flack and Wagner, Acta Cryst. B69 (2013) 249-259).
Absolute structure parameter	−0.5 (5)

Computer programs: *CrysAlis PRO*, Agilent Technologies, Version 1.171.37.34 (release 22-05-2014 CrysAlis171 .NET) (compiled May 22 2014,16:03:01), *SIR92* (Giacovazzo, 1994), *SHELXL2014* (Sheldrick, 2014), *ORTEP* (Farrrugia, 1997), *Mercury*.

Crystallisation of **3.10**, from a saturated hexane solution resulted in crystals of the orthorhombic lattice system in space group P212121. Restraints were required in the crystal structure refinement of **3.10**, using SHELX's software package. The SIMU and RIGU restraints were applied to the carbon atoms of the ligated THF molecule to model its disorder.

7.1.11 [$MgTh_2\mu^2$-$Cl_2\mu^3$-$Cl(OTer^{Mes})_2(C_4H_7)_2\mu$-$\eta^3$:$\eta^3(C_4H_7)H$], **3.11**

Table 7.11 Experimental details

	PO4007: [$MgTh_2\mu^2$-$Cl_2\mu^3$-$Cl(OTer^{Mes})_2(C_4H_7)_2\mu$-$\eta^3$:$\eta^3(C_4H_7)H$]
Crystal data	
Chemical formula	$C_{68}H_{87}Cl_3MgO_4Th_2$
M_r	1563.11
Crystal system, space group	Monoclinic, $P2_1/m$
Temperature (K)	120
a, b, c (Å)	10.8049 (1), 20.0197 (1), 16.7218 (1)

β (°)	92.390 (1)
V (Å^3)	3613.96 (4)
Z	2
Radiation type	Cu $K\alpha$
μ (mm^{-1})	14.59
Crystal size (mm)	0.16 × 0.12 × 0.05

Data collection	
Diffractometer	SuperNova, Dual, Cu at zero, Atlas diffractometer
Absorption correction	Gaussian *CrysAlis PRO*, Agilent Technologies, Version 1.171.37.31 (release 14-01-2014 CrysAlis171 .NET) (compiled Jan 14 2014,18:38:05) Numerical absorption correction based on gaussian integration over a multifaceted crystal model Empirical absorption correction using spherical harmonics, implemented in SCALE3 ABSPACK scaling algorithm.
T_{min}, T_{max}	0.964, 0.984
No. of measured, independent and observed [$I > 2\sigma(I)$] reflections	135421, 7774, 7318
R_{int}	0.054
$(\sin\theta/\lambda)_{max}$ (Å^{-1})	0.630

Refinement	
$R[F^2 > 2\sigma(F^2)]$, $wR(F^2)$, S	0.040, 0.104, 1.13
No. of reflections	7774
No. of parameters	373
No. of restraints	652
H-atom treatment	H atoms treated by a mixture of independent and constrained refinement
	$w = 1/[\sigma^2(F_o^2) + (0.0483P)^2 + 11.5841P]$ where $P = (F_o^2 + 2F_c^2)/3$
$\Delta\rho_{max}$, $\Delta\rho_{min}$ (e Å^{-3})	2.18, −1.38

Computer programs: *CrysAlis PRO*, Agilent Technologies, Version 1.171.37.31 (release 14-01-2014 CrysAlis171 .NET) (compiled Jan 14 2014,18:38:05), *SIR92* (Giacovazzo, 1994), *SHELXL2014* (Sheldrick, 2014), *ORTEP* (Farrrugia, 1997), *Mercury*.

Crystallisation of **3.11**, from a saturated hexane solution resulted in crystals of the monoclinic lattice system in space group P_12_1/m_1. Using the SHELX software package, modelling of the methine type carbon C27, required the DFIX restraint in order to prevent the modelled hydrogen atom from adopting positions that were too close to other atoms. The squeeze

algorithm was required to be used in order to remove the residual electron density of 103 electrons assigned to be highly disordered hexane molecule within the crystal lattice.

7.1.12 $Mg(OTer^{Mes})_2(THF)_2$, **3.12**

Table 7.12 Experimental details

	P14057c: $Mg(OTer^{Mes})_2(THF)_2$
Crystal data	
Chemical formula	$C_{56}H_{66}MgO_4$
M_r	827.39
Crystal system, space group	Monoclinic, $P2_1/c$
Temperature (K)	170
a, b, c (Å)	11.6286 (7), 16.5829 (9), 25.5957 (13)
β (°)	101.067 (5)
V (Å^3)	4844.0 (5)
Z	4
Radiation type	Mo $K\alpha$
μ (mm^{-1})	0.08
Crystal size (mm)	0.48 × 0.41 × 0.06
Data collection	
Diffractometer	Xcalibur, Eos diffractometer
Absorption correction	Multi-scan *CrysAlis PRO*, Agilent Technologies, Version 1.171.36.24 (release 03-12-2012 CrysAlis171 .NET) (compiled Dec 3 2012,18:21:49) Empirical absorption correction using spherical harmonics, implemented in SCALE3 ABSPACK scaling algorithm.
T_{min}, T_{max}	0.728, 1.000
No. of measured, independent and observed [$I > 2\sigma(I)$] reflections	26510, 11092, 5900
R_{int}	0.041
$(\sin\theta/\lambda)_{max}$ (Å^{-1})	0.649
Refinement	
$R[F^2 > 2\sigma(F^2)]$, $wR(F^2)$, S	0.070, 0.189, 1.02
No. of reflections	11092
No. of parameters	562

H-atom treatment	H-atom parameters constrained
$(\Delta/\sigma)_{max}$	0.177
$\Delta\rho_{max}$, $\Delta\rho_{min}$ (e Å^{-3})	0.55, −0.36

Computer programs: *CrysAlis PRO*, Agilent Technologies, Version 1.171.36.24 (release 03-12-2012 CrysAlis171 .NET) (compiled Dec 3 2012,18:21:49), *SIR92* (Giacovazzo, 1994), *SHELXL2014* (Sheldrick, 2014), *ORTEP* (Farrrugia, 1997), *Mercury*.

Crystallisation of **3.12**, from a saturated hexane solution resulted in crystals of the monoclinic lattice system, in space group $P2_1/c$. No special restraints were required in the crystal structure refinement of **3.12**.

7.1.13 $[Th(OTer^{Mes})_2(Cl)_2(4,4'\text{-bipyridyl})_{1.5}]_\infty$, **3.13**

Table 7.13 Experimental details

	P14089b: $[Th(OTer^{Mes})_2(Cl)_2(4,4'\text{-bipyridyl})_{1.5}]_\infty$,
Crystal data	
Chemical formula	$C_{88.35}H_{83.35}Cl_2N_7O_2Th$
M_r	1578.18
Crystal system, space group	Triclinic, *P*1
Temperature (K)	170
a, *b*, *c* (Å)	13.342 (5), 14.040 (5), 23.743 (5)
α, β, γ (°)	95.480 (5), 104.752 (5), 110.128 (5)
V (Å^3)	3955 (2)
Z	2
Radiation type	Mo *K*α
μ (mm^{-1})	2.00
Crystal size (mm)	0.52 × 0.05 × 0.04
Data collection	
Diffractometer	Xcalibur, Eos diffractometer
Absorption correction	Multi-scan *CrysAlis PRO*, Agilent Technologies, Version 1.171.36.24 (release 03-12-2012 CrysAlis171 .NET) (compiled Dec 3 2012,18:21:49) Empirical absorption correction using spherical harmonics, implemented in SCALE3 ABSPACK scaling algorithm.
T_{min}, T_{max}	0.774, 1.000
No. of measured, independent and observed [$I > 2\sigma(I)$] reflections	46423, 18134, 13670
R_{int}	0.050

$(\sin\theta/\lambda)_{max}$ (Å^{-1})	0.649

Refinement	
$R[F^2 > 2\sigma(F^2)]$, $wR(F^2)$, S	0.049, 0.124, 1.00
No. of reflections	18134
No. of parameters	886
No. of restraints	215
H-atom treatment	H atoms treated by a mixture of independent and constrained refinement
$\Delta\rho_{max}$, $\Delta\rho_{min}$ (e Å^{-3})	1.61, −1.18

Computer programs: *CrysAlis PRO*, Agilent Technologies, Version 1.171.36.24 (release 03-12-2012 CrysAlis171 .NET) (compiled Dec 3 2012,18:21:49), *SIR92* (Siemans, 1995), *SHELXL2014* (Sheldrick, 2014), *ORTEP* (Farrugia, 1997), *enCIFer* (Allen *et al.*, 2004).

Crystallisation of **3.13** from a saturated perdeuterated benzene solution afforded single crystals of the triclinic lattice system, in space group P-1. Using the SHELX software package, the AFIX 66, SIMU and RIGU restraints were required in modelling the disorder of lattice bipyridine molecules.

7.1.14 [Th(OTerMes)$_2$((μ-H)$_3$BH)$_2$(DME)], **4.1**

Table 7.14 Experimental details

	PO4019: [Th(OTerMes)$_2$((μ-H)$_3$BH)$_2$(DME)]
Crystal data	
Chemical formula	$C_{52}H_{68}B_2O_4Th\cdot C_7H_8$
M_r	1102.85
Crystal system, space group	Triclinic, *P*1
Temperature (K)	120
a, *b*, *c* (Å)	8.3108 (2), 12.9109 (3), 12.9173 (2)
α, β, γ (°)	99.860 (2), 98.224 (2), 98.203 (2)
V (Å^3)	1331.50 (5)
Z	1
Radiation type	Cu *K*α
μ (mm^{-1})	9.36
Crystal size (mm)	0.08 × 0.04 × 0.02
Data collection	
Diffractometer	SuperNova (Cu) X-ray Source diffractometer
Absorption correction	Gaussian *CrysAlis PRO*, Agilent Technologies, Version 1.171.37.31 (release 14-01-2014

	CrysAlis171 .NET) (compiled Jan 14 2014,18:38:05) Numerical absorption correction based on gaussian integration over a multifaceted crystal model Empirical absorption correction using spherical harmonics, implemented in SCALE3 ABSPACK scaling algorithm.
T_{min}, T_{max}	0.584, 0.822
No. of measured, independent and observed [$I > 2\sigma(I)$] reflections	22296, 8365, 8360
R_{int}	0.041
$(\sin\theta/\lambda)_{max}$ (Å^{-1})	0.630

Refinement	
$R[F^2 > 2\sigma(F^2)]$, $wR(F^2)$, S	0.027, 0.064, 1.08
No. of reflections	8365
No. of parameters	644
No. of restraints	28
H-atom treatment	H atoms treated by a mixture of independent and constrained refinement
$\Delta\rho_{max}$, $\Delta\rho_{min}$ (e Å^{-3})	2.27, −1.55
Absolute structure	Flack x determined using 2821 quotients [(I+)-(I-)]/[(I+)+(I-)] (Parsons, Flack and Wagner, Acta Cryst. B69 (2013) 249-259).
Absolute structure parameter	−0.009 (6)

Computer programs: *CrysAlis PRO*, Agilent Technologies, Version 1.171.37.31 (release 14-01-2014 CrysAlis171 .NET) (compiled Jan 14 2014,18:38:05), *SIR92* (Siemans, 1995), *SHELXL2014* (Sheldrick, 2014), *ORTEP* (Farrugia, 1997), *enCIFer* (Allen *et al.*, 2004).

7.1.15 $Th(OTer^{Mes})_2((\mu\text{-}H)_3BH)_2$, **4.2**

Table 7.15 Experimental details

	P14028d: $Th(OTer^{Mes})_2((\mu\text{-}H)_3BH)_2$
Crystal data	
Chemical formula	$C_{48}H_{50}B_2O_2Th$
M_r	912.54
Crystal system, space group	Monoclinic, $P2_1/n$
Temperature (K)	170
a, b, c (Å)	22.1631 (18), 21.5236 (13), 10.9028 (8)
β (°)	122.674 (11)

V (Å^3)	4377.9 (7)
Z	4
Radiation type	Mo $K\alpha$
μ (mm^{-1})	3.44
Crystal size (mm)	0.44 × 0.06 × 0.05

Data collection	
Diffractometer	Xcalibur, Eos diffractometer
Absorption correction	Multi-scan *CrysAlis PRO*, Agilent Technologies, Version 1.171.36.24 (release 03-12-2012 CrysAlis171 .NET) (compiled Dec 3 2012,18:21:49) Empirical absorption correction using spherical harmonics, implemented in SCALE3 ABSPACK scaling algorithm.
T_{min}, T_{max}	0.673, 1.000
No. of measured, independent and observed [$I > 2\sigma(I)$] reflections	70166, 10027, 7268
R_{int}	0.115
$(\sin\theta/\lambda)_{max}$ (Å^{-1})	0.649

Refinement	
$R[F^2 > 2\sigma(F^2)]$, $wR(F^2)$, S	0.092, 0.195, 1.23
No. of reflections	10027
No. of parameters	490
H-atom treatment	H-atom parameters constrained $w = 1/[\sigma^2(F_o^2) + (0.0145P)^2 + 85.1623P]$ where $P = (F_o^2 + 2F_c^2)/3$
$\Delta\rho_{max}$, $\Delta\rho_{min}$ (e Å^{-3})	3.44, −2.28

Computer programs: *CrysAlis PRO*, Agilent Technologies, Version 1.171.36.24 (release 03-12-2012 CrysAlis171 .NET) (compiled Dec 3 2012,18:21:49), *SIR92* (Giacovazzo, 1994), *SHELXL2014* (Sheldrick, 2014), *ORTEP* (Farrugia, 1997), *enCIFer* (Allen *et al.*, 2004).

7.1.16 $[Th(OTerMes)_2(H_3BH)_2(4,4'\text{-}NC_5H_4C_5H_4N)]_\infty$,**4.3**

Table 7.16 Experimental details

P14040: $[Th(OTerMes)_2(H_3BH)_2(4,4'\text{-}NC_5H_4C_5H_4N)]_\infty$

Crystal data	
Chemical formula	$C_{58}H_{64}B_2N_2Th\cdot 2C_7H_8$

M_r	1249.96
Crystal system, space group	Triclinic, *P*1
Temperature (K)	170
a, *b*, *c* (Å)	12.9640 (2), 14.7824 (2), 17.7705 (3)
α, β, γ (°)	75.461 (1), 77.937 (1), 75.781 (1)
V (Å^3)	3155.84 (9)
Z	2
Radiation type	Mo *K*α
μ (mm^{-1})	2.41
Crystal size (mm)	0.36 × 0.22 × 0.20

Data collection

Diffractometer	Xcalibur, Eos diffractometer
Absorption correction	Multi-scan *CrysAlis PRO*, Agilent Technologies, Version 1.171.36.24 (release 03-12-2012 CrysAlis171 .NET) (compiled Dec 3 2012,18:21:49) Empirical absorption correction using spherical harmonics, implemented in SCALE3 ABSPACK scaling algorithm.
T_{min}, T_{max}	0.926, 1.000
No. of measured, independent and observed [$I > 2\sigma(I)$] reflections	87909, 14469, 13330
R_{int}	0.035
$(\sin\theta/\lambda)_{max}$ (Å^{-1})	0.649

Refinement

$R[F^2 > 2\sigma(F^2)]$, $wR(F^2)$, S	0.023, 0.055, 1.07
No. of reflections	14469
No. of parameters	757
H-atom treatment	H atoms treated by a mixture of independent and constrained refinement
$\Delta\rho_{max}$, $\Delta\rho_{min}$ (e Å^{-3})	0.76, −0.52

Computer programs: *CrysAlis PRO*, Agilent Technologies, Version 1.171.36.24 (release 03-12-2012 CrysAlis171 .NET) (compiled Dec 3 2012,18:21:49), *SIR92* (Siemans, 1995), *SHELXL2014* (Sheldrick, 2014), *ORTEP* (Farrugia, 1997), *enCIFer* (Allen *et al.*, 2004).

7.1.17 $Mg(OTer^{Mes})(BH_4)(THF)_2$, **4.4**

Table 7.17 Experimental details

P14081f: $Mg(OTer^{Mes})(BH_4)(THF)_2$	
Crystal data	
Chemical formula	$C_{32}H_{45}BMgO_3$
M_r	512.80
Crystal system, space group	Monoclinic, $P2_1/n$
Temperature (K)	170
a, b, c (Å)	10.5924 (5), 14.4107 (7), 20.9714 (9)
β (°)	96.272 (4)
V (Å^3)	3182.0 (3)
Z	4
Radiation type	Mo $K\alpha$
μ (mm^{-1})	0.08
Crystal size (mm)	0.40 × 0.19 × 0.13
Data collection	
Diffractometer	Xcalibur, Eos diffractometer
Absorption correction	Multi-scan
T_{min}, T_{max}	0.765, 1.000
No. of measured, independent and observed [$I > 2\sigma(I)$] reflections	30623, 7291, 4093
R_{int}	0.051
$(\sin\theta/\lambda)_{max}$ (Å^{-1})	0.649
Refinement	
$R[F^2 > 2\sigma(F^2)]$, $wR(F^2)$, S	0.072, 0.204, 1.02
No. of reflections	7291
No. of parameters	356
No. of restraints	342
H-atom treatment	H atoms treated by a mixture of independent and constrained refinement
$\Delta\rho_{max}$, $\Delta\rho_{min}$ (e Å^{-3})	0.37, −0.28

Computer programs: *CrysAlis PRO*, Agilent Technologies, Version 1.171.36.24 (release 03-12-2012 CrysAlis171 .NET) (compiled Dec 3 2012,18:21:49), *SIR92* (Giacovazzo, 1994), *SHELXL2014* (Sheldrick, 2014), *ORTEP* (Farrrugia, 1997), *Mercury*.

Crystallisation of **4.4**, from a saturated hexane solution resulted in crystals of the monoclinic lattice system, in space group P121/n1. No special restraints were required in the crystal structure refinement of **4.4**. The borohydride hydrogens were located crystallographically.

7.1.18 $HB(OTer^{Mes})_2$, **4.5**

Table 7.18 Experimental details

	P14142f: $HB(OTer^{Mes})_2$
Crystal data	
Chemical formula	$C_{48}H_{51}BO_2$
M_r	670.69
Crystal system, space group	Orthorhombic, *Fdd*2
Temperature (K)	170
a, *b*, *c* (Å)	44.6191 (10), 21.1401 (6), 8.3981 (2)
V (Å^3)	7921.5 (3)
Z	8
Radiation type	Mo *K*α
μ (mm^{-1})	0.07
Crystal size (mm)	0.37 × 0.18 × 0.13
Data collection	
Diffractometer	Mo Kα diffractometer
Absorption correction	Analytical *CrysAlis PRO*, Agilent Technologies, Version 1.171.37.34 (release 22-05-2014 CrysAlis171 .NET) (compiled May 22 2014,16:03:01) Analytical numeric absorption correction using a multifaceted crystal model based on expressions derived by R.C. Clark & J.S. Reid. (Clark, R. C. & Reid, J. S. (1995). Acta Cryst. A51, 887-897) Empirical absorption correction using spherical harmonics, implemented in SCALE3 ABSPACK scaling algorithm.
T_{min}, T_{max}	0.879, 0.946
No. of measured, independent and observed [$I > 2\sigma(I)$] reflections	13925, 4526, 3006
R_{int}	0.051
$(\sin\theta/\lambda)_{max}$ (Å^{-1})	0.649
Refinement	
$R[F^2 > 2\sigma(F^2)]$, $wR(F^2)$, S	0.053, 0.115, 0.97
No. of reflections	4526
No. of parameters	239
No. of restraints	1
H-atom treatment	H atoms treated by a mixture of independent and constrained refinement
$\Delta\rho_{max}$, $\Delta\rho_{min}$ (e Å^{-3})	0.16, −0.18

Absolute structure	Flack x determined using 1036 quotients [(I+)-(I-)]/[(I+)+(I-)] (Parsons, Flack and Wagner, Acta Cryst. B69 (2013) 249-259).
Absolute structure parameter	1.9 (10)

Computer programs: *CrysAlis PRO*, Agilent Technologies, Version 1.171.37.34 (release 22-05-2014 CrysAlis171 .NET) (compiled May 22 2014,16:03:01), *SIR92* (Giacovazzo, 1994), *SHELXL2014* (Sheldrick, 2014), *ORTEP* (Farrrugia, 1997), *Mercury*.

7.1.19 $(Ter^{Mes}PH)_2$, **5.1**

Table 7.19 Experimental details

	P15104: $(Ter^{Mes}PH)_2$
Crystal data	
Chemical formula	$C_{48}H_{52}P_2$
M_r	690.83
Crystal system, space group	Monoclinic, $P2_1/n$
Temperature (K)	170
a, b, c (Å)	8.4292 (5), 21.5012 (11), 11.6524 (5)
β (°)	110.989 (6)
V (Å^3)	1971.73 (19)
Z	2
Radiation type	Mo $K\alpha$
μ (mm^{-1})	0.14
Crystal size (mm)	0.25 × 0.13 × 0.10
Data collection	
Diffractometer	Xcalibur, Eos diffractometer
Absorption correction	Analytical
T_{min}, T_{max}	0.803, 0.913
No. of measured, independent and observed [$I > 2\sigma(I)$] reflections	19267, 4510, 2400
R_{int}	0.107
$(\sin\theta/\lambda)_{max}$ (Å^{-1})	0.649
Refinement	
$R[F^2 > 2\sigma(F^2)]$, $wR(F^2)$, S	0.068, 0.155, 0.99
No. of reflections	4510
No. of parameters	236

H-atom treatment	H atoms treated by a mixture of independent and constrained refinement
$\Delta\rho_{max}$, $\Delta\rho_{min}$ (e Å^{-3})	0.34, −0.25

Computer programs: *CrysAlis PRO*, Agilent Technologies, Version 1.171.37.34 (release 22-05-2014 CrysAlis171 .NET) (compiled May 22 2014,16:03:01), *SIR92* (Giacovazzo, 1994), *SHELXL2014* (Sheldrick, 2014), *ORTEP* (Farrrugia, 1997), *Mercury*.

Crystallisation of **5.3**, from a saturated toluene solution gave crystals in the monoclinic lattice system of space group P_12_1/n_1. In the crystal structure refinement of **5.3**, no restraints were required in order to create the model obtained.

7.1.20 $U_4K_2Cl_8(\mu^3\text{-})O_2(Ter^{Mes}O)_6$, **3.14**

Table 7.20 Experimental details

	P14008c: $U_4K_2Cl_8(\mu^3\text{-})O_2(Ter^{Mes}O)_6$
Crystal data	
Chemical formula	$C_{144}H_{150}Cl_8K_2O_8U_4$
M_r	3322.55
Crystal system, space group	Monoclinic, *C*2/*c*
Temperature (K)	170
a, *b*, *c* (Å)	30.477 (5), 18.628 (5), 25.753 (5)
β (°)	96.648 (5)
V (Å^3)	14522 (5)
Z	4
Radiation type	Mo *K*α
μ (mm^{-1})	4.70
Crystal size (mm)	0.36 × 0.18 × 0.11
Data collection	
Diffractometer	Xcalibur, Eos diffractometer
Absorption correction	Analytical
T_{min}, T_{max}	0.369, 0.633
No. of measured, independent and observed [$I > 2\sigma(I)$] reflections	6338, 4941, 2449
R_{int}	0.089
$(\sin\theta/\lambda)_{max}$ (Å^{-1})	0.619
Refinement	
$R[F^2 > 2\sigma(F^2)]$, $wR(F^2)$, S	0.185, 0.423, 1.19
No. of reflections	4941
No. of parameters	653

No. of restraints	738
H-atom treatment	H-atom parameters constrained $w = 1/[\sigma^2(F_o^2) + 5246.0068P]$ where $P = (F_o^2 + 2F_c^2)/3$
$(\Delta/\sigma)_{max}$	0.634
Δρmax, Δρmin (e Å−3)	2.49, −1.40

Computer programs: *CrysAlis PRO*, Agilent Technologies, Version 1.171.36.24 (release 03-12-2012 CrysAlis171 .NET) (compiled Dec 3 2012,18:21:49), *SIR92* (Giacovazzo, 1994), *SHELXL2014* (Sheldrick, 2014), *ORTEP* (Farrrugia, 1997), *Mercury*.

Crystallisation of **3.14**, from a saturated toluene solution gave crystals in the monoclinic lattice system of space group C2/c. In the crystal structure refinement of **3.14**, using SHELX's software package, restraints were required in order to create the model obtained. The DFIX restraint was used on carbon atom pairs C45,48 C21,24, C65,70 and C32,37. The AFIX66 restraint was used on the carbons atoms of all of the phenyl rings of the terphenolate ligands. There was also extensive use of the SIMU and DELU restraints.

7.1.21 $^{n}BuTer^{Trip}$, **5.4**

Table 7.21 Experimental details

	PO3015: $^{n}BuTer^{Trip}$
Crystal data	
Chemical formula	$C_{40}H_{58}$
M_r	538.86
Crystal system, space group	Orthorhombic, *Pbca*
Temperature (K)	120
a, *b*, *c* (Å)	22.054 (5), 12.100 (5), 25.323 (5)
V (Å^3)	6758 (3)
Z	8
Radiation type	Mo *K*α
μ (mm^{-1})	0.06
Crystal size (mm)	0.16 × 0.15 × 0.04
Data collection	
Diffractometer	SuperNova, Dual, Cu at zero, Atlas diffractometer
Absorption correction	Gaussian *CrysAlis PRO*, Agilent Technologies, Version 1.171.36.28 (release 01-02-2013 CrysAlis171 .NET) (compiled Feb 1 2013,16:14:44) Numerical absorption correction based on gaussian integration over a multifaceted crystal model
T_{min}, T_{max}	0.769, 0.943

No. of measured, independent and observed [$I > 2\sigma(I)$] reflections	70442, 7041, 5869
R_{int}	0.059
$(\sin\theta/\lambda)_{max}$ (Å^{-1})	0.630

Refinement	
$R[F^2 > 2\sigma(F^2)]$, $wR(F^2)$, S	0.050, 0.133, 1.04
No. of reflections	7041
No. of parameters	374
H-atom treatment	H-atom parameters constrained
$\Delta\rho_{max}$, $\Delta\rho_{min}$ (e Å^{-3})	0.32, −0.31

Computer programs: *CrysAlis PRO*, Agilent Technologies, Version 1.171.36.28 (release 01-02-2013 CrysAlis171 .NET) (compiled Feb 1 2013,16:14:44), *SIR92* (Giacovazzo, 1994), *SHELXL2014* (Sheldrick, 2014), *ORTEP* (Farrrugia, 1997), *Mercury*.

Crystallisation of **5.4**, from a saturated toluene solution gave crystals in the orthorhombic lattice system of space group Pbca. In the crystal structure refinement of **5.4**, no restraints were required in order to create the model obtained.

7.1.22 ClTer^{Trip}, 5.5

Table 7.22 Experimental details

	P13098: ClTer^{Trip}
Crystal data	
Chemical formula	$C_{36}H_{49}Cl$
M_r	517.20
Crystal system, space group	Orthorhombic, $Pca2_1$
Temperature (K)	170
a, b, c (Å)	12.218 (5), 11.022 (5), 25.427 (5)
V (Å^3)	3424 (2)
Z	4
Radiation type	Mo $K\alpha$
μ (mm^{-1})	0.13
Crystal size (mm)	0.56 × 0.38 × 0.19
Data collection	
Diffractometer	Xcalibur, Eos diffractometer

Absorption correction	Multi-scan
T_{min}, T_{max}	0.976, 1.000
No. of measured, independent and observed [$I > 2\sigma(I)$] reflections	13893, 5709, 3913
R_{int}	0.037
$(\sin\theta/\lambda)_{max}$ (Å^{-1})	0.596

Refinement	
$R[F^2 > 2\sigma(F^2)]$, $wR(F^2)$, S	0.118, 0.371, 1.34
No. of reflections	5709
No. of parameters	346
No. of restraints	2
H-atom treatment	H-atom parameters constrained
$\Delta\rho_{max}$, $\Delta\rho_{min}$ (e Å^{-3})	1.92, −0.36
Absolute structure	Flack x determined using 1358 quotients [(I+)-(I-)]/[(I+)+(I-)] (Parsons, Flack and Wagner, Acta Cryst. B69 (2013) 249-259).
Absolute structure parameter	0.61 (6)

Computer programs: *CrysAlis PRO*, Agilent Technologies, Version 1.171.36.24 (release 03-12-2012 CrysAlis171 .NET) (compiled Dec 3 2012,18:21:49), *SIR92* (Giacovazzo, 1994), *SHELXL2014* (Sheldrick, 2014), *ORTEP* (Farrrugia, 1997), *Mercury*.

Crystallisation of **5.5**, from a saturated toluene solution gave crystals in the monoclinic lattice system of space group Pca21. In the crystal structure refinement of **5.5**, restraints were required in order to create the model obtained, using SHELX's software package. The DFIX restraint was used on the chloride to carbon bond and set at 1.79 Å.